

Curtin Medical School

**The role of the HGF/c-MET signalling pathway in  
cellular crosstalk during chronic liver injury**

Sara Pasic

**0000000261687518**

**This thesis is presented for the Degree of  
Doctor of Philosophy  
of  
Curtin University**

**May 2023**

## **Declaration**

To the best of my knowledge, this thesis contains no material previously published by myself or any other person, except where due acknowledgement has been made.

This thesis contains no material which has been accepted for the award of any other degree or diploma at any university.

Sara Pasic

*"I am not afraid of storms, for I am learning how to sail my ship"*

*Louisa May Alcott*

## Abstract

Chronic liver disease (CLD) accounts for approximately 2 million deaths per year worldwide, demonstrating a need for early intervention strategies, before the disease becomes irreversible. During chronic liver injury, fibrosis-driving hepatic stellate cells (HSCs) deposit excess extracellular matrix (ECM) in the liver as an initial wound healing response. However, if chronically stimulated, this type of architectural support may have detrimental effects when scarring becomes excessive in the form of cirrhosis. Liver progenitor cells (LPCs) become activated upon chronic liver insult, proliferate and migrate to sites of injury to replace lost liver tissue and regenerate the liver. HGF/c-MET signalling has been identified as a key pro-regenerative and anti-fibrotic pathway in chronic liver disease. Since HGF-secreting HSCs and c-MET-expressing LPCs co-migrate to sites of injury, this study investigated their unexplored crosstalk and hypothesised that LPCs act as regulatory cells and alter HSC behaviour through the HGF/c-MET signalling pathway.

The project addressed the aims listed below.

1. HGF/c-MET signalling status was first characterised in archival tissue of mice fed a choline-deficient, ethionine-supplemented (CDE) diet. Compared to control tissue, CDE-treated tissue showed a greater expression of fibrosis-associated markers, while demonstrating a decrease in HGF/c-MET signalling components, revealed by western blotting and immunofluorescence. Next, *in vitro* analysis of the LPC line BMOL-TAT confirmed the presence the c-MET receptor, while the HSC line LX-2 revealed expression of the HGF ligand, proposing the cell lines as appropriate models for the study of LPC-HSC crosstalk throughout this thesis.

2. To assess the importance of active HGF/c-MET signalling for LPC biology, CRISPR/Cas9 technology was used to construct a c-MET knockout (KO) BMOL-TAT cell line. BMOL-TAT<sup>c-MET<sup>WT</sup></sup> and BMOL-TAT<sup>c-MET<sup>KO</sup></sup> cell lines were then compared phenotypically. BMOL-TAT<sup>c-MET<sup>KO</sup></sup> cells displayed a rounder phenotype with a significantly greater width/length ratio compared to the BMOL-TAT<sup>c-MET<sup>WT</sup></sup> cells, as evidenced via the Operetta Live Imaging System.



Deletion of the receptor also led to an increase in the cells' adherence in culture. Additionally, BMOL-TAT<sup>c-MET KO</sup> cells were demonstrated to proliferate and migrate slower in culture, as shown by MTS proliferation assay and scratch wound migration assay. Lastly, the cell lines were comparatively evaluated for expression of TGFβ signalling and epithelial-to-mesenchymal transition (EMT) markers by western blotting and immunofluorescence. Overall, c-MET-deleted BMOL-TAT cells demonstrated increased expression of TGFβ signalling and EMT markers, suggesting a shift towards a more pro-fibrotic phenotype. Deletion of the c-MET receptor in BMOL-TAT cells was therefore shown to alter their biology.

3. BMOL-TAT<sup>c-MET WT</sup> and BMOL-TAT<sup>c-MET KO</sup> cells were co-cultured with the LX-2 cell line to assess LPC-HSC crosstalk. Boyden chamber co-culture of BMOL-TAT<sup>c-MET WT</sup> and LX-2 cells exemplified their strong chemoattraction, however LX-2 co-culture with BMOL-TAT<sup>c-MET KO</sup> cells resulted in a repulsive effect. Further, fibrosis-associated marker expression in the LX-2 cells was investigated by western blotting and collagen secretion assay. Following co-culture of LX-2 cells with either BMOL-TAT<sup>c-MET WT</sup> or BMOL-TAT<sup>c-MET KO</sup> cells, LX-2 cells demonstrated altered expression of fibrosis-associated markers and an overall decrease in collagen secretion, suggesting that their collagen expression was HGF/c-MET-independent.

4. Lastly, bulk RNA-sequencing was performed to assess transcriptomic profiles of each cell type following co-culture. LX-2 cells were cultured in Boyden chambers with either BMOL-TAT<sup>c-MET WT</sup> or BMOL-TAT<sup>c-MET KO</sup> cells. BMOL-TAT<sup>c-MET WT</sup> and BMOL-TAT<sup>c-MET KO</sup> were cultured in LX-2-conditioned medium for 30 minutes and 6 hours. Exposing BMOL-TAT<sup>c-MET WT</sup> cells to LX-2-conditioned medium led to a decrease in expression of cell adhesion and matrix deposition genes, and an increase in expression of matrix remodelling genes, suggesting that the cells have an increased capability to migrate to sites of injury, aiding in liver regeneration. Interestingly, BMOL-TAT<sup>c-MET KO</sup> cells under the same conditions demonstrated opposite expression patterns, revealing an increase in expression of cell adhesion and matrix deposition genes, and a decrease in expression of matrix remodelling genes. This

indicates that the observed response of BMOL-TAT cells to LX-2 conditioned medium was c-MET-dependent.

In conclusion, a novel BMOL-TAT<sup>c-MET<sup>KO</sup></sup> cell line was successfully established and was utilised to demonstrate the importance of active HGF/c-MET signalling for the maintenance of LPC biology. Co-culture of BMOL-TAT and LX-2 cells revealed their strong chemoattraction, and a decrease in collagen secretion by LX-2 cells under co-culture conditions suggested that LPCs are potential regulatory cells. The LPC-HSC communicative relationship was greatly weakened following inactivation of c-MET in BMOL-TAT cells. This suggests that the HGF/c-MET signalling pathway is vital for the maintenance of LPC biology and LPC-HSC communication. The results of this thesis demonstrate novel contributions to the previously underexplored field of LPC-HSC crosstalk.

## **Acknowledgement of country**

We acknowledge that Curtin University works across hundreds of traditional lands and custodial groups in Australia, and with First Nations people around the globe. We wish to pay our deepest respects to their ancestors and members of their communities, past, present, and to their emerging leaders. Our passion and commitment to work with all Australians and peoples from across the world, including our First Nations peoples are at the core of the work we do, reflective of our institutions' values and commitment to our role as leaders in the Reconciliation space in Australia.

## Acknowledgements

This PhD journey wouldn't have been possible without the endless encouragement and support from loved ones, mentors and colleagues.

Firstly, I would like to thank Curtin University for providing me an RTP scholarship to pursue my studies.

An enormous thank you to my supervisor Professor Nina Tirnitz-Parker who provided me opportunity, resources and independence throughout my PhD. Beginning my journey with her supervision in my Honours year in 2017, Nina's ongoing support and positivity gave me motivation to pursue a PhD with her in 2019, which I am forever grateful for. Nina has been instrumental in helping me kick start my career in science and she will always be an inspiration and mentor to me. Thank you for the countless stories, training my eye for presentations and for providing enthusiasm when I had little.

Alongside Nina, I am forever indebted to my fellow lab members Dr Rodrigo Carlessi, Dr Benjamin Dwyer, Dr Gayatri Shirolkar, Dr Francis Gratte, Nur Dianah Abu Bakar, Nathan Main and Anjali Ghimire for the support they have provided me. Thank you for always having time to listen to my whinging, silly questions and for broadening my knowledge every single day.

This incredibly challenging journey would have not been capable without the encouragement of my quality friends, you are all treasures to me. A special mention to my PhD friends Zalitha and Melissa, who I spent most of my time with. Whether it was our dinner dates, or our coffee breaks, calculating  $C_1V_1 = C_2V_2$  together, every moment has been extremely valuable to me. My close friends, I will never be able to give you back all the hours I spent complaining, and I am incredibly lucky for all of you. Special mention to my best friend Monica, whom I've spent most of my life with. Thank you for always providing an ear to listen and advice I think back on daily. I would also like to thank my partner Jarryd for the immense patience and compassion you have always provided me. Your work discipline is something I strive toward every day.

Lastly, I would like to give an enormous *hvala* to my Baba and Majka. Fighting and fleeing from a war, before starting a whole new life in a foreign country as refugees, nothing has ever been easy. You have both taught me to always keep pushing no matter the circumstance and I hope that I make you proud.  
*Ljubim vas.*

## **Copyright statement**

I have obtained permission from the copyright owners to use any third-party copyright material reproduced in the thesis or to use any of my own published work in which the copyright is held by another party.

## **Financial support**

This research is supported by an Australian Government Research Training Program (RTP) Scholarship.

## **Publications**

F. G. Gratte, S. Pasic, N. D. B. Abu Bakar, J. Gogoi Tiwari, X. Liu, R. Carlessi, T. Kisseleva, D. A. Brenner, G. A. Ramm, J. K. Olynyk, and J. E. E. Tirnitz-Parker. Previous liver regeneration induces fibro-protective mechanisms during thioacetamide induced chronic liver injury. *Int J Biochem Cell Biol* (2021),134: 105933.

## **Author attributions**

I have obtained permission from the copyright owners to use any third-party copyright material reproduced in the thesis, or to use any of my own published work in which the copyright is held by another party.

Location in thesis: Chapter 5 and Appendix

## **Conference abstracts**

**Sara Pasic**, Pieter Eichhorn, Grant Ramm, Tirnitz-Parker J.E.E. (2022)

The HGF/c-MET signalling pathway is a key regulator of liver progenitor cell biology.

1<sup>st</sup> prize poster presentation at the Annual Liver Cancer Collaborative Meeting, Perth, Australia.

**Sara Pasic**, Pieter Eichhorn, Grant Ramm, Tirnitz-Parker J.E.E. (2022)

The HGF/c-MET signalling pathway. A key player in liver progenitor cell regulatory potential?

1<sup>st</sup> prize oral presentation at the Curtin Medical School Symposium, Perth, Australia

**Sara Pasic**, Pieter Eichhorn, Grant Ramm, Tirnitz-Parker J.E.E. (2022)

The HGF/c-MET signalling pathway is a key regulator of liver progenitor cell function and maintenance of epithelial cell characteristics.

Oral presentation at the Australian Society of Medical Research (ASMR), Perth, Australia

**Sara Pasic**, Pieter Eichhorn, Grant Ramm, Tirnitz-Parker J.E.E. (2022)

The HGF/c-MET signalling pathway is a key regulator of liver progenitor cell function and maintenance of epithelial cell characteristics.

Oral presentation at the Experimental Liver Cancer Forum, Brisbane, Australia (online).

**Sara Pasic**, Pieter Eichhorn, Grant Ramm, Tirnitz-Parker J.E.E. (2021)

HGF/c-MET signalling during cellular crosstalk in chronic liver disease progression.

Oral presentation at the Annual Liver Cancer Collaborative Meeting, Perth, Australia.



## Table of contents

<b>Declaration .....</b>	<b>II</b>
<b>Abstract .....</b>	<b>IV</b>
<b>Acknowledgement of country .....</b>	<b>VII</b>
<b>Acknowledgements .....</b>	<b>VIII</b>
<b>Copyright statement .....</b>	<b>X</b>
<b>Financial support .....</b>	<b>X</b>
<b>Publications .....</b>	<b>XI</b>
<b>Author attributions .....</b>	<b>XI</b>
<b>Conference abstracts .....</b>	<b>XII</b>
<b>Table of contents .....</b>	<b>XIII</b>
<b>List of figures .....</b>	<b>XVII</b>
<b>List of tables .....</b>	<b>XXI</b>
<b>Abbreviations .....</b>	<b>II</b>
<b>Chapter 1: General Introduction .....</b>	<b>1</b>
1.1 The liver .....	2
1.1.1 Anatomy and physiology of the liver .....	2
1.1.2 Hepatic cell types .....	3
1.2 Liver Injury .....	9
1.2.1 Acute liver injury - hepatocyte-mediated regeneration .....	9
1.2.2 Chronic liver disease .....	9
1.3 Liver fibrosis .....	12
1.3.1 The liver injury and regeneration niche .....	14
1.3.2 LPC-HSC crosstalk .....	14
1.4 Murine models of liver fibrosis .....	15
1.4.1 Choline-deficient, ethionine-supplemented (CDE) murine model .....	16
1.4.2 Thioacetamide (TAA) murine model .....	17

1.4.3 Primary HSC model .....	17
1.5 The HGF/c-MET signalling pathway during liver fibrosis.....	18
1.5.1 The HGF/c-MET signalling pathway .....	18
1.5.2 The role of HGF/c-MET signalling in the liver .....	20
1.5.3 HGF/c-MET signalling in liver regeneration .....	20
1.5.4 Crosstalk of the HGF/c-MET and TGF $\beta$ pathways.....	22
1.5.5 HGF/c-MET signalling in liver disease progression .....	24
1.6 Project aims .....	25
<b>Chapter 2: Materials and Methods.....</b>	<b>27</b>
2.1 Materials .....	28
2.1.1 General laboratory chemicals .....	28
2.1.2 Water .....	28
2.1.3 Solutions and buffers .....	28
2.1.4 Antibodies .....	34
2.2 Methods .....	37
2.2.1 CRISPR-facilitated gene editing .....	37
2.2.2 Cell culture techniques.....	39
2.2.3 Histology techniques.....	49
2.2.4 Molecular biology techniques.....	50
2.2.5 RNA sequencing.....	52
<b>Chapter 3: Characterisation of liver progenitor cells and .....</b>	<b>53</b>
<b>hepatic stellate cells in relation to the HGF/c-MET pathway.....</b>	<b>53</b>
<b>in appropriate models of fibrosis .....</b>	<b>53</b>
3.1 Introduction .....	54
3.2 Study Aims.....	55
3.3 Methodology .....	56
3.4 Results .....	57
3.4.1 HGF and c-MET gene expression pattern analysis using single nucleus RNA-sequencing data .....	57

3.4.2 Characterisation of HGF/c-MET signalling components in the CDE model of chronic liver disease.....	61
3.4.3 Characterisation of clonal cell lines BMOL-TAT and LX-2 as appropriate models of LPCs and HSCs.....	66
3.4.4 HGF/c-MET and TGF $\beta$ signalling pathway status in BMOL-TAT and LX-2 clonal cell lines.....	71
3.5 Discussion.....	76
<b>Chapter 4: <i>In vitro</i> deletion of c-MET in liver progenitor cells.....</b>	<b>79</b>
<b>using CRISPR/Cas9 technology.....</b>	<b>79</b>
4.1 Introduction.....	80
4.2 Study aims.....	82
4.3 Methodology.....	83
4.4 Results.....	85
4.4.1 Establishment and confirmation of c-MET knockout BMOL-TAT cells.....	85
4.4.2 Phenotypical assessment of BMOL-TAT <sup>c-MET KO</sup> cells.....	88
4.4.3 The effect of c-MET knockout on cell apoptosis, viability, proliferation and migration.....	94
4.4.4 The effect of c-MET knockout on TGF $\beta$ signalling and epithelial-to-mesenchymal transition markers.....	102
4.5 Discussion.....	107
<b>Chapter 5: Cellular effects of liver progenitor cell-hepatic stellate cell.....</b>	<b>111</b>
<b><i>in vitro</i> co-culture.....</b>	<b>111</b>
5.1 Introduction.....	112
5.2 Study aims.....	114
5.3 Methodology.....	115
5.4 Results.....	117
5.4.1 Spatial arrangement of BMOL-TAT <sup>c-MET WT</sup> and BMOL-TAT <sup>c-MET KO</sup> cells in direct 2D and 3D co-culture with HSCs.....	117

5.4.2 Chemoattraction of BMOL-TAT <sup>c-MET<sup>WT</sup></sup> cells and LX-2 cells.....	124
5.4.3 Expression of fibrogenic markers following indirect co-culture of LX-2 cells and BMOL-TAT <sup>c-MET<sup>WT</sup></sup> cells .....	129
5.4.4 Chemoattraction of BMOL-TAT <sup>c-MET<sup>KO</sup></sup> cells and LX-2 cells.....	134
5.4.5 Expression of TGFβ pathway components and fibrogenic markers following indirect co-culture of LX-2 cells and BMOL-TAT <sup>c-MET<sup>KO</sup></sup> cells	139
5.4.6 LX-2 collagen secretion following indirect co-culture with BMOL-TAT <sup>c-MET<sup>WT</sup></sup> and BMOL-TAT <sup>c-MET<sup>KO</sup></sup> cells .....	142
5.5 Discussion.....	145
<b>Chapter 6: Transcriptional analysis of liver progenitor cell and hepatic stellate cell crosstalk using <i>in vitro</i> co-culture models .....</b>	<b>149</b>
6.1 Introduction .....	150
6.2 Study aims .....	151
6.3 Methodology .....	152
6.4 Results .....	156
6.4.1 Transcriptional profile of LX-2 cells in single culture and co-culture with BMOL-TAT <sup>c-MET<sup>WT</sup></sup> and BMOL-TAT <sup>c-MET<sup>KO</sup></sup> cells.....	156
6.4.2 Transcriptional profile of BMOL-TAT <sup>c-MET<sup>WT</sup></sup> and BMOL-TAT <sup>c-MET<sup>KO</sup></sup> cells in single culture and LX-2-conditioned medium .....	169
6.5 Discussion.....	200
<b>General Discussion .....</b>	<b>204</b>
<b>References.....</b>	<b>213</b>
<b>Appendix .....</b>	<b>243</b>

## List of figures

<b>Figure 1.1: Illustration of the cellular organisation in a liver lobule.....</b>	<b>4</b>
<b>Figure 1.2: Schematic of chronic liver disease progression.....</b>	<b>11</b>
<b>Figure 1.3: Illustration of the role of HGF/c-MET signalling in liver fibrosis resolution.....</b>	<b>22</b>
<b>Figure 2.1: Production of gRNA guides.....</b>	<b>39</b>
<b>Figure 2.2: 3-dimensional cell model illustration of the RASTRUM Bioprinter.....</b>	<b>45</b>
<b>Figure 2.3: Schematic diagram of Boyden chamber co-culture system. .....</b>	<b>48</b>
<b>Figure 3.1: Seurat plot visualisation of healthy, CDE and TAA-treated mouse liver tissue.....</b>	<b>58</b>
<b>Figure 3.2: SnRNA-seq analysis illustration expression pattern of HGF and c-MET in healthy, CDE and TAA-treated livers. ....</b>	<b>60</b>
<b>Figure 3.3: Immunofluorescent detection of collagen 1 expression in 3- month control and CDE-treated tissue. ....</b>	<b>62</b>
<b>Figure 3.4: Immunofluorescent detection of CK19 and <math>\alpha</math>SMA expression in 3-month control and CDE-treated tissue. ....</b>	<b>63</b>
<b>Figure 3.5: Expression analysis and semi-quantitation of fibrosis- associated markers in control and CDE-treated tissue.....</b>	<b>64</b>
<b>Figure 3.6: Expression analysis and semi-quantitation of TGF<math>\beta</math> and HGF/c-MET signalling markers in control and CDE-treated tissue. ....</b>	<b>65</b>
<b>Figure 3.7: Morphological assessment of BMOL-TAT and LX-2 cells... </b>	<b>67</b>
<b>Figure 3.8: Cell proliferation of BMOL-TAT and LX-2 cells. ....</b>	<b>68</b>
<b>Figure 3.9: Immunofluorescent detection of LPC-specific marker expression in BMOL-TAT cells. ....</b>	<b>69</b>
<b>Figure 3.10: Immunofluorescent detection of HSC-specific marker expression in LX-2 cells. ....</b>	<b>70</b>
<b>Figure 3.11: Immunofluorescent detection of HGF/c-MET and TGF<math>\beta</math> signalling components in BMOL-TAT cells. ....</b>	<b>72</b>
<b>Figure 3.12: Immunofluorescent detection of HGF/c-MET and TGF<math>\beta</math> signalling components in LX-2 cells. ....</b>	<b>73</b>

<b>Figure 3.13: Expression analysis and semi-quantitation of TGF<math>\beta</math> and HGF/c-MET signalling markers in BMOL-TAT and LX-2 cells. ....</b>	<b>75</b>
<b>Figure 4.1: Confirmation of c-MET knockout in BMOL-TAT cells. ....</b>	<b>86</b>
<b>Figure 4.2: Confirmation of c-MET knockout through immunofluorescence for phospho-c-MET (p-c-MET). ....</b>	<b>87</b>
<b>Figure 4.3: Morphological assessment of BMOL-TAT<sup>c-MET WT</sup> and BMOL-TAT<sup>c-MET KO</sup> cells. ....</b>	<b>89</b>
<b>Figure 4.4: Morphological assessment by Operetta of BMOL-TAT<sup>c-MET WT</sup> and BMOL-TAT<sup>c-MET KO</sup> cells. ....</b>	<b>92</b>
<b>Figure 4.5: The effect of c-MET knockout in BMOL-TAT cells on cell adherence. ....</b>	<b>93</b>
<b>Figure 4.6: Annexin V apoptosis assay of BMOL-TAT<sup>c-MET WT</sup> and BMOL-TAT<sup>c-MET KO</sup> cells. ....</b>	<b>97</b>
<b>Figure 4.7: Time course cell viability measurements of BMOL-TAT<sup>c-MET WT</sup> and BMOL-TAT<sup>c-MET KO</sup> cells. ....</b>	<b>98</b>
<b>Figure 4.8: Time course cell proliferation measurements of BMOL-TAT<sup>c-MET WT</sup> and BMOL-TAT<sup>c-MET KO</sup> cells. ....</b>	<b>99</b>
<b>Figure 4.9: The effect of c-MET knockout on BMOL-TAT cell migration. ....</b>	<b>101</b>
<b>Figure 4.10: Expression and semi-quantitation of HGF/c-MET and TGF<math>\beta</math> pathway components in BMOL-TAT<sup>c-MET WT</sup> and BMOL-TAT<sup>c-MET KO</sup> cells. ....</b>	<b>104</b>
<b>Figure 4.11: Expression of TGF<math>\beta</math> signalling components by immunofluorescence in BMOL-TAT<sup>c-MET WT</sup> and BMOL-TAT<sup>c-MET KO</sup> cells. ....</b>	<b>105</b>
<b>Figure 4.12: Expression analysis of EMT markers by immunofluorescence in BMOL-TAT<sup>c-MET WT</sup> and BMOL-TAT<sup>c-MET KO</sup> cells. ....</b>	<b>106</b>
<b>Figure 5.1: Spatial arrangement of LX-2 cells in direct 2D co-culture with BMOL-TAT<sup>c-MET WT</sup> and BMOL-TAT<sup>c-MET KO</sup> cells. ....</b>	<b>118</b>
<b>Figure 5.2: Assessment of the spatial arrangement by fluorescent labelling of LX-2 cells in direct 2D co-culture with BMOL-TAT<sup>c-MET WT</sup> and BMOL-TAT<sup>c-MET KO</sup> cells. ....</b>	<b>119</b>

<b>Figure 5.3: Three-dimensional spatial arrangement of BMOL-TAT<sup>c-MET WT</sup> and BMOL-TAT<sup>c-MET KO</sup> cells in single culture and direct co-culture with LX-2 cells.</b>	<b>120</b>
<b>Figure 5.4: Fluorescent labelling of BMOL-TAT<sup>c-MET WT</sup> and BMOL-TAT<sup>c-MET KO</sup> cells in single culture and direct co-culture with LX-2 cells representing their 3D spatial arrangement.</b>	<b>121</b>
<b>Figure 5.5: Annexin V apoptosis assay following direct co-culture of BMOL-TAT<sup>c-MET WT</sup> and BMOL-TAT<sup>c-MET KO</sup> cells with LX-2 cells.</b>	<b>123</b>
<b>Figure 5.6: Boyden chamber migration assay - BMOL-TAT<sup>c-MET WT</sup> cell migration.</b>	<b>126</b>
<b>Figure 5.7: Boyden chamber migration assay - LX-2 cell migration.</b>	<b>128</b>
<b>Figure 5.8: Western blot analysis of LX-2 fibrogenic markers following their indirect co-culture with BMOL-TAT<sup>c-MET WT</sup> cells.</b>	<b>131</b>
<b>Figure 5.9: Western blot analysis of LX-2 fibrogenic markers following their indirect co-culture with SNU-449 cells.</b>	<b>133</b>
<b>Figure 5.10: Boyden chamber migration assay - BMOL-TAT<sup>c-MET KO</sup> cell migration.</b>	<b>136</b>
<b>Figure 5.11: Boyden chamber migration assay - LX-2 cell migration.</b>	<b>138</b>
<b>Figure 5.12: Western blot analysis of LX-2 fibrogenic markers following their indirect co-culture with BMOL-TAT<sup>c-MET KO</sup> cells.</b>	<b>141</b>
<b>Figure 5.13: Collagen assay of LX-2 cells following their indirect co-culture with BMOL-TAT<sup>c-MET WT</sup> and BMOL-TAT<sup>c-MET KO</sup> cells.</b>	<b>144</b>
<b>Figure 6.1: Quality control analysis of LX-2 cells.</b>	<b>159</b>
<b>Figure 6.2: Differential expression analysis of LX-2 SC, LX-2 CC WT and LX-2 CC KO experimental groups.</b>	<b>162</b>
<b>Figure 6.3: Volcano plot of DEGs between LX-2 SC versus LX-2 CC WT experimental groups.</b>	<b>164</b>
<b>Figure 6.4: Volcano plot of DEGs between LX-2 CC WT versus LX-2 CC KO experimental groups.</b>	<b>167</b>
<b>Figure 6.5: Quality control analysis of BMOL-TAT<sup>c-MET WT</sup> cells.</b>	<b>172</b>
<b>Figure 6.6: Quality control analysis of BMOL-TAT<sup>c-MET WT</sup> and BMOL-TAT<sup>c-MET KO</sup> cells in conditioned medium experiments.</b>	<b>175</b>
<b>Figure 6.7: Differential gene expression analysis of WT SC versus WT CM 30 versus WT CM 6 comparison groups.</b>	<b>179</b>

<b>Figure 6.8: Enrichment analysis of the WT SC versus WT CM 6 experimental group.....</b>	<b>182</b>
<b>Figure 6.9: Volcano plot of DEGs between WT SC versus WT CM 6 experimental groups.....</b>	<b>184</b>
<b>Figure 6.10: Differential expression analysis of WT CM 30, WT CM 6, KO CM 30 and KO CM 6 comparison groups.....</b>	<b>190</b>
<b>Figure 6.11: Enrichment analysis of WT CM 6 versus KO CM 6 comparison groups. ....</b>	<b>193</b>
<b>Figure 6.12: Volcano plot of DEGs between WT CM 6 versus KO CM 6 experimental groups.....</b>	<b>195</b>
<b>Figure 6.13 Heatmaps graphically representing the top DEGs between WT SC versus WT CM 6 and WT CM 6 versus KO CM 6 experimental groups.....</b>	<b>199</b>
<b>Figure A.1: <i>In vitro</i> growth of primary control and TAA-treated HSCs in 2D culture. ....</b>	<b>245</b>
<b>Figure A.2: Fluorescent detection of <math>\alpha</math>SMA expression in primary HSCs of control and TAA-treated mice. ....</b>	<b>246</b>
<b>Figure A.3: Brightfield microscopy of primary HSCs from control and TAA-treated mice in 3D culture.....</b>	<b>247</b>
<b>Figure A.4: Immunofluorescent detection of <math>\alpha</math>SMA expression in 3D cultured primary HSCs isolated from control and TAA-treated mice..</b>	<b>248</b>



## List of tables

<b>Table 2.1: List of primary antibodies.....</b>	<b>35</b>
<b>Table 2.2: List of secondary antibodies.....</b>	<b>36</b>
<b>Table 6.1: Reference table of RNA-sequencing treatment groups and abbreviations.....</b>	<b>155</b>
<b>Table 6.2: DEGs between LX-2 SC versus LX-2 CC WT comparison groups involved in liver disease.....</b>	<b>165</b>
<b>Table 6.3: DEGs between LX-2 CC WT versus LX-2 CC KO cells involved in liver disease. ....</b>	<b>168</b>
<b>Table 6.4: DEGs between the WT SC versus WT CM 6 comparison group involved in liver disease.....</b>	<b>187</b>
<b>Table 6.5: DEGs between the WT CM 6 versus KO CM 6 comparison group involved in liver disease.....</b>	<b>198</b>

## Abbreviations

$\alpha$ SMA	alpha-smooth muscle actin
BCA	bicinchoninic assay
BMOL	bipotential murine oval liver
CCL <sub>4</sub>	carbon tetrachloride
CDE	choline-deficient, ethionine-supplemented
CK	cytokeratin
CLD	chronic liver disease
CM	conditioned medium
c-MET	tyrosine-protein kinase MET
CoH	canals of Hering
Col1a	collagen type 1 alpha
CRISPR	clustered regularly interspaced short palindromic repeat
DAPI	4',6-diamidino-2-phenylindole dihydrochloride
ddH <sub>2</sub> O	double de-ionised water
DEG	differentially expressed gene
DMSO	dimethyl sulfoxide
ECL	enhanced chemiluminescence
ECM	extracellular matrix
EDTA	ethylenediaminetetraacetic acid
EMT	epithelial-to-mesenchymal transition
EpCAM	epithelial cell adhesion molecule
FACS	fluorescence-activated cell sorting
FBS	fetal bovine serum

FC	fold change
FDR	false discovery rate
GFP	green fluorescent protein
GO	gene ontology
gRNA	genomic RNA
HCC	hepatocellular carcinoma
HGF	hepatocyte growth factor
HRP	horseradish peroxidase
HSC	hepatic stellate cell
Hu	human
IF	immunofluorescence
kDa	kilodalton
KO	knockout
LPC	liver progenitor cell
LSEC	liver sinusoidal epithelial cell
MET	mesenchymal-to-epithelial transition
MMP	matrix metalloproteinase
mRNA	messenger RNA
Mu	mouse
panCK	pan-cytokeratin
PBS	phosphate-buffered saline
PCA	principal component analysis
PFA	paraformaldehyde
PI	propidium iodide
RIN	RNA integrity number

RIPA	radio-immunoprecipitation assay
RNA	ribonucleic acid
SEM	standard error of the mean
snRNA-seq	single nucleus RNA sequencing
TAA	thioacetamide
TAT	tyrosine aminotransferase
TBST	tris-buffered saline with tween
TGF $\beta$	transforming growth factor beta
TIMP	tissue inhibitor of metalloproteinases
TKI	tyrosine kinase inhibitor
WB	western blot
WT	wildtype

## **Chapter 1: General Introduction**

## 1.1 The liver

### 1.1.1 Anatomy and physiology of the liver

The liver is the largest internal organ in the body, with fundamental roles in maintaining whole body homeostasis including detoxification, regulating blood glucose levels, protein and lipid metabolism as well as plasma protein synthesis (Trefts, Gannon, & Wasserman, 2017).

Accounting for approximately 2-3% of an individual's body weight, the liver is located in the right upper quadrant of the abdominal cavity (Abdel-Misih & Bloomston, 2010). Of the two lobes, the right is larger, located on the posterior side, and separates into two smaller superficial lobes, the caudate and quadrate lobes (Sear, 1992). Liver lobes are composed of liver lobules, rich with blood supply to meet functional and metabolic needs (Kruepunga, Hakvoort, Hikspoors, Köhler, & Lamers, 2019). As a highly vascularised organ, the liver receives approximately 25% of total cardiac output (Abdel-Misih & Bloomston, 2010). Its dual blood supply is delivered through the hepatic artery, which contributes to roughly 30% of the total blood supply, with the portal vein delivering the remainder of the total blood flow (Abdel-Misih & Bloomston, 2010). The blood moves through the vascular portion of the hepatic sinusoids, starting at the portal triad (hepatic artery, portal vein and bile duct) and toward the central vein, before ultimately draining into the hepatic venous system (Abdel-Misih & Bloomston, 2010). The intrahepatic biliary tree is responsible for the production and transport of bile throughout the liver and accessory organs. Bile travels in through the bile canaliculi, a bile network between hepatocytes, further transitioning into larger bile ducts, including the terminal bile ducts, and eventually through the interlobular bile duct (Sear, 1992).

To execute its diverse metabolic functions, such as blood glucose metabolism, detoxification and bile production, the liver is spatially organised into highly structured metabolic zones along the portal-to-central axis (Trefts et al., 2017). Three main zones in this architecture exist: (1) the periportal, (2) the intermediate and (3) pericentral zones (T. Kietzmann, 2017). The periportal

area receives blood with the highest concentration of oxygen, nutrients and glucose (Cunningham & Porat-Shliom, 2021). Conversely, as blood reaches the pericentral areas, significantly lower levels of oxygen and nutrients are present, favouring functions such as glutamine synthesis and lipogenesis (T. Kietzmann, 2017) (Cunningham & Porat-Shliom, 2021). Köhn-Gaone and colleagues reported distinctive pathological responses in different mouse models of chronic liver injury. Thioacetamide (TAA) treatment resulted in progressive injury in pericentral regions (zone 3), however choline-deficient, ethionine-supplemented (CDE) diet administration led to an early fibrosis peak in the periportal area (zone 1) (Köhn-Gaone et al., 2016). Despite the importance of zonation to normal liver function, it is unclear to what degree chronic liver disease disrupts this zonation and whether this drives disease development and progression (Cunningham & Porat-Shliom, 2021).

### **1.1.2 Hepatic cell types**

The liver sinusoidal functional unit is structurally organised to contain the principal cells of the liver (Sear, 1992). Within this vascular matrix, the hepatocytes co-exist with liver sinusoidal epithelial cells (LSECs) along the epithelial layer. Moreover, ducts are formed by the close spatial arrangement of cholangiocytes (Marrone, Shah, & Gracia-Sancho, 2016). Within the sinusoid, the resident macrophages, named Kupffer cells, are activated upon liver injury and release mediators such as interleukin 6 (IL6), to recruit resident cell types to sites of injury (Marrone et al., 2016). Between the sinusoidal epithelial layers, at the Space of Disse, hepatic stellate cells (HSCs) reside and contribute to myofibroblastic activity when activated upon injury stimulus (Figure 1.1) (Marrone et al., 2016). Further, when disease progresses from acute to chronic via repeated viral, chemical or carcinogenic insult, liver progenitor cells (LPCs) become activated at the Canals of Hering (CoH) (Figure 1.1).

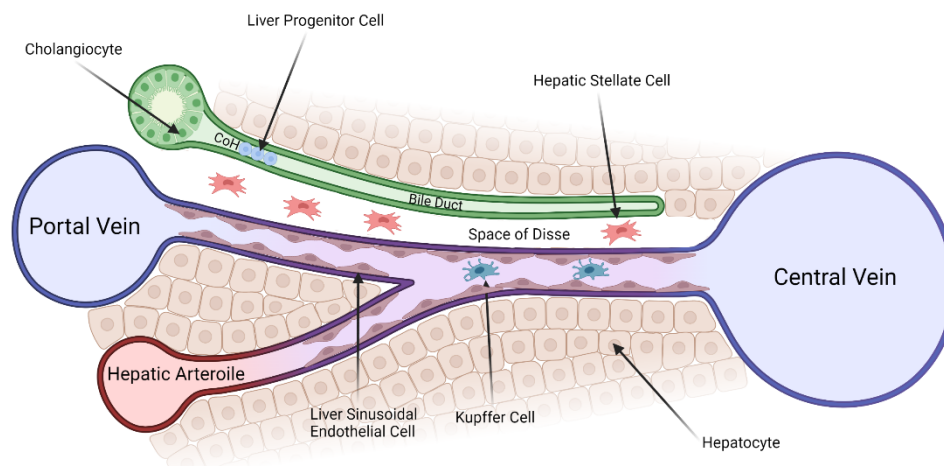


**Figure 1.1: Illustration of the cellular organisation in a liver lobule.**

Representation of cells within the liver lobule and their location. The portal triad consists of the portal vein, hepatic arteriole and bile duct. Blood travels from the hepatic arteriole and portal vein towards the central vein through the sinusoids bordered by liver sinusoidal endothelial cells (LSECs). Kupffer cells are located at the luminal side of sinusoids and hepatic stellate cells (HSCs) are positioned between the hepatocytes and sinusoids at the Space of Disse. Bile is collected into bile ducts, bordered by cholangiocytes near the Canals of Hering (CoH). Here, upon chronic liver injury, liver progenitor cells (LPCs) may activate. Figure created using BioRender.

### 1.1.2.1 Hepatocytes

Hepatocytes are the main parenchymal cell type of the liver and make up 70-80% of the total cell population (Schulze, Schott, Casey, Tuma, & McNiven, 2019). They present cuboidal in shape, ranging from 20-30  $\mu\text{m}$  in size and line the liver sinusoids (Schulze et al., 2019). Hepatocytes are involved in several homeostatic functions including secretion of bile, lipid uptake, drug metabolism and tissue regeneration. Therefore, they contain many mitochondria along with other organelles such as lysosomes, free ribosomes and both smooth and rough endoplasmic reticulum to elicit their large range of functions (Schulze et al., 2019). Additionally, some populations, closer to the central area are



binucleated (Gandillet et al., 2003). The position of the hepatocyte within the different metabolic zones of the liver, determines its function (Kholodenko & Yarygin, 2017). Hepatocytes are therefore differentially exposed to gradients of oxygen, hormones and nutrients depending on their placement in the periportal (1), the intermediate (2) and pericentral (3) zones (Kholodenko & Yarygin, 2017). This metabolic zonation theory was explored by Jungermann *et al.*, suggesting that the closer hepatocytes are to zone one, the greater their exposure to oxygen and therefore aiding in  $\beta$ -oxidation, ureagenesis, and gluconeogenesis (Jungermann & Katz, 1989). Conversely, the closer hepatocytes are to zone three, greater functions in ketogenesis, lipogenesis and glycolysis are observed (Thomas Kietzmann, 2017) (Jungermann & Katz, 1989).

#### **1.1.2.2 Cholangiocytes**

Cholangiocytes are biliary epithelial cells that represent approximately 2-3% of all hepatic cells (Tabibian, Masyuk, Masyuk, O'Hara, & LaRusso, 2013). They form the biliary tree in the sub-lobular architecture of the liver (Figure 1.1). Cholangiocytes are flattened or cuboidal in smaller ducts, changing to columnar in larger ducts (Tabibian et al., 2013). In the hepatic biliary tree, cholangiocytes develop from bipotential hepatoblasts, the same precursor cells as for hepatocytes (P. S. Vestentoft et al., 2011). The cells' main function is to transport bile past the Canals of Hering and into the intestine (Tabibian et al., 2013). Before this occurs, cholangiocytes biochemically modify bile through secretin-induced bicarbonate. This eventually causes an influx of water into the lumen, aiding in the transport of the bile into the intestine (Maroni et al., 2015).

#### **1.1.2.3 Liver sinusoidal endothelial cells**

Pooled blood enters the liver through the hepatic artery and portal vein, where it travels between the hepatic plates and into the sinusoids (Trefts et al., 2017). This blood flow is directed by specialised cells named liver sinusoidal

endothelial cells (LSECs) (Shetty, Lalor, & Adams, 2018) (Figure 1.1). LSECs are the most abundant non-parenchymal cells of the liver and are phenotypically distinct from other liver cell types. LSECs are characterised through the presence of fenestrae, or membranous pores organised into sieve plates, and no basement membrane (Shetty et al., 2018). Key functions of LSECs include the elimination of blood-borne waste, maintenance of hepatocyte homeostasis and mediation of immune responses during acute and chronic liver injury (DeLeve & Maretti-Mira, 2017). Interestingly, LSECs have been reported to play a key role in hepatic fibrosis, as they undergo capillarisation. This process is defined by a phenotypic change, whereby the cells lose their fenestrae and develop a more organised basement membrane (DeLeve & Maretti-Mira, 2017). This, in turn, activates HSCs and therefore, contributes to fibrogenesis (DeLeve & Maretti-Mira, 2017). Research into LSECs is important, however difficult. This is due to limited availability of suitable biomarkers, and co-expression with other vascular endothelial cells. However, regularly used markers include von Willebrand factor and platelet-derived cell adhesion molecule 1 (Shetty et al., 2018).

#### **1.1.2.4 Hepatic stellate cells**

Hepatic stellate cells (HSCs) were first described as “Sternzellen” cells, a German term translating to “star cells”, due to their elongated morphology (Geerts, 2001). HSCs are present in the Space of Disse, located between the extracellular space between the liver sinusoids (Figure 1.1) (Geerts, 2001). They account for approximately 5% of the non-parenchymal cell population and carry out vital functions in healthy and diseased livers. In a healthy liver, HSCs are in a quiescent state, and their main function is to store Vitamin A in lipid droplets (Friedman, 2008). These lipid-storing cells also have roles in retinoid production, remodelling of the extracellular matrix, secretion of cytokines and regulation of the sinusoid diameter (Friedman, 2008). Upon liver injury, HSCs become activated through two main cytokines; transforming growth factor beta (TGF $\beta$ ) and platelet-derived growth factor (PDGF) (Troeger et al., 2012). They then undergo changes in their structure, expanding their myofibroblastic potential. Their characteristic functional changes include

increased cellular proliferation and migration, production of extracellular matrix proteins and expression of specific myofibroblastic cell surface markers including alpha-smooth muscle actin ( $\alpha$ SMA), vimentin and desmin (Friedman, 2008). If resolution of liver injury ensues, HSCs undergo apoptosis or inactivation into a quiescent-like phenotype through the downregulation of fibrosis-associated genes  $\alpha$ SMA and collagen I (Troeger et al., 2012).

#### 1.1.2.5 Liver progenitor cells

Liver progenitor cells (LPCs) are generally 7-20  $\mu$ M in size and contain a relatively large nucleus in proportion to their cytoplasm (Bria et al., 2017). When stained with haematoxylin and eosin, they contain a lightly basophilic cytoplasm and light blue staining nuclei, with them named “oval” cells in rodents due to their shape (Dollé et al., 2010).

There is controversy in the literature in regard to their origin. The most common historical hypothesis is that LPCs are bipotential and arise from an area termed the Canals of Hering (CoH), which is the anatomical boundary between the terminal bile ductules and the first hepatocytes of the hepatic plate (Figure 1.1) (Xin Wang et al., 2003). LPCs proliferate upon activation, migrate to sites of injury, and then differentiate into either hepatocytes or cholangiocytes, depending on the underlying injury stimulus (Xin Wang et al., 2003). This hypothesis was supported by Theise *et al.*, where acetaminophen-induced liver necrosis activated the LPC population, with the cells spreading from the CoH towards the pericentral area of the hepatic lobule (Theise et al., 1999). A different study by Tarlow *et al.* used hepatocyte-chimeric lineage tracing, followed by RNA sequencing analysis in mice administered a 3,5-diethoxycarbonyl-1,4-dihydrocollidine (DDC) diet and demonstrated that mature hepatocytes can undergo metaplasia, and add to the LPC pool (Tarlow et al., 2014).

LPCs represent a very dynamic and heterogeneous cell population, with their phenotype and marker expression shifting, depending on the cells' proliferation and differentiation status (Kohn-Gaone, Gogoi-Tiwari, Ramm, Olynyk, &

Tirnitz-Parker, 2016). Consequently, they share many markers with hepatocytes, cholangiocytes and cancer stem cells (Kawai et al., 2015). Tirnitz-Parker and colleagues identified oval cells positively expressing both hepatocytic (muscle 2-pyruvate kinase, transferrin) and biliary cell markers (A6, cytokeratin 19) in chronically injured, CDE-treated mice, suggesting bipotentiality (J. E. E. Tirnitz-Parker, Tonkin, Knight, Olynyk, & Yeoh, 2007). Importantly, LPCs are not detectable in healthy livers and are only activated during chronic liver injury. However, their role in chronic liver disease has been controversially discussed over time. LPCs have been demonstrated to have a strong association with the progression of chronic liver disease, since their numbers positively correlate to the stage of disease (Lowes, Brennan, Yeoh, & Olynyk, 1999). However, LPCs have also been highlighted to have a pro-regenerative role in the early stages of liver disease, where they are capable of replacing lost parenchymal tissue by differentiation into biliary epithelial cells or hepatocytes (Raven et al., 2017).

#### **1.1.2.6 Kupffer cells**

Kupffer cells were first described by Karl Wilhelm von Kupffer in 1876 and thought to be a part of the endothelium of blood vessels (Dixon, Barnes, Tang, Pritchard, & Nagy, 2013). However, in 1898, Tadeusz Browiecz identified these cells as resident macrophages of the liver (Naito, Hasegawa, & Takahashi, 1997). Kupffer cells are located at the sinusoids near LSECs, and account for approximately 30% of total healthy liver cells (Dixon et al., 2013). The largest percentage of Kupffer cells are in the periportal region, having a role in innate immunity, as first contacts with substances transported in the blood from the gastro-intestinal tract and through the hepatic vein (Nguyen-Lefebvre & Horuzsko, 2015). When Kupffer cells encounter foreign antigens, they become activated and have roles in defence such as phagocytosis of micro-organisms or apoptotic cells, recruitment of monocytes and release of anti-inflammatory cytokines (Yuan-yuan, Mu-qing, Zhi-gang, Qing, & Ji-yu, 2017) (Dixon et al., 2013). Kupffer cells can be identified through immune detection using specific markers such as F4/80 and CD68 to identify their location and proliferative patterns during homeostasis and liver injury (Dixon

et al., 2013). Currently, there is evidence that Kupffer cells regulate the activation and survival of HSCs. However, the exact underlying mechanisms are still largely unknown (Xuanyan Cai et al., 2020).

## **1.2 Liver Injury**

### **1.2.1 Acute liver injury - hepatocyte-mediated regeneration**

Acute liver injury is caused by drug- or toxin-induced liver injury such as paracetamol poisoning or excessive alcohol consumption. Further, hepatic ischaemia, metabolic syndrome and various forms of viral hepatitis, including hepatitis A, B and E, are known causes (Stravitz & Lee, 2019). Acute liver injury usually has a rapid onset and can lead to hepatic failure due to sudden hepatic necrosis and apoptosis of key liver cell players, mainly hepatocytes (Stravitz & Lee, 2019). If the stimulus is not constant and injury is not extensive, hepatocyte-mediated regeneration occurs, where hepatocytes restore the liver mass by proliferation of remaining healthy hepatocytes. This was demonstrated by Michalopoulos and colleagues by partial hepatectomy (PHx), where two thirds of a rat liver were resected and liver mass was restored in five to seven days (Michalopoulos, 2010). Here, an upregulation of the TGF $\beta$  and hepatocyte growth factor (HGF) pathways primed the hepatocytes for an increase in proliferation and replication (Michalopoulos, 2010). If impairment of cells and lack of key signalling pathways is evident, liver mass cannot be effectively restored, signifying that alternate intervention strategies need to be implemented such as liver transplantation (Stravitz & Lee, 2019).

### **1.2.2 Chronic liver disease**

Chronic liver diseases (CLD) mainly include alcoholic (ALD) or non-alcoholic fatty liver disease (NAFLD), cholestasis, steatohepatitis, haemochromatosis and viral hepatitis (Cheemerla & Balakrishnan, 2021). It has been described that approximately 844 million people worldwide have CLD (Marcellin & Kutala, 2018) with a mortality rate of roughly two million people per year (Asrani,

Devarbhavi, Eaton, & Kamath, 2019). Poor diet, excessive alcohol consumption, metabolic syndrome, hepatitis and genetic predispositions (Ferlay et al., 2015) all play pivotal roles in the initiation and advancement of CLD. When continuously exposed to the injury stimulus, chronic inflammation leads to excessive deposition of ECM, distorting the liver architecture. Dysregulation of this wound healing response, termed fibrosis, may advance to cirrhosis, whereby further scarring and formation of widespread nodules occurs (Ferlay et al., 2015). Cirrhosis is largely irreversible due to excessive damage to the liver, with liver transplantation considered as the main curative treatment avenue. However, limited availability of transplantable livers, potential organ rejection and high procedural costs often make organ transplantation an undesirable option and many end-stage liver disease patients develop liver cancers such as hepatocellular carcinoma (HCC) (Cheemerla & Balakrishnan, 2021). Of the treatment options available for liver cancer, tyrosine kinase inhibitors (TKIs) have shown promise. In particular, Sorafenib is routinely administered to advanced HCC patients due to increasing patient lifespans from 10.7 to 14.7 months (A. Huang, Yang, Chung, Dennison, & Zhou, 2020). Still, sorafenib is associated with high toxicity in some patients, limited anti-tumour activity and acquired drug resistance, indicating a need for other treatment options (A. Huang et al., 2020). Recently, immune checkpoint inhibitors (ICIs), which fall under the broad category of programmed cell death protein-1 (PD-1) inhibitors, have been trialled for the treatment of advanced HCC, especially in patients who have demonstrated resistance to Sorafenib. Immune checkpoints are expressed by immune cells and apply a physiologic break that prevent their activation. It has been demonstrated that immune checkpoint proteins can be dysregulated by tumours, establishing drug resistance (Onuma et al., 2020). Therefore, ICIs were designed to prevent activation of immune checkpoints and an overall decrease in drug resistance has been reported (A. Huang et al., 2020). However, despite the success in some patients, approximately 85% of HCC patients do not respond to ICIs (Onuma et al., 2020). Discovery of novel biomarkers to accurately predict treatment responses and define appropriate

drug candidates for patients is therefore the focus of future liver cancer research.

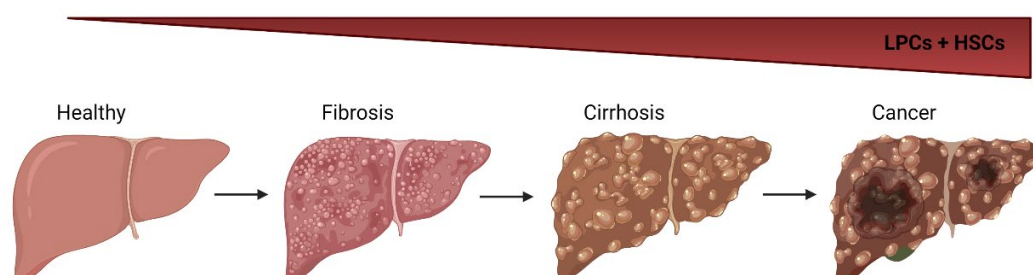


**Figure 1.2: Schematic of chronic liver disease progression.**

Representation of the liver during stages of disease. As disease progresses, increased numbers of proliferating LPCs and HSCs are also evident. Figure created using BioRender.

### 1.2.2.1 Chronic liver disease - liver progenitor cell-mediated regeneration versus disease progression

Subject to the underlying injury stimulus, hepatocytes or cholangiocytes proliferate to restore liver mass and return homeostasis (Kholodenko & Yarygin, 2017). However, chronic chemical or carcinogenic insult halts this process, and LPCs become activated. LPCs proliferate, migrate to sites of injury and ultimately differentiate into hepatocytes or cholangiocytes, depending on the stimulus and type of disease, eventually restoring liver mass (Kohn-Gaone et al., 2016). The specific role of LPCs during chronic liver disease remains to be elucidated and may depend on the injury context.

Studies suggest that LPCs are critical for tissue regeneration as they replace lost parenchyma. This was reported by Dai and colleagues, where overexpression of growth factor 11 in mice increased the number of leucine-rich repeat-containing G-protein coupled receptor 5 (LGR5<sup>+</sup>) LPCs, resulting in hepatic regeneration (Dai et al., 2020). Another study activated the LPC pool in mice through a 3,5-diethoxycarbonyl-1,4-dihydrocollidine (DDC) diet.

Thereafter, deletion of the c-MET receptor in LPCs impaired their proliferation, migration and ultimately inhibited liver regeneration (Ishikawa et al., 2012).

Conversely, LPC numbers have been reported to be directly proportional to disease severity (Lowes et al., 1999) and suppression of LPCs was demonstrated to exert antitumorigenic effects in the liver (Knight, Tirnitz-Parker, & Olynyk, 2008). Therefore, LPCs have been suggested to represent cancer-initiating cells or cancer stem cell-like cells (Greenbaum & Wells, 2011). As several LPC markers overlap with cancer stem cell markers, including CD133 and Sox9, it can be challenging to distinguish between the respective cell types.

Their cancer stem cell-like activity has been previously reported, where advanced liver pathologies correlate with increased levels of (Kuramitsu et al., 2013). Further, following administration of tumour necrosis factor-like weak inducer of apoptosis (TWEAK)-neutralising antibody in mice, a strong downregulation of pro-fibrogenic mRNA, reduced levels of LPCs and improved overall regeneration was evident (Kuramitsu et al., 2013). Taken together, the reported pro- and anti-regenerative roles of LPCs appear to be dependent on the injury stimulus and stage of disease.

### **1.3 Liver fibrosis**

Fibrosis is a natural wound healing response that provides structural support when the liver architecture is compromised following tissue damage from chemical, viral or carcinogenic insult (T. A. Wynn, 2008). However, when exacerbated, it is characterised by excessive accumulation of extracellular matrix (ECM) components such as fibronectin, collagen, laminin and proteoglycans (Thomas A. Wynn & Ramalingam, 2012). During liver fibrosis, this accumulation of ECM in and around inflamed or damaged tissue, may lead to permanent scarring, or cirrhosis, distorting tissue architecture (Thomas A. Wynn & Ramalingam, 2012).



Early intervention is widely considered as the most promising method to combatting the progression of fibrosis. However, as excess fibrotic scarring and ECM overproduction persists, resolving fibrosis may become increasingly difficult (Bataller & Brenner, 2005). Liver fibrosis interventions include liver biopsy, followed by histological examination, as it is considered the gold-standard method for the assessment of liver fibrosis (Afdhal & Nunes, 2004). However, biopsy is invasive and there are risks of sampling error and infection (Bataller & Brenner, 2005). Alternatively, routine laboratory tests such as serum alanine aminotransferase (ALT) level assessment have been utilised in the detection of fibrosis, due to its direct relation to hepatic fibrosis. However, the inability to differentiate intermediate grades of fibrosis is a limitation and may in fact describe fibrosis in nearby organs instead (Fontana & Lok, 2002). Further, transient elastography provides a liver stiffness measurement for the degree of liver fibrosis examined. Yet, this technique has sub-optimal accuracy in obese patients and resulting measurements may be influenced by elevated ALT concentrations (Cheng & Wong, 2017). Therefore, there is a demand for reliable, reproducible, and non-invasive methods for assessing liver fibrosis.

HSCs are known as the main collagen-producing cells in the liver (Bataller & Brenner, 2005). When liver injury occurs, HSCs are activated by cytokines such as tumour necrosis factor (TNF) and transforming growth factor beta (TGF $\beta$ ) (Fabregat et al., 2016) (Tsuchida & Friedman, 2017). Following activation, HSCs undergo a major phenotypic change, becoming myofibroblastic. Upon sustained activation, these myofibroblastic cells deposit excessive ECM and become invasive, pro-fibrogenic cells (Bataller & Brenner, 2005). Activated, myofibroblastic HSCs express markers  $\alpha$ SMA, desmin, collagen I and vimentin (Shang, Hosseini, Liu, Kisseleva, & Brenner, 2018). Ogawa and colleagues demonstrated that treatment of the human HSC line LX-2 with the multi-kinase inhibitor Lenvatinib led to a significant decrease in TGF $\beta$ -induced HSC activation (Ogawa et al., 2021). Other key molecular pathways involved during activation and regulation of myofibroblastic HSCs include Wnt/ $\beta$ -catenin, HGF/c-MET and hedgehog signalling (Yan, Zeng, Xing, & Li, 2021).

### 1.3.1 The liver injury and regeneration niche

Irrespective of the injury stimulus, LPCs are generally in close proximity to inflammatory cell populations and activated HSCs, forming a histological phenomenon named the injury and regeneration niche (Kohn-Gaone et al., 2016). Their spatial proximity suggests that the cells' crosstalk during fibrosis to either resolve or progress disease (Kohn-Gaone et al., 2016). A recent study investigated the cellular dynamics in the liver injury and regeneration niche, with a particular focus on LPCs and HSCs. Here, 2-acetylaminofluorene treatment and a partial hepatectomy was performed to promote liver injury. Proliferation of cytokeratin 19<sup>+</sup> LPCs and desmin<sup>+</sup> HSCs was induced following injury in the periportal areas. The HSCs were determined to have elevated levels of galectins, while knockdown of galectin-1 and galectin-3 led into a significant function loss in HSCs and their communication with LPCs, ultimately hindering liver regeneration (Ge et al., 2020). Further studies into the close communicative relationship between LPCs, HSCs and immune cells are needed to aid in understanding their intricate signals for either regeneration or disease progression.

### 1.3.2 LPC-HSC crosstalk

LPCs and HSCs have been reported to co-migrate to sites of injury (Dwyer, Olynyk, Ramm, & Tirnitz-Parker, 2014) (Van Hul, Abarca-Quinones, Sempoux, Horsmans, & Leclercq, 2009). Despite a lack of investigation into bi-directional, mutual regulation of LPCs and HSCs, recently published data suggest that LPCs are regulators of HSCs (Gratte et al., 2021). In this study, primary murine HSCs, when co-cultured with the clonal LPC line BMOL-TAT, downregulated the fibrosis-associated markers  $\alpha$ SMA, TGF $\beta$ , and collagen 1, suggesting that LPCs regulate HSC pro-fibrotic behaviour (Gratte et al., 2021). Further, it has been reported that LPCs can inhibit HSC activation through IL6-mediated activation of NF- $\kappa$ B signalling (Gajalakshmi et al., 2016). Ruddell and colleagues also demonstrated the clear migratory relationship between the two cell types, through chemotactic recruitment (Ruddell et al., 2009). Lymphotoxin-beta receptor (LT $\beta$ R)-expressing HSCs were revealed to signal

with nearby  $LT\beta$ -expressing liver progenitor cells (Ruddell et al., 2009). This study suggests that HSCs may be involved in paracrine signalling with adjacent  $LT\beta$ -expressing LPCs, recruiting them to regenerate the injured liver (Ruddell et al., 2009) (Dwyer et al., 2014).

The pro-fibrotic relationship between LPCs and HSCs has also been reported. The TWEAK signalling pathway is known to modulate the LPC response during HSC-mediated liver fibrosis (J. E. Tirnitz-Parker et al., 2010). In this study, Fn14 receptor knockout mice were utilised to investigate the effects of a lack of corresponding TWEAK ligand downstream signalling on cellular dynamics during CLD induction and maintenance. A decrease in LPC and inflammatory cell numbers was demonstrated, as well as an overall reduction in collagen deposition (J. E. Tirnitz-Parker et al., 2010). Similarly, another study evidenced that blocking of canonical hedgehog signalling in myofibroblasts led to an attenuation of liver fibrosis and a decrease in proliferating LPCs (Michelotti et al., 2013).

As exemplified, contextual factors including cell type and disease state have an immense impact on liver regeneration versus disease progression. With limited knowledge available into the bi-directional crosstalk between LPCs and HSCs and the critical pathways involved, filling the gap in this area of research will help strengthen our understanding of the cells' co-regulatory relationship.

#### **1.4 Murine models of liver fibrosis**

In humans, CLD arises from a variety of genetic and lifestyle causes, resulting in a highly complex condition. To recapitulate the disease in a laboratory setting, rodents are largely used (Y. Liu et al., 2012) (Yanguas et al., 2016). Due to their marked genetic similarity to humans, they add benefit for reproducibility in experiments, while reflecting many features and mechanisms of human disease progression (Y. Liu et al., 2012). Dietary and toxin-induced models of chronic liver disease are largely used to mimic human pathology (Y. Liu et al., 2012). Dietary manipulation involving either overnutrition or nutrition deficiency is commonly used to acquire a non-alcoholic fatty liver disease

phenotype. Examples of dietary manipulation include high-fat diet and choline-deficient, ethionine-supplemented diet. Additionally, toxin-induced models of chronic liver disease include thioacetamide (TAA) and the commonly used carbon-tetrachloride (CCL<sub>4</sub>) (Y. Liu et al., 2012). CCL<sub>4</sub> leads to hepatocyte death and acute necrosis that initiates a wound healing process. With repetition, liver fibrosis develops progressively, which may lead to cirrhosis and ultimately HCC (Domenicali et al., 2009) (T. Uehara, Pogribny, & Rusyn, 2014). A major limitation of dietary and toxin-induced models is the variable disease severity, which may be strongly dependent on the mouse strain and length of treatment. Thus, scientists may transition to the use of genetically engineered mice (Y. Liu et al., 2012). This technology allows insertion or disruption of endogenous genes and has also emerged as a powerful tool for the study of gene function in chronic liver disease (Brown, Heinrich, & Greten, 2018). Numerous genetically modified models in combination with dietary or toxin-induced models have emerged, allowing scientists to evaluate the relationship of various genes with the progression of disease (J. E. Tirnitz-Parker et al., 2010) (Chung et al., 2016) (Ishikawa et al., 2012).

#### **1.4.1 Choline-deficient, ethionine-supplemented (CDE) murine model**

The choline-deficient, ethionine-supplemented (CDE) diet has been largely used to recapitulate CLD in mice, as it induces fibrosis, fat loading and in long-term administration, carcinogenesis (Gogoi-Tiwari et al., 2017). Choline is known to be an essential nutrient in mammals and its deficiency causes impairment to hepatic triglyceride release (Liedtke et al., 2013). A choline-deficient diet, in combination with ethionine, results in stronger CLD development by inhibiting hepatocyte proliferation, while increasing LPC proliferation (Liedtke et al., 2013). Ethionine is a methionine antagonist and is usually provided in the drinking water at a concentration of 0.15% (Gogoi-Tiwari et al., 2017) (Liedtke et al., 2013). Vast research has been undertaken using this diet-induced CLD model to understand liver cell dynamics over time (Köhn-Gaone et al., 2016) (Gogoi-Tiwari et al., 2017). It is now clear that the CDE diet stimulates periportal injury, steatosis, and fibrosis with LPC and HSC proliferation peaking as early as two weeks, followed by slow normalisation of

general liver disease parameters over time (Köhn-Gaone et al., 2016). These data identify the CDE model as an appealing model to study pathological changes in early- and late-stage disease.

#### **1.4.2 Thioacetamide (TAA) murine model**

Thioacetamide (TAA) requires to be metabolised in order to become toxic. This bioactivation process is catalysed by cytochrome P450 (CYP450) isoenzymes and ultimately results in the formation of thioacetamide sulphur dioxide, which is toxic (Yanguas et al., 2016). Typically, TAA is administered intra-peritoneally at a dose of 100 and 200 mg/kg body weight three times per week for approximately 6-8 weeks to establish centrilobular necrosis and mild inflammatory cell infiltration (Yanguas et al., 2016). Additionally, TAA may be administered orally through drinking water at a dose of 150 mg/kg, for two to four months, for mice to develop significant fibrosis (Yanguas et al., 2016) (Liedtke et al., 2013).

The TAA model has been largely utilised to induce fibrosis, cirrhosis, and liver cancer (Köhn-Gaone et al., 2016) (Wallace et al., 2015) (Lee et al., 2018). Severe TAA-induced liver damage is associated with pericentral lipid oxidative damage as well as gradual increases in inflammatory, fibrogenic and LPC responses. In advanced stages portal-portal bridging and tissue necrosis are also observed (Aydin et al., 2010) (Bao et al., 2021) (Yanguas et al., 2016) (Köhn-Gaone et al., 2016).

#### **1.4.3 Primary HSC model**

Primary isolated HSCs are considered the gold standard of *in vitro* HSC experimentation. The well-described methodology for the isolation of primary HSCs is based on a density gradient centrifugation method using Nycodenz (Mederacke, Dapito, Affò, Uchinami, & Schwabe, 2015). This allows separation from other liver cell types, acquiring a highly viable population of HSCs (Mederacke et al., 2015). To obtain further purity of isolates, cell sorting

with an ultraviolet laser, able to excite vitamin A, produces an ultrapure population of HSCs (>99%) (Mederacke et al., 2015). In combination with murine models of fibrosis such as TAA administration, differing HSC phenotypes can be isolated successfully. However, primary HSCs generally autoactivate and become myofibroblastic upon seeding on plastic. Therefore, isolated cells may not reflect the pathophysiological phenotype exhibited during *in vivo* liver fibrogenesis (Yanguas et al., 2016) (Z. Liu et al., 2021). Culturing primary HSCs with an optimised growth medium containing epidermal growth factor (EGF) and fibroblast growth factor 2 (FGF2) may circumvent these issues, as it retains cells in an undifferentiated state (El Taghdouini, Najimi, Sancho-Bru, Sokal, & van Grunsven, 2015).

## **1.5 The HGF/c-MET signalling pathway during liver fibrosis**

### **1.5.1 The HGF/c-MET signalling pathway**

The HGF/c-MET signalling pathway is well-conserved across species and plays numerous roles in liver biology comprising of fetal liver development, cellular proliferation, survival, motility, and when aberrantly activated, liver tumour formation (Ishikawa et al., 2012) (Organ & Tsao, 2011).

The c-MET proto-oncogene, also known as mesenchymal-to-epithelial transition factor or tyrosine-protein kinase MET, is located on chromosome 7q21-31 (Organ & Tsao, 2011). The protein product of this gene is the c-MET tyrosine kinase. This receptor lies on the cell surface and is expressed by epithelial cells of many organs, including liver progenitor cells (Organ & Tsao, 2011) (Wu, Cheng, Shi, Feng, & Guan, 2014). The receptor c-MET is originally expressed as a 150 kDa single-chain precursor, which, after proteolytic cleavage, is then converted into its mature form (Uchikawa, Chen, Xiao, Zhang, & Bai, 2021). The mature form comprises of the  $\alpha$ - (32 kDa) and  $\beta$ -subunits (120 kDa) that are linked by disulphide bonds (Uchikawa et al., 2021).

Structurally, the extracellular portion of c-MET encompasses the semaphorin (SEMA) domain, where N-terminal residues fold and create the  $\alpha$ -subunit and

part of the  $\beta$ -subunit (Uchikawa et al., 2021) (Organ & Tsao, 2011). The plexin-semaphorin-integrin (PSI) domain follows the SEMA domain in the extracellular portion and extends roughly 50 residues. The PSI domain is connected to the transmembrane helix via four immunoglobulin-plexin-transcription (IPT) domains, which leads to the intracellular portion of the receptor (Organ & Tsao, 2011). When hepatocyte growth factor (HGF) induces the dimerisation of c-MET, the intracellular kinase domains (KDs) undergo autophosphorylation, leading to receptor activation (Uchikawa et al., 2021).

HGF, also known as scatter factor (SF) (Weidner et al., 1991), is the cognate ligand of c-MET that is expressed by HSCs and is secreted as an 83 kDa single-chain precursor protein containing an N-terminal domain, four kringle (K1-K4) domains, and a serine protease homology (SPH) domain (Uchikawa et al., 2021). Like its receptor, HGF undergoes proteolytic cleavage to produce  $\alpha$ - and  $\beta$ -subunits (57 and 26 kDa, respectively) (Organ & Tsao, 2011) (Zhang et al., 2018). Naturally occurring alternatively spiced isoforms of HGF also exist, as they activate the same receptor with high affinity, however differ in cellular activity and biological function (Mungunsukh, McCart, & Day, 2014). The NK1 variant contains the N-terminal hairpin and the first kringle domain. However, the NK2 variant extends through the second kringle domain (Mungunsukh et al., 2014). Studies suggest that the NK1 isoform signals similarly to pro-HGF, where it induces epithelial cell proliferation and motility, while the NK2 isoform acts as an antagonist for HGF-induced cellular proliferation, as it is elevated in human fibrotic diseases, potentially playing a role in arresting regeneration (Mungunsukh et al., 2014).

The HGF/c-MET signalling pathway has been extensively described (H. Wang et al., 2020) (Organ & Tsao, 2011) (Zhang et al., 2018). HGF binding to c-MET results in receptor homodimerisation and phosphorylation at residue points Y1234 and Y1235 (Maulik et al., 2002). Consequently, tyrosines 1349 and 1356 in the carboxy-terminal end are then phosphorylated. Following phosphorylation of the receptor, signalling effectors such as growth factor receptor-bound protein 2 (GRB2) and the scaffolding adaptor GAB1 (growth-factor-receptor-bound protein 2 (Grb2-associated binder 1) mediate most of



the complex cellular responses to c-MET activation (Figure 1.3). Unique to c-MET, GAB1 directly, or indirectly through GAB2, can create binding sites for additional adaptor proteins including Y1313, which activates phosphatidylinositol 3-kinase (PI3K) signalling (H. Wang et al., 2020) (Birchmeier, Birchmeier, Gherardi, & Vande Woude, 2003) (Maulik et al., 2002). Several downstream pathways may then be activated through adapter proteins, including mitogen-activated protein kinase (MAPK), signal transducer and activator of transcription (STAT3) and extracellular signal-regulated kinase (ERK), which all play vital roles in cell growth, viability, motility, morphogenesis and immune system regulation (Figure 1.3) (Zhang et al., 2018) (Seif et al., 2017).

### **1.5.2 The role of HGF/c-MET signalling in the liver**

The HGF/c-MET signalling pathway has roles in many epithelial organ systems including the kidney, lung and liver (Kato, 2017). HGF was first described as a strong mitogen for mature hepatocytes, however its roles in cell proliferation, motility, differentiation and morphogenesis makes it vital during embryogenesis (Kato, 2017). The significance of HGF during fetal development was described in 1995 by two groups, suggesting that mice lacking HGF established severely impaired placentas and failed to complete development, dying *in utero* (Schmidt et al., 1995) (Y. Uehara et al., 1995). The importance of HGF carries on to adult liver physiology in roles such as mitogenesis and regeneration (Huh et al., 2004). Activation of the c-MET receptor on LPCs, by secretion of the ligand HGF by HSCs, promotes the proliferative and migratory behaviour of liver progenitor cells, which is essential for tissue repair and regeneration (Petrini, 2015) (Ishikawa et al., 2012).

### **1.5.3 HGF/c-MET signalling in liver regeneration**

The HGF/c-MET signalling pathway has been noted to promote regeneration during chronic liver damage (Petrini, 2015) (Huh et al., 2004). HGF, secreted by HSCs, initiates its biological effect by binding to the c-MET receptor,



expressed by LPCs (Zhang et al., 2018). This induces a variety of cellular responses, including LPC proliferation and motility, previously reported to aid in the regeneration of the fibrotic liver (Ishikawa et al., 2012) (Suárez-Causado et al., 2015) (Figure 1.3).

The importance of HGF expression for LPC homeostatic function was first described in the rat by Hu and colleagues (Z. Hu, Evarts, Fujio, Marsden, & Thorgeirsson, 1993). Acetylaminofluorene treatment combined with partial hepatectomy was used to induce proliferation and differentiation of LPCs. It was revealed that expression of HGF and c-MET significantly increased following partial hepatectomy, as well as progenitor cell proliferation (Z. Hu et al., 1993). In situ hybridisation indicated that HGF was localised to HSCs, whereas the c-MET receptor was confirmed to be expressed by the LPCs, suggesting an intimate relationship between these two cell types during wound healing (Z. Hu et al., 1993).

With knowledge of the c-MET localising to LPCs in the liver, Ishikawa and colleagues, demonstrated that deletion of c-MET in LPCs had a profound effect on liver tissue remodelling. Significantly reduced levels of metalloproteinase 9 (MMP9) and overall reduced numbers of proliferating LPCs were observed, suggesting failure of LPC mobilisation (Ishikawa et al., 2012). This was also described by Marquardt *et al.* in the same year, whereby c-MET deletion in hepatocytes was associated with decreased hepatocyte proliferation, HSC activation, excessive necrosis, ultimately leading to aggravated hepatic fibrogenesis (Marquardt et al., 2012). Additionally, HGF/c-MET signalling also increases invasion of progenitor cells through extracellular matrix of fibrotic tissues - a process that requires PI3K and metalloproteinase activation, further allowing their successful migration to sites of injury to aid in the regeneration of the injured liver (Suárez-Causado et al., 2015).

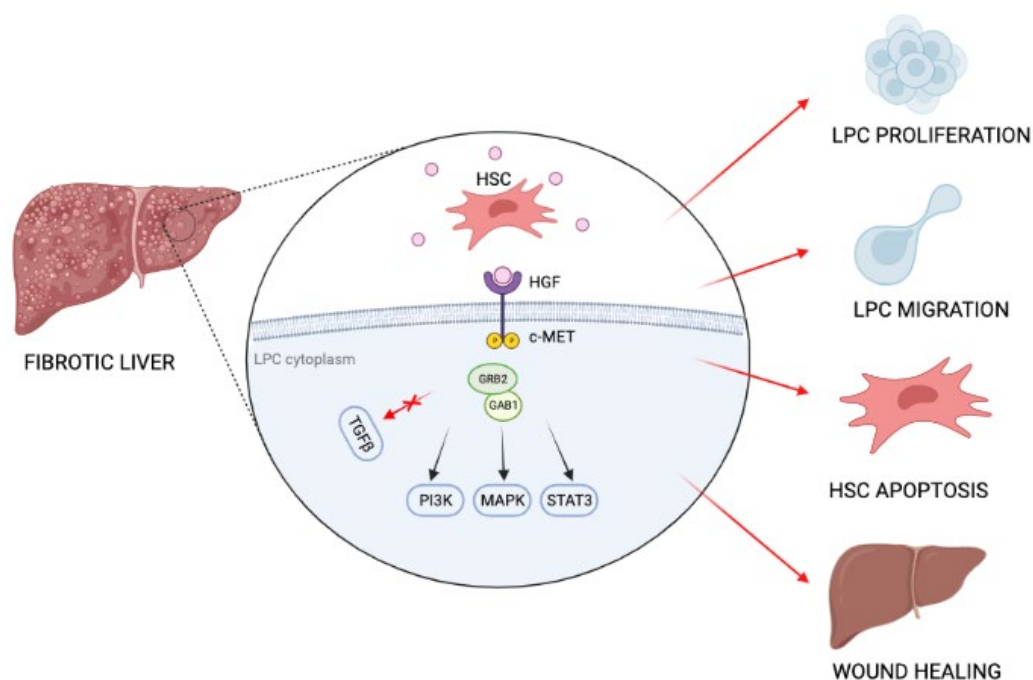


**Figure 1.3: Illustration of the role of HGF/c-MET signalling in liver fibrosis resolution.**

Illustration of the HGF/c-MET signalling pathway during liver fibrosis identifies upregulation of downstream signalling pathways PI3K, MAPK, STAT3 and downregulation of the TGF $\beta$  signalling pathway. Upregulation of HGF/c-MET signalling increases LPC proliferation, LPC migration, HSC apoptosis and wound healing, ultimately aiding in liver fibrosis resolution. Figure created using BioRender.

#### 1.5.4 Crosstalk of the HGF/c-MET and TGF $\beta$ pathways

Quiescent HSCs activate into myofibroblastic cells during fibrosis, producing ECM and ultimately leading to the development of excessive scarring in the liver, when dysregulated (Z. Liu et al., 2021). The HGF/c-MET signalling pathway has been described to attenuate liver fibrosis (Li et al., 2018) (Narmada et al., 2013) (Inagaki et al., 2008) (Kwiecinski et al., 2011). In many cases, a decrease in expression of fibrosis-associated markers was demonstrated by HGF/c-MET inhibiting the TGF $\beta$  signalling pathway (Inagaki et al., 2008) (Kwiecinski et al., 2011). TGF $\beta$  is known as a key disease-

progressing cytokine, due to it directly activating HSCs and causing hepatocyte death (Fabregat et al., 2016).

TGF $\beta$  signals by binding to transmembrane type I and type II receptors (T $\beta$ RI and T $\beta$ RII). Once bound, the receptors form a ligand-induced heteromeric complex that activates a type I kinase (Fabregat et al., 2016). Upon activation, the extracellular signal is transmitted intracellularly, and phosphorylation of specific proteins named R-SMADS, (SMAD2 and SMAD3) occurs. Activated SMAD2 and SMAD3 form a complex with SMAD4, and this complex is translocated into the nucleus, functioning as transcription factors that act together with the corepressor SMAD7, to regulate TGF $\beta$  signalling responses including cell growth, migration, apoptosis and differentiation (Fabregat et al., 2016). TGF $\beta$  has been reported to induce its pro-fibrotic role through activating the transcription of EMT-related components snail and slug: two zinc-finger transcription factors that repress E-cadherin (Akhurst & Hata, 2012). Further, increased expression of TGF $\beta$  has been reported to induce hepatocyte apoptosis and mediate the over-activation of HSCs, causing excessive ECM deposition (Dooley & Dijke, 2012).

The HGF/c-Met pathway's anti-fibrotic action is suggested to be the direct effect of its antagonistic role of inhibiting TGF $\beta$  expression (Papa et al., 2017). Kwiecinski and colleagues described that a micro-RNA, miR-29, suppresses the production of collagen I and IV (Kwiecinski et al., 2011). The same study reported that upregulation of miR-29 was dependent on HGF and that conversely, TGF $\beta$  downregulates the micro-RNA's expression (Kwiecinski et al., 2011). Additionally, HGF has been noted to suppress fibrogenesis via nuclear export of SMAD3, a TGF $\beta$  pathway component, via galectin-7 (Inagaki et al., 2008). Moreover, it has been reported in pulmonary fibrosis, that HGF induces the expression of SMAD7, a suppressor of the TGF $\beta$  signalling pathway and therefore downregulating the expression of the fibrosis-associated markers  $\alpha$ SMA, collagen 1 and fibronectin in rat alveolar epithelial cells (Shukla et al., 2009). Although HGF and TGF $\beta$  are evidently cross-talking, their antagonistic relationship has been highlighted to be context specific.

### 1.5.5 HGF/c-MET signalling in liver disease progression

It has been evidenced that LPC numbers directly and positively correlate to the stage of underlying chronic liver disease (Lowe et al., 1999). Though LPCs are generally thought to aid in liver regeneration in the early stages of liver injury by replacing lost tissue (Raven et al., 2017), in later stages of disease, they may then become targets of transformation and assume a cancer-stem cell-like phenotype (Knight et al., 2008) (Sancho-Bru et al., 2012). Conventionally, the HGF/c-MET axis is critical for liver development, morphogenesis and regeneration. Yet, when dysregulated, it leads to uncontrolled proliferation and invasion of resident liver cell types such as LPCs and HSCs (Goyal, Muzumdar, & Zhu, 2013). Elevated expression and mutations of HGF and c-MET have been reported in cancers such as lung, bladder and liver, and correlate with poor outcome (Goyal et al., 2013) (C.-T. Hu, Wu, Cheng, & Wu, 2017). The mechanisms involved in aberrant activation of the signalling pathway include abnormal paracrine or autocrine ligand production, overexpression of HGF and c-MET leading to genetic mutation and constitutive kinase activation downstream (Venepalli & Goff, 2013).

As compared to liver fibrosis, HGF tissue expression is reduced in HCC as compared to surrounding tissue (Kiss, Wang, Xie, & Thorgeirsson, 1997) (Goyal et al., 2013). However, plasma HGF levels are consistently higher in patients with HCC, demonstrating that HGF is not a reliable prognostic marker for disease state (Goyal et al., 2013). Conversely, c-MET expression is greatly increased in liver tumours, as compared to surrounding normal liver tissue (Suzuki et al., 1994), suggesting that c-MET has a tumour-promoting role in HCC (Goyal et al., 2013).

*In vitro* characterisation and manipulation models of HGF/c-MET have been documented. Xie and colleagues demonstrated that the HCC line MHCC97-H, known for enhanced scattering, proliferation and invasion, also had an increased expression of c-MET. To modulate the cell biology, they silenced c-

MET expression in the HCC line by RNA interference (RNAi) and noticed a decrease in cell motility and invasion (Xie et al., 2010).

Targeted HCC therapy has been aimed at the HGF/c-MET pathway. However, HCC is highly heterogeneous and while therapies are effective in some patients, others experience toxic side effects or present with drug resistance to established kinase-based c-MET targeting drugs. Since treatment options are limited in advanced HCC, prevention of disease progression from early to late-stage chronic liver disease is therefore desirable.

## 1.6 Project aims

Chronic liver injury leads to the activation and expansion of LPCs. Their pro-regenerative role in the early stages of disease has been reported, illustrating their function in replacing lost parenchymal tissue by differentiation into biliary epithelial cells or hepatocytes (Köhn-Gaone et al., 2016) (Raven et al., 2017). During early stages of disease, fibrosis-driving HSCs become activated, which have a key role in ECM production in the liver. However, if the injury stimulus persists, HSCs become over-activated, leading to extensive scarring of the liver (Tsuchida & Friedman, 2017).

LPCs and HSCs sit spatially proximal in the fibrotic niche, with few studies exploring the cells' interrelationship during disease. Given the largely unexplored co-regulation between LPCs and HSCs, this study hypothesises that LPCs have pro-regenerative roles by regulating HSC behaviour via the anti-fibrotic HGF/c-MET signalling pathway.

To explore this hypothesis, the first aim of this study was to characterise several models of fibrosis as a proof-of-principle for following chapters. Fibrosis stages of the CDE model in relation to the HGF/c-MET signalling pathway were examined. Thereafter, a transition to clonal cell lines BMOL-TAT (LPC) and LX-2 (HSC) was undertaken.

Following the characterisation of the HGF/c-MET signalling pathway in selected cell lines, the second aim of this study involved the CRISPR/Cas9-

mediated knockout of the c-MET receptor in the LPC line BMOL-TAT. Following deletion of the c-MET receptor, the BMOL-TAT cells were evaluated phenotypically, functionally, and fibrosis-associated markers were assessed.

As LPCs and HSCs are known to be spatially proximal during liver disease *in vivo*, the third aim of the study was to assess the cellular crosstalk between wildtype and c-MET knockout LPCs with HSCs in relation to the cells' arrangement, migration, HGF/c-MET signalling and fibrosis-related readouts.

Lastly, aim four was to undertake bulk RNA-sequencing analysis of LPCs and HSCs in direct co-culture or following conditioned medium experiments. Experimental set ups allowed to compare the communication between HSCs and BMOL-TAT<sup>c-MET<sup>WT</sup></sup> versus BMOL-TAT<sup>c-MET<sup>KO</sup></sup> cells to gain a deeper understanding of the cells' c-MET signalling-dependent cellular crosstalk.

**Chapter 2: Materials and Methods**

## **2.1 Materials**

### **2.1.1 General laboratory chemicals**

All chemicals were research grade and attained from commercial suppliers. Supplier information has been specified throughout Chapter 2, wherever required.

### **2.1.2 Water**

Milliq H<sub>2</sub>O was obtained in the laboratory from the Aquatec purification system (Aquatec, VIC, Australia) to prepare solutions and buffers for downstream experiments. Nuclease-free water (Bioline, NSW, Australia) was used for molecular techniques involving RNA extraction.

### **2.1.3 Solutions and buffers**

#### **2.1.3.1 Phosphate-buffered saline (PBS)**

Phosphate-buffered saline (1X PBS) was prepared using 137mM NaCl (Chem supply Australia SA, Australia), 2.7mM KCl (Chem supply Australia SA, Australia), 4.3mM Na<sub>2</sub>HPO<sub>4</sub> (Sigma-Aldrich, NSW, Australia), and 1.47mM KH<sub>2</sub>PO<sub>4</sub> (Chem supply Australia SA, Australia), adjusted to pH 7.4 and stored at room temperature. For cell culture, sterile PBS (Fisher Biotech, WA, Australia) was used.

#### **2.1.3.2 Methanol-acetone solution for fixation**

A solution of methanol (Sigma-Aldrich, NSW, Australia) and acetone (VWR, Qld, Australia) (ratio 1:1, v/v) was prepared and stored at -20°C.



#### **2.1.3.3 4% Paraformaldehyde (PFA) solution for fixation**

A PFA solution was prepared by dissolving 10 g of PFA (Sigma-Aldrich, NSW, Australia) in 250 ml PBS and heating at 60°C in a biological safety cabinet. The solution was then aliquoted and stored at -20°C.

#### **2.1.3.4 Triton X-100 solution for permeabilisation**

A 0.1% Triton X-100 (Sigma-Aldrich, NSW, Australia) solution was prepared in PBS and stored at room temperature.

#### **2.1.3.5 Coverslip etching solution**

A solution using Milliq H<sub>2</sub>O (11.3 ml), ethanol (17.1 ml) and 3 g NaOH (VWR, Qld, Australia) was prepared.

#### **2.1.3.6 MTT solution for MTT assay**

MTT solution was prepared by dissolving 3-[4, 5-dimethylthiazolyl-2]-2, 5-diphenyltetrazolium bromide (MTT; Sigma-Aldrich, NSW, Australia) in sterile PBS at a concentration of 5 mg/ml and stored at -20°C.

#### **2.1.3.7 Annexin V buffer for cell apoptosis assay**

A 10X Annexin V buffer was prepared by dissolving 0.1M HEPES, 1.4M NaCl and 25mM CaCl<sub>2</sub> in Milliq H<sub>2</sub>O. This was adjusted to pH 7.4 and filter-sterilised. The solution was diluted to 1X concentration before use.

### **2.1.3.8 Propidium iodide solution for cell apoptosis assay**

Propidium iodide 10X stock solution (Sigma-Aldrich, NSW, Australia) was prepared by dissolving the powder at a concentration of 1 mg/ml in 1X sterile PBS. Stock solution was diluted 1:10 in 1X PBS to achieve the working solution.

### **2.1.3.9 FACS buffer**

FACS buffer was prepared for flow cytometry by combining 1X sterile PBS with 5% FBS.

### **2.1.3.10 MES SDS running buffer solution for western blot**

NuPAGE™ MES SDS Running Buffer 20X (Thermo Fisher Scientific, WA, Australia) was diluted in Milliq H<sub>2</sub>O to a 1X concentration.

### **2.1.3.11 Tris/glycine transfer buffer solution for western blot**

A transfer buffer solution was prepared with 100 ml of 10X Tris/glycine buffer (Bio-Rad laboratories, NSW, Australia), 200 ml of methanol and 700 ml of Milliq H<sub>2</sub>O to create a 1X solution.

### **2.1.3.12 Tris-buffered saline with tween (TBST) solution for western blot**

A 10X solution of TBST was prepared by dissolving 24 g Tris (Sigma-Aldrich, NSW, Australia) and 88 g NaCl in 900 ml of Milliq H<sub>2</sub>O. The pH was then adjusted to 7.6 to a final volume of 1 L. A 1X working solution was then made by diluting 100 ml of 10X TBST in 900 ml of Milliq H<sub>2</sub>O and 1% of tween-20 (Sigma-Aldrich, NSW, Australia).

#### **2.1.3.13 Ponceau solution for western blot**

Ponceau solution was prepared by dissolving 0.1% Ponceau S (Thermo Fisher Scientific, WA, Australia) in 1% (v/v) acetic acid (Sigma-Aldrich, NSW, Australia).

#### **2.1.3.14 Blocking solution for western blot**

A 5% blocking solution was prepared by dissolving skim milk powder (Woolworths, WA, Australia) in 1X TBST solution.

#### **2.1.3.15 0.05% Crystal violet stain for cells**

A crystal violet stain was prepared by dissolving 1 g of crystal violet (Sigma-Aldrich, NSW, Australia) in 50 ml of ethanol (Sigma-Aldrich, NSW, Australia). The total volume was then adjusted to 1 L with Milliq H<sub>2</sub>O.

#### **2.1.3.16 Yeast Extract Tryptone (2YT) broth for bacterial culture**

A 2YT broth was prepared using 16 g/L Bacto Tryptone (Sigma-Aldrich, NSW, Australia), 10 g/L yeast extract (Thermo Fisher Scientific, WA, Australia) and 5 g/L NaCl in 1 L of Milliq H<sub>2</sub>O. The pH was adjusted to 7.0 using 5M NaOH and the broth was sterilised by autoclaving.

#### **2.1.3.17 LB-ampicillin agar for bacterial selection**

Agar solution was prepared by dissolving 15 g of Bacto agar (Thermo Fisher Scientific, WA, Australia) in 1 L of LB medium. This was then sterilised by autoclaving and 100 µg/ml ampicillin (Sigma-Aldrich, NSW, Australia) was added. LB-ampicillin plates were then poured.

### **2.1.3.18 Trypsin-ethylenediaminetetraacetic acid (EDTA) solution for cell culture**

A 10X Trypsin-EDTA solution (Sigma-Aldrich, NSW, Australia) was diluted to 0.05% using sterile PBS, aliquoted to 50 ml aliquots and stored at -20°C. Once thawed, aliquots were stored at 4°C and used within a month.

### **2.1.3.19 Williams' E maintenance medium for BMOL-TAT cell culture**

Williams' E medium (Life Technologies, VIC, Australia) supplemented with 2.5 µg/ml fungizone (Life Technologies, VIC, Australia), 48.4 ng/ml penicillin (Life Technologies, VIC, Australia), 675 ng/ml streptomycin (Life Technologies, VIC, Australia), 292.3 ng/ml glutamine (Sigma-Aldrich, NSW, Australia), 15 ng/ml insulin-like growth factor (IGF)-II (GroPep, SA, Australia), 10 ng/ml EGF (BD Biosciences, CA, USA), 5 µg/ml insulin (Humulin; Eli Lilly, IN, USA) and 2% fetal bovine serum (FBS) (Serana, Pessin, Germany) was used as maintenance medium for BMOL-TAT cells. The FBS concentration was 5% for only one passage after thawing and 2% thereafter for routine cell culture.

### **2.1.3.20 DMEM high glucose maintenance medium for LX-2 and SNU-449 cell culture**

DMEM high glucose (Life Technologies, VIC, Australia) supplemented with 2.5 µg/ml fungizone (Life Technologies, VIC, Australia), 48.4 ng/ml penicillin (Life Technologies, VIC, Australia), 675 ng/ml streptomycin (Life Technologies, VIC, Australia), and 10% fetal bovine serum (FBS) (Serana, Pessin, Germany) was used as maintenance medium for LX-2 and SNU-449 cells.

### **2.1.3.21 DMEM high glucose medium for co-culture**

DMEM high glucose (Life Technologies, VIC, Australia) supplemented with 2.5 µg/ml fungizone (Life Technologies, VIC, Australia), 48.4 ng/ml penicillin (Life Technologies, VIC, Australia), 675 ng/ml streptomycin (Life Technologies, VIC, Australia), and 5% fetal bovine serum (FBS) (Serana, Pessin, Germany) was used as medium for LX-2 co-culture with either BMOL-TAT or SNU-449 cells.

### **2.1.3.22 LX-2-conditioned medium**

LX-2-conditioned medium was prepared by growing LX-2 cells in DMEM high glucose maintenance medium until approximately 80% confluency was reached. Cell culture medium was aspirated and centrifuged at 300 G for 5 minutes to remove dead cells and debris. Conditioned medium was stored at -20°C until use.

### 2.1.4 Antibodies

Primary and secondary antibodies used in experiments along with their experimental conditions are listed. All antibodies were diluted in antibody diluent (Dako, NSW, Australia) before use.

Antibody	Host	Reactivity	Dilution	Clone	Fixation	Supplier
<b>A6</b>	rat	mouse	1:200 IF		Meth/Ace	Gift from Dr Valentina Factor, National Cancer Institute, Bethesda, MD, USA
<b>CK19</b>	rat	mouse	1:150 IF	AB_213 3570	Meth/Ace	TROMA-III, Developmental Studies Hybridoma Bank, IA, USA
<b>PanCK</b>	rabbit	mouse	1:200 IF	Z0622	Meth/Ace	Dako, NSW, Australia
<b>CD133</b>	rat	mouse	1:200 IF	13A4	Meth/Ace	e-Bioscience, CA, USA
<b>EpCAM</b>	rabbit	mouse	1:200 IF		Meth/Ace	Abcam, VIC, Australia
<b>EpCAM</b>	rat	mouse	1:200 Flow	Ber-EP4	-	BD Biosciences, CA, USA
<b><math>\alpha</math>SMA</b>	mouse	mouse, human	1:2000 IF 1:2000 WB	M0851	Meth/Ace	Sigma-Aldrich NSW, Australia
<b>Desmin</b>	rat	human	1:200 IF	ab3236 2	Meth/Ace	Abcam, VIC, Australia
<b>GFAP</b>	rat	human	1:500 IF	13-0300	Meth/Ace	Thermo Fisher Scientific, WA, Australia
<b>Vimentin</b>	rabbit	human	1:100 IF	D21H3	Meth/Ace	Cell Signaling Technology, MA, USA
<b>Collagen 1</b>	rabbit	human	1:500 IF, WB		Meth/Ace	Sigma-Aldrich NSW, Australia
<b>TGF<math>\beta</math>1</b>	rabbit	mouse, human	1:100 IF 1:1000 WB	EPR211 43	Meth/Ace	Abcam, VIC, Australia
<b>TGF<math>\beta</math>R1</b>	rabbit	mouse, human	1:500 IF, WB	EPR209 23-13	Meth/Ace	Abcam, VIC, Australia
<b>SMAD2/3</b>	goat	mouse, human	1:200 IF, WB		Meth/Ace	Life Technologies, VIC, Australia
<b>p-SMAD2</b>	rabbit	mouse, human, rat	1:100 IF	138D4	Meth/Ace	Cell Signaling Technology, MA, USA

<b>t-SMAD2</b>	mouse	mouse, human, rat, monkey	1:100 IF	L16D3	Meth/Ace	Cell Signaling Technology, MA, USA
<b>HGF</b>	rabbit	human	1:100 IF 1:1000 WB	EPR122 30	Meth/Ace	Abcam, VIC, Australia
<b>c-MET</b>	mouse	mouse	1:100 IF 1:1000 WB	3D4	Meth/Ace	Life Technologies, VIC, Australia
<b>p-c-MET</b>	rabbit	mouse	1:100 IF 1:1000 WB	D26	Meth/Ace	Cell Signaling Technology, MA, USA
<b>E-cadherin</b>	rabbit	mouse, human	1:200 IF	24E10	Meth/Ace	Cell Signaling Technology, MA, USA
<b>N- cadherin</b>	mouse	mouse, human, rat	1:200	ab7605 7	Meth/Ace	Abcam, VIC, Australia
<b>Annexin V</b>	-	-	1:100 647 conjugate Flow		-	Thermo Fisher Scientific, WA, Australia
<b>DAPI</b>	-	-	1:100 IF		Meth/Ace	Thermo Fisher Scientific, WA, Australia
<b>Hoechst</b>	-	-	1:1000 IF		4% PFA	Thermo Fisher Scientific, WA, Australia
<b>Phalloidin</b>	-	-	1:1000 647 conjugate IF		4% PFA	Thermo Fisher Scientific, WA, Australia

**Table 2.1: List of primary antibodies.**

IF, immunofluorescence; WB, western blotting; Meth/Ace, methanol/acetone.

<b>Epitope</b>	<b>Host</b>	<b>Reactivity</b>	<b>Dilution</b>	<b>Conjugate</b>	<b>Supplier</b>
IgG	goat	rabbit	1:500	Alexa Fluor 488	Life Technologies, VIC, Australia
IgG	goat	rabbit	1:500	Alexa Fluor 594	Life Technologies, VIC, Australia
IgG	goat	rat	1:500	Alexa Fluor 488	Life Technologies, VIC, Australia
IgG	goat	rat	1:500	Alexa Fluor 594	Life Technologies, VIC, Australia
IgG	goat	mouse	1:500	Alexa Fluor 488	Life Technologies, VIC, Australia
IgG	goat	mouse	1:500	Alexa Fluor 594	Life Technologies, VIC, Australia
IgG	rabbit	goat	1:500	Alexa Fluor 594	Life Technologies, VIC, Australia
IgG	goat	rabbit	1:2000	HRP-linked	Cell Signaling Technology, MA, USA
IgG	goat	mouse	1:2000	HRP-linked	Cell Signaling Technology, MA, USA
IgG	donkey	goat	1:2000	HRP-linked	Cell Signaling Technology, MA, USA

**Table 2.2: List of secondary antibodies.**

HRP, horseradish peroxidase.



## **2.2 Methods**

### **2.2.1 CRISPR-facilitated gene editing**

#### **2.2.1.1 Vector preparation**

Stefan Stricker from the Helmholtz Institute Munich provided plasmid #B, which was modified for our own gRNA guide production (Figure 2.1A).

A quantity of 40  $\mu\text{l}$  of #B plasmid was digested using BamHI and HindIII for 1.5 hours, and then heat-inactivated at 95°C for 3 minutes. The product was run on a 0.8% agarose electrophoresis gel for approximately 40 minutes at 130V. The top band (~760 bp) of the 4069 bp product was cut and purified in a gel purification column following the manufacturer's instructions (Qiagen, VIC, Australia) and utilised for downstream CRISPR experiments. The product was eluted to a total of 120  $\mu\text{l}$  and approximately 100 ng/ $\mu\text{l}$  of linearised plasmid was achieved.

#### **2.2.1.2 gRNA guide preparation**

The gRNA cassettes (#B7 and #B8) were resuspended to a final concentration of 10 ng/ $\mu\text{l}$ . For each guide, 100 ng was digested with BamHI and HindIII for 30 minutes. The products were then purified by PCR clean up, following the manufacturer's instructions (Qiagen, VIC, Australia). Finally, gRNA guides were eluted to a concentration of approximately 15 ng/ $\mu\text{l}$ .

#### **2.2.1.3 Vector and insert ligation**

Ligation reactions were completed at a vector:insert molar ratio of approximately 1:4. This was completed with 50 ng vector (#B), 1.5  $\mu\text{l}$  of inserts (#B7, #B8) and 0.5  $\mu\text{l}$  of T4 ligase overnight at 16°C.

#### **2.2.1.4 Transformation**

For transformation, 2  $\mu$ l of ligation products were transformed in 20  $\mu$ l of NEB competent cells (New England Biolabs, MA, USA). Cells were left to recover for 1 hour at 37°C in 400  $\mu$ l SOC medium (Thermo Fisher, WA, Australia). Then, 150  $\mu$ l of cell suspension was plated on LB Ampicillin plates.

#### **2.2.1.5 Colony selection and miniprep**

All LB ampicillin plates resulted in approximately 30 colonies. One colony from each plate of either gRNA guide #B7 or #B8 was picked and cultured in 2YT medium overnight at 37°C. The resulting turbid solution was used to elute plasmid DNA using the plasmid DNA miniprep kit according to the manufacturer's instructions (New England Biolabs, MA, USA).

#### **2.2.1.6 Confirmation of insert integration**

All resulting plasmids were verified to have correct insertions. This was confirmed by digesting the insert out of the vector using BamHI and HindIII. The digested vector had an excised fragment size of 760 bp and #B7 and #B8 had fragment sizes of 392 bp, as expected (Figure 2.1B), confirming that the inserts and plasmids were correctly ligated. Additionally, these gRNA guides were sent to Genomics WA for validation of correct ligation (Figure 2.1C).

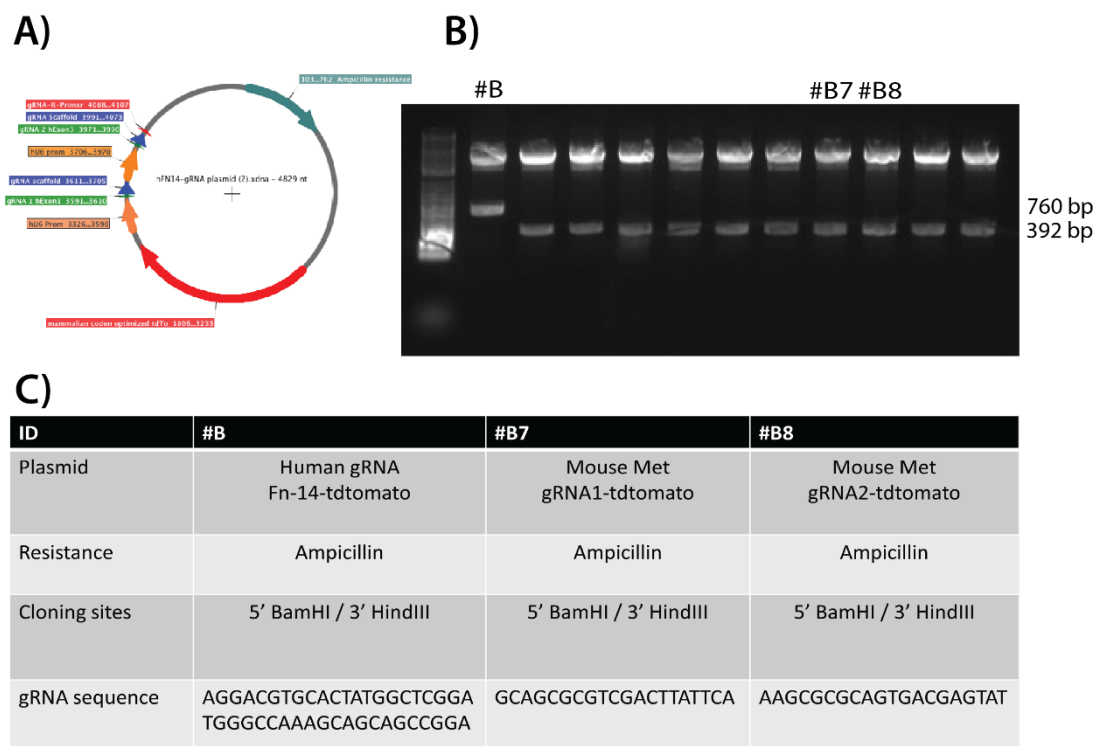


**Figure 2.1: Production of gRNA guides.**

A) Plasmid #B provided by Helmholtz Institute Munich. B) Plasmids digested to correct size: #B, 760 bp; #B7, 392 bp; #B8, 392 bp. C) Table of plasmids #B, #B7 and #B8 and their corresponding characteristics.

## 2.2.2 Cell culture techniques

### 2.2.2.1 Bipotential murine oval liver tyrosine aminotransferase (BMOL-TAT) cell line

The clonal ‘bipotential murine oval liver - tyrosine aminotransferase’ (BMOL-TAT) cell line represents liver progenitor cells with a tyrosine amino transferase (TAT) glucocorticoid response element (GRE) lacZ reporter gene. It was characterised and supplied by my supervisor, Nina Tirnitz-Parker (J. E. E. Tirnitz-Parker et al., 2007).

#### **2.2.2.2 LX-2 hepatic stellate cell line**

The clonal hepatic stellate cell line LX-2 was purchased from Sigma-Aldrich, NSW, Australia.

#### **2.2.2.3 SNU-449 hepatocellular carcinoma cell line**

The clonal hepatocellular carcinoma cell line SNU-449 was obtained from ATCC, Manassas, VA, USA.

#### **2.2.2.4 Thawing of cell lines**

Cryovials were removed from liquid nitrogen storage and placed in a 37°C water bath. When vials were approximately 80% thawed, the cell suspension was transferred to a T25 flask (Thermo Scientific, VIC, Australia) containing 4 ml of growth medium (2.1.3.19, 2.1.3.20). Cell cultures were maintained at 37°C, 5% CO<sub>2</sub> and 90% humidity in an IR Direct Heat CO<sub>2</sub> incubator (In Vitro Technologies, VIC, Australia). When cells had attached (approximately after 4 hours), the DMSO-containing cell culture medium was replaced with fresh growth medium.

#### **2.2.2.5 Cell line maintenance and subculturing**

Cell lines were cultured at 37°C in a 5% CO<sub>2</sub> humidified atmosphere. The cell culture medium was changed every second day (2.1.3.19, 2.1.3.20). When cells had reached confluency, they were sub-cultured by removing the medium and washing them twice with sterile PBS. Cells were then dissociated with 1 ml of 0.05% Trypsin-EDTA solution and incubated at 37°C for 3 minutes, or until dislodged. Thereafter, 2 ml growth medium of the respective cell line was added to halt the dissociation. The solution was then collected into a 15 ml tube and centrifuged at 500 G for 5 minutes. The pellet was resuspended in 1 ml of growth medium, from which an appropriate volume was taken to seed each flask or well as required.

### **2.2.2.6 Cryopreservation of cell lines**

Cells were routinely passaged as described above (2.2.2.5). After cell pellet production, cells were resuspended in freezing medium containing 40% growth medium (2.1.3.19, 2.1.3.20), 50% FBS and 10% DMSO. The cell solution was then distributed into cryovials to a volume of 1 ml and placed in a Mr. Frosty™ Freezing Container (Thermo Fisher Scientific, WA, Australia) and moved to a -80°C freezer to regulate the rate of freezing to 1°C per minute. After overnight incubation at -80°C, the cryovials were placed in liquid nitrogen for long-term storage.

### **2.2.2.7 Cell transfection and sorting**

The BMOL-TAT cells were sub-cultured as previously described and seeded in a 6-well plate at a density of  $1.5 \times 10^5$  cells/well. Cells were left to attach overnight at 37°C and 5% CO<sub>2</sub>. The following day, 800 ng of previously prepared CRISPR guides (#B7 and #B8, positive for tdtomato) and a Cas9 plasmid (#A; positive for GFP) were transfected into BMOL-TAT cells using Lipofectamine 3000, diluted in Opti-MEM, according to the manufacturer's instructions (Thermo Fisher Scientific WA, Australia). The transfection efficiency was evaluated 48 hours after transfection.

Cell sorting was then completed on the BD FACS Jazz cell sorter (BD Biosciences, WA, Australia). Cells were trypsinised and sorted based on their cell marker fluorescence. Positive cells (GFP<sup>+</sup> and tdtomato<sup>+</sup>) were collected in a 1.5 ml microcentrifuge tube, along with the negatively transfected population (GFP<sup>-</sup> and tdtomato<sup>-</sup>), which was used as a control. The cells were then plated in a 24-well plate for a post-sorting 24-hour recovery period before single cell manual sorting was performed.

### **2.2.2.8 CRISPR cell knockout expansion**

Following the post-sorting recovery period, cells were trypsinised, counted and manually single cell-sorted into 96-well plates. The cell culture medium was

replaced every three days and after approximately 14 days, wells were screened for single cell colonies. When colonies had taken up 75% of the well, they were transferred to a 24-well plate, and slowly expanded to a T-75 flask, before being cryopreserved. Protein was also extracted for knockout confirmation experiments by western blot (2.2.4.3).

#### **2.2.2.9 MTT assay**

The MTT colorimetric assay is centred on the ability of cellular oxidoreductase enzymes to convert the tetrazolium dye MTT (Sigma-Aldrich, NSW, Australia) to insoluble, purple formazan.

At the start of the experiment, cells were plated at 2,000 cells/well in a 96-well plate (Thermo Fisher Scientific, WA, Australia) for 24, 48 and 72 hours.

At each time point, the respective cells were incubated with 10  $\mu$ l of MTT solution for 4 hours at 37°C and 5% CO<sub>2</sub> to dissolve the resultant formazan crystals. Following incubation, 100  $\mu$ l of DMSO was added for 30 minutes, at room temperature, in the dark and the absorbance was measured at 590 nm using a plate reader (EnSight Multimode Plate Reader, PerkinElmer, VIC, Australia).

#### **2.2.2.10 MTS assay**

The CellTiter 96® AQueous one solution cell proliferation assay (Promega, WI, USA) is a colorimetric method that was used to determine cell proliferation. The reagent contains a novel tetrazolium compound (MTS) that is bio-reduced by cells to a coloured formazan product, which is then solubilised in tissue culture medium.

At the start of the experiment, cells were plated at 2,000 cells/well in a 96-well plate for 24, 48 and 72 hours. At the end of each time point, the respective cells were incubated with 20  $\mu$ l of MTS solution for 2 hours at 37°C and 5% CO<sub>2</sub> for soluble formazan to be produced by cellular reduction of MTS. Following incubation, the absorbance was immediately measured at 490 nm using a plate reader (EnSight Multimode Plate Reader, PerkinElmer, VIC, Australia).

### **2.2.2.11 Cell adherence assay**

A cell adherence assay was performed to compare the adhesive capacity between BMOL-TAT wildtype and c-MET knockout cell lines. Cell lines were plated in a 96-well plate at a density of  $3 \times 10^4$  cells/well and left to incubate at 37°C and 5% CO<sub>2</sub> for 24 hours. Following incubation, cells were then washed twice with sterile PBS and incubated with 200 µl of 0.05% trypsin-EDTA from 0-7.5 minutes. Non-adherent cells were washed off with sterile PBS and the remaining adherent cells were fixed with 100 µl ice cold methanol for five minutes. The methanol was then aspirated and 50 µl of 0.05% crystal violet solution was added for 10 minutes. Crystal violet solution was then aspirated, and wells were washed with Milliq H<sub>2</sub>O until the solution ran clear, and then air-dried. The dye taken up by the cells was then solubilised with the addition of 1% SDS on a shaker for 15 minutes. Following incubation, the absorbance was measured at 595 nm using a plate reader (EnSight Multimode Plate Reader, PerkinElmer, VIC, Australia).

### **2.2.2.12 Wound healing assay**

A wound healing assay assesses the migratory capacity of a given cell type. BMOL-TAT wildtype and c-MET knockout cell lines were seeded into separate Ibidi 35 mm culture 2-well inserts (Ibidi, Grafelfing, Germany) at a density of  $7 \times 10^4$  cells/well in a 24-well plate and left to attach overnight at 37°C and 5% CO<sub>2</sub>. The following day, the inserts were carefully removed with sterile forceps, leaving a 500 µm cell-free gap. The wells were washed with sterile PBS and 1 ml of growth medium was added to the wells. The cells were then placed on the Nikon A1+ confocal microscope and live cell imaging was performed for 48 hours. Following imaging, analysis of digital images was achieved using Software Guide ZEN 2.1 (blue edition).

### 2.2.2.13 OPERETTA cell morphology analysis

The Operetta CLS™ High-Content Analysis System was used to assess potential morphological differences between cell types. BMOL-TAT wildtype and c-MET knockout cell lines were seeded in a 96-well plate at a density of 3,000 cells/well and incubated overnight at 37°C and 5% CO<sub>2</sub>. The cells were then fixed with 4% PFA for 10 minutes, washed with 1X PBS twice and stained with the nuclear dye Hoechst 33342 and the cytoskeletal dye Phalloidin, according to the concentration in Table 2.1. Following staining, the 96-well plate was imaged by the Operetta CLS™ High-Content Analysis System at a 10x magnification and analysed using a pre-determined Harmony 4.9 software pipeline named 'calculate morphology properties' to assess cell number, cell length (µm), cell width (µm), cell area (µm), roundness and cell width/length ratio.

### 2.2.2.14 Bioprinting

The Rastrum 3D bioprinter (Inventia, NSW, Australia) uses digital printing technology to resuspend cells in a 3D matrix with polyethylene glycol (PEG) bioink formulations that mimic the mechanical and biochemical properties of the relevant *in vivo* tissue (RGD, ~0.7 kPa). The 3D cultures created by RASTRUM used two components: bioink and activator. Prior to cell preparation, the bioink formulation was printed in a 96-well plate to form the inert base. Cells were then sub-cultured as previously described (2.2.2.5), and cell pellets were resuspended in the activator solution to form an instant gel. This instant gel solution was then loaded into the bioprinter and each cell/matrix formulation was printed at approximately 700 cells/well. Upon completion of the print run, 150 µl of culture medium (2.1.3.19, 2.1.3.20) was added to each well. The 3D cell model then allows for imaging and harvesting of cells for downstream analyses (Figure 2.2).



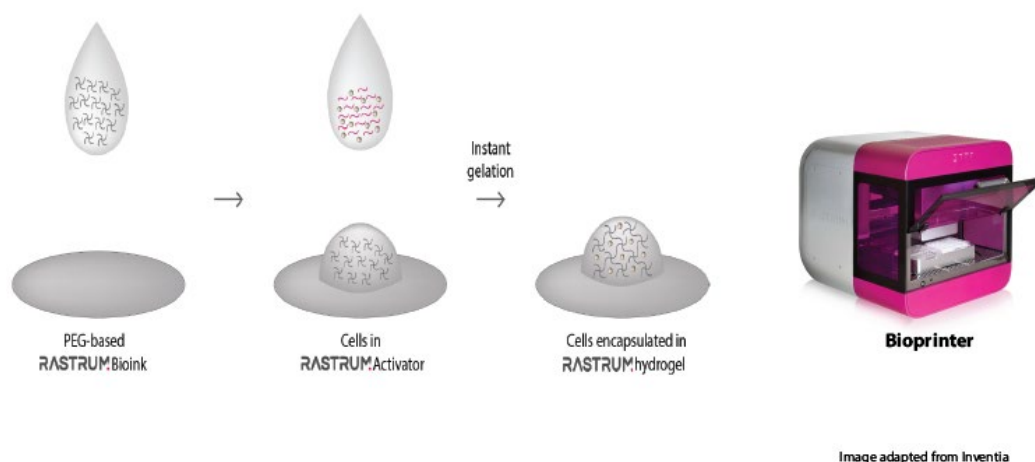


**Figure 2.2: 3-dimensional cell model illustration of the RASTRUM Bioprinter.**

Illustration of 3D bioprinting.

#### 2.2.2.15 Direct co-culture

LX-2, BMOL-TAT wildtype and c-MET knockout cells were sub-cultured as normal (2.2.2.5) and resuspended in co-culture medium (2.1.3.21). BMOL-TAT wildtype and BMOL-TAT c-MET knockout cells were plated in a 6-well plate at 250,000 cells/well for single culture, and 125,000 cells/well for co-culture wells. Cells were allowed to attach for four hours at 37°C with 5% CO<sub>2</sub>, and LX-2 cells were then plated at 250,000 cells/well for single culture and 125,000 cells/well in the co-culture wells. The cells were then incubated at 37°C with 5% CO<sub>2</sub> for 48 hours and cells were collected for downstream processing.

#### 2.2.2.16 Apoptosis assay

Annexin V, which stains positive in apoptotic cells, and PI, which stains positive in necrotic cells, was used to assess cell apoptosis the BMOL-TAT sister cell lines in single culture and following direct co-culture with LX-2 cells. BMOL-TAT wildtype and c-MET knockout cells were cultured in 6-well plates until they

reached 90% confluency for single culture experimentation. For co-culture analysis, LX-2, BMOL-TAT wildtype or c-MET knockout cells were cultured in direct co-culture as described above (2.2.2.14). Cells were then re-suspended in 100  $\mu$ l of FACS buffer with 1:200 dilution of epithelial cell adhesion molecule (EpCAM) to label LPCs and incubated for 30 minutes in the dark. Cells were then washed twice with FACS buffer. Next, 1X Annexin V buffer was used to dilute PI to a working concentration of 100  $\mu$ g/ml. Then, 5  $\mu$ l of Annexin V and 1  $\mu$ l of PI was added and samples were incubated in the dark for 15 minutes. Finally, 400  $\mu$ l of 1X Annexin V buffer was added and samples were run on the BD LSRFortessa™ X-20 cell analyzer. Results were analysed using the FlowJo™ Software.

#### **2.2.2.17 Conditioned medium culture**

Wildtype and c-MET knockout BMOL-TAT cells were seeded in 6-well plates at a concentration of 200,000 cells/well and incubated at 37°C with 5% CO<sub>2</sub> for 24 hours. Next, LX-2-conditioned medium (2.1.3.22) was added to cells and incubated at 37°C with 5% CO<sub>2</sub> for either 30 minutes or 6 hours, prior to downstream analyses.

#### **2.2.2.18 Indirect co-culture assay - Boyden chamber**

Wildtype and c-MET knockout BMOL-TAT cells and SNU-449 cells were sub-cultured as normal (2.2.2.5) and resuspended in co-culture medium (2.1.3.21). The cells were then seeded in transwell inserts with a 0.4  $\mu$ m pore size (Corning, NY, USA), at a density of 100,000 cells/cm<sup>2</sup>. Inserts were then placed in a 12-well plate (Thermo Fisher Scientific, WA, Australia) and incubated for 24 hours at 37°C with 5% CO<sub>2</sub> to allow the cells to adapt to the new medium and adhere to the porous polycarbonate membrane surface. Simultaneously, LX-2 cells were seeded in replicate wells of a separate sterile 12-well plate in co-culture medium at a density of 100,000 cells/cm<sup>2</sup>. The LX-2 cells were also incubated at 37°C with 5% CO<sub>2</sub> for 24 hours. Following 24 hours, all media were carefully replaced from the inserts (1.5 ml) and the

wells (0.5 ml). The inserts were transferred with sterilised forceps to an HSC-adhered well to generate the Boyden chamber co-culture system (Figure 2.3A). After 48 hours of incubation, the transwell inserts were then carefully removed and analysed independently for downstream processing.

### 2.2.2.19 Indirect co-culture assay for migration - Boyden chamber

The BMOL-TAT wildtype, c-MET knockout cells and LX-2 cells were sub-cultured as normal (2.2.2.5) and resuspended in co-culture medium with 1% FBS. The cells were then seeded in transwell inserts with a 0.8  $\mu\text{m}$  pore size (Sigma-Aldrich, NSW, Australia), or 12-well plate at a density of 100,000 cells. Inserts were then placed in the wells of the 12-well plate with sterile forceps and incubated for 4 hours at 37°C with 5% CO<sub>2</sub>. This incubation allows the cell type in the insert to migrate through the polycarbonate membrane and get caught if chemoattracted to the cell type in the well beneath (Figure 2.3B). Following the 4-hour incubation, all media were carefully aspirated, inserts and wells were washed with sterile PBS and 0.5 ml of 0.05% crystal violet solution was added to the inserts for 10 minutes and at room temperature. Inserts were then thoroughly washed with sterile PBS until clear and air-dried for 30 minutes. Images of five non-overlapping fields of view were taken on the Olympus BX51 microscope and the Olympus camera DP70 (Olympus, VIC, Australia). Percentage of cell area was then calculated using ImageJ software (NIH).

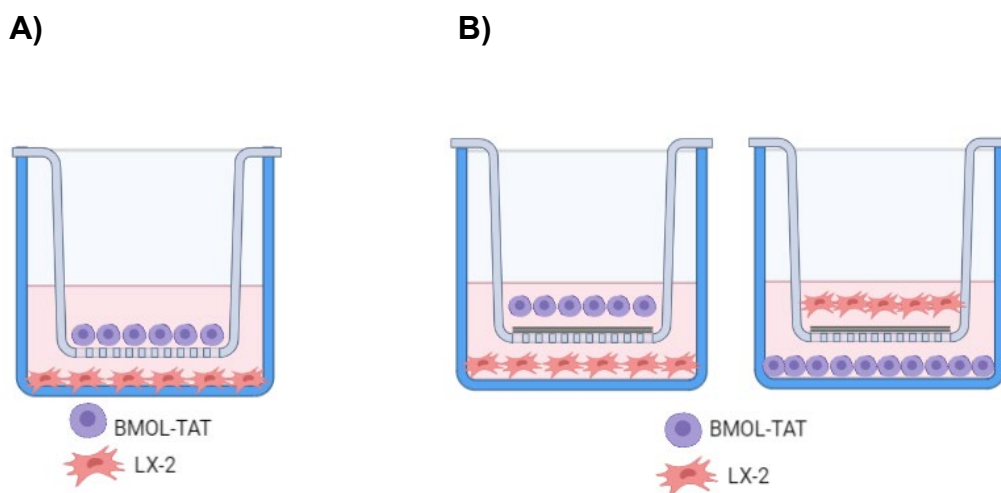


**Figure 2.3: Schematic diagram of Boyden chamber co-culture system.**

- A) Indirect co-culture with BMOL-TAT cells in insert and LX-2 cells beneath.  
B) Migration assay co-culture with BMOL-TAT cells in insert, LX-2 cells beneath and *vice versa*.

**2.2.2.20 Collagen assay**

This assay allows rapid and simple quantification of human pro-collagen 1 in cell supernatants through Fluorescence Resonance Energy Transfer (FRET) from Europium cryptate (donor), to d2 (acceptor) antibodies. The human LX-2 cell line was either cultured alone or in Boyden chamber co-culture with either BMOL-TAT wildtype and BMOL-TAT c-MET knockout cell lines for 48 hours. Collagen levels were then determined by adding 12  $\mu$ l of resulting supernatant to 1.5  $\mu$ l of donor and acceptor antibodies in a 384-well plate. In addition, wells with collagen standard of known concentrations were plated. This plate was then incubated at room temperature for three hours. An EnSpire® Multimode Plate Reader (Perkin-Elmer Life Sciences, Australia) was used to determine the fluorescence of all wells at 620 nm and 665 nm. A 665/620 ratio between readings was then created to fit a standard curve with the 4 Parameter Logistic (4PL) model.

**2.2.2.21 Cytospin preparation**

Cells were resuspended in their usual growth medium (2.1.3.19, 2.1.3.20) at a volume of  $0.25 \times 10^6$  cells/ml. Next, 200  $\mu$ l of single cell suspension was loaded into the chamber of a cytospin cartridge, with a glass slide attached, and loaded into the Cytospin™ 4 cytocentrifuge (Thermo Fisher Scientific, WA, Australia). Cells were centrifuged at 300 G for 5 minutes to adhere to the glass slides and were then fixed as per the antibody requirements for 5 minutes and processed for downstream immunofluorescence experiments (2.2.3.4).

### **2.2.2.22 Etched coverslips**

Glass coverslips were etched by immersion in the chemical mixture with occasional gentle agitation for 30 minutes followed by thorough washing in Milliq H<sub>2</sub>O. After air-drying and sterilisation by UV irradiation for at least 30 minutes, coverslips were stored in a sterile dry container until use. For experimentation, sterile coverslips were placed into a 24-well plate (Thermo Fisher, WA, Australia) with sterile forceps prior to seeding of a single suspension of cells at a density of  $2 \times 10^4$  cells/well. Cells were allowed to adhere to the glass overnight before extracting the coverslips, fixing for five minutes and processing for downstream experiments.

## **2.2.3 Histology techniques**

### **2.2.3.1 Sample processing**

Archival 3-month mouse liver sections were previously embedded in optimal cutting temperature (OCT, Sakura Finetek, South Holland, Netherlands) and 7  $\mu$ m sections were cut and transferred to Superfrost®Plus slides using a Leica CM1520 cryostat microtome (Leica). Sides were stored at -80°C.

### **2.2.3.2 PFA fixation**

Frozen tissue sections were air-dried for 1 hour before being incubated in 4% PFA solution for 10 minutes. Sections were then washed in PBS for 5 minutes. Next, the sections were permeabilised by incubation in 0.1% Triton X-100 solution for 10 minutes and again washed in PBS for 5 minutes.

### **2.2.3.3 Acetone-methanol fixation**

Frozen tissue sections were immediately placed in ice-cold methanol-acetone solution for 5 minutes. The slides were then air-dried for 1 hour at room

temperature. Afterwards, the sections were rehydrated in PBS for 10 minutes prior to further experimentation.

#### **2.2.3.4 Immunofluorescence analysis of tissue and cells**

Fixed cells were washed with sterile PBS and blocked with serum-free protein blocking solution (Dako, NSW, Australia) for 20 minutes at room temperature to block non-specific binding. They were then incubated with primary antibodies (Table 2.1) diluted in antibody diluent (Dako, NSW, Australia) for 1 hour at room temperature. The cells were washed three times with PBS before proceeding further with secondary antibody incubation in the dark for 1 hour. Following this, the cells were washed in PBS three times and mounted with ProLong Gold antifade reagent with DAPI (Life Technologies, VIC, Australia). Fluorescent images were taken using the Olympus BX51 microscope and the Olympus camera DP70 (Olympus, VIC, Australia).

#### **2.2.4 Molecular biology techniques**

##### **2.2.4.1 Protein extraction**

Protein lysate was extracted from BMOL-TAT wildtype, BMOL-TAT c-MET knockout, SNU-449 cells and LX-2 cell lines at 90% confluency. Cells were washed with sterile PBS before incubation in Radio Immunoprecipitation Assay (RIPA) lysis buffer (Sigma-Aldrich, NSW, Australia), with the addition of protease and phosphatase inhibitor cocktail (Cell Signaling Technology, MA, USA). Following this, adherent cells were lifted using a cell scraper before homogenising with a sonicator (Bioruptor Plus, diagenode, VIC, Australia). Finally, homogenised cells were centrifuged at 14,000 G for 10 minutes. The supernatant containing the final protein product was collected and transferred to a new 1.5 ml microcentrifuge tube. Extracted proteins were stored at -80°C, until further use.

#### **2.2.4.2 Protein concentration assay**

The concentration of protein, extracted from cells was determined using the Pierce bicinchoninic acid (BCA) protein assay kit (Thermo Fisher Scientific, WA, Australia). For this colorimetric assay, diluted albumin standards and working reagent were prepared by serial dilution in MilliQ H<sub>2</sub>O. Further, 10 µl of standards and samples were pipetted into a 96-well plate and the absorbance was measured at 562 nm using a plate reader (EnSight Multimode Plate Reader, PerkinElmer, VIC, Australia). Absorbance measurements of standards were then used to interpolate the protein concentration for each sample.

#### **2.2.4.3 Western blot**

Samples were prepared after BCA protein quantification to ensure equal protein concentrations of 20 µg. In addition, 4X Laemmli sample buffer (Bio-Rad Laboratories, NSW, Australia) was added, and samples were denatured for 5 minutes at 95°C. Samples were loaded along with a Precision Plus Protein Standards ladder (Bio-Rad Laboratories, NSW, Australia) and separated using Bolt 4-12% Bis-Tris Plus precast gels (Thermo Fisher, WA, Australia) at 200V for 30 minutes. Gels were transferred onto a 0.2 µm nitrocellulose membrane (Bio-Rad Laboratories, NSW, Australia) for 1 hour at 100V. Protein transfer was checked using REVERT Total Protein Stain (LICOR, NE, USA). REVERT Total Protein Stain gel image can also be used as a loading control for analysis, according to the manufacturer's instructions. Membranes were blocked with 5% skim milk powder in 1X TBST for 1 hour at room temperature. Membranes were then incubated with primary antibodies (Table 2.1) overnight at 4°C. The next day, blots were incubated with appropriate HRP-labelled secondary antibodies (Table 2.2) and the signal was detected using the enhanced chemiluminescence (ECL) kit (Bio-Rad Laboratories, NSW, Australia) and ChemiDoc MP imaging system (Bio-Rad Laboratories, NSW, Australia). Western blot semi-quantification was performed using the Biorad ImageLab software and protein expression was normalised to REVERT total protein stain.

#### **2.2.4.4 RNA extraction**

Total RNA was extracted from at least  $3 \times 10^5$  cultured cells using the Isolate II RNA mini kit (Bioline, NSW, Australia), according to the manufacturer's instructions. Eluted RNA was dissolved in UltraPure DNase/RNase-free water (Bioline, NSW, Australia) and stored at  $-80^\circ\text{C}$  for future use. The RNA concentration and purity were determined using the NanoDrop 1000 spectrophotometer (Thermo Scientific, VIC, Australia). RNA purity was assessed through A260/230 and A260/280 ratios. RNA samples with values greater than 1.7 for A260/230 and greater than 1.8 for A260/280 were deemed of sufficient quality for further analysis.

#### **2.2.5 RNA sequencing**

Four biological samples of BMOL-TAT and LX-2 treatment groups were analysed at 90% confluency and RNA sequencing was performed by Azenta Life Sciences. Firstly, RNA integrity was assessed by Agilent 2100 Bioanalyzer and every sample had an RNA Integrity Number (RIN)  $>7$ . Next, poly A and non-strand specific libraries were constructed and high-throughput sequencing using Illumina NovaSeq PE150 to sequence 20M pair reads platform was performed. FASTQ sequencing data were generated and bioinformatically analysed by Azenta Life Sciences. Reads were aligned to either the human or murine genome using Hisat2 (v2.0.1). Differential expression analysis was performed using the Bioconductor package DESeq2 (V1.6.3). Genes with a differential expression higher than 2-fold change and a false discovery rate (FDR)  $<0.05$  were considered as differentially expressed genes (DEGs). Gene ontology analysis was completed using GOSeq, which accounts for gene length bias and read count bias when performing GO analysis. Lastly, KEGG pathway analysis was completed using the Kyoto Encyclopedia of Genes and Genomes (KEGG) database to identify pathways of differentially expressed genes that are significantly enriched against the transcriptome background.



**Chapter 3: Characterisation of liver progenitor cells and  
hepatic stellate cells in relation to the HGF/c-MET pathway  
in appropriate models of fibrosis**

### 3.1 Introduction

Chronic liver disease (CLD) accounts for approximately two million annual deaths worldwide, with liver cancer listed as the 16th leading cause of death globally (Asrani et al., 2019). Success of tyrosine kinase inhibitor (TKI) treatment strategies in conjunction with immunotherapy is variable due to heterogeneity between patients (Cheemerla & Balakrishnan, 2021). Additionally, co-morbidities including metabolic syndrome and hypertension are frequent, with approaches to treatment becoming increasingly difficult (Cheemerla & Balakrishnan, 2021). With the ever-increasing number of individuals with CLD worldwide, there is a clear need for early treatment and prevention strategies. Focused research into earlier stages of disease, would provide insight into targetable disease-associated interactions amongst cells.

Upon chronic insult, LPCs and HSCs are activated (Gogoi-Tiwari et al., 2017). Fibrosis, when exacerbated, becomes a pathological feature of chronic disease, distorting normal tissue architecture (T. A. Wynn, 2008). Considering that LPCs and HSCs co-migrate to sites of injury, (Ruddell et al., 2009) there is interest in investigating their cellular crosstalk.

Active HGF/c-MET signalling elicits anti-fibrotic effects in the liver, in part by antagonising the pro-fibrotic TGF $\beta$  signalling pathway (Marquardt et al., 2012) (Papa et al., 2017). The HGF ligand is secreted by the HSCs (Weidner et al., 1991), while the c-MET receptor is present on the LPCs (Uchikawa et al., 2021). Therefore, the HGF/c-MET signalling pathway is a potential candidate for mutual regulation and its investigation will aid to understand the complex communicative relationship between the LPCs and HSCs during liver fibrosis.

To date, several models of fibrosis have been utilised to investigate the HGF/c-MET signalling pathway (Suárez-Causado et al., 2015) (Almalé et al., 2019) (Ishikawa et al., 2012). This chapter aims to provide a proof-of-principle, to confirm appropriate models of fibrosis, not previously characterised, in relation to the HGF/c-MET pathway for further use throughout this thesis.

### 3.2 Study Aims

In this chapter, the study aims were (a) to investigate the cellular expression pattern of HGF and c-MET using single nucleus RNA-sequencing (snRNA-seq) of archival control, CDE- and TAA-treated mouse liver tissue and confirm HGF expression by HSCs and c-MET presence in LPCs, (b) to characterise HGF/c-MET signalling components as well as fibrogenic markers at different timepoints of archival tissue from CDE-treated mice and (c) to identify and characterise appropriate cells lines for expression of the same components. These data then served as the experimental basis for the rest of this project.

### 3.3 Methodology

For a previous study in our laboratory, snRNA-seq was completed on three biological replicates of archival control, CDE- and TAA-treated C57BL/6J mouse tissue, at 32- and 24-week timepoints, respectively (Carlessi et al., 2022). The bioinformatic analysis was undertaken by Dr. Rodrigo Carlessi at Curtin University using the bioinformatic tool R-studio and data was stored on the UCSC Browser (Appendix). Resulting data were utilised to determine c-MET expression by LPCs and HGF expression by HSCs, respectively.

Archival control and CDE-treated mouse liver tissues were retrieved from a previous study using various timepoints (2-week, 3-week and 3-month) to confirm the CDE diet as a suitable fibrosis model as well as HGF expression by HSCs and c-MET expression in LPCs. Two-week control tissue was used after previous confirmation of unchanged expression of all markers over time in healthy livers. Immunofluorescent staining of frozen sections of 3-month control and CDE-treated livers was completed with HSC markers collagen 1 and  $\alpha$ SMA, along with the LPC marker CK19 (2.2.3.4, Table 2.1). The same 2-week control, 3-week and 4-month CDE-treated tissue was sampled to assess fibrogenic marker expression (collagen 1,  $\alpha$ SMA) along with HGF/c-MET and TGF $\beta$  signalling components (phospho-c-MET, total c-MET, HGF, SMAD2/3, TGF $\beta$ R1, TGF $\beta$ 1) at the protein level by western blot (2.2.4.3, Table 2.1).

Further, the clonal LPC and HSC cell lines BMOL-TAT and LX-2, respectively, were characterised morphologically by brightfield microscopy. Their proliferation status was indirectly assessed by MTT assay (2.2.2.9). Immunofluorescent staining of standard cell type-specific markers was also completed (LPC; A6, CK19, PanCK, EpCAM and HSC;  $\alpha$ SMA, collagen 1, desmin, vimentin) (2.2.3.4, Table 2.1). Lastly, presence of the c-MET receptor on the BMOL-TAT cells and the HGF ligand on the LX-2 cells was confirmed using immunofluorescent staining and western blot analysis. The TGF $\beta$  pathway components SMAD2/3, TGF $\beta$ R1 and TGF $\beta$ 1 were also assessed in both cell lines using the same methods (2.2.3.4, 2.2.4.3, Table 2.1).

### 3.4 Results

#### 3.4.1 HGF and c-MET gene expression pattern analysis using single nucleus RNA-sequencing data

Single nucleus RNA-sequencing was performed by Dr. Rodrigo Carlessi at Curtin University. Generated transcriptomes from three biological replicates of healthy, CDE- and TAA-treated mouse tissue illustrated nine major clusters of cell types, which included T and natural killer cells (T\_NK), myeloid cells, hepatocytes (Hep), mesenchymal cells, endothelial cells (Endo), plasmacytoid dendritic cells (pDCs), mesothelial cells (Meso), B cells and biliary epithelial cells (BECs). These populations were classified through gene expression profile similarity represented in a Seurat plot, dependent on their respective source of either healthy (39.8%), CDE (35.6%) or TAA (24.65%) livers (Figure 3.1).

Utilising the snRNA-seq data from the UCSC browser, HGF expression was evident in the mesenchymal population, as well as in endothelial and myeloid cells, at lower expression frequencies (Figure 3.2A).

Expression of the c-MET receptor was observed in hepatocytes, biliary epithelial cells (including LPCs as a subpopulation) and mesothelial cells (Figure 3.2B).

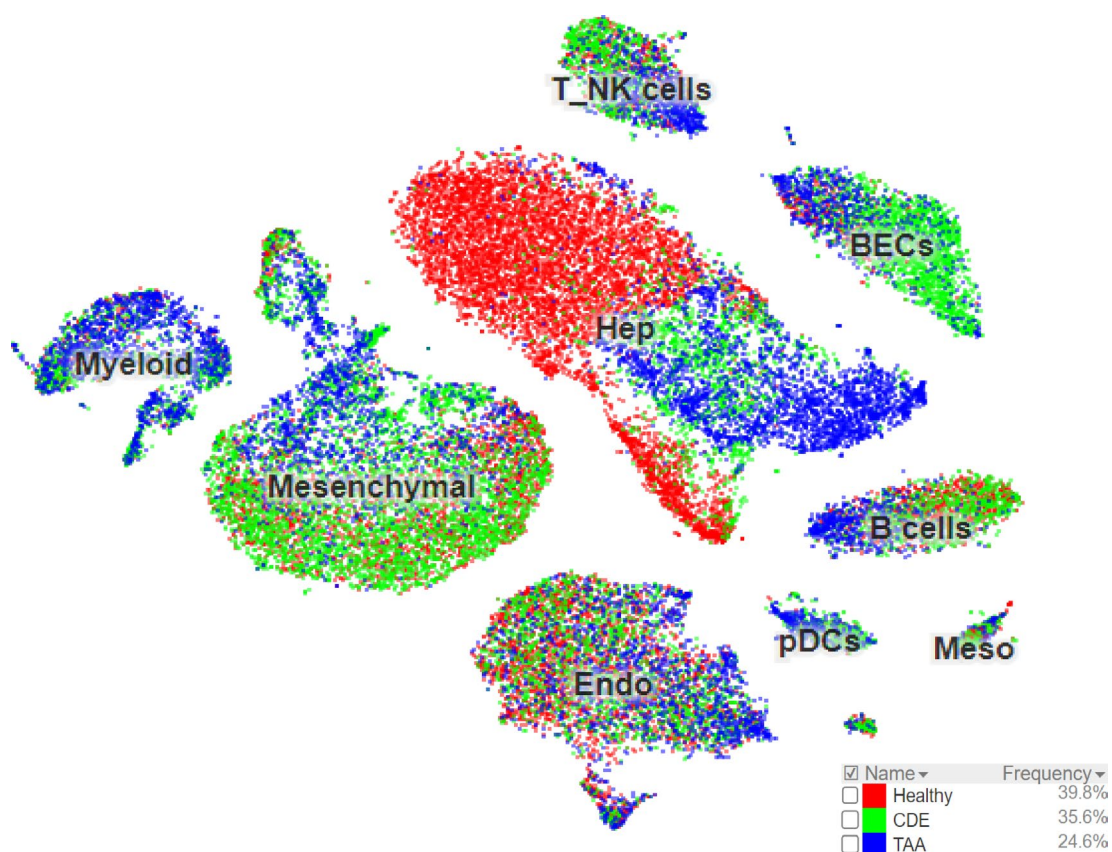
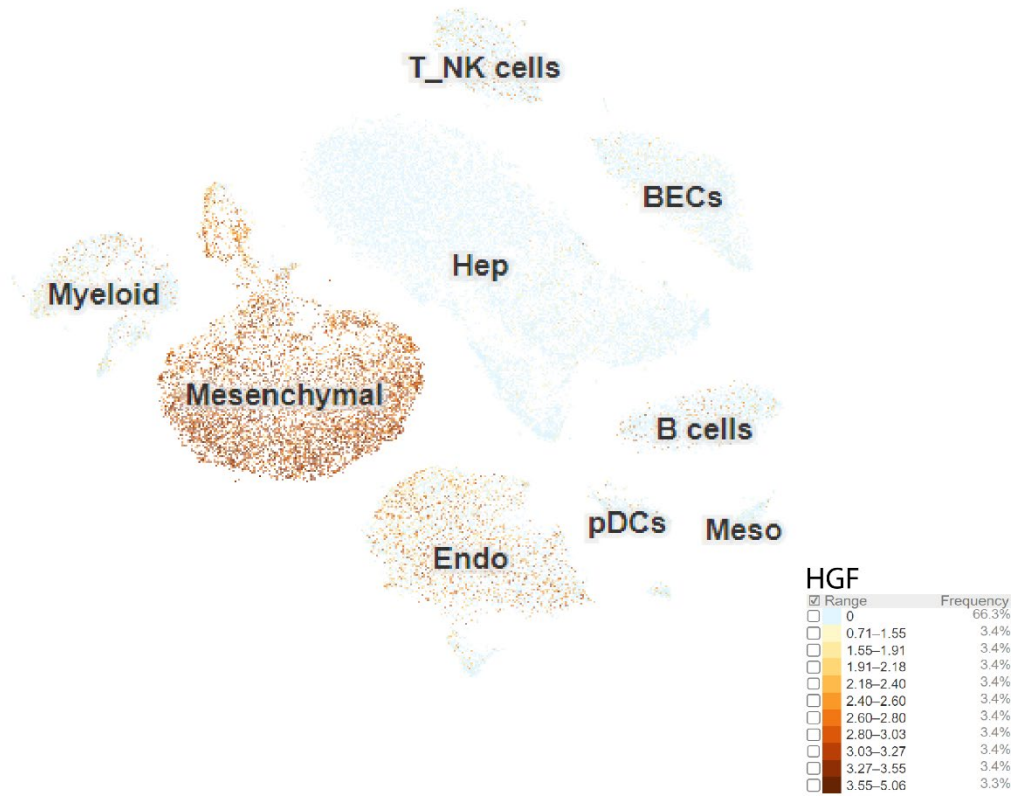


**Figure 3.1: Seurat plot visualisation of healthy, CDE and TAA-treated mouse liver tissue.**

Seurat plot visualisation of snRNA-seq analysis illustrating clustering of nuclei isolated from healthy, CDE- and TAA-treated mouse liver. Nuclei clustered based on gene expression profile similarity. Cell type identities were then assigned for each cluster. Seurat plot demonstrating nine major populations of liver cells included T and natural killer cells (T\_NK), myeloid cells, hepatocytes (Hep), mesenchymal cells, endothelial cells (Endo), plasmacytoid dendritic cells (pDCs), mesothelial cells (Meso), B cells and biliary epithelial cells (BECs).

Data represent n=3.

(A)



(B)

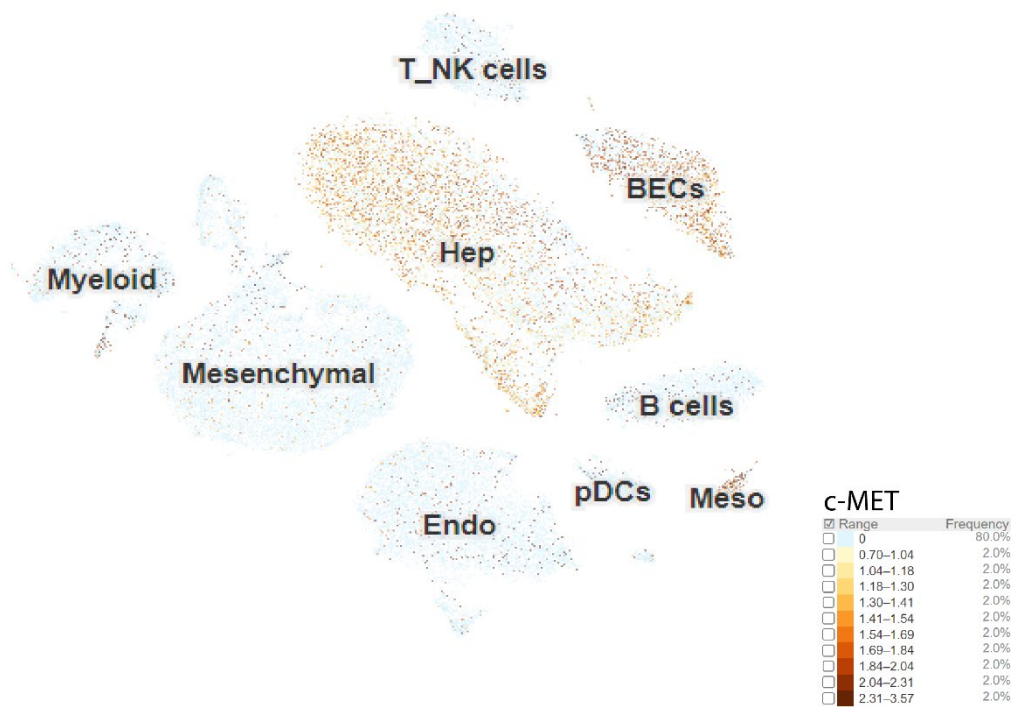


**Figure 3.2: SnRNA-seq analysis illustration expression pattern of HGF and c-MET in healthy, CDE and TAA-treated livers.**

Seurat plot illustrating expression of genes (A) HGF, most predominantly in mesenchymal and endothelial cells (Endo) and (B) c-MET, primarily expressed by hepatocytes (Hep) and biliary endothelial cells (BECs).

Data represent n=3.



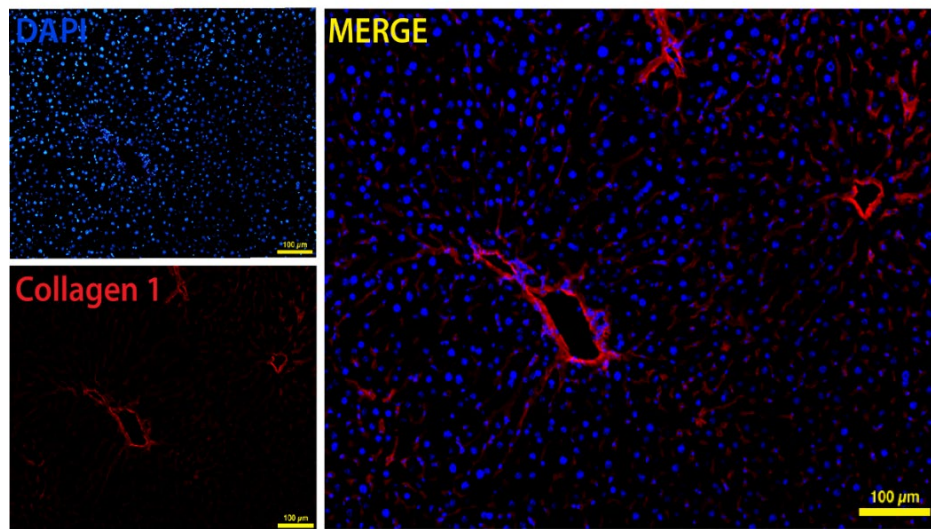
### **3.4.2 Characterisation of HGF/c-MET signalling components in the CDE model of chronic liver disease**

Immunofluorescent staining of control and CDE-treated 3-month mouse tissue was completed for markers CK19 (LPCs),  $\alpha$ SMA and collagen 1 (HSCs). While CK19 staining was restricted to biliary cells and  $\alpha$ SMA<sup>+</sup>/collagen 1<sup>+</sup> and cell numbers were relatively low in healthy livers, CDE treatment induced a strong upregulation of all tested markers with parenchymal tissue infiltration (Figure 3.3B, Figure 3.4B). Western blot analysis also demonstrated conversion of pro-collagen 1 into activated collagen 1 and an increase in  $\alpha$ SMA expression in 3-week and 4-month CDE-treated tissue, as compared to control tissue (Figure 3.5).

Further, western blot analysis was completed to assess TGF $\beta$  and HGF/c-MET signalling pathway components in livers subjected to CDE-induced chronic liver injury. Disease progression positively correlated with upregulation of the TGF $\beta$  pathway, as judged by an increase in the expression of TGF $\beta$ 1, TGF $\beta$ R1 and SMAD2/3 (Figure 3.6). Considering that the TGF $\beta$  and HGF/c-MET pathways have been shown to antagonise each other (Papa et al., 2017), it was also important to investigate HGF signalling components. As disease progressed, the expression of pro-HGF (83kDa) and active HGF (69kDa) decreased, as well as phosphorylated levels of c-MET (Figure 3.6).

**(A)**

Control 3M

**(B)**

CDE 3M

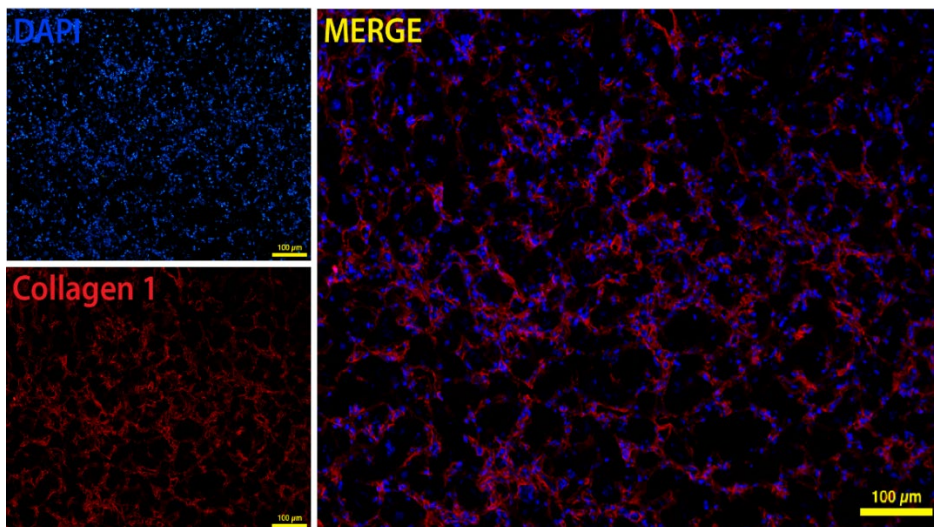


**Figure 3.3: Immunofluorescent detection of collagen 1 expression in 3-month control and CDE-treated tissue.**

While collagen 1 expression was relatively low and mainly restricted to vessels in healthy 3-month control liver (A), its expression was greatly increased and observed in parenchymal liver areas in 3-month CDE-treated tissue. DAPI was used for nuclear quantitation.

Scale bar depicting 100 μm.

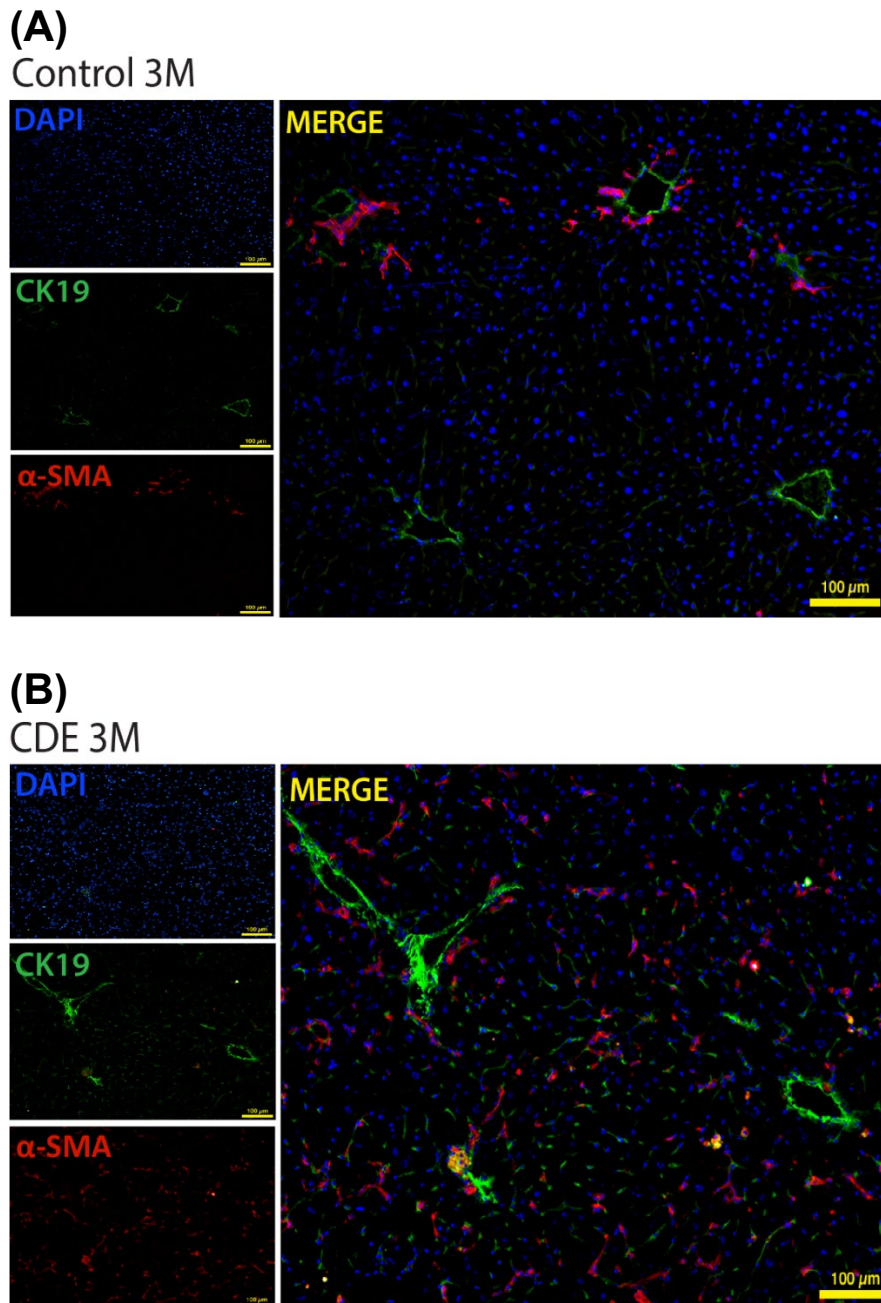


**Figure 3.4: Immunofluorescent detection of CK19 and  $\alpha$ SMA expression in 3-month control and CDE-treated tissue.**

The LPC marker CK19 (green) and the HSC marker  $\alpha$ SMA (red) were only expressed in portal areas in healthy liver (A). However, both cell types were greatly increased in numbers and observed to have migrated into parenchymal areas in mice subjected to 3-month CDE treatment (B). DAPI was used for nuclear quantitation.

Scale bar depicting 100  $\mu$ m.

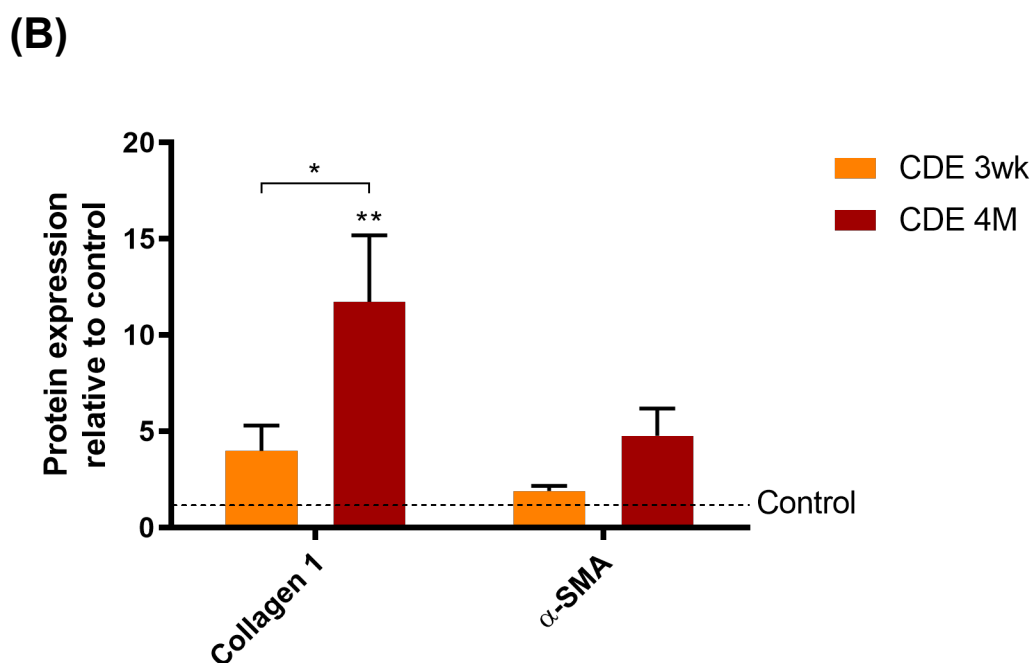
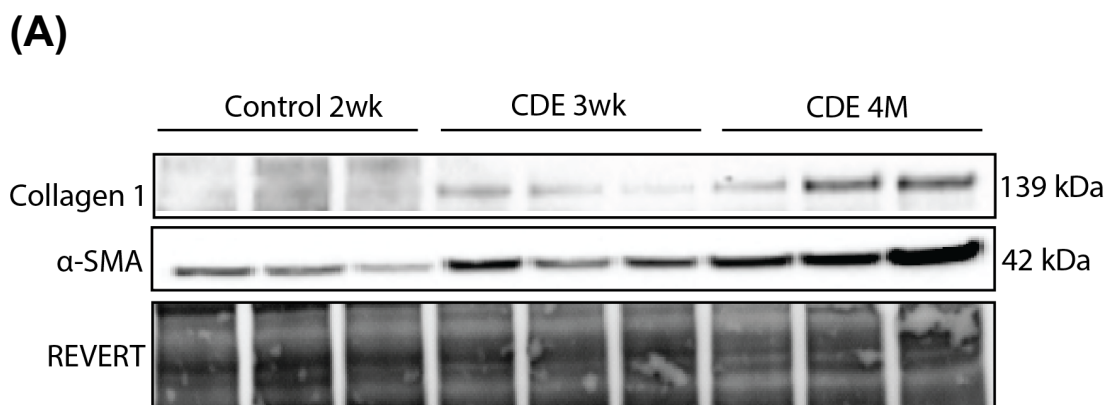


**Figure 3.5: Expression analysis and semi-quantitation of fibrosis-associated markers in control and CDE-treated tissue.**

Protein expression analysis of collagen 1 and αSMA by western blot (A) and semi-quantitation by densitometry (B) revealed a significant increase in collagen 1 in CDE-treated tissue, as compared to healthy control liver. An increased expression of αSMA is evident from control 2-week to 4-month CDE-treated tissue.

Data represent the mean  $\pm$  SEM.  $n=3$ , \*  $P < 0.05$ , \*\*  $P < 0.01$ .

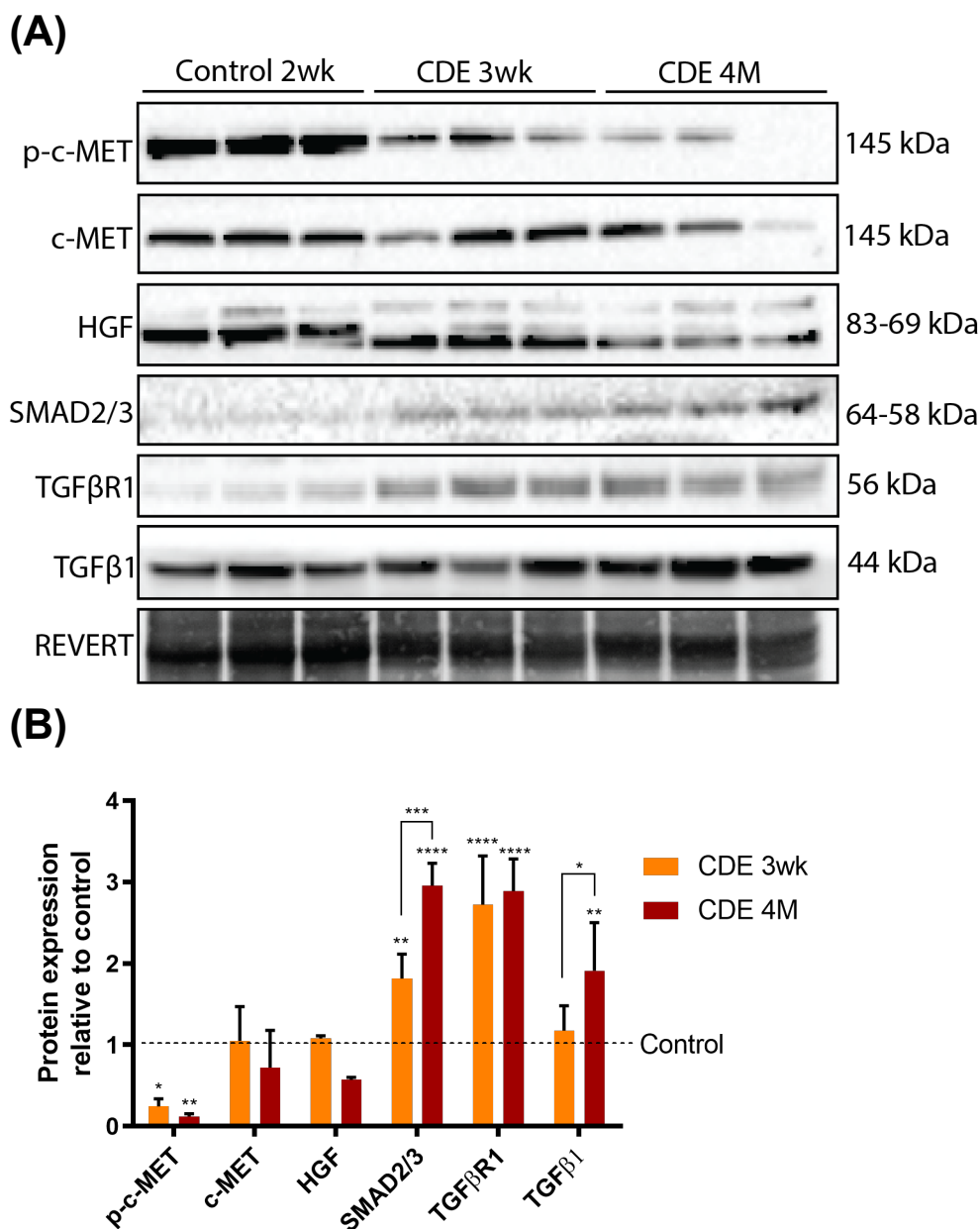


**Figure 3.6: Expression analysis and semi-quantitation of TGFβ and HGF/c-MET signalling markers in control and CDE-treated tissue.**

Expression and phosphorylation levels of the HGF/c-MET pathway components p-c-MET, c-MET and HGF were assessed by western blot analysis (A) and semi-quantitation by densitometry (B). A significant increase in TGFβ pathway components SMAD2/3 and TGFβR1 was observed with the progression of disease.

Data represent the mean  $\pm$  SEM.  $n = 3$ .  $P^* < 0.05$ ,  $P^{**} < 0.01$ ,  $P^{***} < 0.001$ ,  $P^{****} < 0.0001$ .



### **3.4.3 Characterisation of clonal cell lines BMOL-TAT and LX-2 as appropriate models of LPCs and HSCs**

As an epithelial cell line, the clonal LPC line BMOL-TAT presents a rounder, cobblestone morphology, while the mesenchymal clonal HSC line LX-2 displays an elongated, spindle-like phenotype (Figure 3.7).

The BMOL-TAT and LX-2 cell lines follow linear growth over 72 hours, as indirectly judged by MTT assay. A faster doubling time was observed in BMOL-TAT cells, indicated by the higher absorbance readings over 72 hours, as compared to the LX-2 cell line (Figure 3.8). Future experimental set ups therefore considered the difference in doubling time (~1:1.4 seeding ratio) for optimal growth of both cell lines when co-cultured.

Furthermore, immunofluorescent staining was performed on BMOL-TAT and LX-2 cells using cell type-specific markers. BMOL-TAT cells were confirmed to express the LPC markers A6, PanCK, CK19 and EpCAM (Figure 3.9), while LX-2 cells expressed the HSC-specific markers  $\alpha$ SMA, desmin, vimentin and collagen 1 (Figure 3.10). Thus, BMOL-TAT and LX-2 cell lines were established as appropriate LPC and HSC models for further experimentation.

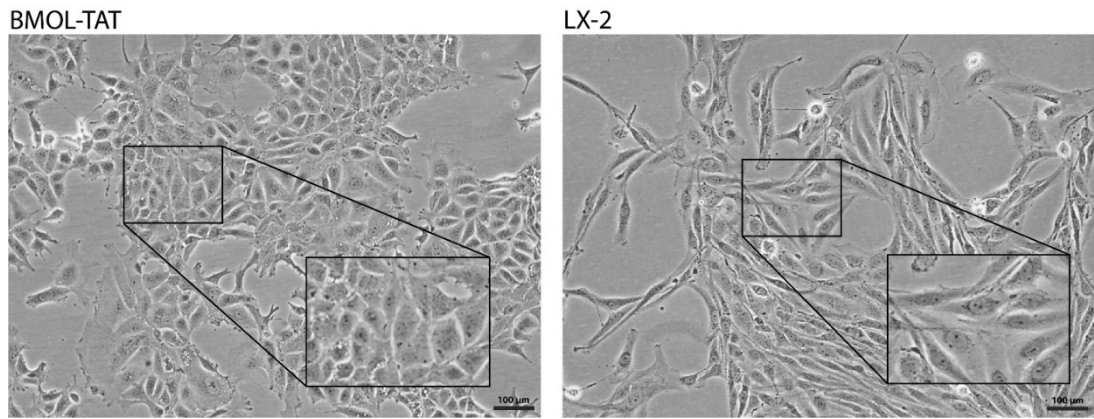


**Figure 3.7: Morphological assessment of BMOL-TAT and LX-2 cells.**

Brightfield microscopy images displaying BMOL-TAT and LX-2 cells at approximately 70% confluency. BMOL-TAT cells present standard epithelial LPC morphology, with cobblestone growth, while LX-2 cells exhibit an elongated mesenchymal shape, a standard phenotype of activated HSCs. Scale bar depicting 100  $\mu\text{m}$ .

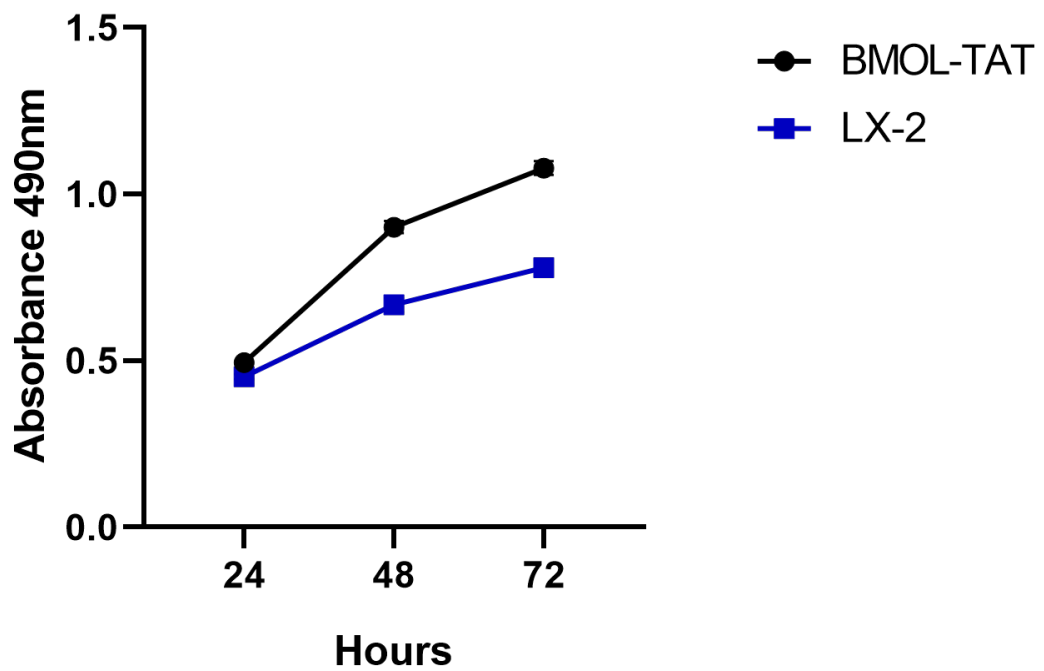


**Figure 3.8: Cell proliferation of BMOL-TAT and LX-2 cells.**

The LPC and HSC cell lines BMOL-TAT and LX-2 were cultured over 72 hours. The MTT assay revealed that both cell lines grow linearly, with faster doubling time in the BMOL-TAT cell line.

Data represent the mean  $\pm$  SEM. n= 3.



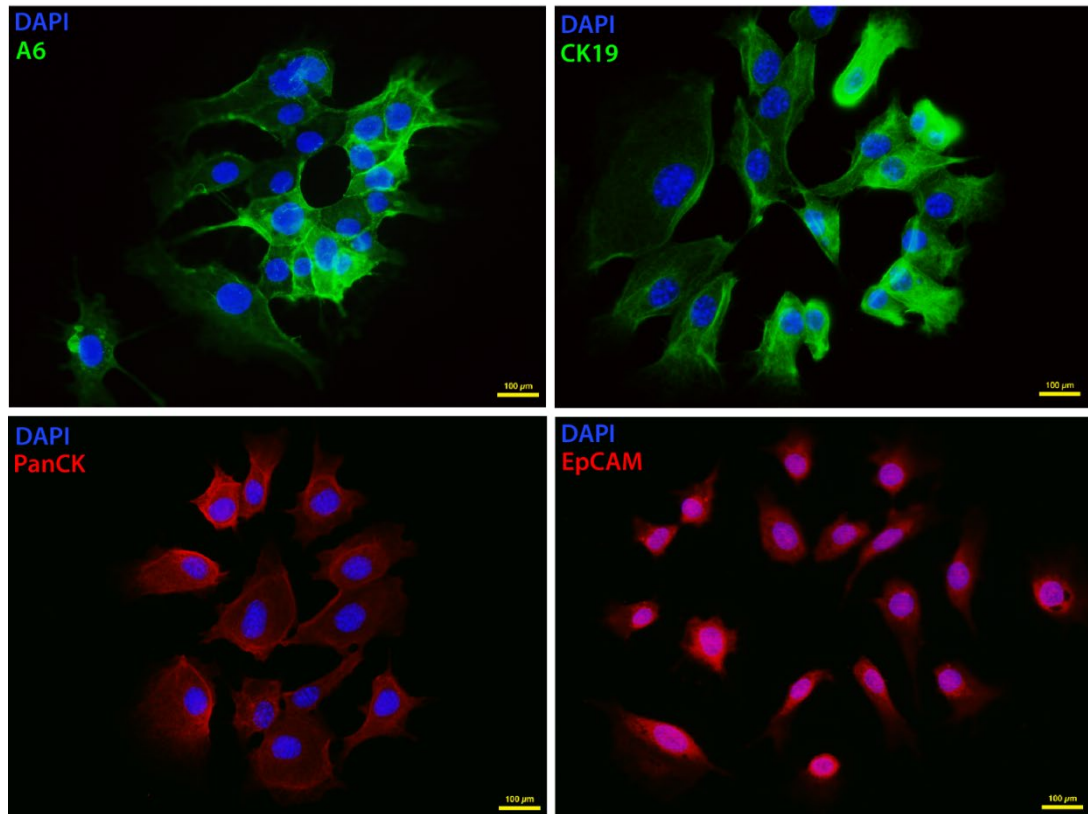


**Figure 3.9: Immunofluorescent detection of LPC-specific marker expression in BMOL-TAT cells.**

Immunofluorescent staining demonstrating that BMOL-TAT cells express the LPC markers A6, CK19, PanCK and EpCAM.

Scale bar depicting 100 µm.

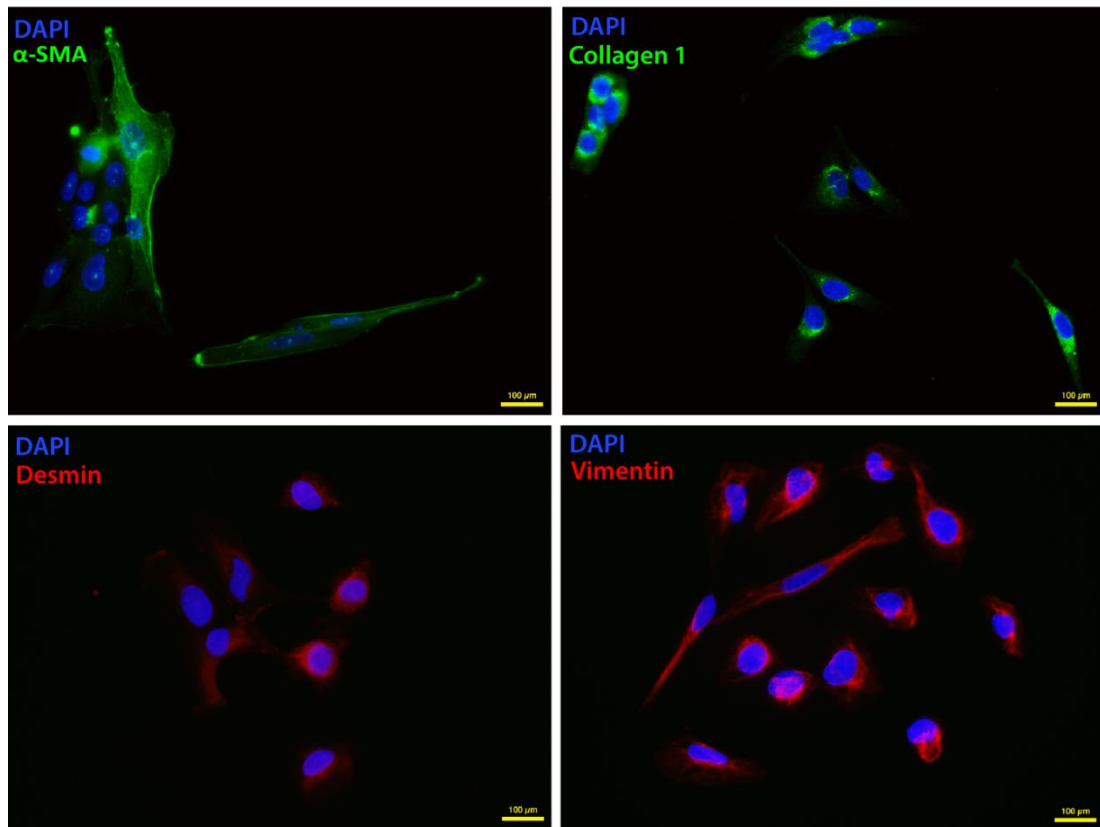


**Figure 3.10: Immunofluorescent detection of HSC-specific marker expression in LX-2 cells.**

Immunofluorescent staining demonstrating that LX-2 cells express HSC-specific markers  $\alpha$ SMA, collagen 1, desmin and vimentin.

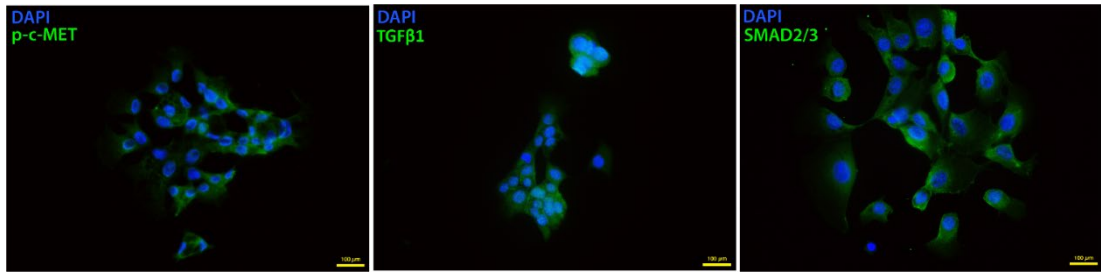
Scale bar depicting 100  $\mu$ m.

#### **3.4.4 HGF/c-MET and TGF $\beta$ signalling pathway status in BMOL-TAT and LX-2 clonal cell lines**

Immunofluorescent analysis of the clonal LPC line BMOL-TAT revealed phosphorylation of c-MET, denoting active c-MET signalling (Figure 3.11). Similarly, the clonal HSC line LX-2 demonstrated expression of the HGF ligand (Figure 3.12). In addition, immunofluorescent staining determined that both cell lines signal through TGF $\beta$  pathway components, TGF $\beta$ 1 and SMAD2/3 (Figure 3.11, Figure 3.12).

Moreover, western blot analysis indicated that c-MET is exclusively phosphorylated in BMOL-TAT cells, whereas the ligand HGF is expressed in both BMOL-TAT and LX-2 cells (Figure 3.13). The TGF $\beta$  pathway components SMAD2/3, TGF $\beta$ R1 and TGF $\beta$ 1 were expressed in both cell types, however greater expression levels were evident in BMOL-TAT cells (Figure 3.13).

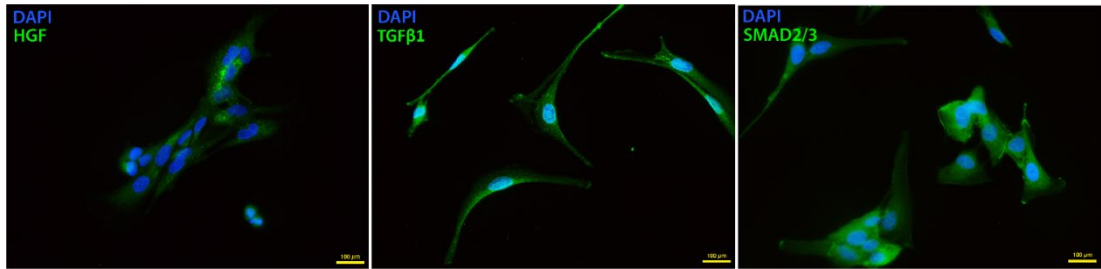
This signalling pathway characterisation established a baseline level of signalling activity in the selected cell types before molecular pathway manipulation was carried out, as described in the following chapters.



**Figure 3.11: Immunofluorescent detection of HGF/c-MET and TGF $\beta$  signalling components in BMOL-TAT cells.**

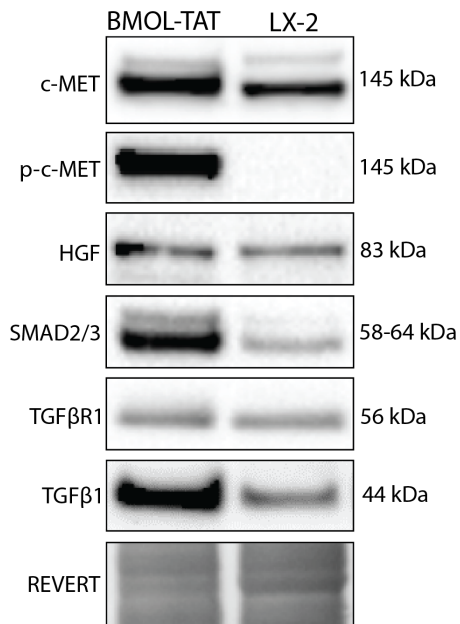
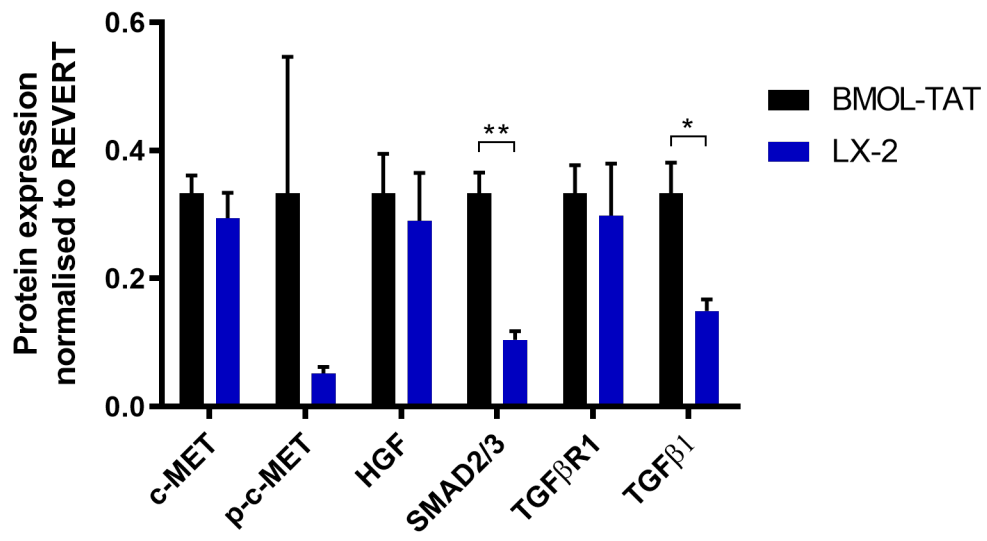
BMOL-TAT cells demonstrating phosphorylation of c-MET (p-c-MET) and expression of markers TGF $\beta$ 1 and SMAD2/3.

Scale bar depicting 100  $\mu$ m.



**Figure 3.12: Immunofluorescent detection of HGF/c-MET and TGF $\beta$  signalling components in LX-2 cells.**

LX-2 cells demonstrating expression of markers HGF, TGF $\beta$ 1 and SMAD2/3. Scale bar depicting 100  $\mu$ m.

**(A)****(B)**

**Figure 3.13: Expression analysis and semi-quantitation of TGF $\beta$  and HGF/c-MET signalling markers in BMOL-TAT and LX-2 cells.**

An absence of p-c-MET was observed in the LX-2 cells and expression of HGF was evident in both cell lines, demonstrated by western blot (A) and semi-quantitation by densitometry (B). Lower expression levels of TGF $\beta$  pathway components SMAD2/3 and TGF $\beta$ R1 and TGF $\beta$ 1 was confirmed in LX-2 cells. Data represent the mean  $\pm$  SEM. n= 3. \* P < 0.05, \*\* P < 0.01.

### 3.5 Discussion

Selecting appropriate *in vitro* and *in vivo* models for investigating underlying mechanisms of fibrosis is vital before accurate conclusions can be drawn. Access to archival TAA- and CDE-treated mouse tissue allowed for investigation into HGF/c-MET signalling components in different timepoints of liver disease, before *in vitro* cell models were selected for further study. Thioacetamide (TAA) supplementation to the drinking water and the choline-deficient, ethionine-supplemented (CDE) diet are well-characterised models of liver disease. Both models demonstrate inflammation, LPC activation, fibrosis and eventually lead to HCC. While the CDE diet induces portal injury and is characterised by hepatocyte fat loading and mild fibrosis, TAA supplementation targets central lobular areas and gives rise to more severe fibrotic changes that eventually progress to cirrhosis and HCC. A comparison of these two distinct models previously facilitated the study of different pathological processes in a time course manner (Köhn-Gaone et al., 2016).

Additionally, access to archival CDE- and TAA-treated single nucleus RNA-sequencing data provided further insight into HGF and c-MET gene expression within a variety of liver cell populations (Carlessi et al., 2022). HGF expression was identified in the mesenchymal cell population, consistent with the literature (Weidner et al., 1991). Further, expression of the c-MET receptor was demonstrated to be in hepatocytes and biliary endothelial cells, with LPCs recognised as a subset of the BEC population.

Having confirmed HSCs as a main HGF ligand-producing cell type and LPCs/BECs as c-MET-expressing cells by snRNA-seq, further immunofluorescence and western blot analysis of 3-month CDE-treated tissue established a significant increase in collagen 1 expression, compared to control tissue. In addition, increased expression of  $\alpha$ SMA and CK19 in CDE tissue confirmed the activation of HSCs and LPCs, demonstrating a relevance of studying HGF/c-MET in the context of LPC and HSC biology during fibrotic liver disease.



A previous study highlighted that the HGF/c-MET signalling pathway and the TGF $\beta$  pathway can antagonise each other (Papa et al., 2017). Western blot analysis confirmed reduced expression of HGF and c-MET and therefore less phosphorylated c-MET, indicating a downregulation in HGF/c-MET signalling with disease progression. Conversely, expression levels of the fibrosis-associated markers TGF $\beta$ , TGF $\beta$ R1 and SMAD2/3 all increased over time, consistent with previous reports (Dooley & Dijke, 2012). Considering that the HGF/c-MET signalling pathway is known to be anti-fibrotic (Borowiak et al., 2004) (Almalé et al., 2019), the decrease in signalling may be detrimental to disease resolution.

Since it can be difficult to interpret cell type-specific data and molecular mechanisms while cells are *in situ* in a complex microenvironment, clonal cell lines were utilised to assess LPCs and HSCs in isolation. The LPC line BMOL-TAT (J. E. E. Tirnitz-Parker et al., 2007) and HSC line LX-2 (L. Xu et al., 2005) are well-characterised representative *in vitro* models. BMOL-TAT cells presented standard epithelial morphology, while LX-2 cells displayed the expected mesenchymal phenotype. Both cell lines grew linearly over 72 hours and expressed standard cell type-specific markers, suggesting these cells are appropriate for further investigation into cellular HGF/c-MET crosstalk.

Lastly, it was necessary to characterise the BMOL-TAT and LX-2 lines with regards to cell type-specific contribution to HGF/c-MET signalling as a fundamental basis for future pathway modulation studies. As determined by immunofluorescence and western blot analysis, both cell lines express TGF $\beta$  components TGF $\beta$ , TGF $\beta$ R1 and SMAD2/3, with higher levels evident in the LPC line BMOL-TAT. As demonstrated through snRNA-seq data, only LPCs express c-MET, which was confirmed for BMOL-TAT cells. Interestingly, HGF expression was not limited to the HSC line, LX-2, with expression also evident in the LPC line, BMOL-TAT, suggesting autocrine HGF/c-MET signalling pathway activity.

The combination of COVID-19 constraints, and availability of C57BL/6 mice hampered the planned investigation into primary HSCs in relation to the

HGF/c-MET signalling pathway (Appendix). Nonetheless, characterisation of the CDE model and clonal cell lines BMOL-TAT and LX-2 in relation to the HGF/c-MET signalling pathway had not previously been studied and provided a novel basis for further experimentation, where respective pathway modulation and co-culture experiments were carried out.

**Chapter 4: *In vitro* deletion of c-MET in liver progenitor cells  
using CRISPR/Cas9 technology**

## 4.1 Introduction

In Chapter 3, the anti-fibrotic role of the HGF/c-MET pathway was discussed. LPC/HSC-associated processes including fibrosis were investigated at progressing stages of liver disease in archival CDE-treated liver tissue, along with the baseline HGF/c-MET signalling status of the investigated LPC and HSC lines, BMOL-TAT and LX2, respectively.

LPCs have recently been determined to function as regulatory cells that can impact the fibrogenic status of nearby HSCs (Gratte et al., 2021). This finding prompted investigations into the anti-fibrotic role of the HGF/c-MET pathway in LPCs. The data presented in Chapter 3 described HSCs as producers of HGF and confirmed that LPCs express the receptor c-MET. Therefore, the impact of c-MET deletion in LPCs and the resulting biological effects on processes including proliferation, migration and fibrogenic potential were studied in Chapter 4.

CRISPR/Cas9 technology has become a gold standard method for knocking out a gene to investigate the resulting downstream effects (Uddin, Rudin, & Sen, 2020). CRISPR/Cas9, which stands for clustered regularly interspaced short palindromic repeats and CRISPR-associated protein 9, was first discovered in 1993. Since then, this system has been extensively studied and identified as a key element in the adaptive immune system in prokaryotes (Bolotin, Quinquis, Sorokin, & Ehrlich, 2005) (Uddin et al., 2020). Researchers use CRISPR/Cas9 technology by introducing a small fragment of RNA with a guide sequence that attaches to a specific DNA target sequence, along with the dual RNA-guided Cas9 endonuclease enzyme. The cell then uses its own DNA repair machinery to delete the specified piece of genetic material (Rodríguez-Rodríguez, Ramírez-Solís, Garza-Elizondo, Garza-Rodríguez, & Barrera-Saldaña, 2019). Since CRISPR/Cas9 is inexpensive and highly specific, this technology was selected to delete the c-MET receptor from the BMOL-TAT LPC line and facilitate the study of consequential downstream cellular effects. Numerous studies have highlighted the significance of c-MET in the liver, specifically through *in vivo* studies. Huh and colleagues used

Cre/loxP-mediated gene targeting to create conditional c-MET knockout (KO) mice in hepatocytes (Huh et al., 2004). These mice were additionally subjected to carbon tetrachloride (CCL<sub>4</sub>) treatment, which caused impaired hepatocyte migration and significantly reduced liver regeneration compared to wildtype mice, as demonstrated by a delayed wound healing response (Huh et al., 2004). A similar study that administered CCL<sub>4</sub> to c-MET knockout mice, demonstrated that loss of c-MET in hepatocytes altered the hepatic microenvironment and aggravated hepatic fibrogenesis due to greater HSC activation and invasion (Marquardt et al., 2012).

Studies that specifically focused on c-MET deletion in LPCs revealed an impairment of LPC function, which led to exacerbated liver fibrosis. This was reported by an *in vivo* study by Ishikawa and colleagues, which demonstrated that LPC-specific deletion of c-MET in the 3,5-diethocarbonyl-1,4-dihydrocollidine (DDC) model of chronic liver injury resulted in overall reduced LPC numbers and migration to sites of injury (Ishikawa et al., 2012). Similarly, c-MET deletion from isolated primary murine LPCs by Castillo *et al.* caused a decrease in cell viability and increased levels of apoptosis (del Castillo et al., 2008). These studies provide direct evidence for c-MET having a critical role in driving effective liver regeneration and suggest that disruption of the receptor directly affects the respective microenvironment, and therefore tissue remodelling.

Together, these data, mainly obtained through *in vivo* investigations, suggest that HGF/c-MET signalling plays a role in LPC proliferation and migration. While *in vivo* studies can provide a depth of information on cellular processes during liver disease and regeneration, it is often difficult to discern the underlying mechanisms and distinguish direct from indirect effects on a particular cell population. This chapter describes the establishment of a novel cell culture model to specifically study the role of HGF/c-MET signalling in LPCs *in vitro*.

## 4.2 Study aims

The first aim of this chapter was to establish a clonal c-MET knockout LPC line using CRISPR/Cas9 technology. The second aim was to study the downstream effects of c-MET knockout on LPC proliferation, migration and fibrogenic pathway expression, as compared to the wildtype (WT) cell line.

### 4.3 Methodology

To study the role of the HGF/c-MET pathway in LPCs *in vitro* by CRISPR/Cas9-mediated deletion of the c-MET receptor, the well-characterised LPC line BMOL-TAT (J. E. E. Tirnitz-Parker et al., 2007) was selected.

BMOL-TAT cells were seeded in a 6-well plate at a cell density of  $1.5 \times 10^5$  cells/well. The following day, the cells were transfected with CRISPR guides (#A, #B7 and #B8), which demonstrated sufficient transfection efficiency (>35%). Green fluorescent protein (GFP)-positive cells were then sorted and seeded in a 24-well plate for post-sorting recovery overnight, before single cell manual sorting was completed (2.2.2.7). Cultures were then expanded, protein was collected (2.2.4.1) and cell lines assessed for potential c-MET KO status by western blot analysis (2.2.4.3) and immunofluorescence (2.2.3.4). Confirmed c-MET KO cells (BMOL-TAT<sup>c-MET KO</sup>) were cryopreserved. The same experimental workflow was implemented with wildtype BMOL-TAT cells, without the addition of CRISPR guides. This ultimately selected for an appropriate wildtype control cell line for downstream experiments (BMOL-TAT<sup>c-MET WT</sup>).

Phenotypical differences between BMOL-TAT<sup>c-MET WT</sup> and BMOL-TAT<sup>c-MET KO</sup> cells were assessed by brightfield microscopy. Further, sister cell lines were fixed with 4% PFA and stained with the nuclear dye Hoechst and cytoskeletal dye Phalloidin. Cell morphology parameters including area, roundness, width, length, and ratio of width to length were analysed by the Operetta CLS™ High-Content Analysis System and quantified using Harmony 4.9 software through a predefined protocol. Cell adherence was assessed using a cell trypsinisation assay.

Next, a cell apoptosis assay was performed by flow cytometry (2.2.2.16) to analyse whether deletion of c-MET affected LPC viability in culture. Cell functionality was assessed by MTT and MTS assays over 72 hours to study

proliferation (2.2.2.9, 2.2.2.10). Further, wound healing assays were completed over 34 hours to investigate cell migration (2.2.2.12).

Finally, protein was extracted from BMOL-TAT<sup>c-MET<sup>WT</sup></sup> and BMOL-TAT<sup>c-MET<sup>KO</sup></sup> cells to compare the changes in the expression of TGF $\beta$  pathway components at the protein level using western blot analysis for SMAD2/3, TGF $\beta$ R1, TGF $\beta$ 1 and  $\alpha$ SMA (2.2.4.3, Table 2.1). Immunofluorescence on cytospin sections were performed to detect phospho-SMAD2 and total-SMAD2, as well as the EMT markers E-cadherin, N-cadherin, and vimentin (2.2.3.4, Table 2.1).

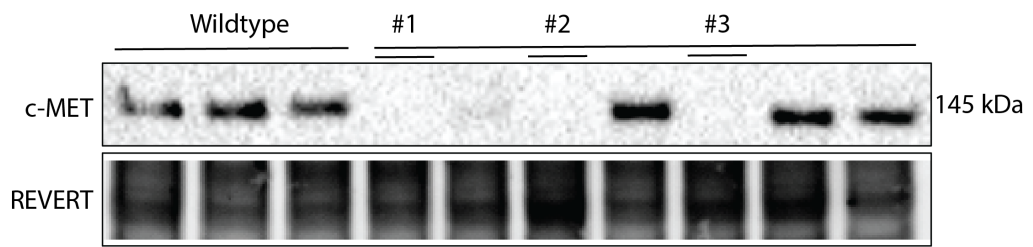


## 4.4 Results

### 4.4.1 Establishment and confirmation of c-MET knockout BMOL-TAT cells

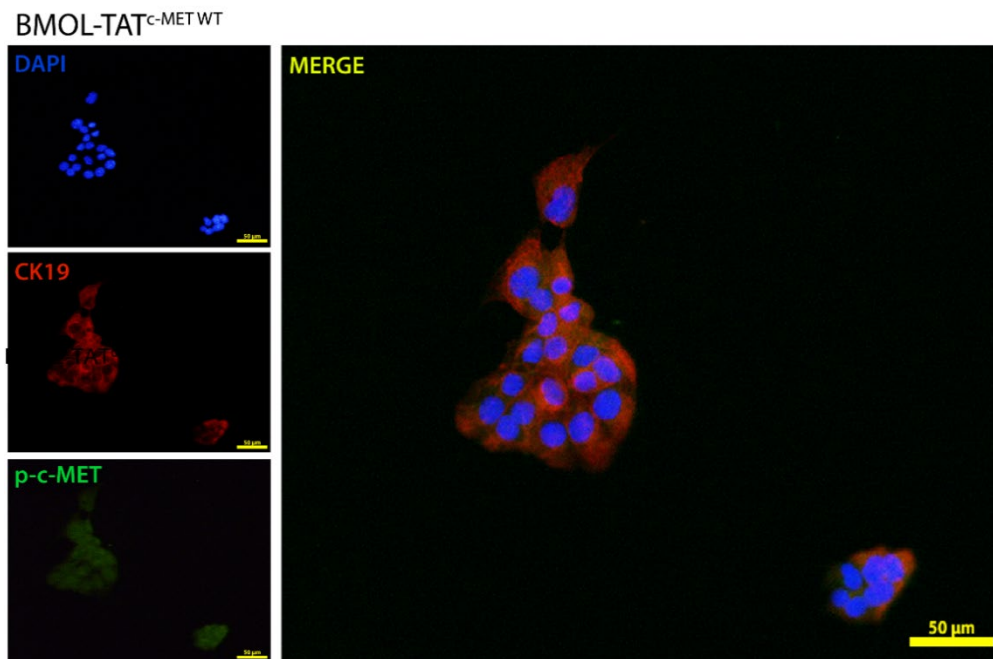
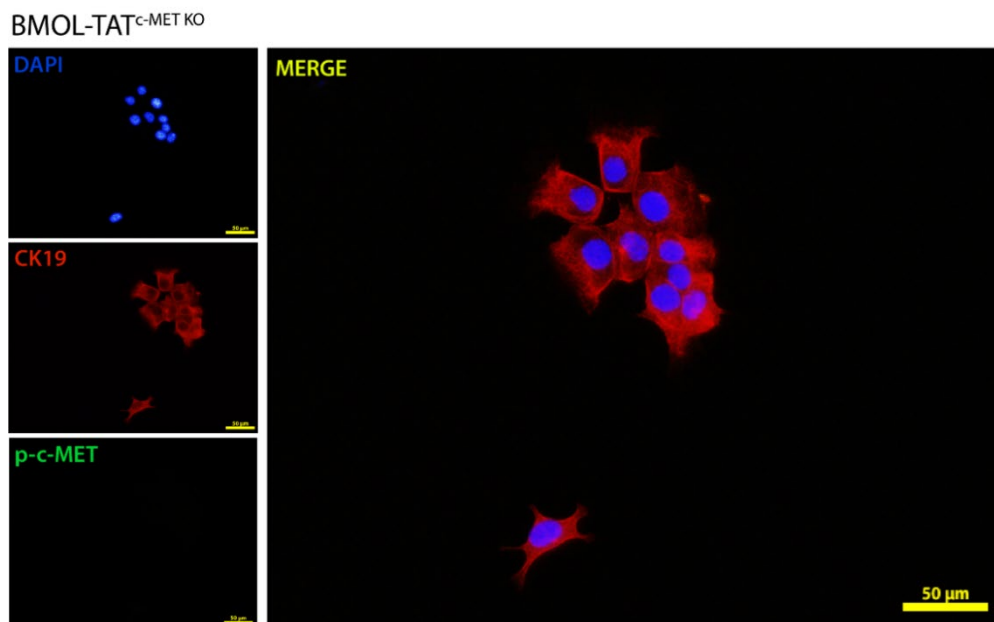
The HGF receptor, c-MET, was deleted of the LPC cell line BMOL-TAT by CRISPR/Cas9 technology.

Three BMOL-TAT<sup>c-MET KO</sup> cell lines were confirmed by western blot analysis through the absence of the protein (Figure 4.1). Further validation of knockout #1 was performed by immunofluorescent co-staining with phospho-c-MET and CK19, an LPC marker (Figure 4.2). Knockout cell line #1 was used for further experimentation throughout this thesis.



**Figure 4.1: Confirmation of c-MET knockout in BMOL-TAT cells.**

Successful CRISPR deletion of the c-MET receptor was confirmed in three clones (#1, #2, #3) of BMOL-TAT cells using western blot analysis.

**(A)****(B)**

**Figure 4.2: Confirmation of c-MET knockout through immunofluorescence for phospho-c-MET (p-c-MET).**

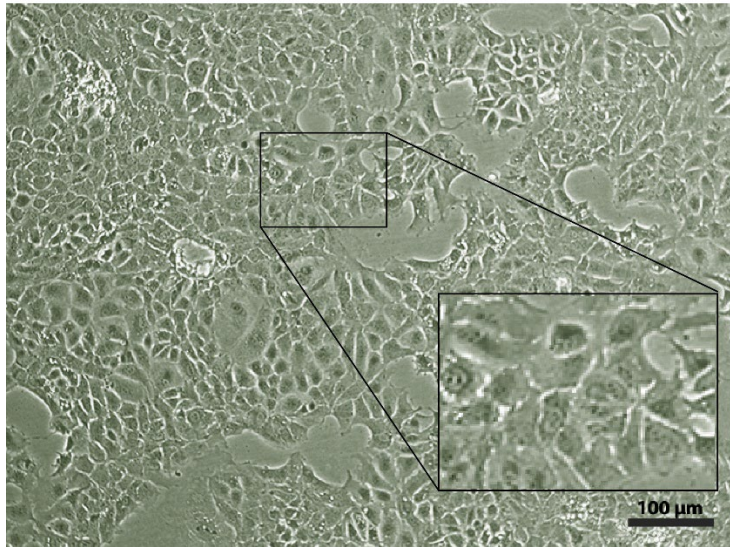
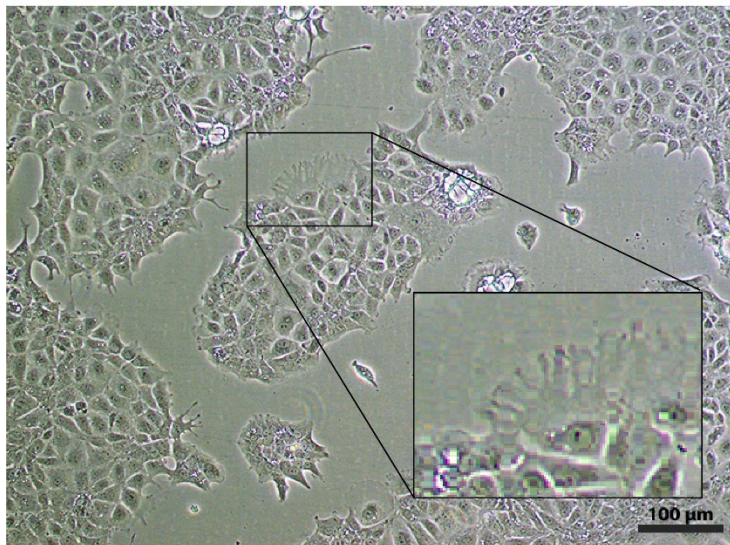
While BMOL-TAT<sup>c-MET WT</sup> cells (A) express CK19 (red) and p-c-MET (green), BMOL-TAT<sup>c-MET KO</sup> clone #1 displayed no detectable phosphorylation of c-MET (B), further confirming successful CRISPR/Cas9-mediated receptor deletion. Scale bar depicting 50  $\mu$ m.

#### 4.4.2 Phenotypical assessment of BMOL-TAT<sup>c-MET KO</sup> cells

Morphological assessment by brightfield microscopy demonstrated that the BMOL-TAT<sup>c-MET KO</sup> cells presented finger-like projections, compared to the BMOL-TAT<sup>c-MET WT</sup> cells (Figure 4.3). Additionally, the BMOL-TAT<sup>c-MET KO</sup> cells grew in a clump-like morphology, rather than a more scattered arrangement, more commonly seen by the wildtype cells (Figure 4.3).

Morphological differences were further assessed using the Operetta CLS<sup>TM</sup> High-Content Analysis System. Figure 4.4AB demonstrates BMOL-TAT<sup>c-MET WT</sup> and BMOL-TAT<sup>c-MET KO</sup> cells stained with the nuclear dye Hoechst 33342 and the cytoskeletal dye Phalloidin. Following analysis via the Harmony 4.9 software with selected cells (Figure 4.4CD), BMOL-TAT<sup>c-MET KO</sup> cells were identified to be significantly rounder, wider, have a greater cell area ( $\mu\text{m}$ ) and width/length ratio as compared to BMOL-TAT<sup>c-MET WT</sup> cells (Figure 4.4E).

As well as the identification of phenotypical changes between cell types, the BMOL-TAT<sup>c-MET KO</sup> cells appeared to be more adherent. To experimentally investigate this, a cell adherence assay using 0.05% trypsin was completed to compare cell attachment between the BMOL-TAT<sup>c-MET KO</sup> and BMOL-TAT<sup>c-MET WT</sup> cells. As seen in Figure 4.5, the BMOL-TAT<sup>c-MET KO</sup> cells were significantly more adherent at 1-minute post-trypsin, with a similar trend evident throughout the rest of the time course.

**(A)**BMOL-TAT<sup>c-MET WT</sup>**(B)**BMOL-TAT<sup>c-MET KO</sup>

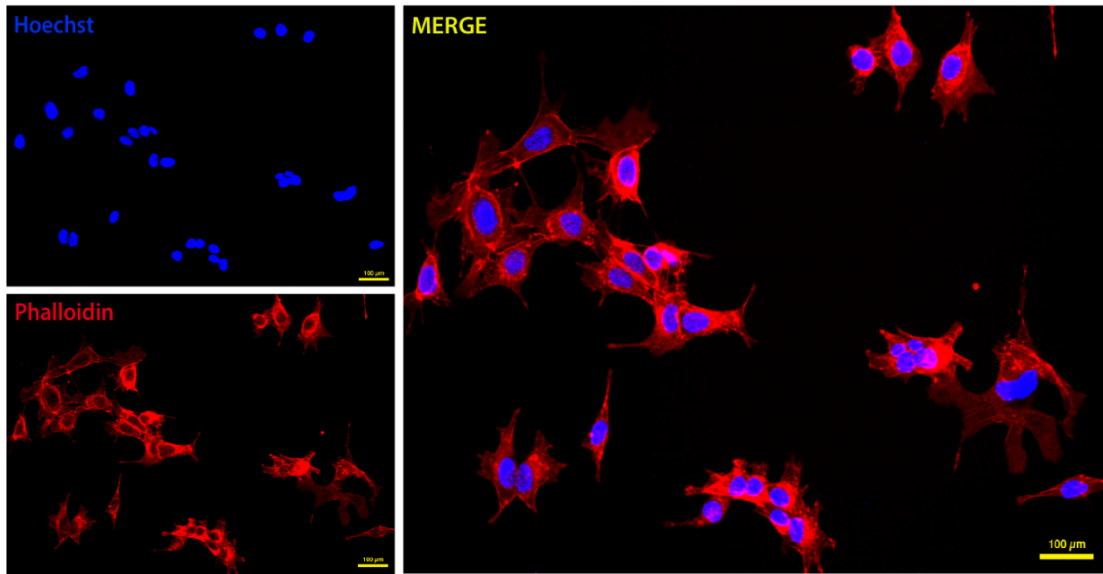
**Figure 4.3: Morphological assessment of BMOL-TAT<sup>c-MET WT</sup> and BMOL-TAT<sup>c-MET KO</sup> cells.**

Brightfield microscopy of both sister cell lines revealed that BMOL-TAT<sup>c-MET WT</sup> cells grow in the expected cobblestone-like phenotype (A), whereas deletion of the c-MET receptor displayed clump-like growth and finger-like projections (B).

Scale bar depicting 100  $\mu\text{m}$ .

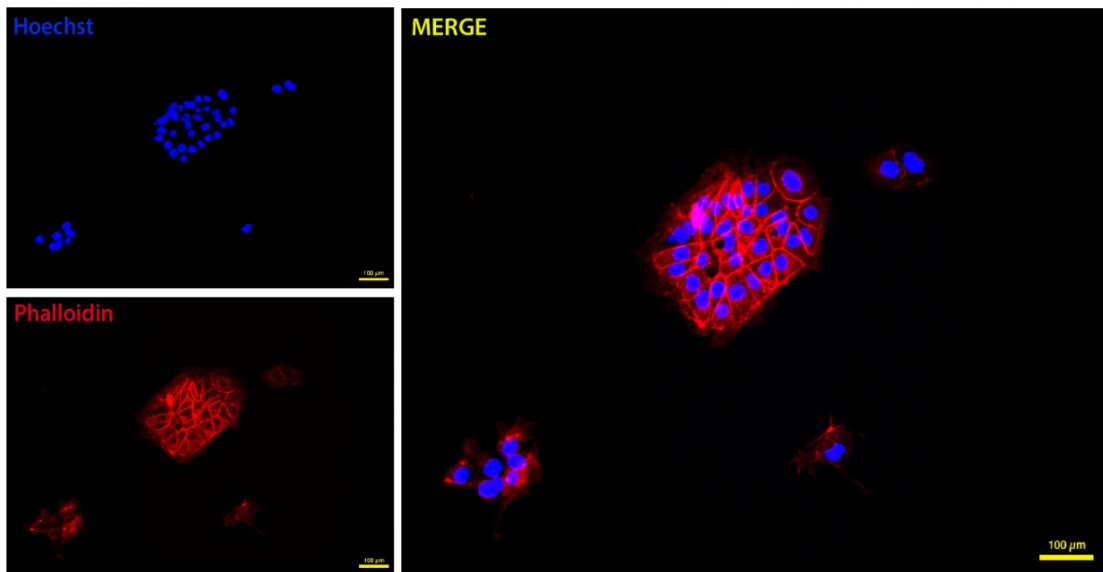
**(A)**

BMOL-TAT<sup>c-MET WT</sup>



**(B)**

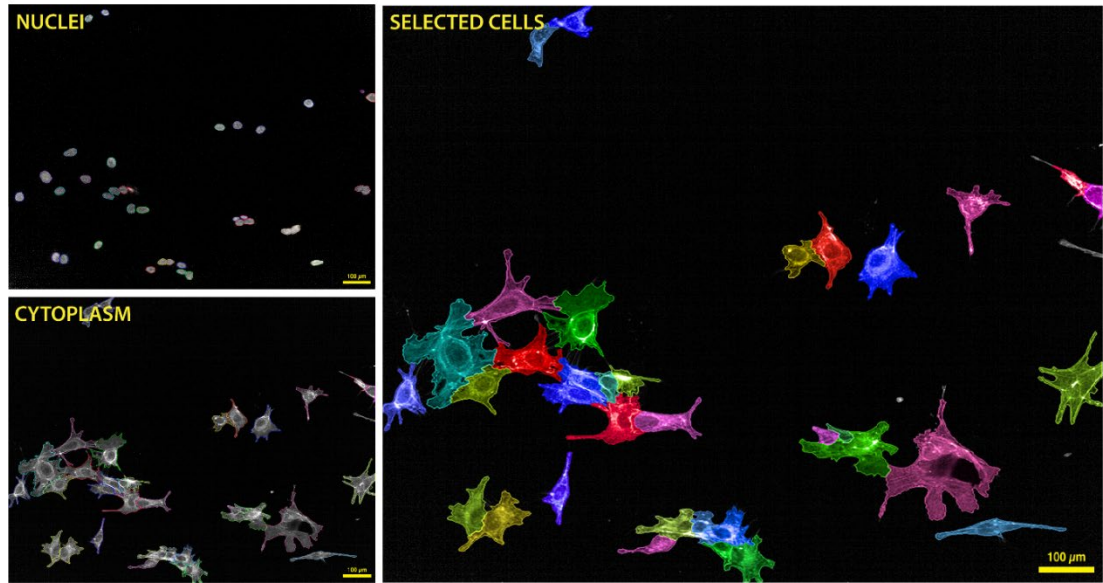
BMOL-TAT<sup>c-MET KO</sup>





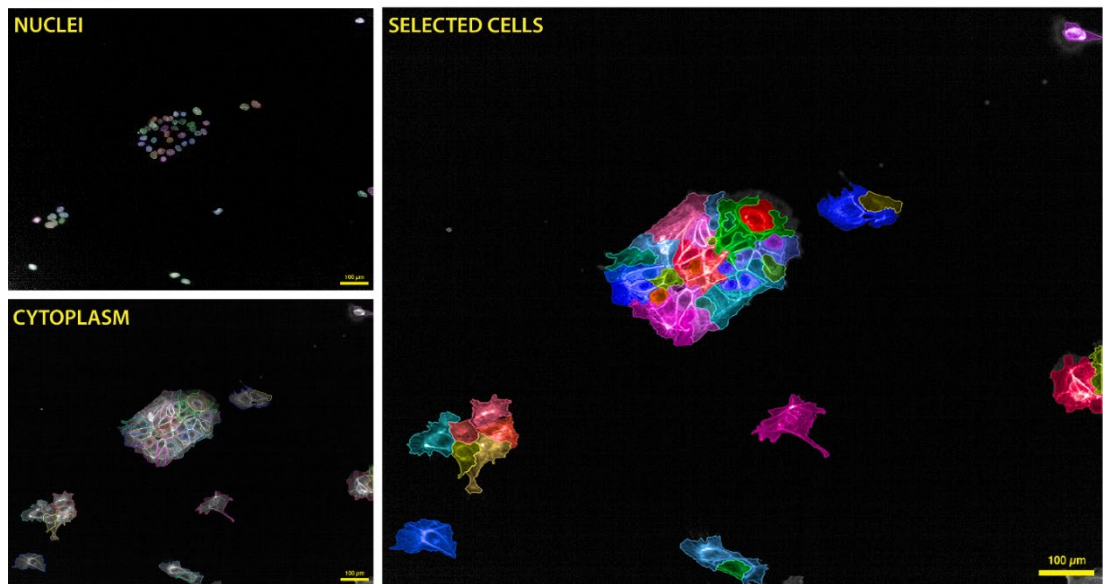
(C)

BMOL-TAT<sup>C-MET WT</sup>



(D)

BMOL-TAT<sup>C-MET KO</sup>



(E)

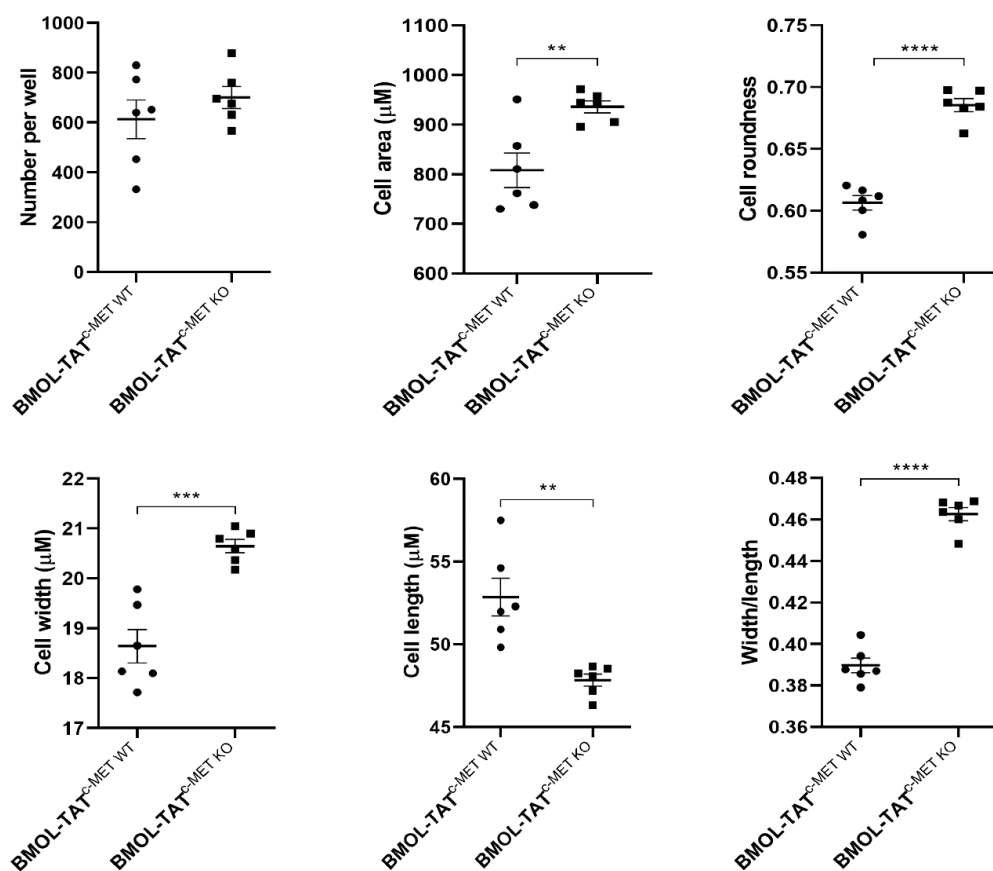


**Figure 4.4: Morphological assessment by Operetta of BMOL-TAT<sup>c-MET</sup> WT and BMOL-TAT<sup>c-MET</sup> KO cells.**

The Operetta CLS<sup>TM</sup> High-Content Analysis System demonstrating Hoechst 33342 and Phalloidin staining of BMOL-TAT<sup>c-MET</sup> WT and BMOL-TAT<sup>c-MET</sup> KO cells (A, B). Images were segmented with Harmony software 4.9 to find nuclei and cytoplasm of selected cells (C, D). Quantification of cell segmentation illustrated in (E). BMOL-TAT<sup>c-MET</sup> KO cells present to be significantly rounder, with a greater cell area and width/length ratio.

Scale bar depicting 100 μm. Data represent the mean ± SEM. n = 3.

\*\*P < 0.01, \*\*\*P < 0.001 and \*\*\*\*P < 0.0001.



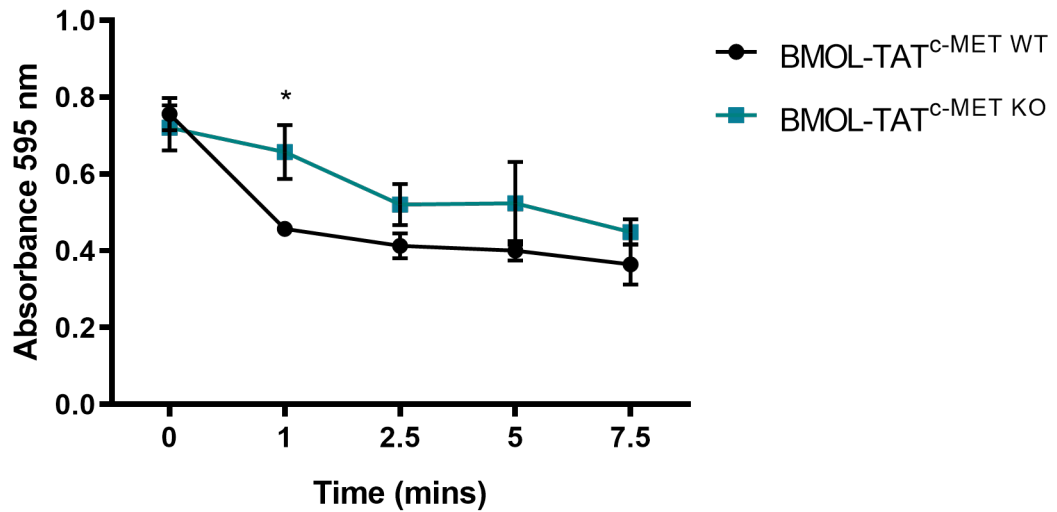


**Figure 4.5: The effect of c-MET knockout in BMOL-TAT cells on cell adherence.**

A cell adherence assay revealed significantly greater adherence of c-MET deleted cells compared to the respective controls at the 1-minute timepoint of trypsinisation.

Data represent the mean  $\pm$  SEM. n= 3. \*P < 0.05.

#### 4.4.3 The effect of c-MET knockout on cell apoptosis, viability, proliferation and migration

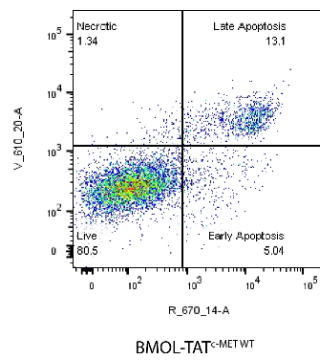
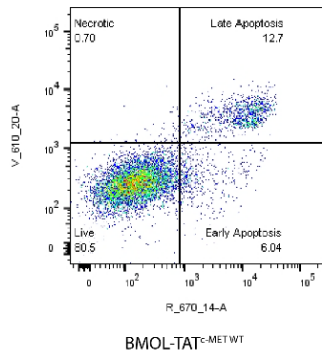
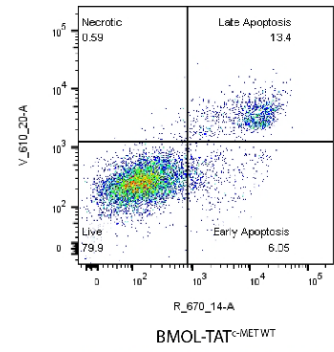
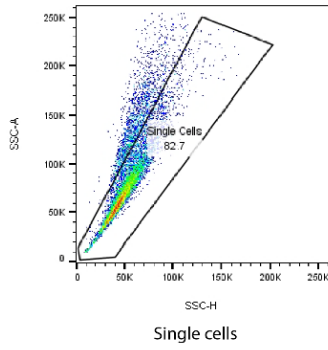
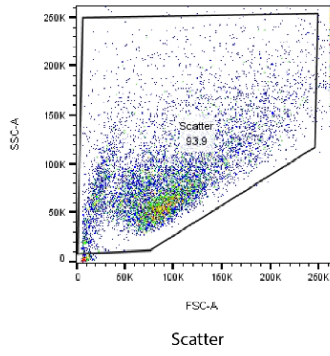
Visually, a higher degree of apoptosis was observed in the c-MET-deleted BMOL-TAT sister cell line when in culture. To measure the degree of apoptosis and whether this effect was c-MET-dependent, an Annexin V apoptosis assay was performed. In comparison to BMOL-TAT<sup>c-MET WT</sup> cells in single culture, BMOL-TAT<sup>c-MET KO</sup> cells demonstrated a higher degree of early (Annexin V-FITC<sup>+</sup>/PI<sup>-</sup>), and late-stage apoptosis (Annexin V-FITC<sup>+</sup>/PI<sup>+</sup>) (Figure 4.6).

The BMOL-TAT<sup>c-MET WT</sup> and BMOL-TAT<sup>c-MET KO</sup> cell viability rates were indirectly assessed through an MTT assay, measuring mitochondrial metabolic rates. After 72 hours, the BMOL-TAT<sup>c-MET KO</sup> cells were significantly less viable than their wildtype counterparts (Figure 4.7).

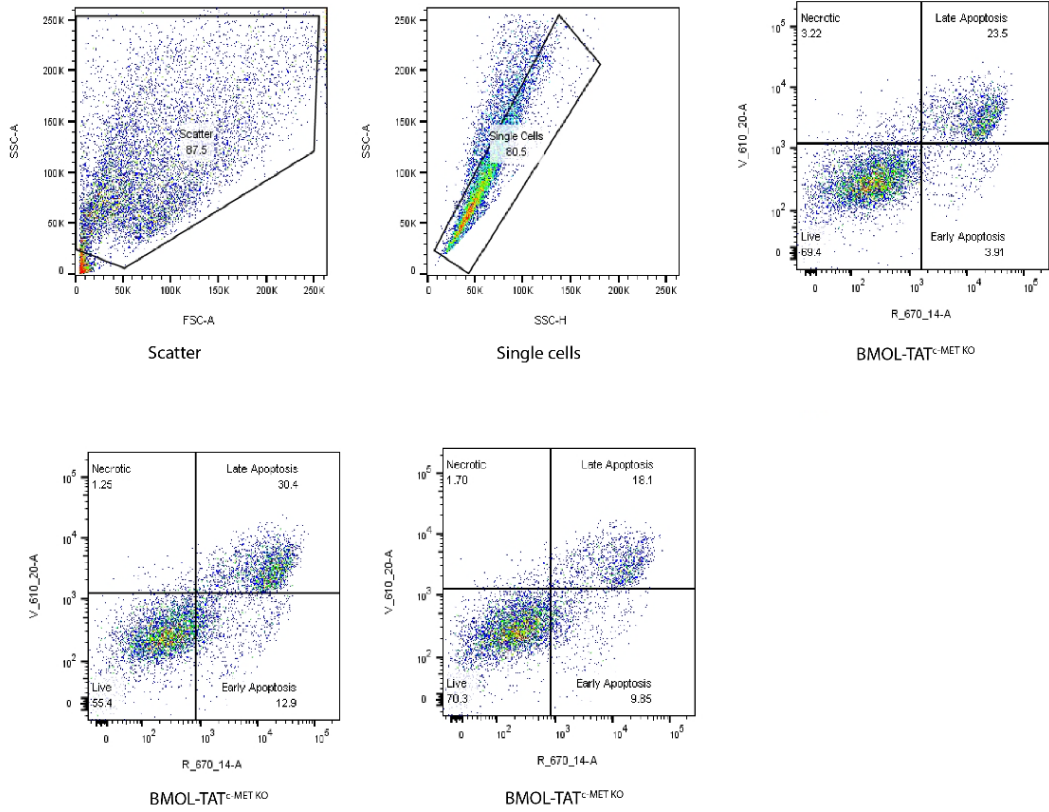
A similar experiment, the MTS assay, was undertaken to directly measure the proliferative capacity of the BMOL-TAT<sup>c-MET WT</sup> and BMOL-TAT<sup>c-MET KO</sup> cells. The BMOL-TAT<sup>c-MET KO</sup> cells were significantly less proliferative, as compared to the BMOL-TAT<sup>c-MET WT</sup> cells (Figure 4.8).

Next, migratory differences between BMOL-TAT<sup>c-MET WT</sup> and BMOL-TAT<sup>c-MET KO</sup> cells were assessed, through a wound healing experiment. Following live cell imaging over 34 hours, it was evident that the BMOL-TAT<sup>c-MET KO</sup> cells had a reduced migratory capacity with no wound closure at 28 hours, when compared to their wildtype counterparts (Figure 4.9).

(A)



(B)



(C)

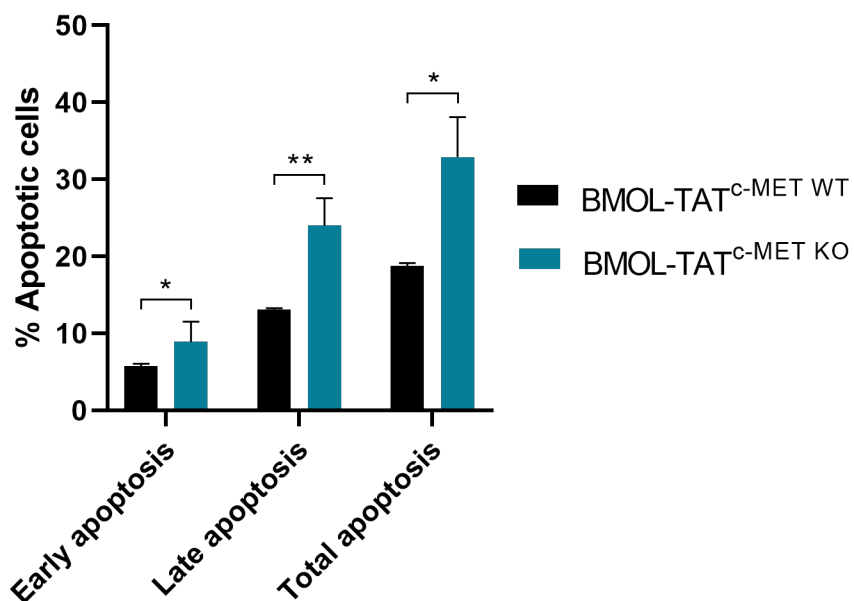


**Figure 4.6: Annexin V apoptosis assay of BMOL-TAT<sup>c-MET</sup> WT and BMOL-TAT<sup>c-MET</sup> KO cells.**

Culture of BMOL-TAT<sup>c-MET</sup> KO cells resulted in significantly higher levels of early (Annexin V-FITC<sup>+</sup>/PI<sup>-</sup>), and late-stage (Annexin V-FITC<sup>+</sup>/PI<sup>+</sup>) apoptosis (B,C), compared to the BMOL-TAT<sup>c-MET</sup> WT cells cultured under the same conditions (A,C).

Data represent the mean  $\pm$  SEM. n= 3. \*\*\*P < 0.001, \*\*\*\*P < 0.0001.

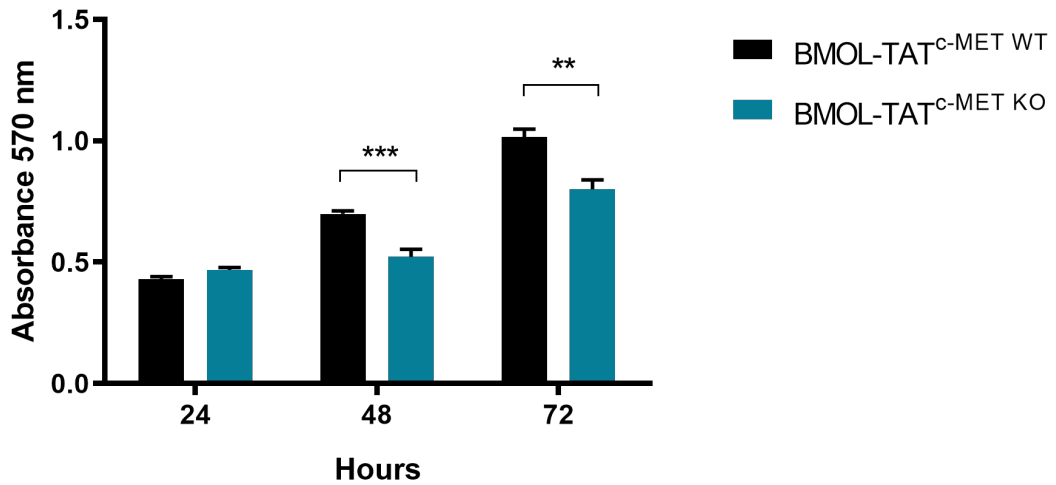


**Figure 4.7: Time course cell viability measurements of BMOL-TAT<sup>c-MET</sup> WT and BMOL-TAT<sup>c-MET</sup> KO cells.**

CRISPR/Cas9-mediated c-MET deletion resulted in significantly reduced BMOL-TAT cell viability at 48 and 72 hours of culture compared to BMOL-TAT<sup>c-MET</sup> WT control cells, as demonstrated by MTT assay. Data represent the mean  $\pm$  SEM.  $n=3$ . \*\* $P < 0.01$  and \*\*\* $P < 0.001$ .

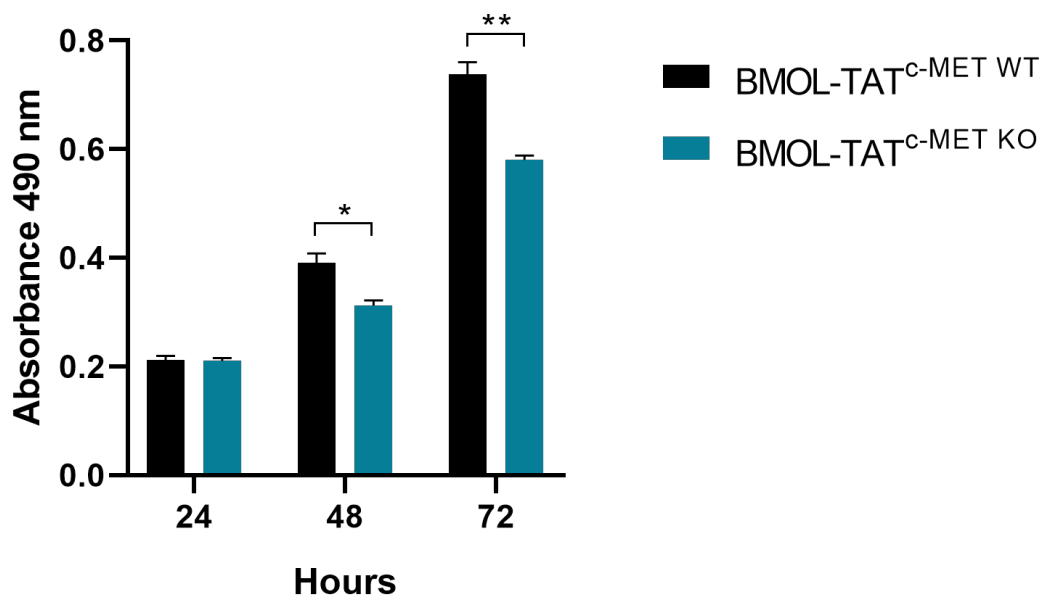
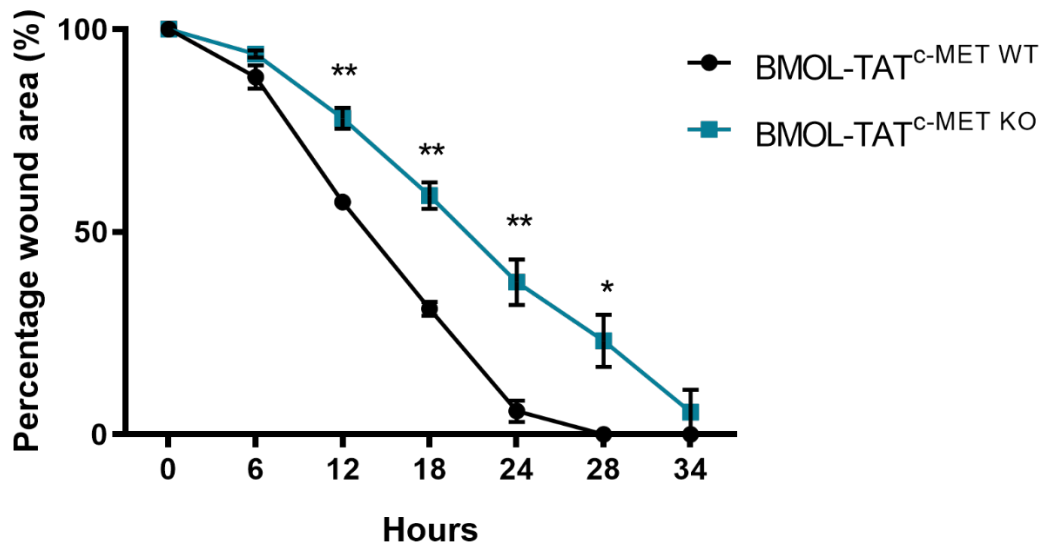


**Figure 4.8: Time course cell proliferation measurements of BMOL-TAT<sup>c-MET</sup> WT and BMOL-TAT<sup>c-MET</sup> KO cells.**

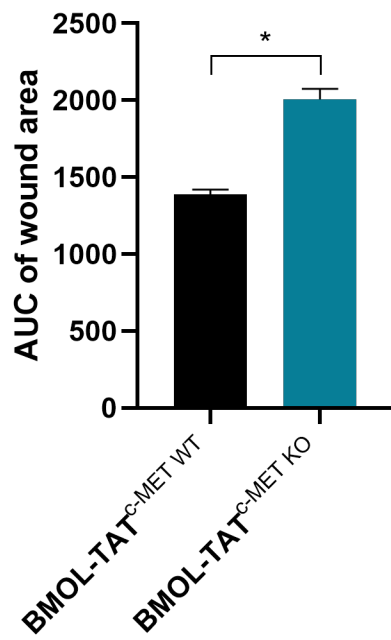
CRISPR/Cas9-mediated c-MET deletion resulted in significantly reduced BMOL-TAT cell proliferation at 48 and 72 hours of culture compared to BMOL-TAT<sup>c-MET</sup> WT control cells, as demonstrated by MTS assay.

Data represent the mean  $\pm$  SEM. n=3. \*P < 0.05 and \*\*P < 0.01.

(A)



(B)





(C)

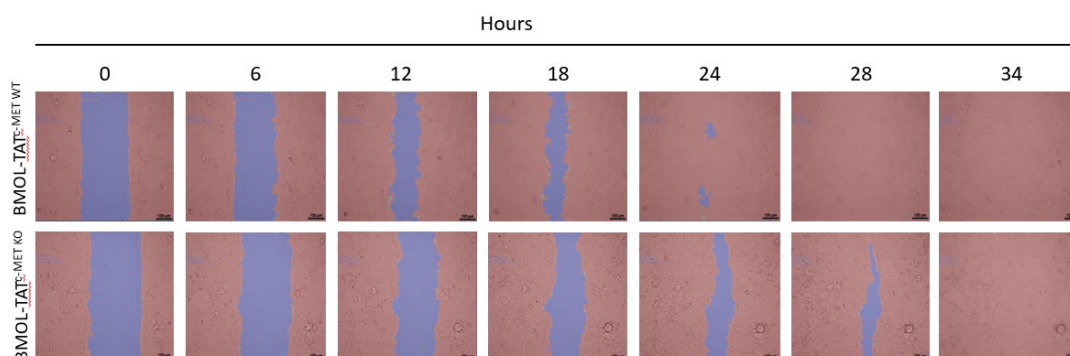


**Figure 4.9: The effect of c-MET knockout on BMOL-TAT cell migration.**

BMOL-TAT<sup>c-MET</sup> WT and BMOL-TAT<sup>c-MET</sup> KO cells were subjected to a wound healing assay and incubated for 34 hours in total. (A) Deletion of the c-MET receptor in BMOL-TAT cells resulted in significantly slower cell migration and wound closure compared to the c-MET control cell line, as judged by percentage of wound area (A) and a significantly greater area under the curve (AUC) (B). The reduced migratory capacity of the BMOL-TAT<sup>c-MET</sup> KO cells is also visually demonstrated by brightfield microscopy (C).

Data represent the mean  $\pm$  SEM. n= 3. \*P < 0.05, \*\*P < 0.01.

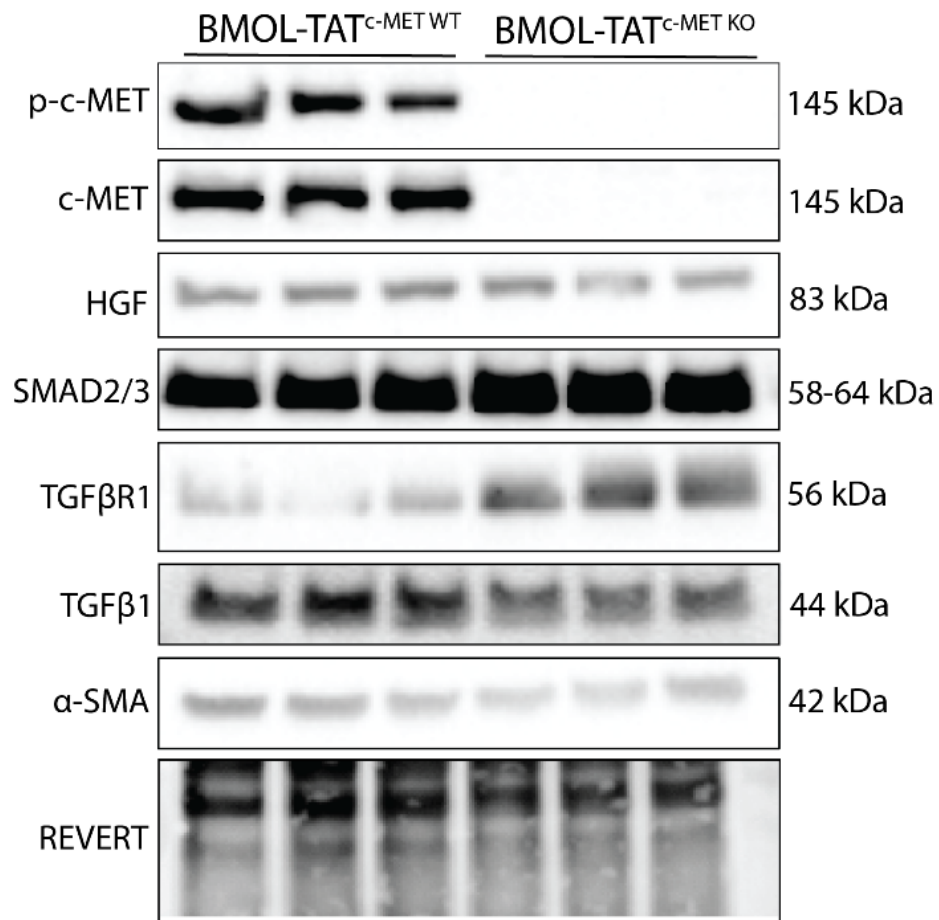
#### 4.4.4 The effect of c-MET knockout on TGF $\beta$ signalling and epithelial-to-mesenchymal transition markers

Western blot analysis on BMOL-TAT<sup>c-MET KO</sup> confirmed no detectable levels of c-MET and p-c-MET, as compared to their wildtype counterparts. However, HGF was demonstrated to be constitutively expressed by the knockout cells. Lack of the c-MET receptor appeared to significantly increase the levels of the TGF $\beta$  pathway components SMAD2/3 and TGF $\beta$ R1, in knockout cells. Despite the increase in TGF $\beta$  signalling components, the expression of the fibrogenic marker  $\alpha$ SMA remained unchanged (Figure 4.10).

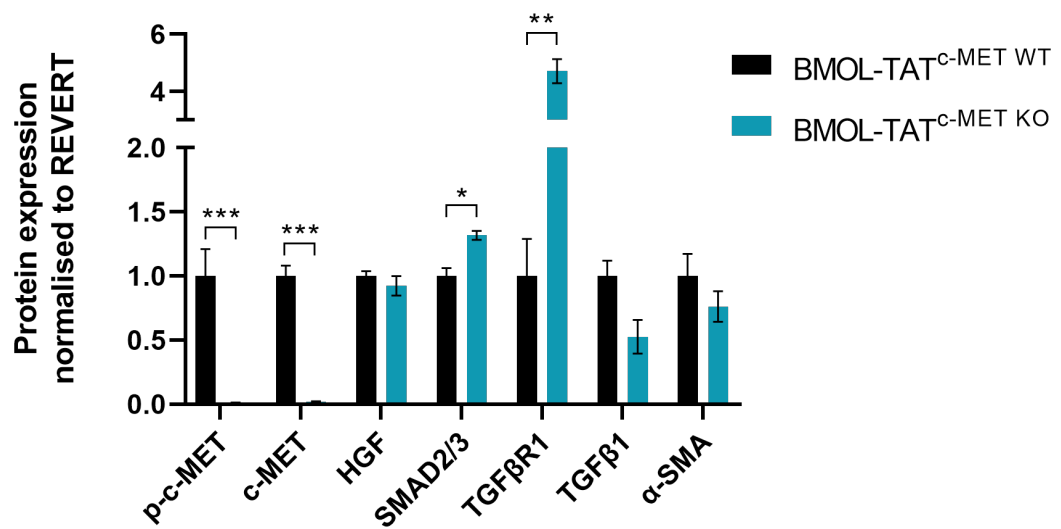
Immunofluorescent staining of phospho-SMAD2 and total-SMAD2 further demonstrated the upregulation of TGF $\beta$  pathway components in BMOL-TAT<sup>c-MET KO</sup> cells, compared to their wildtype counterparts (Figure 4.11).

Considering that TGF $\beta$  pathway components were upregulated in BMOL-TAT<sup>c-MET KO</sup> cells, investigating a potential EMT shift was of interest. Immunofluorescent analysis of the BMOL-TAT<sup>c-MET WT</sup> and BMOL-TAT<sup>c-MET KO</sup> cells revealed that the mesenchymal markers N-cadherin and vimentin were highly expressed by the BMOL-TAT<sup>c-MET KO</sup> cells, which was associated with reduced expression of the epithelial marker E-cadherin, as compared to BMOL-TAT<sup>c-MET WT</sup> cells (Figure 4.12). This suggests that the BMOL-TAT<sup>c-MET KO</sup> cells have undergone partial EMT-like changes.

(A)



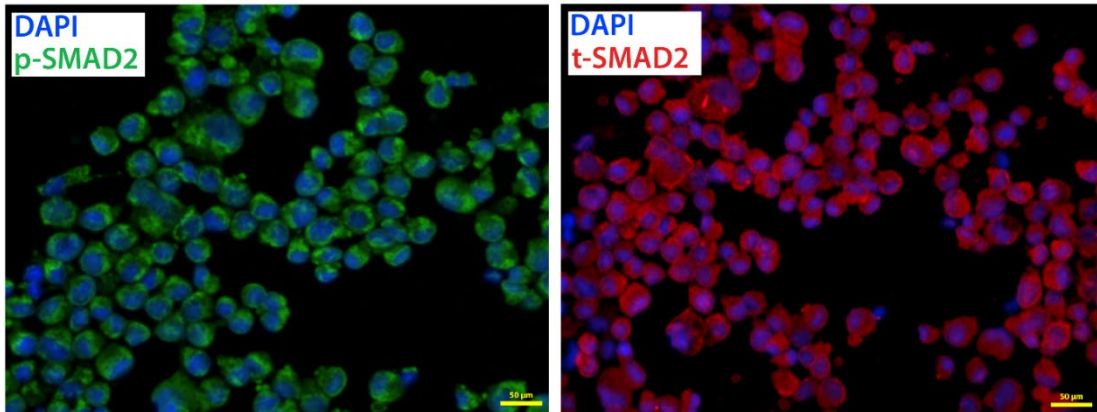
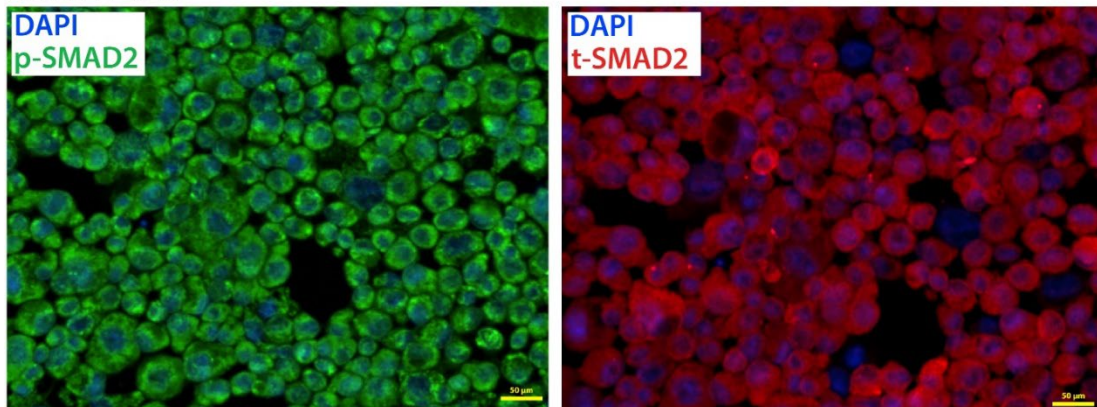
(B)



**Figure 4.10: Expression and semi-quantitation of HGF/c-MET and TGF $\beta$  pathway components in BMOL-TAT<sup>c-MET WT</sup> and BMOL-TAT<sup>c-MET KO</sup> cells.**

Analysis of phospho-c-MET (p-c-MET) and c-MET by western blot (A) and semi-quantitation by densitometry (B) confirmed complete knockout of the c-MET receptor in the BMOL-TAT<sup>c-MET KO</sup> cell line. While the expression of HGF,  $\alpha$ SMA and TGF $\beta$ 1 was not significantly altered between both lines, protein levels of SMAD2/3 and TGF $\beta$ R1 were significantly increased following c-MET deletion.

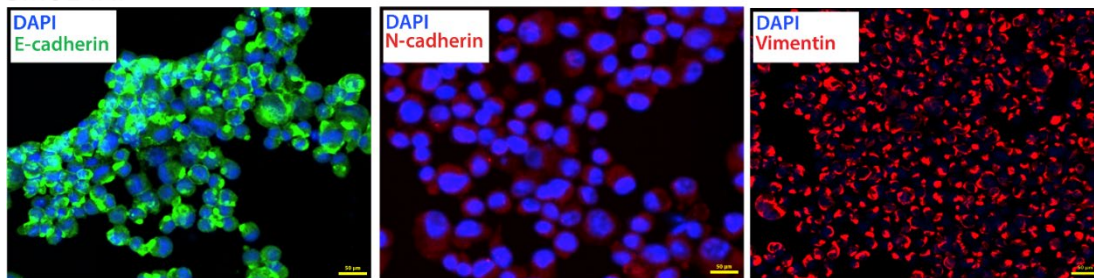
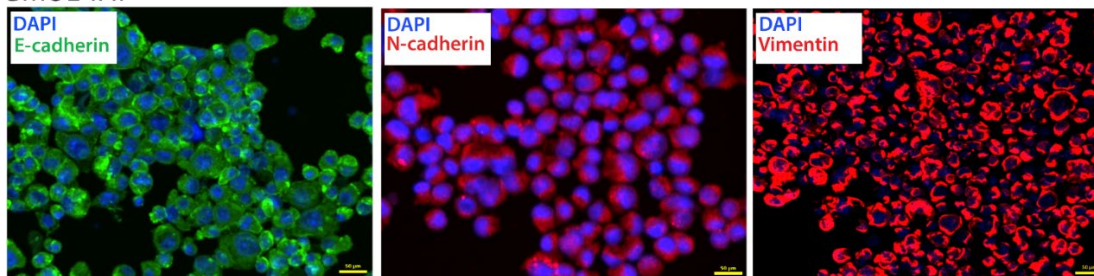
Data represent the mean  $\pm$  SEM. n= 3. \*P < 0.05, \*\*P < 0.01, \*\*\*P < 0.001.

**(A)**BMOL-TAT<sup>c-MET WT</sup>**(B)**BMOL-TAT<sup>c-MET KO</sup>

**Figure 4.11: Expression of TGF $\beta$  signalling components by immunofluorescence in BMOL-TAT<sup>c-MET WT</sup> and BMOL-TAT<sup>c-MET KO</sup> cells.**

Increased phosphorylation of SMAD2 (p-SMAD2) as well as increased expression of total SMAD2 (t-SMAD2) was evident in BMOL-TAT<sup>c-MET KO</sup> cells (B) compared to BMOL-TAT<sup>c-MET WT</sup> cells (A).

Scale bar depicting 50 µm, data represent n=3.

**(A)**BMOL-TAT<sup>c-MET WT</sup>**(B)**BMOL-TAT<sup>c-MET KO</sup>

**Figure 4.12: Expression analysis of EMT markers by immunofluorescence in BMOL-TAT<sup>c-MET WT</sup> and BMOL-TAT<sup>c-MET KO</sup> cells.**

A greater expression of the epithelial marker E-cadherin was evident the in BMOL-TAT<sup>c-MET WT</sup> cells (A). Conversely, in the BMOL-TAT<sup>c-MET KO</sup> cells, greater expression of mesenchymal markers N-cadherin and vimentin was demonstrated (B).

Scale bar depicting 50  $\mu$ m.

## 4.5 Discussion

Many studies have identified LPCs cells as pro-fibrotic in nature (Best et al., 2015) (Roskams, 2006). However, over the last decade, LPCs have been recognised as a highly heterogenous population, with their phenotype and function dependent on the surrounding microenvironment (Kohn-Gaone et al., 2016). Recent experimental evidence suggests that LPCs may act as regulatory cells, potentially modulating the fibrogenic response through cell-cell communication with HSCs (Gratte et al., 2021). It has also been reported that the HGF/c-MET pathway has an anti-fibrotic role during chronic liver disease, influencing LPC function. In Chapter 3, it was established that the c-MET receptor is present on LPCs. The work presented in Chapter 4 then focused on deleting c-MET through CRISPR/Cas9 technology to generate a suitable *in vitro* model to study the direct effects of HGF/c-MET signalling on LPC biology.

CRISPR/Cas9 technology is known to be an accurate method of deleting a gene of interest (Uddin et al., 2020) and was therefore selected to target the c-MET receptor in the LPC line BMOL-TAT. The standard procedure is performed using a high-throughput sorter to separate the guide-transfected cells (Giuliano, Lin, Girish, & Sheltzer, 2019). However, in BMOL-TAT cells, this method led to reduced viability and inability to survive single cell culture to generate a clonal cell line. Instead, limiting dilution cloning (Greenfield, 2019) (Ye, Wilhelm, Gentshev, & Szalay, 2021) was performed, where cells were sorted, and allowed to recover for 24 hours, followed by manual single cell seeding. This gentler technique aided in generating three successful clonal BMOL-TAT<sup>c-MET KO</sup> cell lines. Considering that c-MET is an essential gene during fetal development and deletion of c-MET in mice is embryonically lethal, (Ishikawa et al., 2012) (Bladt, Riethmacher, Isenmann, Aguzzi, & Birchmeier, 1995), creating a clonal c-MET knockout cell line was challenging but was successfully completed.

Studies greatly focus on c-MET deletion in whole organ systems (Borowiak et al., 2004) (Huh et al., 2004), which represent complex environments with



multifaceted interplays between cells. Therefore, it can be difficult to find separation between direct and indirect effects in such microenvironments. Successful generation of a c-MET LPC *in vitro* model made it possible to study the direct effects of c-MET receptor signalling loss on LPC biology. Phenotypically, the BMOL-TAT<sup>c-MET KO</sup> cells displayed a clump-like morphology compared to the BMOL-TAT<sup>c-MET WT</sup> cells. The c-MET ligand HGF, also known as 'scatter factor', has been noted by Chan *et al.*, to induce scattering of pancreatic adenocarcinoma cells, with inhibition of HGF generating clumping of cells in culture (G. K. Y. Chan, Lutterbach, Pan, Kariv, & Szewczak, 2008). This finding was reproduced in the novel BMOL-TAT<sup>c-MET KO</sup> model, where lack of c-MET signalling reduced cell scattering, and increased cell adherence.

Visual assessment of BMOL-TAT<sup>c-MET WT</sup> and BMOL-TAT<sup>c-MET KO</sup> cells in culture led to greater apoptosis in the BMOL-TAT<sup>c-MET KO</sup> cells. To investigate whether this apoptotic effect was dependent on the presence or absence of the c-MET receptor in BMOL-TAT cells, an Annexin V apoptosis assay by flow cytometry was performed. The results demonstrated an increase in early- and late-stage cell apoptosis in the BMOL-TAT<sup>c-MET KO</sup> cells, as compared to their wildtype counterparts, suggesting that deletion of the c-MET receptor decreases their viability. The importance of c-MET on LPC viability has been previously reported by Castillo and colleagues, where c-MET-deleted LPCs were more susceptible to apoptosis (del Castillo *et al.*, 2008). In future, investigating the underlying mechanism for this elevated apoptosis in c-MET knockout cells will be of interest.

Further, compared to the wildtype control cells, the BMOL-TAT<sup>c-MET KO</sup> cell line showed a significant reduction in cell viability and proliferation by 48 hours, as judged by MTT and MTS assays. These results are consistent with the literature, as c-MET KO mice have been reported to have decreased amounts of viable LPCs (Ishikawa *et al.*, 2012). In addition, it has been established that the c-MET receptor has importance for LPC expansion during chronic liver disease (Almalé *et al.*, 2019) (Suárez-Causado *et al.*, 2015). Therefore, a decrease in BMOL-TAT<sup>c-MET KO</sup> cell proliferation further corroborates this finding.



Next, assessment of cell migration following c-MET deletion was explored. BMOL-TAT<sup>c-MET KO</sup> cells had a significant decrease in migratory capacity compared to their wildtype counterpart, as judged by a wound healing assay. This has been previously reported in an *in vivo* study by Suárez-Causado and colleagues, where deletion of c-MET in LPCs caused apoptosis and growth arrest in cells, which could not be saved by the addition of HGF (Suárez-Causado et al., 2015). Additionally, the activation of c-MET by HGF, has been noted to be vital for inducing metalloproteinase (MMP) activity in migrating LPCs, in turn, degrading extracellular matrix and contributing to tissue repair. On the background of the HGF/c-MET pathway having anti-fibrotic effects in the liver, these results provided evidence that without c-MET regulation, LPCs cannot migrate to sites of injury and aid in the wound healing process.

Further, investigation into protein expression confirmed the deletion of c-MET in the knockout cells. However, interestingly, HGF was still expressed at comparable levels to BMOL-TAT<sup>c-MET WT</sup> cells, suggesting autocrine activation. This result was also identified by Castillo *et al.*, who proposed that the constitutive expression of HGF had anti-apoptotic effects in LPCs (del Castillo et al., 2008). Moreover, the HGF/c-MET signalling pathway has been noted to antagonise TGF $\beta$  signalling (Papa et al., 2017). Therefore, western blot analysis for relevant pathway components was undertaken and demonstrated a significant increase in key TGF $\beta$  pathway components including TGF $\beta$ R1 and SMAD2/3 in BMOL-TAT<sup>c-MET KO</sup> cells. This was confirmed by immunofluorescence, which demonstrated the increased phosphorylation of SMAD2 in BMOL-TAT<sup>c-MET KO</sup> cells, indicating increased TGF $\beta$  pathway signalling. As an upregulation of TGF $\beta$  is characteristic of an EMT process (Almalé et al., 2019), immunofluorescent staining was performed and determined that BMOL-TAT<sup>c-MET KO</sup> cells had greater expression of the mesenchymal markers N-cadherin and vimentin and lower expression levels of the epithelial marker E-cadherin, compared to BMOL-TAT<sup>c-MET WT</sup> cells. This suggests that in the absence of c-MET, the cells have undergone a partial EMT-like change.

In the future, injecting the BMOL-TAT<sup>c-MET KO</sup> cells into immunocompromised mice or subjecting LPC-specific c-MET KO mice to a chronic liver injury diet, would allow for a more complete characterisation of LPCs without c-MET regulation. Further, exploring the mechanism for the antagonistic role of HGF/c-MET and TGF $\beta$  signalling in relation to EMT is of interest in *in vitro* and *in vivo* models. Nonetheless, this chapter describes the establishment of a novel LPC-specific c-MET cell culture model and provides an important contribution to our understanding of the vital role of the HGF/c-MET pathway in terms of LPC biology, EMT and TGF $\beta$  pathway regulation *in vitro*.

**Chapter 5: Cellular effects of liver progenitor cell-hepatic stellate cell  
*in vitro* co-culture**

Parts of this chapter have already been peer-reviewed and published. The manuscript is included in the Appendix of this document.

F. G. Gratte, **S. Pasic**, N. D. B. Abu Bakar, J. Gogoi Tiwari, X. Liu, R. Carlessi, T. Kisseleva, D. A. Brenner, G. A. Ramm, J. K. Olynyk, and J. E. E. Tirnitz-Parker. Previous liver regeneration induces fibro-protective mechanisms during thioacetamide induced chronic liver injury. *Int J Biochem Cell Biol* (2021),134: 105933.

## 5.1 Introduction

In the literature, LPCs have traditionally been portrayed as pro-fibrotic in nature (Jakubowski et al., 2005) (Spee et al., 2010) (Kohn-Gaone et al., 2016). This hypothesis is based on the general finding that increasing LPC numbers positively correlate with progressing stages of liver disease (Lowes et al., 1999). Yet, it is not understood whether LPC presence and action are key regulatory factors or rather a consequence of liver disease progression. In the so-called liver disease and regeneration niche, the LPCs interact with the HSCs (Kohn-Gaone et al., 2016) to establish and regulate their surrounding hepatic microenvironment (Van Hul et al., 2009). Since LPCs and fibrosis-driving HSCs are generally spatially proximal, there is the significant potential for cellular crosstalk to drive liver regeneration or induce disease progression. Van Hul and colleagues investigated this cellular niche in chronically injured mice fed a CDE diet and reported that LPCs infiltrate the liver parenchyma alongside  $\alpha$ SMA-positive cells, hypothesised to be HSCs (Van Hul et al., 2009). Regenerative LPC-HSC crosstalk has been reported by Ruddell *et al.* using the same mouse model stated above, where the interaction of ligand/receptor communication of lymphotoxin  $\beta$ -expressing LPCs and lymphotoxin  $\beta$  receptor-positive HSCs regulated the cells' co-migration to injury sites (Ruddell et al., 2009) (Dwyer et al., 2014).

Recently published data, also presented in this chapter, suggest that LPCs are involved in the regulation of HSCs and, therefore, fibrogenesis (Gratte et al., 2021). Primary murine HSCs, when indirectly co-cultured in a Boyden chamber system with the clonal LPC line BMOL-TAT, downregulated the fibrosis-associated markers TGF $\beta$ ,  $\alpha$ SMA and collagen 1, suggesting that LPCs influence HSC behaviour (Gratte et al., 2021). However, the underlying mechanisms of this regulation are unknown.

The HGF/c-MET pathway has been described to promote liver cancer (Venepalli & Goff, 2013) (H. Wang et al., 2020), yet to be anti-fibrotic in other contexts, where it favours LPC expansion and migration, aiding in liver regeneration (Borowiak et al., 2004) (Inagaki et al., 2008) (Ishikawa et al.,

2012). Consequently, this suggests that the downstream effects of the HGF/c-MET signalling pathway axis are context- and disease stage-dependent. As HSCs secrete the ligand HGF and the LPCs present the c-MET receptor on their surface (Organ & Tsao, 2011), this signalling pathway was considered as an appropriate candidate to study cellular effects during LPC-HSC crosstalk.

## 5.2 Study aims

In Chapter 4, the establishment of a novel cell culture model using CRISPR/Cas9 technology to study the role of HGF/c-MET signalling in LPCs *in vitro* was described. The BMOL-TAT<sup>c-MET KO</sup> cells had an altered phenotype, with decreased proliferative and migratory capacities.

Since the previous *in vitro* c-MET knockout studies assessed cells in isolation, the aim of this chapter was to investigate the BMOL-TAT<sup>c-MET WT</sup> and BMOL-TAT<sup>c-MET KO</sup> cells in co-culture with the HSC line LX-2. This was achieved in a direct co-culture system, and indirectly, using Boyden chambers to better understand the importance of HGF/c-MET crosstalk in cellular phenotype regulation, with a particular focus on fibrogenesis.

### 5.3 Methodology

To investigate the hypothesis that LPCs regulate HSC behaviour through the HGF/c-MET signalling pathway, the BMOL-TAT<sup>c-MET WT</sup> and BMOL-TAT<sup>c-MET KO</sup> LPC lines were co-cultured with the HSC line LX-2, characterised in Chapters 3 and 4.

Following 48-hour direct 2D co-culture of either BMOL-TAT<sup>c-MET WT</sup> or BMOL-TAT<sup>c-MET KO</sup> cell lines with LX-2 cells (2.2.2.15), their morphology and spatial arrangement was examined using brightfield microscopy, followed by immunofluorescence of specific markers for each cell type (LPC, CK19; HSC,  $\alpha$ SMA) (2.2.3.4, Table 2.1). Additionally, a cell apoptosis assay was performed by flow cytometry (2.2.2.16) to analyse whether direct cell contact with LX-2 cells induced cell death in BMOL-TAT cells and whether this effect was c-MET-dependent. The same co-culture combinations and spatial arrangement analysis was achieved following direct 3D co-culture using the Inventia RASTRUM Bioprinter (2.2.2.14) with liver-specific matrix conditions (RGD,  $\sim$ 0.7 kPa), simulating the liver ECM microenvironment more closely.

Next, indirect co-culture was performed to analyse cellular crosstalk between the BMOL-TAT<sup>c-MET WT</sup> or BMOL-TAT<sup>c-MET KO</sup> cells with LX-2 cells. The Boyden chamber system is a reliable method to recapitulate *in vivo* crosstalk since it creates close spatial arrangement of the cells and allows diffusion of signalling molecules across the membrane. Migration of the wildtype and c-MET knockout BMOL-TAT cell line toward the LX-2 cell line and *vice versa* was analysed by a Boyden chamber migration assay, following a 4-hour incubation period (2.2.2.19).

Next, after 48-hour Boyden chamber co-culture of LX-2 cells with either BMOL-TAT<sup>c-MET WT</sup> or BMOL-TAT<sup>c-MET KO</sup> cells (2.2.2.18), total protein was extracted from the LX-2 cells to determine changes in fibrogenic markers ( $\alpha$ SMA, vimentin and collagen 1) as well as HGF/c-MET and TGF $\beta$  signalling pathway components (HGF, c-MET, TGF $\beta$ 1, TGF $\beta$ R1 and SMAD2/3) through western blot analysis (2.2.4.3, Table 2.1).

Lastly, following the same 48-hour Boyden chamber set up, the fibrotic status of the LX-2 cells was assessed using a commercially available collagen assay (2.2.2.20).



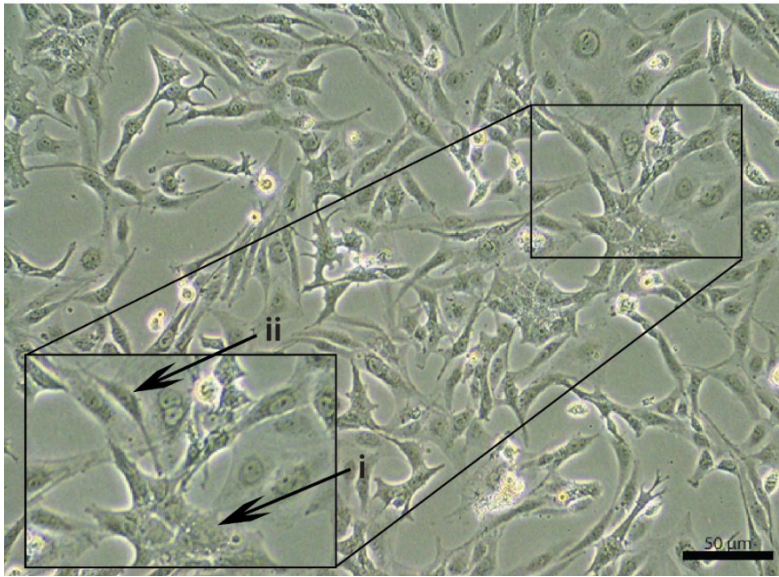
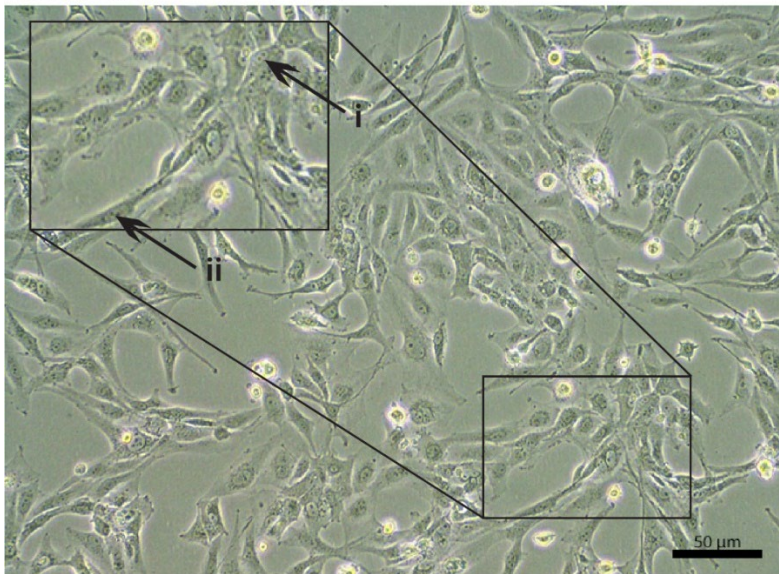
## 5.4 Results

### 5.4.1 Spatial arrangement of BMOL-TAT<sup>c-MET</sup> WT and BMOL-TAT<sup>c-MET</sup> KO cells in direct 2D and 3D co-culture with HSCs

Following direct 2D co-culture of LX-2 cells with either BMOL-TAT<sup>c-MET</sup> WT and BMOL-TAT<sup>c-MET</sup> KO cells, brightfield microscopy (Figure 5.1) and immunofluorescent staining (Figure 5.2) revealed that the BMOL-TAT cells organise themselves in cluster-like formations independent of their c-MET signalling status, whereas the LX-2 cells form branch-like networks between themselves and each BMOL-TAT cell line, consistent with an epithelial LPC and a mesenchymal HSC phenotype.

Furthermore, the spatial relationship between the investigated cell types was analysed in a 3D co-culture model using the Inventia RASTRUM Bioprinter. With the addition of a tissue-like matrix containing RGD, ~0.7 kPa, both the BMOL-TAT<sup>c-MET</sup> WT and BMOL-TAT<sup>c-MET</sup> KO cells displayed a spheroid-like morphology, whereas the LX-2 cells formed network-like structures, connecting groups of cells together, consistent with their growth characteristics in the 2D cultures (Figures 5.3 and 5.4).

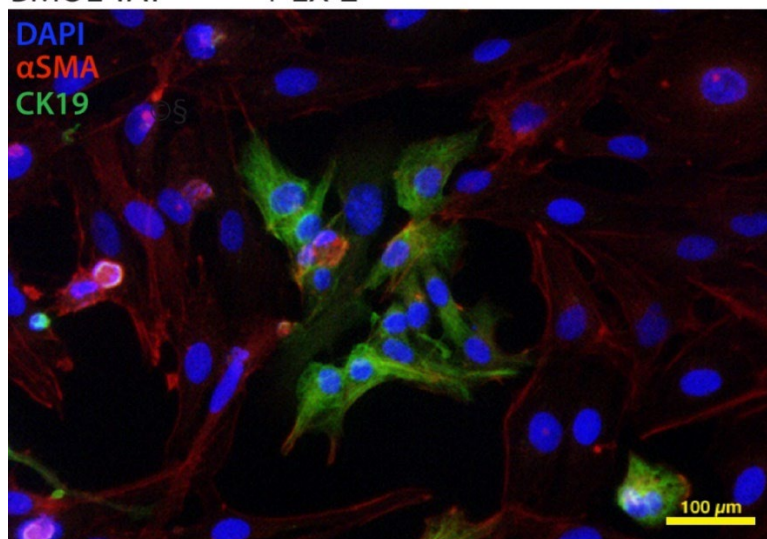
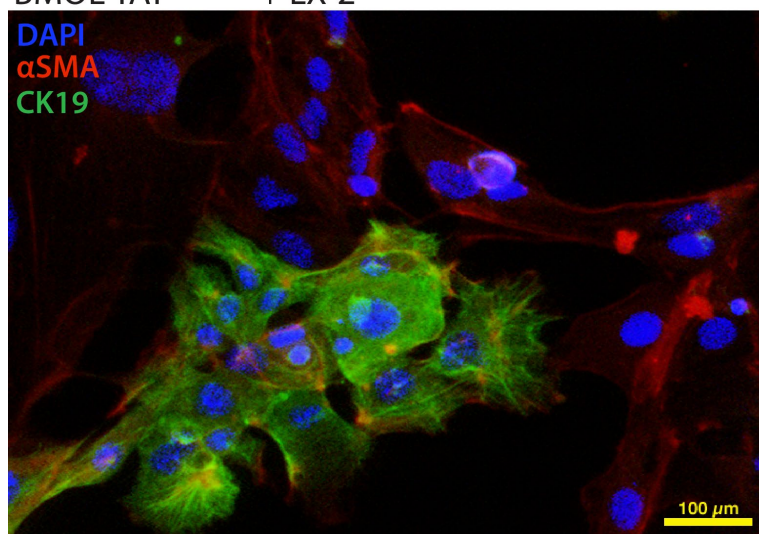
Visual assessment of BMOL-TAT cells in direct co-culture with LX-2 cells resulted in increased amounts of cell debris, therefore an Annexin V apoptosis assay was carried out. In comparison to single culture of the BMOL-TAT sister cell lines, their 2D direct co-culture with LX-2 cells stimulated a high degree of early- (Annexin V-FITC<sup>+</sup>/PI<sup>-</sup>), and late-stage (Annexin V-FITC<sup>+</sup>/PI<sup>+</sup>) apoptosis (Figure 5.5). Importantly, apoptosis was identified to be c-MET-independent. These data suggest that direct co-culture methods cause cell apoptosis in BMOL-TAT cells, proposing that indirect co-culture methods may be a more reliable and reproducible way of assessing cell functionality during crosstalk.

**(A)**BMOL-TAT<sup>c-MET WT</sup> + LX-2**(B)**BMOL-TAT<sup>c-MET KO</sup> + LX-2

**Figure 5.1: Spatial arrangement of LX-2 cells in direct 2D co-culture with BMOL-TAT<sup>c-MET WT</sup> and BMOL-TAT<sup>c-MET KO</sup> cells.**

Brightfield microscopy images of LX-2 cells (i) in direct 24-hour 2D co-culture with BMOL-TAT<sup>c-MET WT</sup> (A) and BMOL-TAT<sup>c-MET KO</sup> (B) cells (ii) revealed that both BMOL-TAT cell lines grow in a cluster-like formation surrounded by network-like growth of the LX-2 cells.

Scale bar depicting 50  $\mu\text{m}$ .

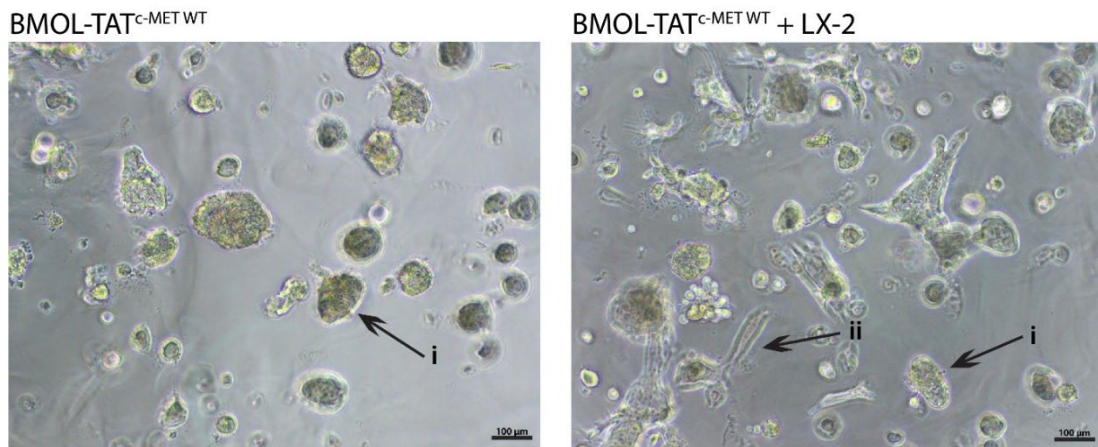
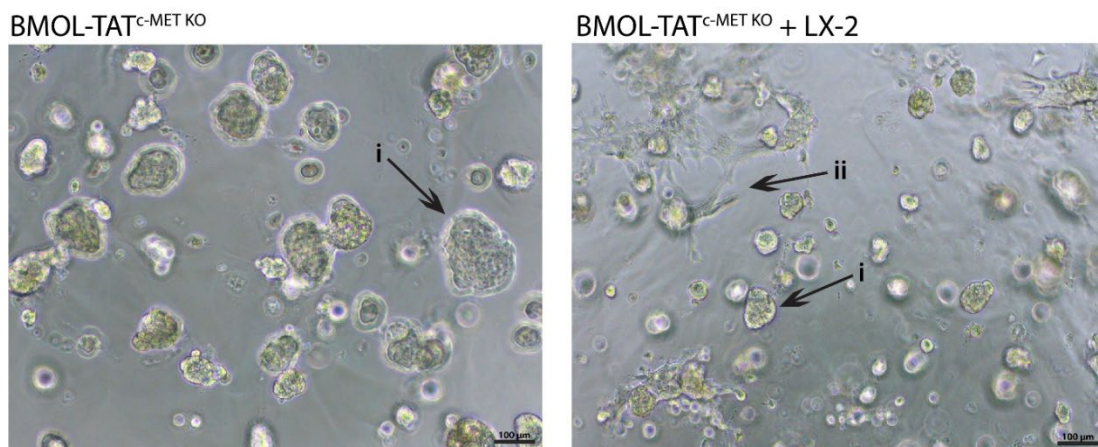
**(A)**BMOL-TAT<sup>c-MET WT</sup> + LX-2**(B)**BMOL-TAT<sup>c-MET KO</sup> + LX-2

**Figure 5.2: Assessment of the spatial arrangement by fluorescent labelling of LX-2 cells in direct 2D co-culture with BMOL-TAT<sup>c-MET WT</sup> and BMOL-TAT<sup>c-MET KO</sup> cells.**

Fluorescently labelled LX-2 cells ( $\alpha$ SMA) in direct 24-hour 2D co-culture with BMOL-TAT<sup>c-MET WT</sup> (A; CK19) and BMOL-TAT<sup>c-MET KO</sup> (B; CK19) cells. Wildtype and c-MET-deleted BMOL-TAT cell lines are arranged in cluster-like formations, surrounded by network-like growth arrangement of LX-2 cells.

Scale bar depicting 100  $\mu$ m.



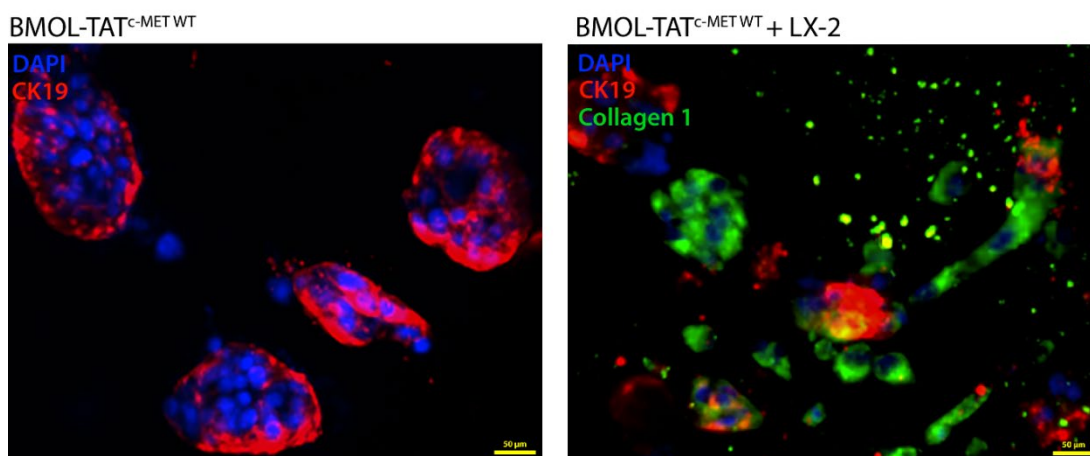
**(A)****(B)**

**Figure 5.3: Three-dimensional spatial arrangement of BMOL-TAT<sup>c-MET WT</sup> and BMOL-TAT<sup>c-MET KO</sup> cells in single culture and direct co-culture with LX-2 cells.**

Brightfield microscopy images of BMOL-TAT<sup>c-MET WT</sup> (A) and BMOL-TAT<sup>c-MET KO</sup> cells (B) in single culture (left) and in direct co-culture with LX-2 cells (right) after seven days in culture. Their 3D arrangement revealed that both BMOL-TAT cell lines grow in a cluster-like formations (i) surrounded by network-like growth of the LX-2 cells (ii).

Scale bar depicting 100  $\mu$ m.

(A)



(B)

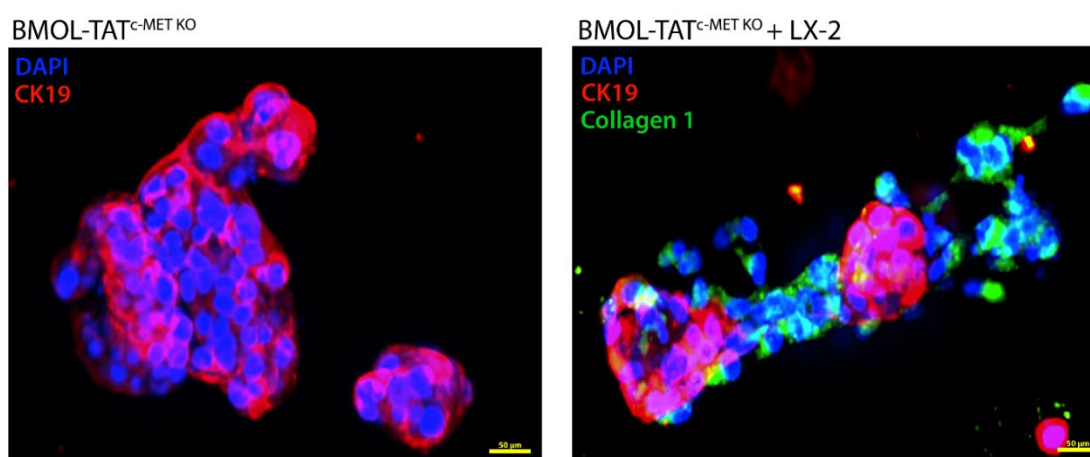
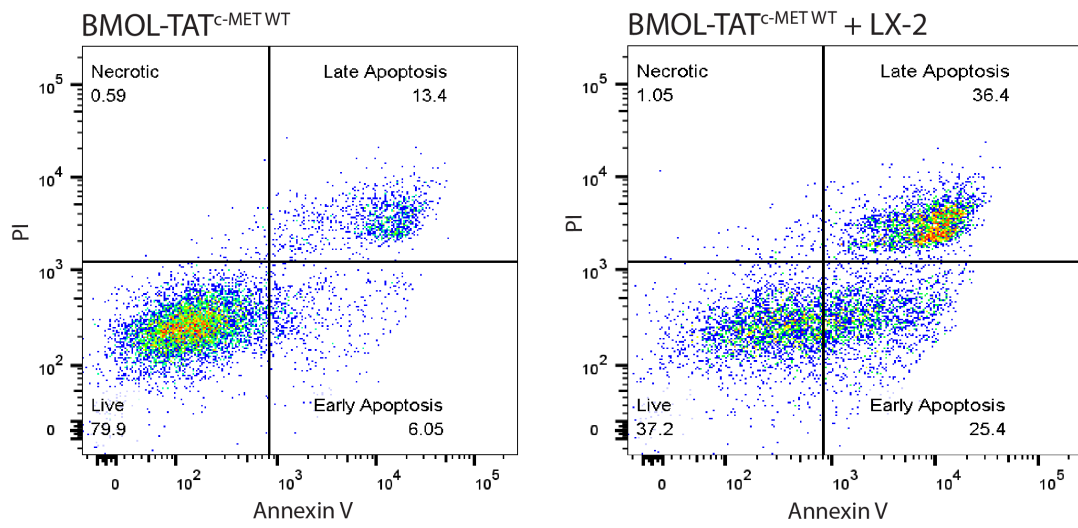


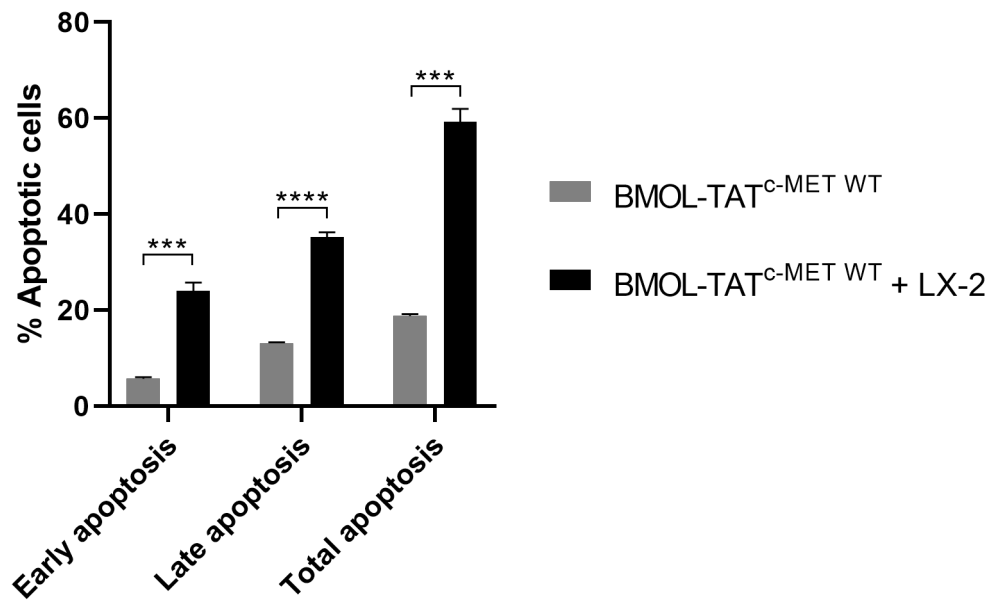
**Figure 5.4: Fluorescent labelling of BMOL-TAT<sup>c-MET<sup>WT</sup></sup> and BMOL-TAT<sup>c-MET<sup>KO</sup></sup> cells in single culture and direct co-culture with LX-2 cells representing their 3D spatial arrangement.**

Fluorescently labelled (CK19, red) BMOL-TAT<sup>c-MET<sup>WT</sup></sup> (A) and BMOL-TAT<sup>c-MET<sup>KO</sup></sup> (B) cells in single culture (left) and in direct 7-day co-culture with LX-2 cells (right; collagen 1, green). The cells' 3D organisation confirmed the 2D arrangement results, with both BMOL-TAT sister cell lines arranged in cluster-like formations, with LX-2 cells forming spheroids and networks around them. Scale bar depicting 50  $\mu$ m.

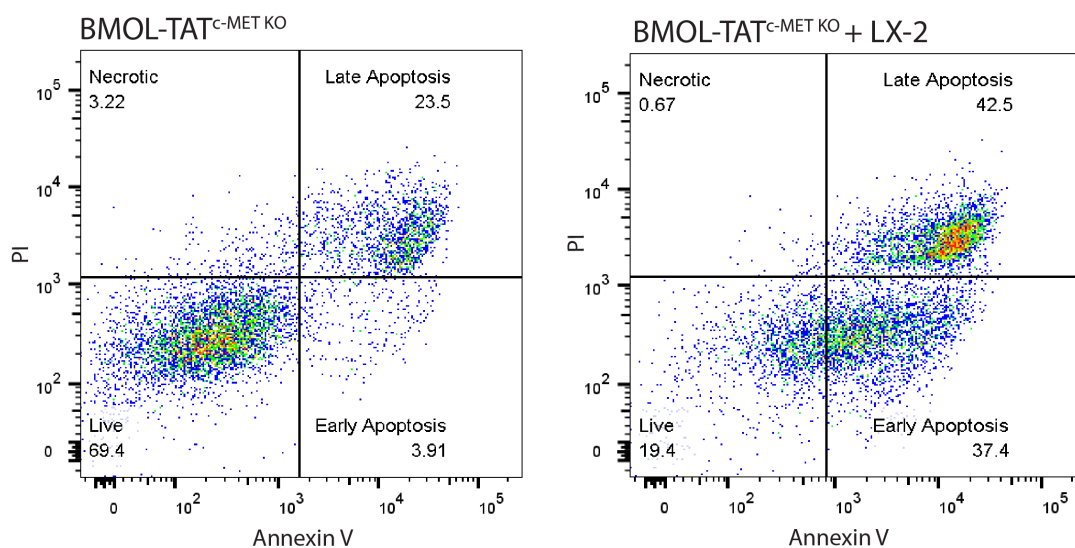
(A)



(B)



(C)



(D)

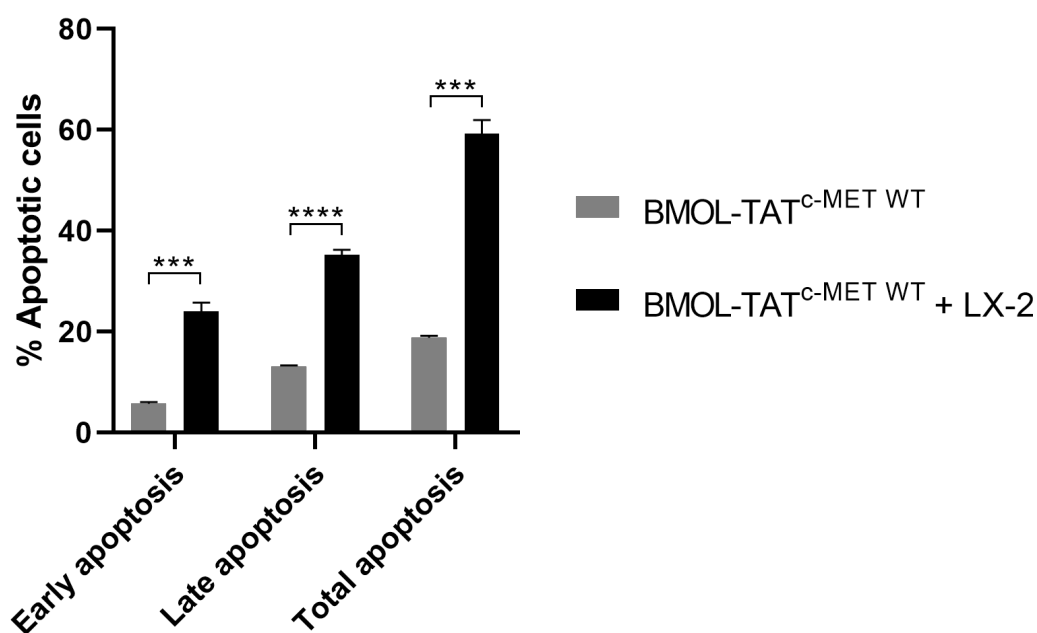


**Figure 5.5: Annexin V apoptosis assay following direct co-culture of BMOL-TAT<sup>c-MET WT</sup> and BMOL-TAT<sup>c-MET KO</sup> cells with LX-2 cells.**

Direct co-culture of BMOL-TAT<sup>c-MET WT</sup> and BMOL-TAT<sup>c-MET KO</sup> cells with LX-2 cells resulted in significantly higher levels of early- (Annexin V-FITC<sup>+</sup>/PI<sup>-</sup>), and late-stage (Annexin V-FITC<sup>+</sup>/PI<sup>+</sup>) apoptosis, compared to the cells grown in single culture.

Data represent the mean  $\pm$  SEM.  $n=3$ . \*\*\* $P < 0.001$ , \*\*\*\* $P < 0.0001$ .

#### 5.4.2 Chemoattraction of BMOL-TAT<sup>c-MET WT</sup> cells and LX-2 cells

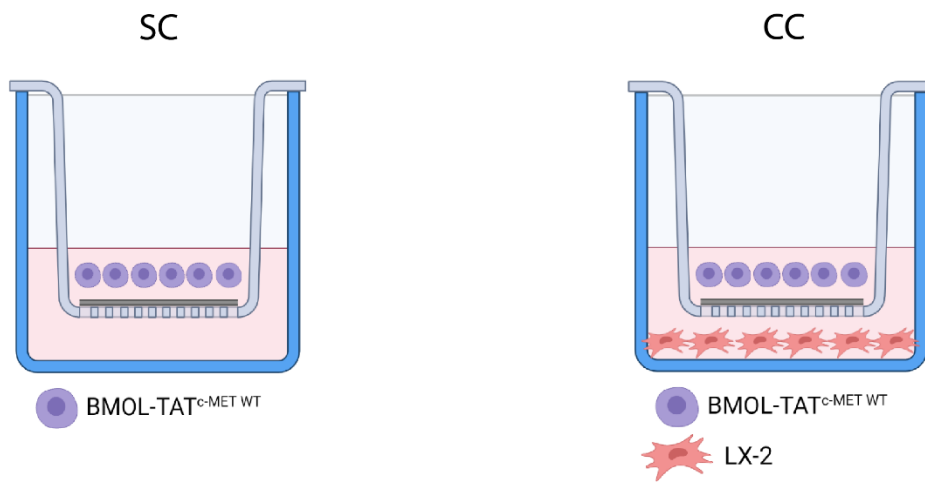
Using Boyden chambers, an indirect co-culture migration assay was performed to assess the level of chemoattraction of BMOL-TAT<sup>c-MET WT</sup> cells to LX-2 cells, and *vice versa*. The appropriate timeframe of migration was optimised to be four hours, as longer timeframes would allow the membrane in the insert to become saturated with cells, missing the linear stage of migration.

BMOL-TAT<sup>c-MET WT</sup> cells in the insert were strongly chemoattracted to the LX-2 cells in the well below, compared to no chemoattractant being present in the single culture experimental group (Figure 5.6).

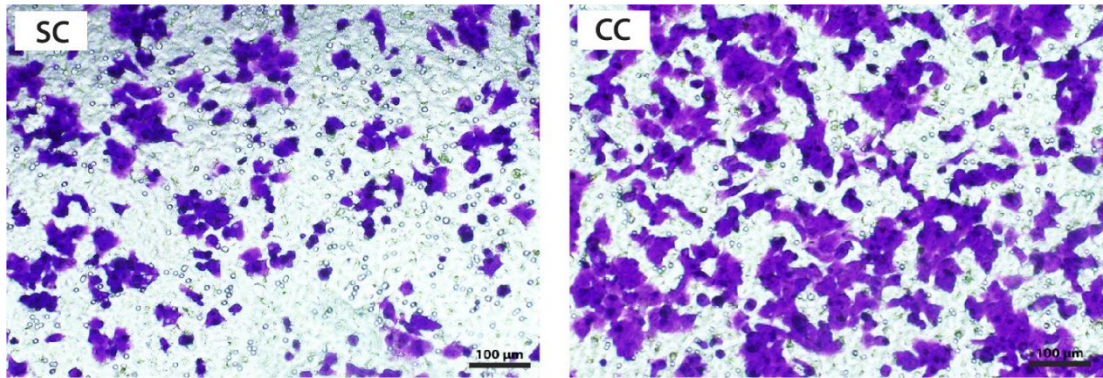
This result was mirrored when the LX-2 cells were placed in the insert and the BMOL-TAT<sup>c-MET WT</sup> cells were situated in the well below (Figure 5.7), demonstrating that both cell types positively influence each other's migration through the secretion of chemoattractant molecules.



(A)



(B)



(C)

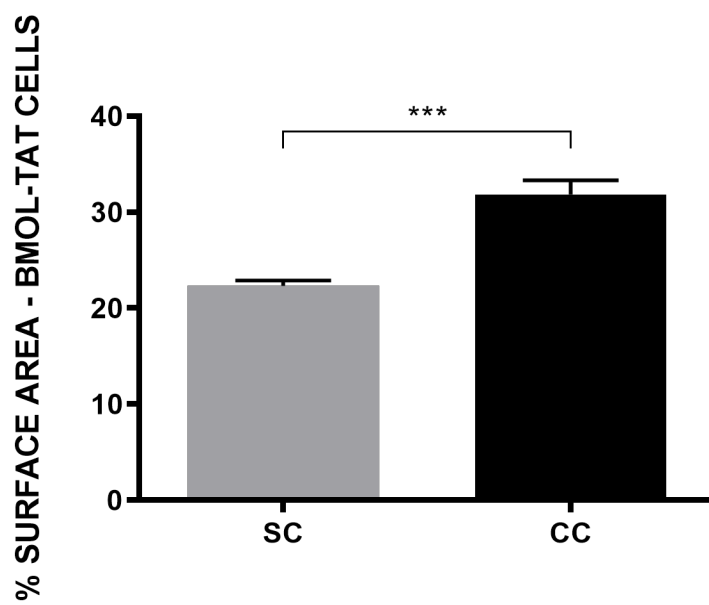


**Figure 5.6: Boyden chamber migration assay - BMOL-TAT<sup>c-MET</sup> WT cell migration.**

BMOL-TAT<sup>c-MET</sup> WT cells were subjected to a 4-hour Boyden chamber migration assay with either no cells or LX-2 cells as a potential chemoattractant. (A) Illustration of cell arrangement in Boyden chamber. (B) Crystal violet staining revealed an increase in BMOL-TAT<sup>c-MET</sup> WT cell migration with LX-2 cells in well underneath. (C) Quantification of the positively stained surface area demonstrated a significant increase in BMOL-TAT<sup>c-MET</sup> WT cell migration with LX-2 cells in well underneath, compared to no cells.

Data represent the mean  $\pm$  SEM, n= 3, \*\*\*P < 0.01.

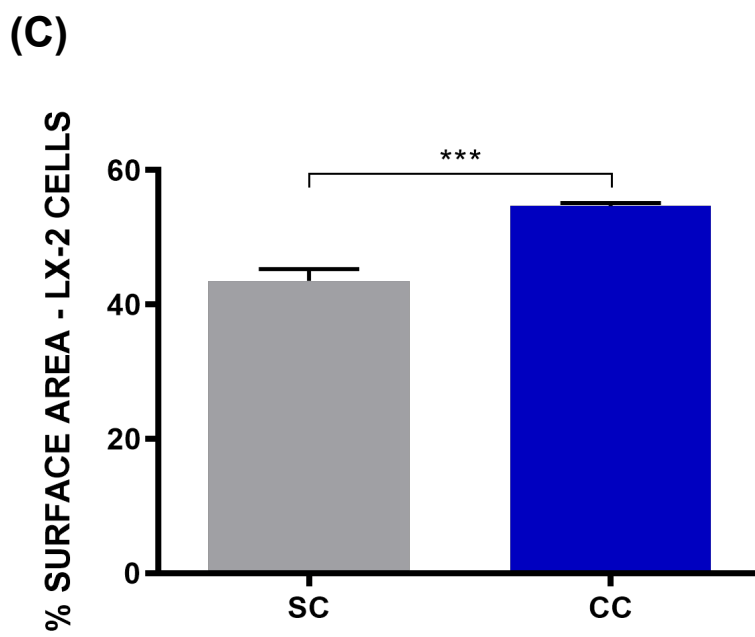
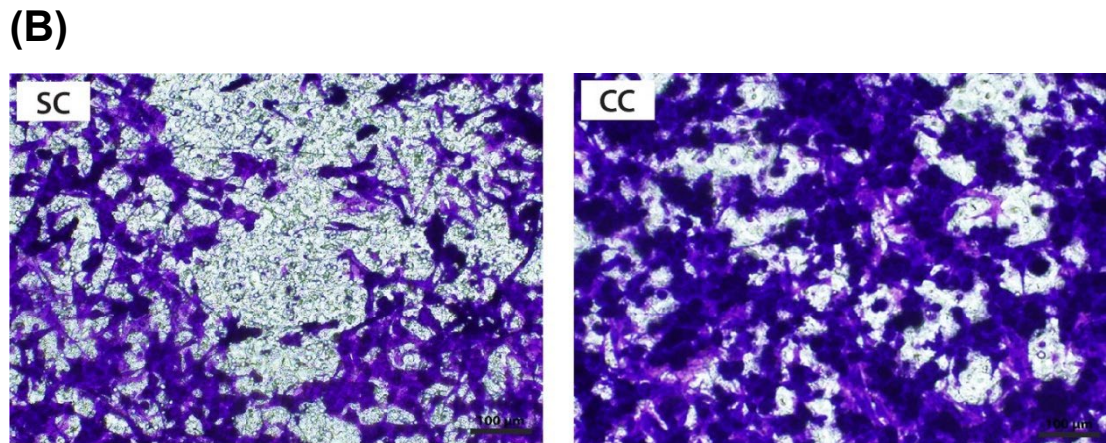
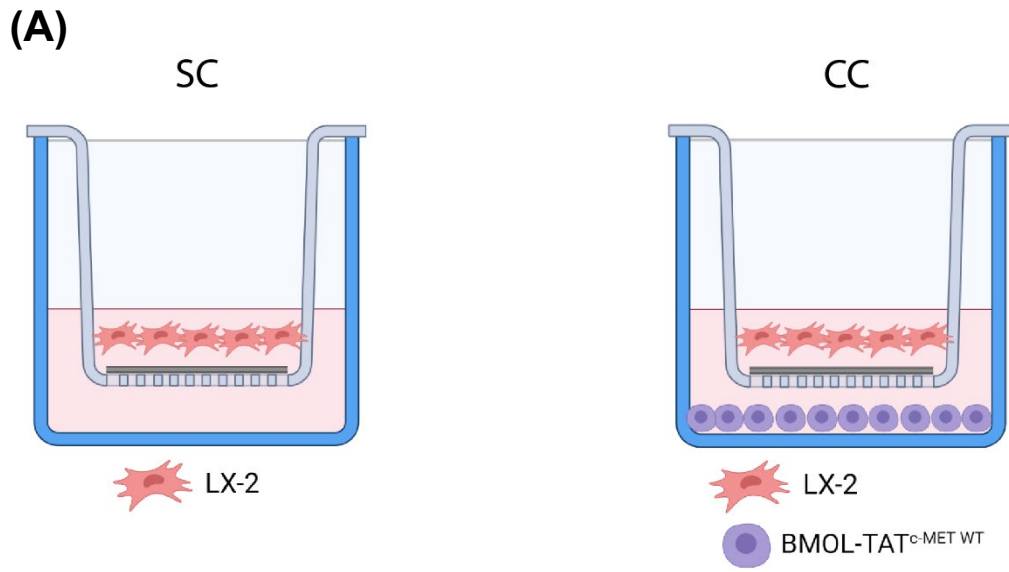


**Figure 5.7: Boyden chamber migration assay - LX-2 cell migration.**

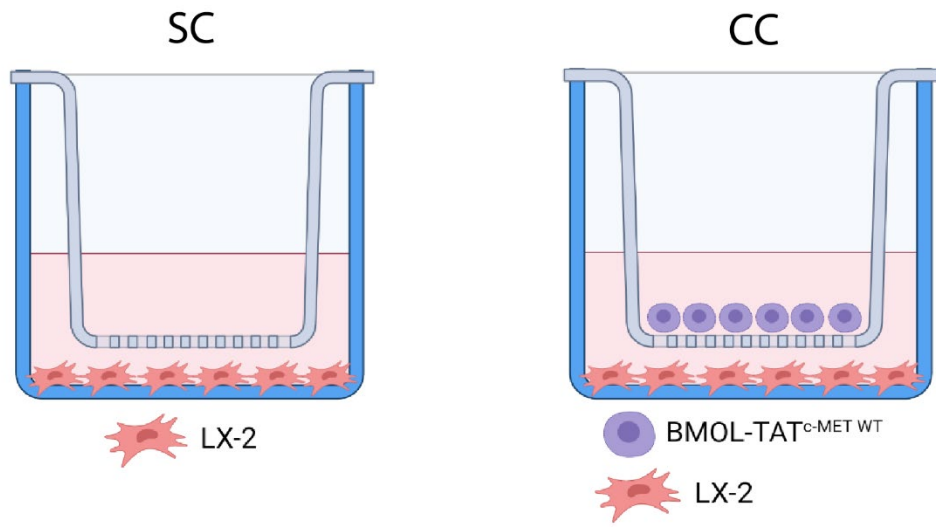
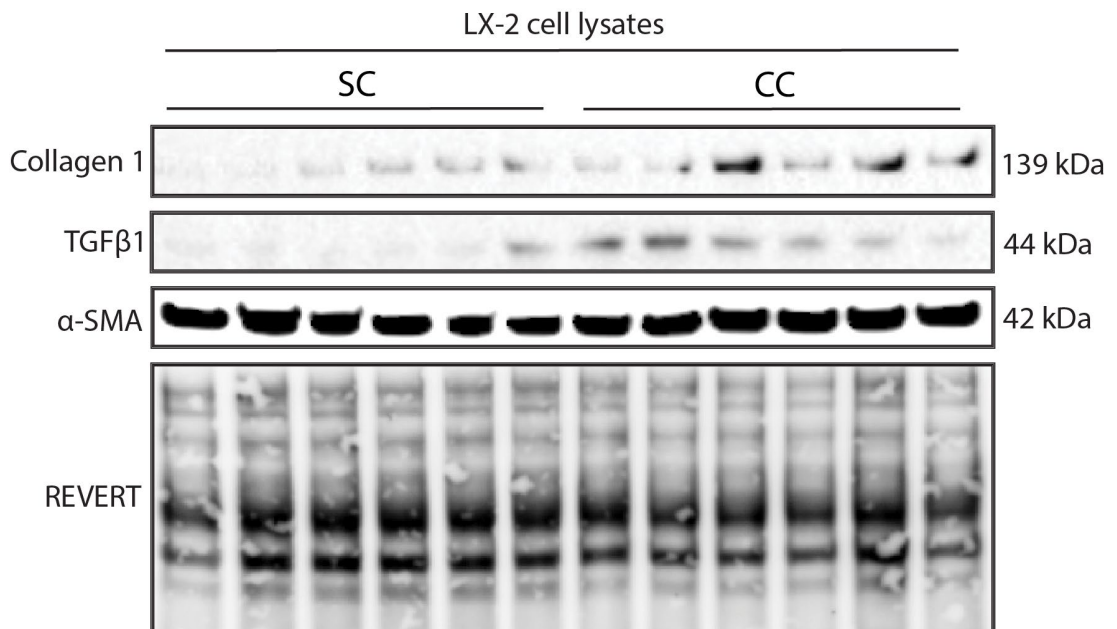
LX-2 cells were subjected to a 4-hour Boyden chamber migration assay with either no cells or BMOL-TAT<sup>c-MET</sup> <sup>WT</sup> cells as a potential chemoattractant. (A) Illustration of cell arrangement in Boyden chamber. (B) Crystal violet staining displayed an increase in LX-2 cell migration with BMOL-TAT<sup>c-MET</sup> <sup>WT</sup> cells in well underneath. (C) Quantification of positively stained surface area further demonstrated a significant increase in LX-2 cell migration with BMOL-TAT<sup>c-MET</sup> <sup>WT</sup> cells as a chemoattractant.

Data represent the mean  $\pm$  SEM, n= 3, \*\*\*P < 0.01.

### 5.4.3 Expression of fibrogenic markers following indirect co-culture of LX-2 cells and BMOL-TAT<sup>c-MET WT</sup> cells

Following a 48-hour co-culture of LX-2 cells with BMOL-TAT<sup>c-MET WT</sup> cells, western blot analysis for protein expression of collagen 1, TGF $\beta$ 1 and  $\alpha$ SMA was undertaken. Densitometry of the obtained bands demonstrated that LX-2 cells significantly increased expression of the fibrotic markers collagen 1 and TGF $\beta$ 1 following co-culture (Figure 5.8).

To evaluate whether this increase in fibrosis-associated markers in LX-2 cells is specific to co-culture with BMOL-TAT<sup>c-MET WT</sup> cells, the LX-2 cells were also co-cultured with SNU-499 cells, a human hepatocellular carcinoma cell line. “Figure 5.9 reveals that the previously observed fibrotic response in the LX-2 cells was not replicated with the SNU-499 cell line, suggesting that the fibrogenic potential of the LX-2 cells may be BMOL-TAT-dependent.”

**(A)****(B)**

(C)

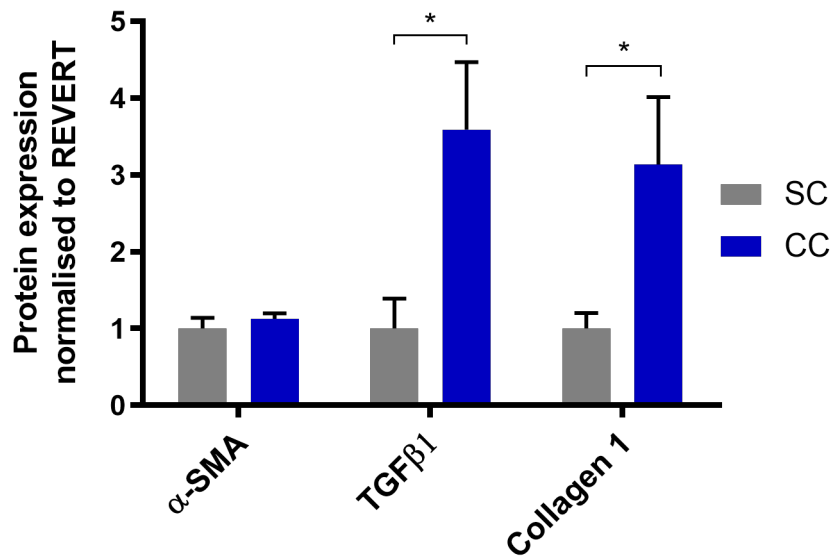
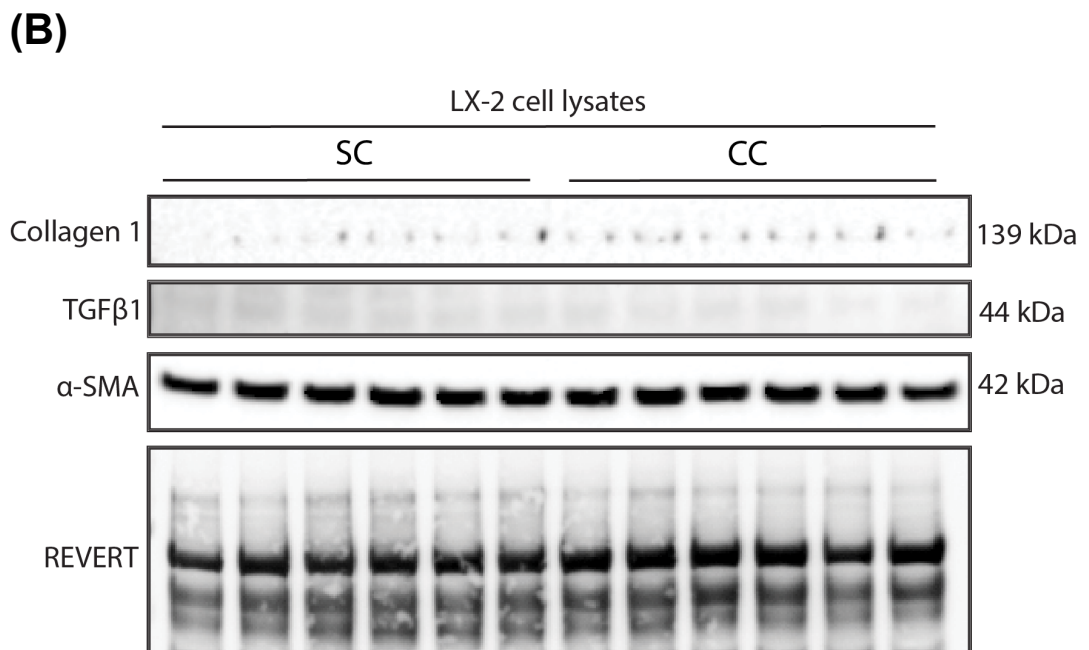
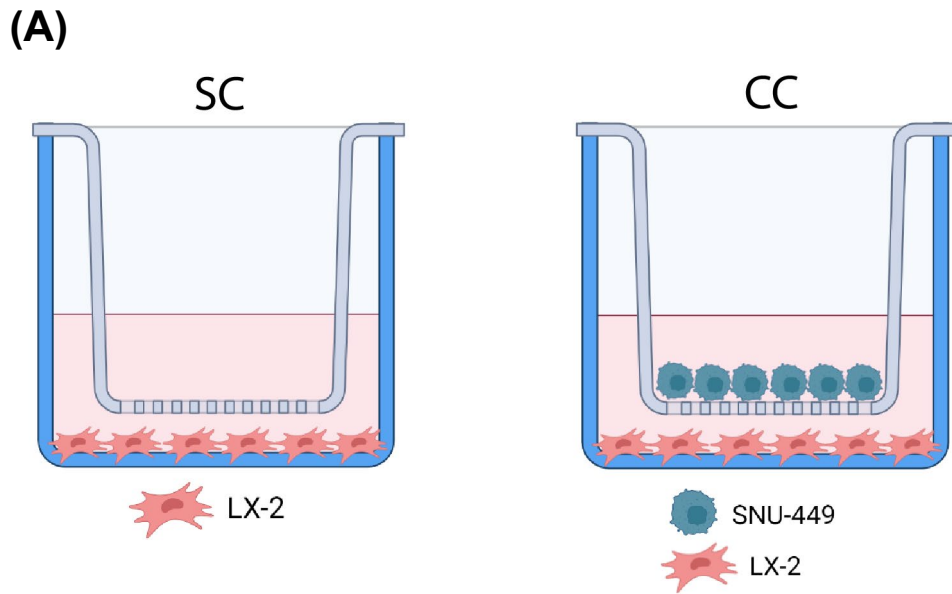


**Figure 5.8: Western blot analysis of LX-2 fibrogenic markers following their indirect co-culture with BMOL-TAT<sup>c-MET WT</sup> cells.**

Illustration of cell arrangement in Boyden chamber (A). Expression analysis of  $\alpha$ SMA, TGF $\beta$ 1 and collagen 1 using western blot (B) and semi-quantification by densitometry (C). While  $\alpha$ SMA levels remained unchanged, TGF $\beta$ 1 and collagen 1 expression significantly increased in LX-2 cells following co-culture with BMOL-TAT<sup>c-MET WT</sup> cells.

Data represent the mean  $\pm$  SEM. n= 3. \*P < 0.05.





(C)

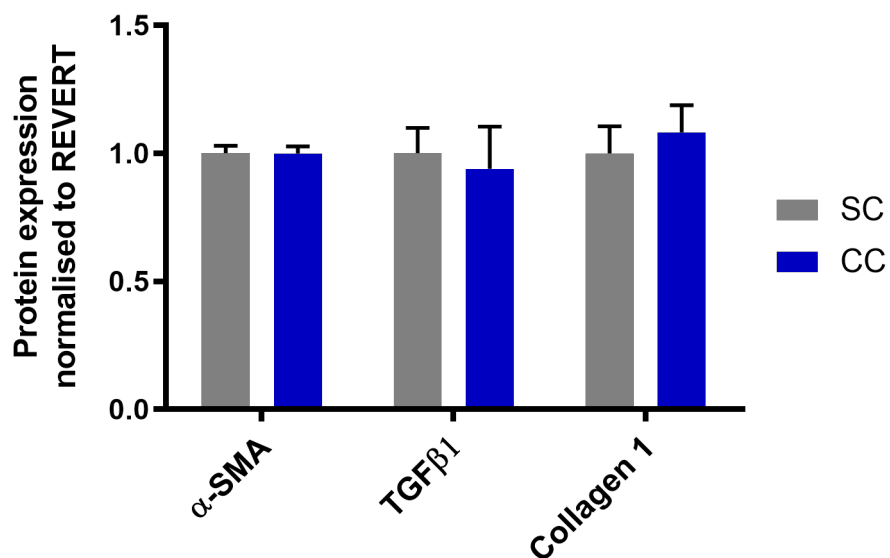


**Figure 5.9: Western blot analysis of LX-2 fibrogenic markers following their indirect co-culture with SNU-449 cells.**

Illustration of cell arrangement in Boyden chamber (A). Expression analysis of  $\alpha$ SMA, TGF $\beta$ 1 and collagen 1 using western blot (B) and semi-quantification by densitometry (C). Expression of all fibrogenic markers remained unchanged following LX-2 co-culture with SNU-449 cells.

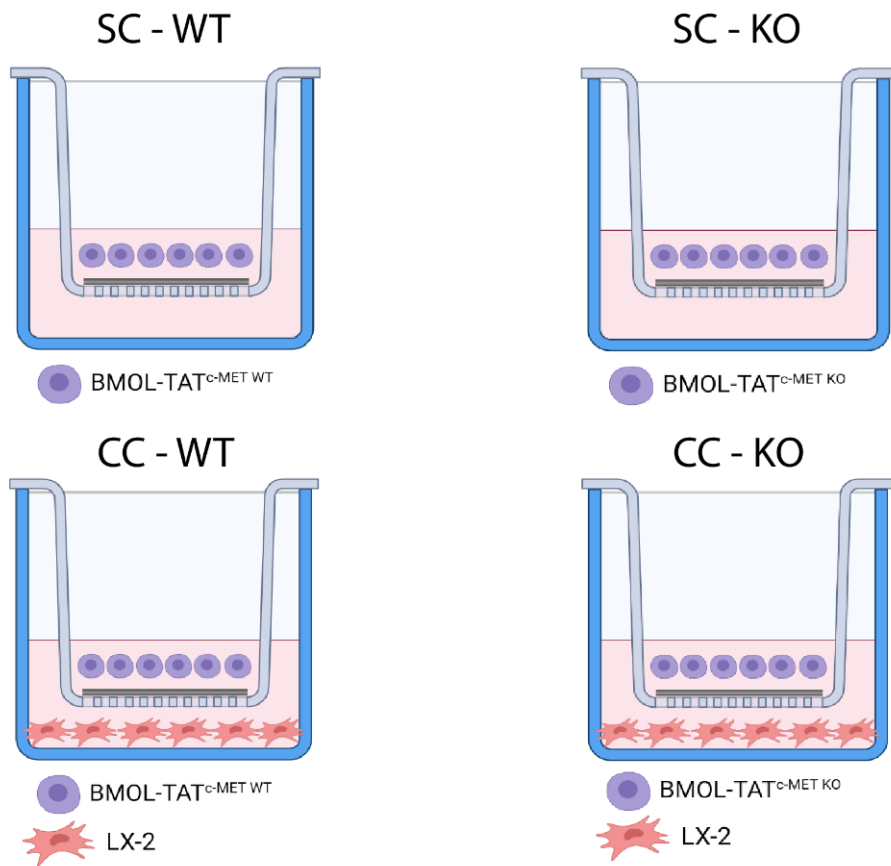
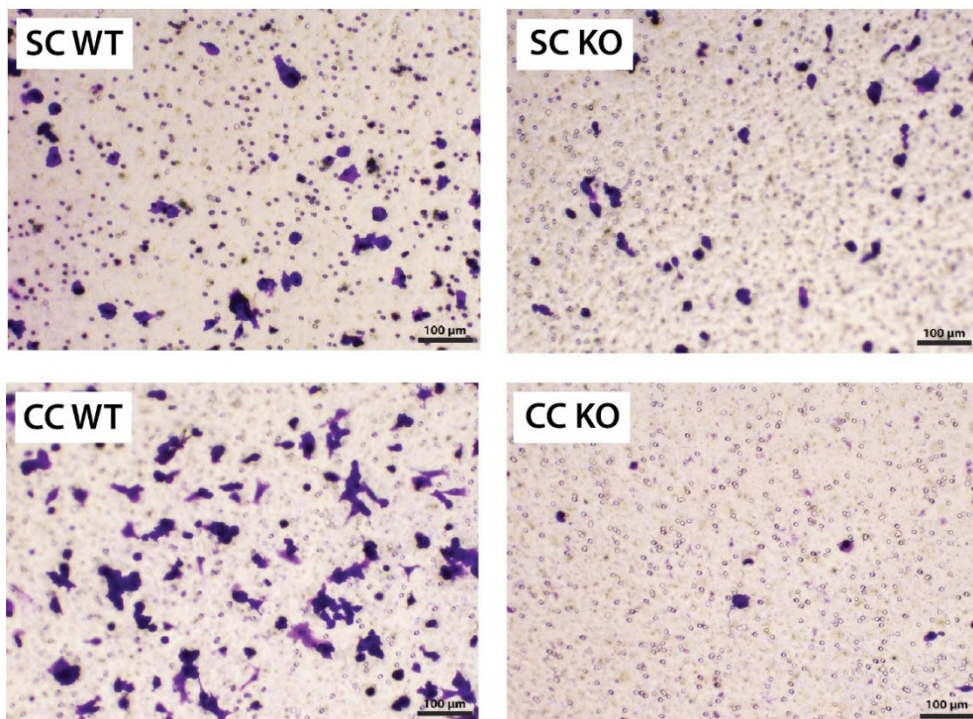
Data represent the mean  $\pm$  SEM. n= 3. \*P < 0.05.

#### 5.4.4 Chemoattraction of BMOL-TAT<sup>c-MET KO</sup> cells and LX-2 cells

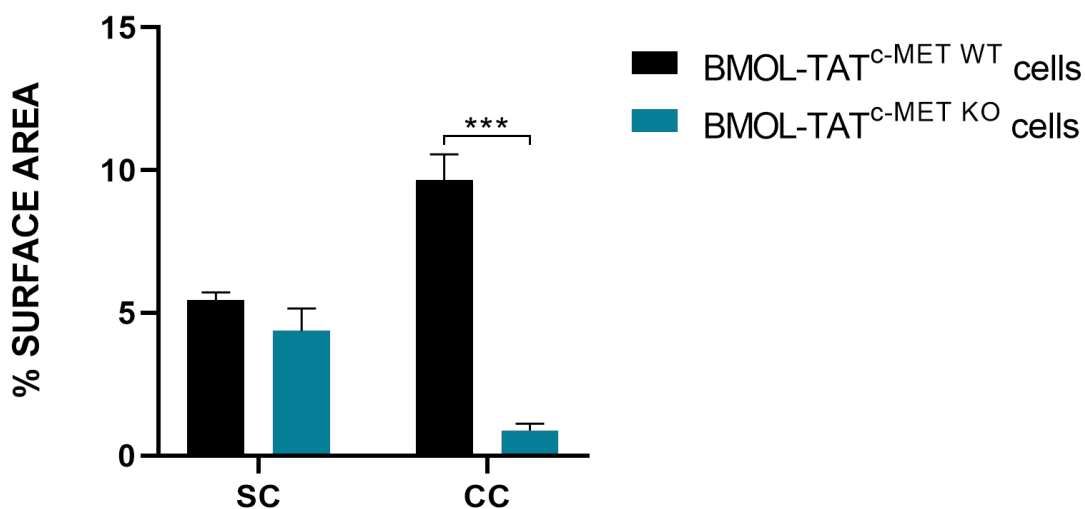
To assess the chemoattractive abilities of BMOL-TAT<sup>c-MET KO</sup> cells and LX-2 cells, they were subjected to an indirect co-culture migration assay, using Boyden chambers.

Figure 5.10 indicates that placement of LX-2 cells in the bottom well resulted in reduced BMOL-TAT<sup>c-MET KO</sup> cell migration towards them, as compared to their wildtype counterparts. The same decrease in chemoattraction was evident when assessing LX-2 cell migration toward the BMOL-TAT<sup>c-MET KO</sup> cells in the well underneath (Figure 5.11).

These data suggest that a lack of functional HGF/c-MET signalling interaction between cells negatively affected cell migration. The comparison of data obtained in wildtype versus knockout cells even suggests a 'repulsive' effect, with less BMOL-TAT<sup>c-MET KO</sup> cell migration in LX-2 co-culture compared to single culture.

**(A)****(B)**

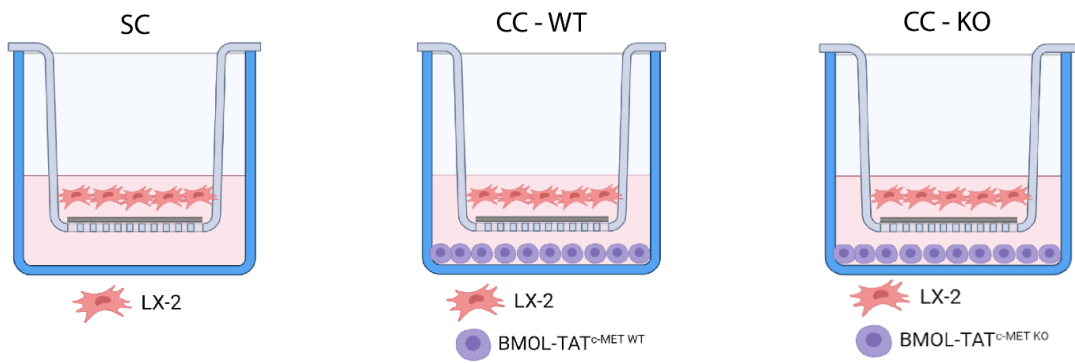
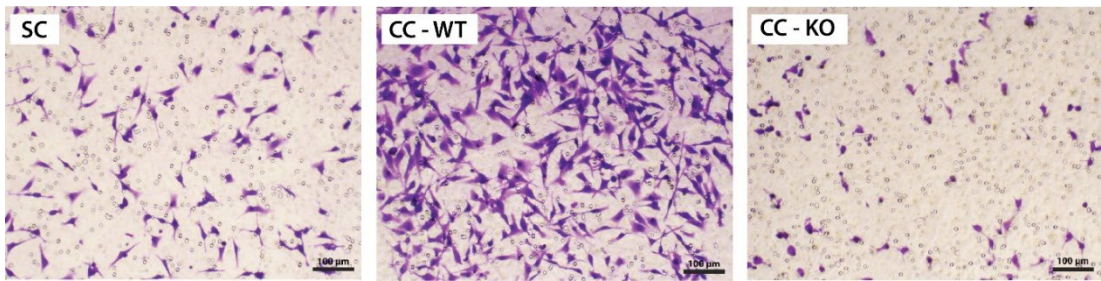
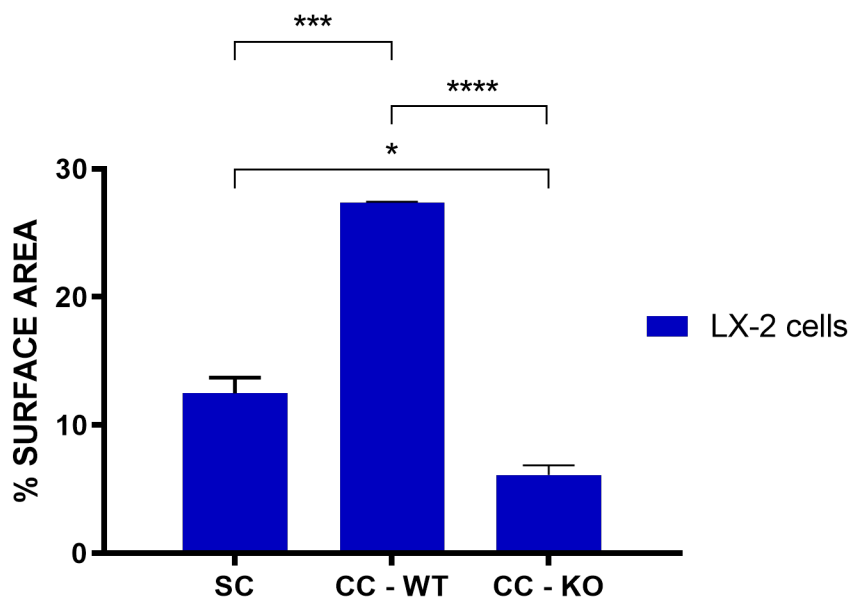
(C)



**Figure 5.10: Boyden chamber migration assay - BMOL-TAT<sup>c-MET</sup> KO cell migration.**

BMOL-TAT<sup>c-MET</sup> KO cells were cultured in a Boyden chamber co-culture system alone or with LX-2 cells underneath. Co-cultures were incubated for 4 hours in total and compared to BMOL-TAT<sup>c-MET</sup> WT cells under the same conditions. (A) Illustration of cell arrangement in Boyden chamber. (B) Crystal violet staining and (C) quantification of cell migration through measurement of positively stained surface area. A significant decrease in BMOL-TAT<sup>c-MET</sup> KO cell migration was observed with LX-2 cells in the well underneath, compared to no cells.

Data represent the mean  $\pm$  SEM,  $n = 3$ , \* $P < 0.05$ .

**(A)****(B)****(C)**

**Figure 5.11: Boyden chamber migration assay - LX-2 cell migration.**

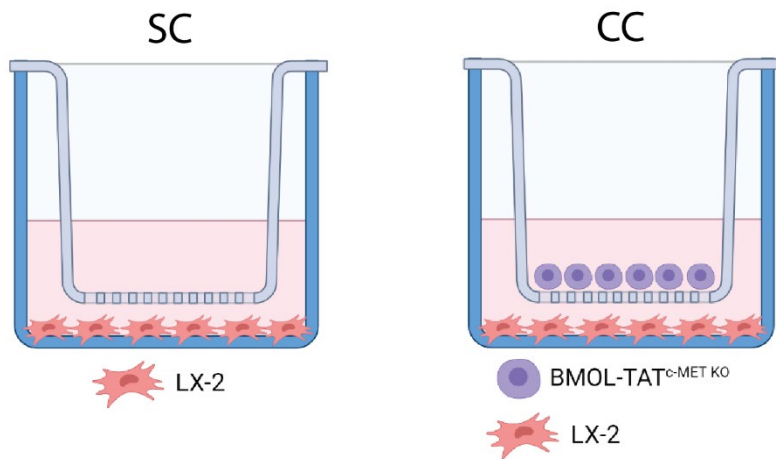
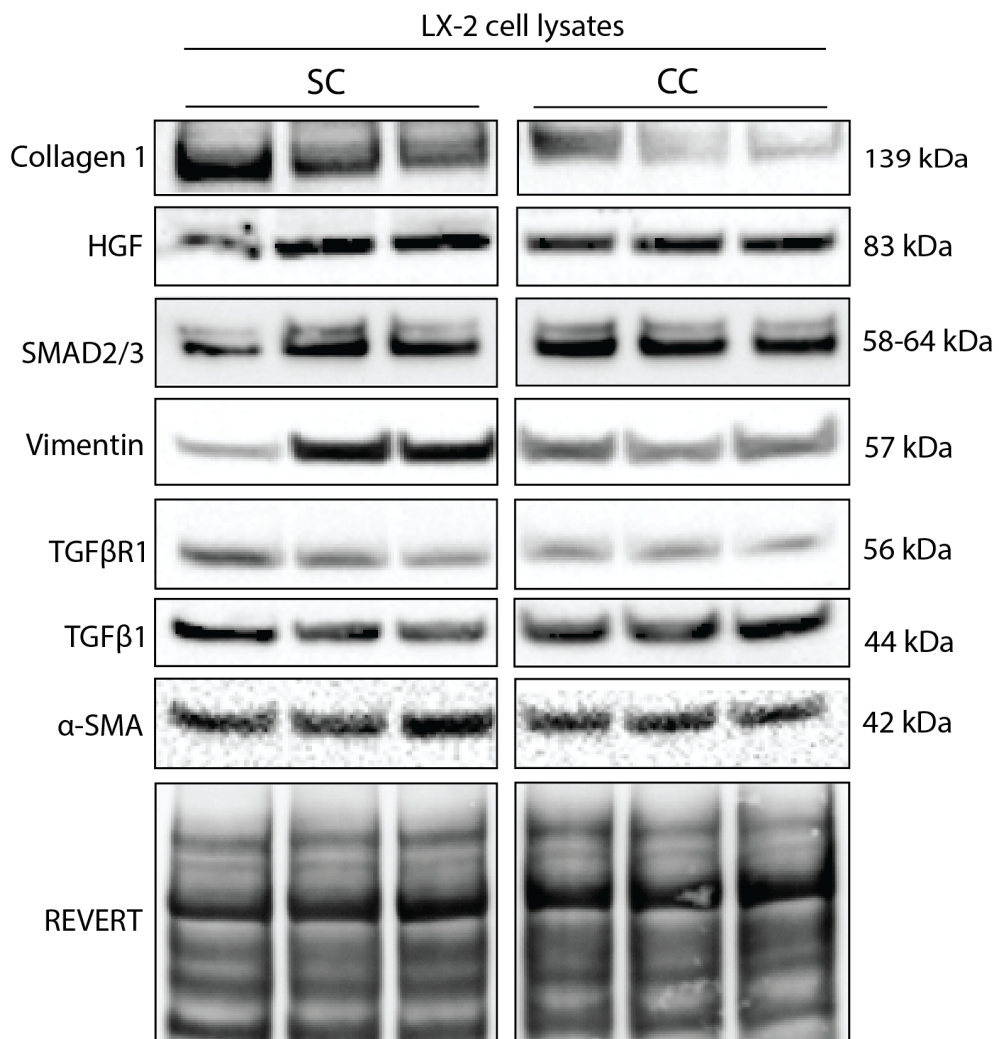
LX-2 cells were cultured in a Boyden chamber co-culture system alone or with BMOL-TAT<sup>c-MET<sup>KO</sup></sup> cells underneath. Co-cultures were incubated for 4 hours in total and compared to BMOL-TAT<sup>c-MET<sup>WT</sup></sup> cells under the same conditions. (A) Illustration of cell arrangement in Boyden chamber. (B) Crystal violet staining and (C) quantification of cell migration through measurement of positively stained surface area. A significant decrease in LX-2 cell migration was observed with BMOL-TAT<sup>c-MET<sup>KO</sup></sup> cells in the well underneath, compared to no cells.

Data represent the mean  $\pm$  SEM, n= 3, \*P < 0.05.

#### **5.4.5 Expression of TGF $\beta$ pathway components and fibrogenic markers following indirect co-culture of LX-2 cells and BMOL-TAT<sup>c-MET KO</sup> cells**

LX-2 cells were co-cultured with BMOL-TAT<sup>c-MET KO</sup> cells in Boyden chambers for 48 hours. Thereafter, western blot analysis was used to investigate the fibrogenic potential and TGF $\beta$  pathway expression of LX-2 cells.

Following co-culture, protein expression of HGF, SMAD2/3 and  $\alpha$ SMA remained unaltered in LX-2 cells (Figure 5.12). However, the expression of fibrosis-associated markers collagen 1 and vimentin significantly decreased (Figure 5.12). Furthermore, the expression of TGF $\beta$ 1 was augmented, whereas the expression of the receptor TGF $\beta$ R1 was reduced in LX-2 cells following co-culture (Figure 5.12).

**(A)****(B)**



(C)

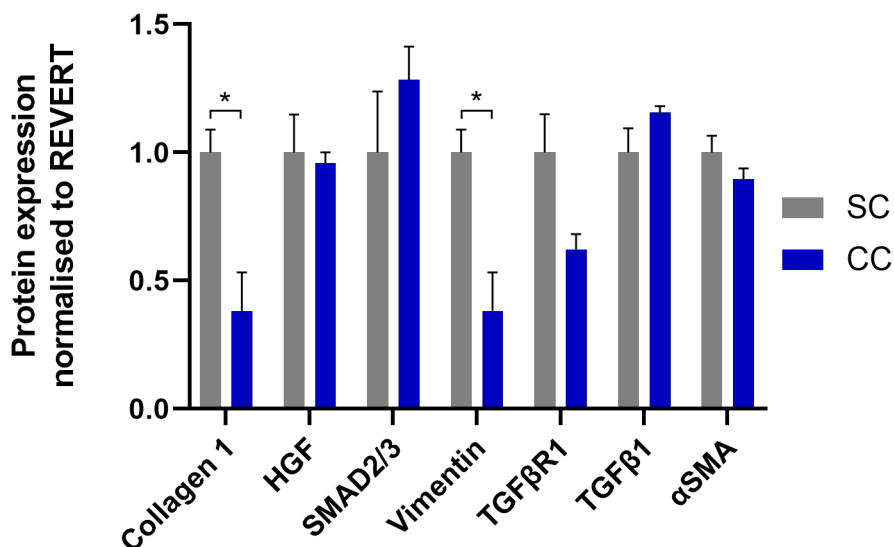


**Figure 5.12: Western blot analysis of LX-2 fibrogenic markers following their indirect co-culture with BMOL-TAT<sup>c-MET KO</sup> cells.**

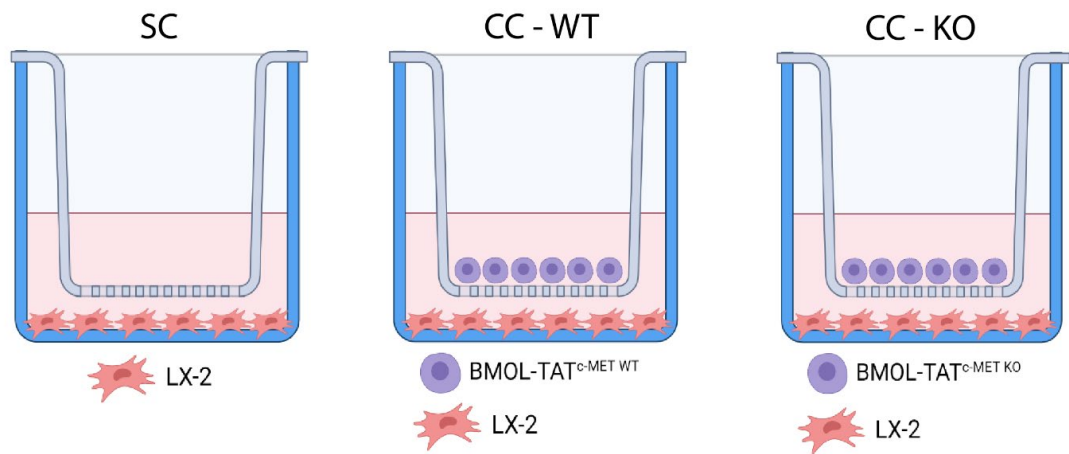
Illustration of cell arrangement in Boyden chamber (A). Expression analysis of collagen 1, HGF, SMAD2/3, vimentin, TGFβR1, TGFβ1 and αSMA using western blot (B) and semi-quantification by densitometry (C). Co-culture of LX-2 with BMOL-TAT<sup>c-MET KO</sup> cells resulted in a significant decrease in the fibrogenic markers collagen 1 and vimentin compared to single culture, while expression of other investigated markers was not significantly altered.

Data represent the mean ± SEM. n= 3. \*P < 0.05.

#### **5.4.6 LX-2 collagen secretion following indirect co-culture with BMOL-TAT<sup>c-MET WT</sup> and BMOL-TAT<sup>c-MET KO</sup> cells**

As collagen 1 is mainly secreted by HSCs, a human-specific collagen assay from the cell culture supernatant was performed to analyse the amount of collagen produced from the LX-2 cells, following their co-culture with BMOL-TAT<sup>c-MET WT</sup> and BMOL-TAT<sup>c-MET KO</sup> cells. The results demonstrated that co-culture of LX-2 cells with either BMOL-TAT cell line led to a decrease in collagen secretion compared to LX-2 cells grown in single culture conditions (Figure 5.13), confirming that cellular LPC-HSC crosstalk induced an HGF/c-MET-independent reduction in LX-2 collagen secretion.

(A)



(B)

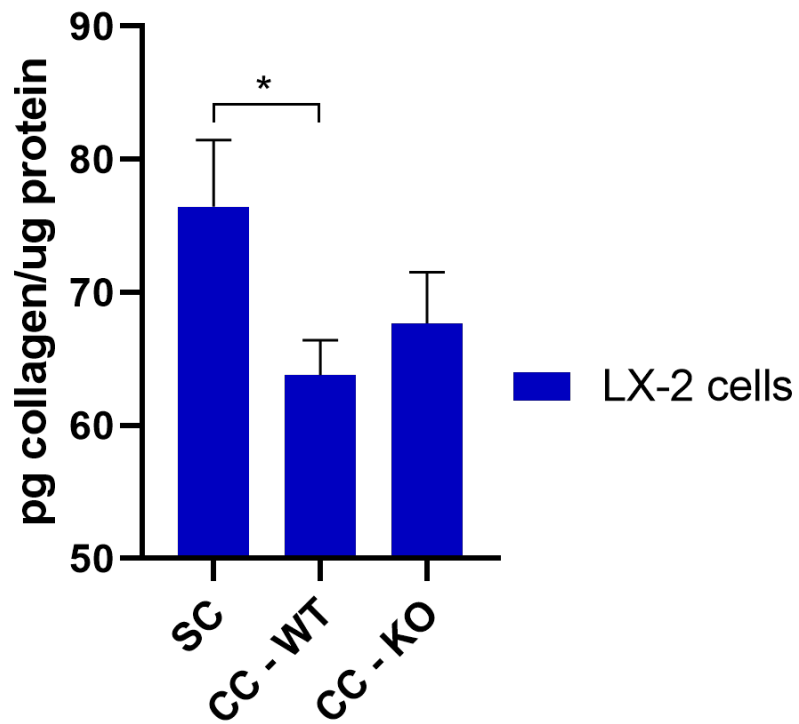


**Figure 5.13: Collagen assay of LX-2 cells following their indirect co-culture with BMOL-TAT<sup>c-MET WT</sup> and BMOL-TAT<sup>c-MET KO</sup> cells.**

Illustration of cell arrangement in Boyden chamber (A). Quantification of collagen protein revealed a significant decrease in collagen secretion by LX-2 cells following their co-culture with BMOL-TAT<sup>c-MET WT</sup> cells, compared to single culture (B). The same trend was observed when LX-2 cells were co-cultured with BMOL-TAT<sup>c-MET KO</sup> cells.

Data represent the mean  $\pm$  SEM. n= 3. \*P < 0.05.

## 5.5 Discussion

LPCs may represent tumour-initiating cells, however up to date clear experimental evidence for this hypothesis is lacking. Since LPCs are observed as part of Ductular Reactions in almost every chronic liver disease aetiology and at different injury and regeneration stages (Kohn-Gaone et al., 2016) (Köhn-Gaone et al., 2016) (Sancho-Bru et al., 2012), their specific roles may be highly context-specific.

Evidence for a pro-regenerative role of LPCs was proposed by Dai and colleagues who reported that growth differentiation factor 11 increased the numbers of LGR5<sup>+</sup> progenitor cells in the liver, attenuating fibrosis. However, an underlying mechanism for this anti-fibrotic effect was not provided (Dai et al., 2020). Additionally, it was demonstrated that co-culture of LPCs with primary HSCs caused a downregulation of fibrosis-associated markers (Gratte et al., 2021), suggesting LPCs as regulatory cells with the potential to influence cell behaviour in their microenvironment via cellular crosstalk. It has been established that the HGF/c-MET pathway is upregulated in advanced stages of liver cancer, however thought to have anti-fibrotic effects during chronic liver disease (Ishikawa et al., 2012) (Huh et al., 2004). This prompted investigations into the pathways' involvement in the anti- or pro-regenerative role of LPCs during their crosstalk with HSCs.

As presented in Chapter 4 of this thesis, knocking out the c-MET receptor in the LPCs, significantly affected the cells' ability to migrate and proliferate, reflecting a detrimental effect on the cells' normal biology. In this chapter, BMOL-TAT<sup>c-MET<sup>WT</sup></sup> and BMOL-TAT<sup>c-MET<sup>KO</sup></sup> cells displayed cluster-like formations, independent of their HGF/c-MET signalling status, when co-cultured directly with LX-2 cells in 2D and 3D culture. In the 3D model, created by the Inventia RASTRUM bioprinter, the underlying RGD ~0.7kPa matrix provided an additional layer of complexity seen in a tissue system. As LX-2 cells are mesenchymal cells, they are highly motile, facilitated by their cell polarisation and complex interactions with the extracellular matrix during

fibrosis (Yamada & Sixt, 2019). Therefore, it was not surprising that the LX-2 cells displayed network-like structures.

Visual assessment of BMOL-TAT<sup>c-MET<sup>WT</sup></sup> and BMOL-TAT<sup>c-MET<sup>KO</sup></sup> cells in direct culture with LX-2 cells suggested that co-culture may have induced cell death. This hypothesis was further investigated through assessment of cellular apoptosis using an Annexin V assay by flow cytometry. The results demonstrated an increase in early- and late-stage cell apoptosis of BMOL-TAT<sup>c-MET<sup>WT</sup></sup> and BMOL-TAT<sup>c-MET<sup>KO</sup></sup> cells when in co-culture with LX-2 cells, as compared to the cells in single culture. Importantly, this apoptotic result in BMOL-TAT cells was independent of their c-MET signalling status. The resulting undesirable cell death led to further experimentation utilising a Boyden chamber system, which facilitated co-culture without direct cell-cell contact. Boyden chambers are a gold standard technique in recapitulating *in vivo* crosstalk to ensure reproducibility since they still allow diffusion of soluble signalling factors across the cell-impermeable membrane.

Migration was therefore assessed using Boyden chambers, which revealed that BMOL-TAT<sup>c-MET<sup>WT</sup></sup> cells and LX-2 cells are greatly chemoattracted to each other. This chemotactic behaviour was reported by Ruddell and colleagues in 2008, whereby lymphotoxin  $\beta$  (LT $\beta$ ), expressed by progenitor cells, aids in a wound healing response via direct effects on LT $\beta$ R-positive hepatic stellate cells, supporting co-migration during liver injury (Ruddell et al., 2009). Knocking out c-MET from the LPC line BMOL-TAT, resulted in a decrease in their chemoattraction towards the LX-2 cells, and vice versa compared to single culture. The reduced migratory levels of the BMOL-TAT<sup>c-MET<sup>KO</sup></sup> cells below levels of their wildtype counterparts may be explained by the morphological changes occurring as a result of knocking out the c-MET receptor and may have an additional influence on their migratory behaviour. This novel result highlights the importance of the HGF/c-MET signalling pathway for effective co-migration of LPCs and HSCs during liver injury, not previously assessed in a co-culture system.

The fibrogenic response of the LX-2 cells was investigated following their indirect co-culture with BMOL-TAT<sup>c-MET</sup> WT cells. Published data suggest that the pro-fibrotic nature of HSCs can be altered, depending on the disease context and communication with nearby cells (Dai et al., 2020) (Z. Liu et al., 2021) (Ruddell et al., 2009) (Gratte et al., 2021). This was exemplified by Gratte *et al.*, where co-culture of primary HSCs with BMOL-TAT<sup>c-MET</sup> WT cells decreased HSC expression of fibrogenic markers including  $\alpha$ SMA, TGF $\beta$ 1 and collagen 1 at the transcriptional level (Gratte et al., 2021). Interestingly, western blot data from the same study and presented in this thesis, demonstrated that co-culturing clonal HSCs (LX-2 cells) and BMOL-TAT<sup>c-MET</sup> WT cells led to the upregulation of the same fibrogenic markers at the protein level, revealing context-specific regulation of LPC-induced HSC behaviour. Importantly, this response was found to be LPC-specific, as co-culturing LX-2 cells with a clonal hepatocellular carcinoma cell line, SNU-499, eventuated in no change in the HSC fibrogenic response. This suggests that HSC behaviour can be regulated by LPCs, and may be dependent on the activation status and origin of the cell.

To gauge the anti-fibrotic potential of the HGF/c-MET signalling pathway, co-culture of the LX-2 cells with the BMOL-TAT<sup>c-MET</sup> KO cells was performed, which demonstrated a significant decrease in the fibrosis-associated markers collagen 1 and vimentin, along with TGF $\beta$ R1, determined by western blot analysis. The presented data oppose the HGF/c-MET anti-fibrotic hypothesis and rather point towards the pathways' involvement during liver cancer (H. Wang et al., 2020).

Activated HSCs secrete collagen during their response to liver injury, making this an appropriate marker for the study of their functionality (Karsdal et al., 2020). Therefore, a collagen secretion assay was completed with supernatants, following LX-2 co-culture with BMOL-TAT<sup>c-MET</sup> WT and BMOL-TAT<sup>c-MET</sup> KO cells. Interestingly, the LX-2 cells significantly decreased their collagen secretion following co-culture with BMOL-TAT<sup>c-MET</sup> WT cells. This result differs from the observed increase in collagen at the protein level, suggesting that collagen is being internalised and not secreted. This

internalisation of collagen by HSCs has been reported by means of endocytosis, to promote the breakdown of ECM in fibrotic tissue (Bi et al., 2014). Further, LX-2 cell collagen secretion decreased following co-culture with BMOL-TAT<sup>c-MET KO</sup> cells, reflecting the western blot result. This demonstrates that collagen expression also decreases without active HGF/c-MET signalling, suggesting that LPC regulation of HSC behaviour is dependent on other signalling pathways and regulators.

Future experiments including co-culturing immune cells with LPCs and HSCs would allow for a more comprehensive characterisation of cellular communication during liver injury. Moreover, undertaking the above co-culture experiments with primary cells would be of interest to investigate fibrosis read outs that are more closely to an *in vivo* model. Nonetheless, the evidence presented here in Chapter 5 provides a contribution to our understanding of LPC-HSC crosstalk during fibrosis and the impact of the HGF/c-MET signalling pathway on cellular communication and downstream migration and fibrosis.



**Chapter 6: Transcriptional analysis of liver progenitor cell and hepatic stellate cell crosstalk using *in vitro* co-culture models**

## 6.1 Introduction

It has been well documented that LPCs and HSCs are in spatial proximity during the progression of chronic liver disease (Kohn-Gaone et al., 2016) (Van Hul et al., 2009). Ruddell *et al.* demonstrated that both cell types migrate to the site of injury together via lymphotoxin beta-induced signalling, with HSCs producing the ligand and LPCs expressing the lymphotoxin beta receptor and responding with chemokine secretion to attract the HSCs (Ruddell et al., 2009). However, other signalling consequences of LPC-HSC crosstalk are not known, and it remains of interest to investigate its impact on other aspects of the cells' biology.

The HGF/c-MET signalling pathway, as described previously, has anti-fibrotic potential through enhancing LPC expansion and increasing apoptosis of HSCs (Borowiak et al., 2004), (Huh et al., 2004). The HSCs secrete the ligand HGF and the LPCs present the c-MET receptor on their surface (Organ & Tsao, 2011). Examining LPC-HSC crosstalk, with a focus on the HGF/c-MET signalling pathway during early liver disease, will provide insight into how both cell types communicate to regulate regeneration and reveal potential therapeutic targets.

As described in Chapter 5, co-culture of LPCs and HSCs demonstrated their chemoattraction, with c-MET deletion in LPCs greatly hindering this behaviour. The work in this chapter investigated LPC-HSC crosstalk at the transcriptional level using bulk RNA-sequencing to get broader insights into the underlying signalling networks that orchestrate the cells' co-regulation.

## 6.2 Study aims

The aim of this chapter was to further study the BMOL-TAT<sup>c-MET<sup>WT</sup></sup> and BMOL-TAT<sup>c-MET<sup>KO</sup></sup> cells in co-culture with the HSC line LX-2. Bulk RNA-sequencing was performed following Boyden chamber co-culture or conditioned medium experiments to assess transcriptional changes during cellular crosstalk.

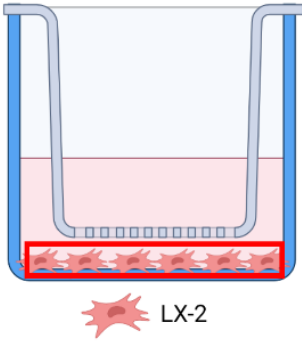
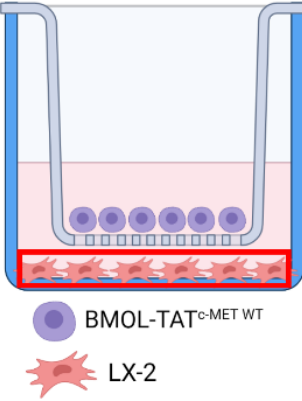
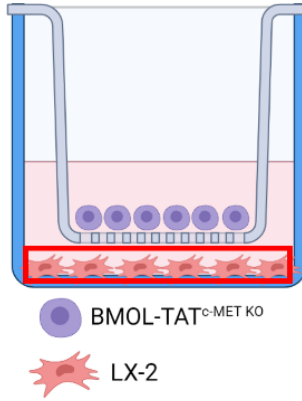
### 6.3 Methodology

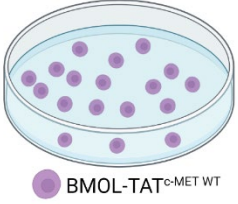
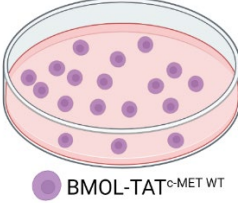
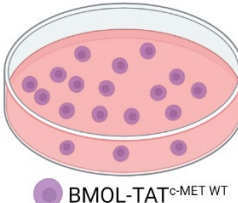
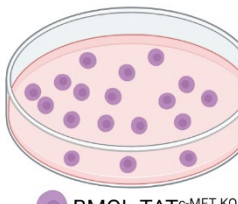
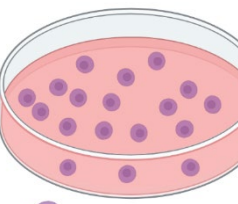
LX-2 cells were co-cultured in Boyden chambers for 48 hours with either BMOL-TAT<sup>c-MET<sup>WT</sup></sup> or BMOL-TAT<sup>c-MET<sup>KO</sup></sup> cells in the insert above, as previously described (2.2.2.18). LX-2 cell RNA was isolated using the Bioline RNA column extraction kit, following the manufacturer's instructions (2.2.4.4). Four biological replicates were collected for each experimental group, and RNA was tested for appropriate quality and quantity using the Nanodrop 1000 spectrophotometer.

Poor quality and quantity of BMOL-TAT<sup>c-MET<sup>WT</sup></sup> and BMOL-TAT<sup>c-MET<sup>KO</sup></sup> cell RNA was attained from inserts in the Boyden chambers and accessibility issues of co-culture plates due to COVID-related delivery delays resulted in a change in experimental set up for the collection of BMOL-TAT<sup>c-MET<sup>WT</sup></sup> and BMOL-TAT<sup>c-MET<sup>KO</sup></sup> cell RNA. Consequently, BMOL-TAT<sup>c-MET<sup>WT</sup></sup> and BMOL-TAT<sup>c-MET<sup>KO</sup></sup> cells were seeded in 6-well plates, incubated until the cultures reached approximately 80% confluency and LX-2 cell-conditioned medium was added for either 30 minutes or 6 hours, to assess various timepoints for transcriptional events (2.2.2.17). Total RNA was collected using the Bioline RNA column extraction kit (2.2.4.4). Four biological replicates were collected for each sample group, and all RNA samples were tested for appropriate quality and quantity using the Nanodrop 1000 spectrophotometer.

Samples were shipped to Azenta Life Sciences, Suzhou, China, for quality control, Poly A selection, non-strand specific library preparation and sequencing using Illumina NovaSeq PE150 at 20 M pair reads and 6 Gb/sample.

Raw FASTQ files along with standard bioinformatic analysis (quality control, alignment to reference genome, PCA, differential gene expression and enrichment analysis by gene ontology and KEGG pathway analysis) was delivered through Alicloud (Appendix).

Experimental group	Abbreviation	Illustration
LX-2 cells in single culture	LX-2 SC	
LX-2 cells in co-culture with BMOL-TAT <sup>c-MET</sup> WT cells	LX-2 CC WT	
LX-2 cells in co-culture with BMOL-TAT <sup>c-MET</sup> KO cells	LX-2 CC KO	

BMOL-TAT <sup>c-MET</sup> WT cells in single culture	WT SC	
BMOL-TAT <sup>c-MET</sup> WT cells in LX-2-conditioned medium for 30 minutes	WT CM 30	
BMOL-TAT <sup>c-MET</sup> WT cells in LX-2-conditioned medium for 6 hours	WT CM 6	
BMOL-TAT <sup>c-MET</sup> KO cells in LX-2-conditioned medium for 30 minutes	KO CM 30	
BMOL-TAT <sup>c-MET</sup> KO cells in LX-2-conditioned medium for 6 hours	KO CM 6	

**Table 6.1: Reference table of RNA-sequencing treatment groups and abbreviations.**

The 'Experimental group' column details the experimental state of the cells for RNA-sequencing. The 'Abbreviation' column to be used as reference throughout this chapter. The "Illustration" column visually representing the experimental groups. Four biological replicates were collected for each experimental group.

## 6.4 Results

### 6.4.1 Transcriptional profile of LX-2 cells in single culture and co-culture with BMOL-TAT<sup>c-MET WT</sup> and BMOL-TAT<sup>c-MET KO</sup> cells

#### 6.4.1.1 Quality control analysis

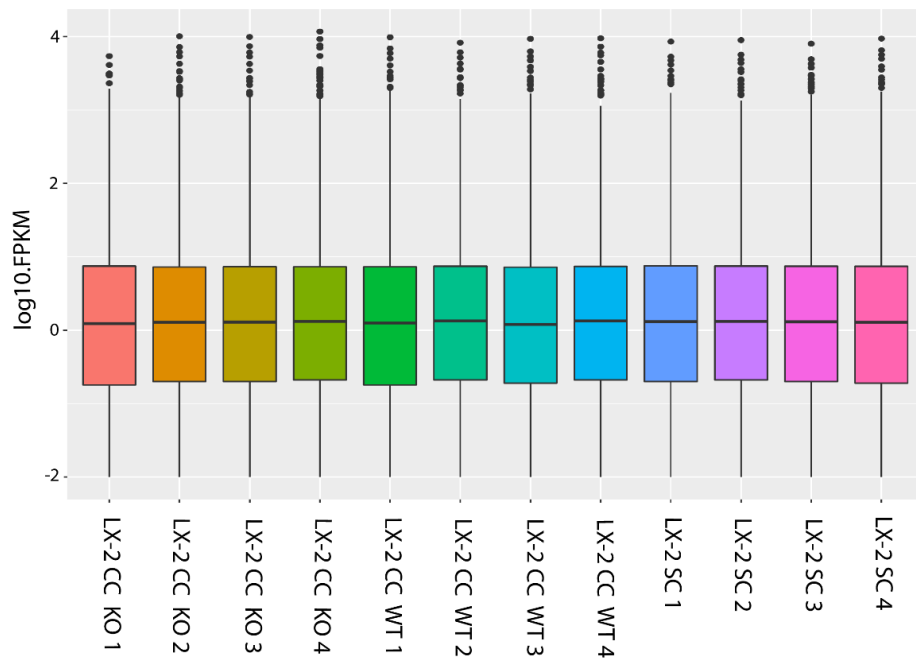
All samples of isolated total RNA from LX-2 cultures were confirmed to be of acceptable quality (RIN  $\geq 7$ ) prior to RNA-sequencing.

The Boxplot illustrating the log<sub>10</sub> (FPKM; fragments per kilobase of exon per million mapped fragments) gene expression of each sample was consistent (mean  $\sim 0$ ) (Figure 6.1A).

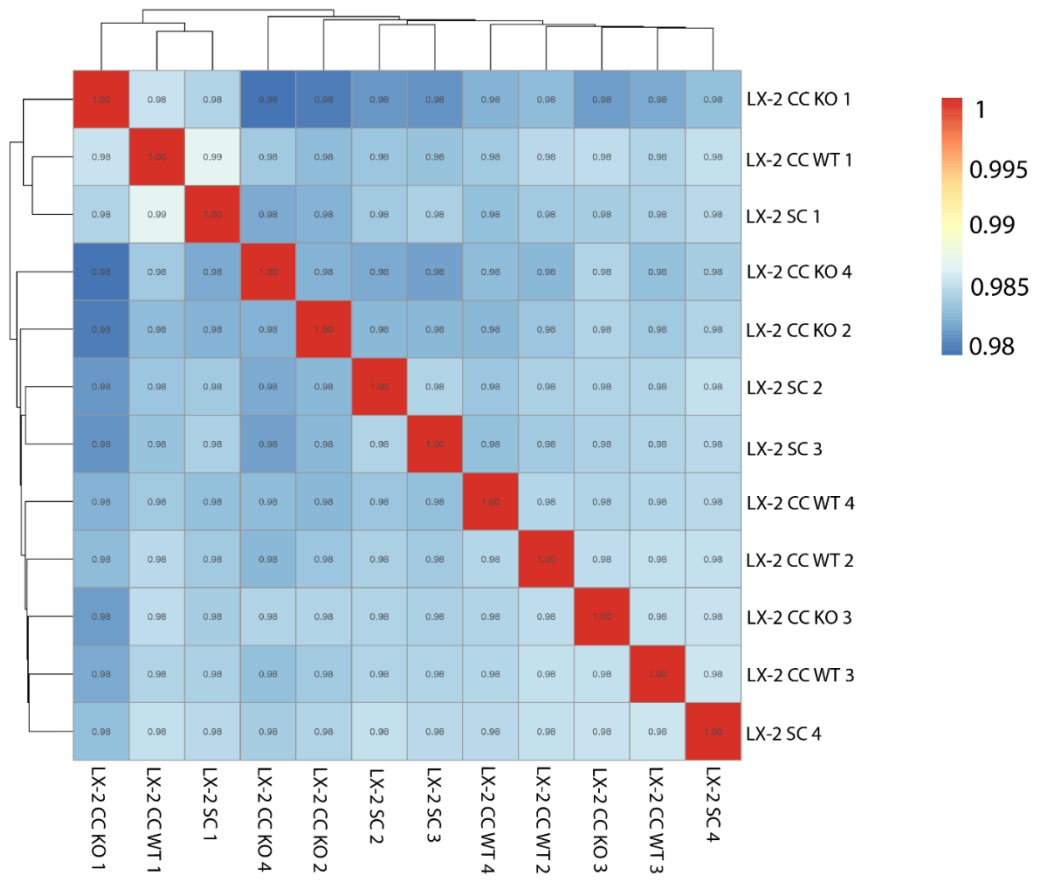
The Pearson coefficient correlates gene expression between biological samples to provide information about the reliability of the experiment. With the values in Figure 6.1B all  $\geq 0.98$ , this demonstrates a positive linear relationship between samples.

Lastly, principal component analysis (PCA) provides us with the ability to analyse sample relationship depending on the distance between them. Figure 6.1C demonstrates that biological samples of each group tend to cluster together, due to their high sample relationship. Although minor, each experimental group displays sample diversity, with the LX-2 CC KO samples displaying a more distinct transcriptional profile compared to LX-2 SC and LX-2 CC WT experimental groups.



**(A)**

(B)



(C)

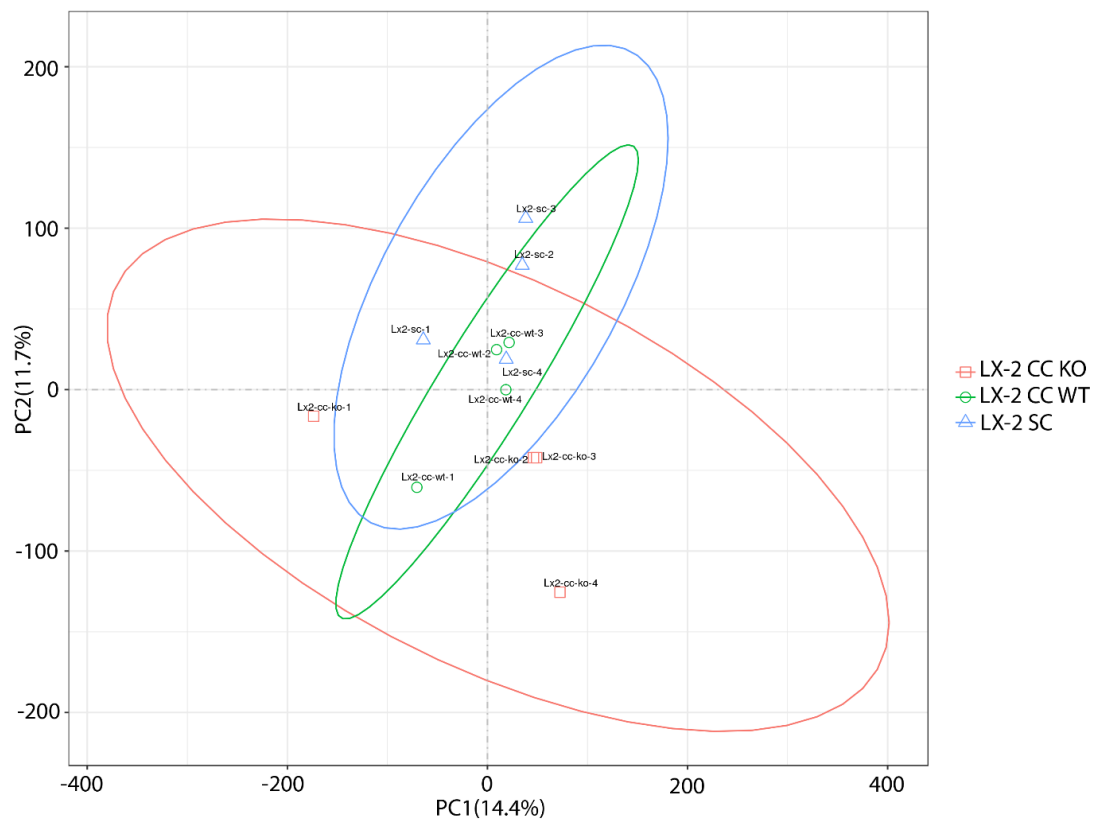


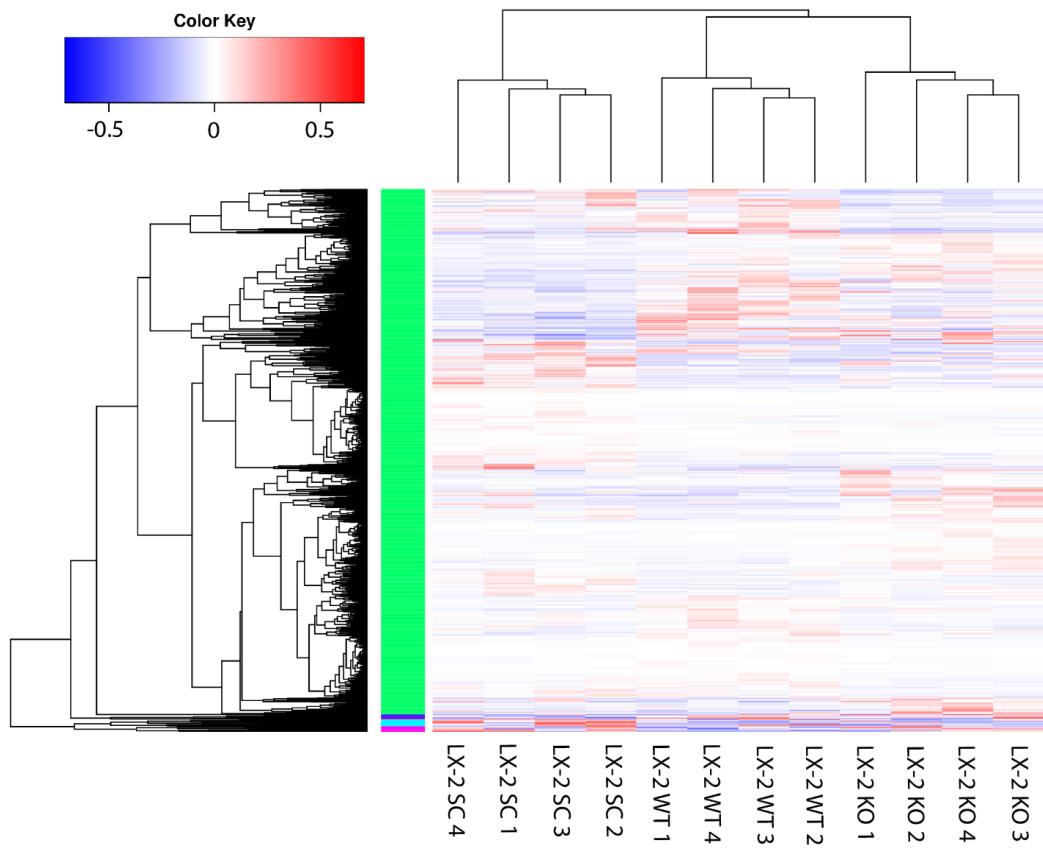
**Figure 6.1: Quality control analysis of LX-2 cells.**

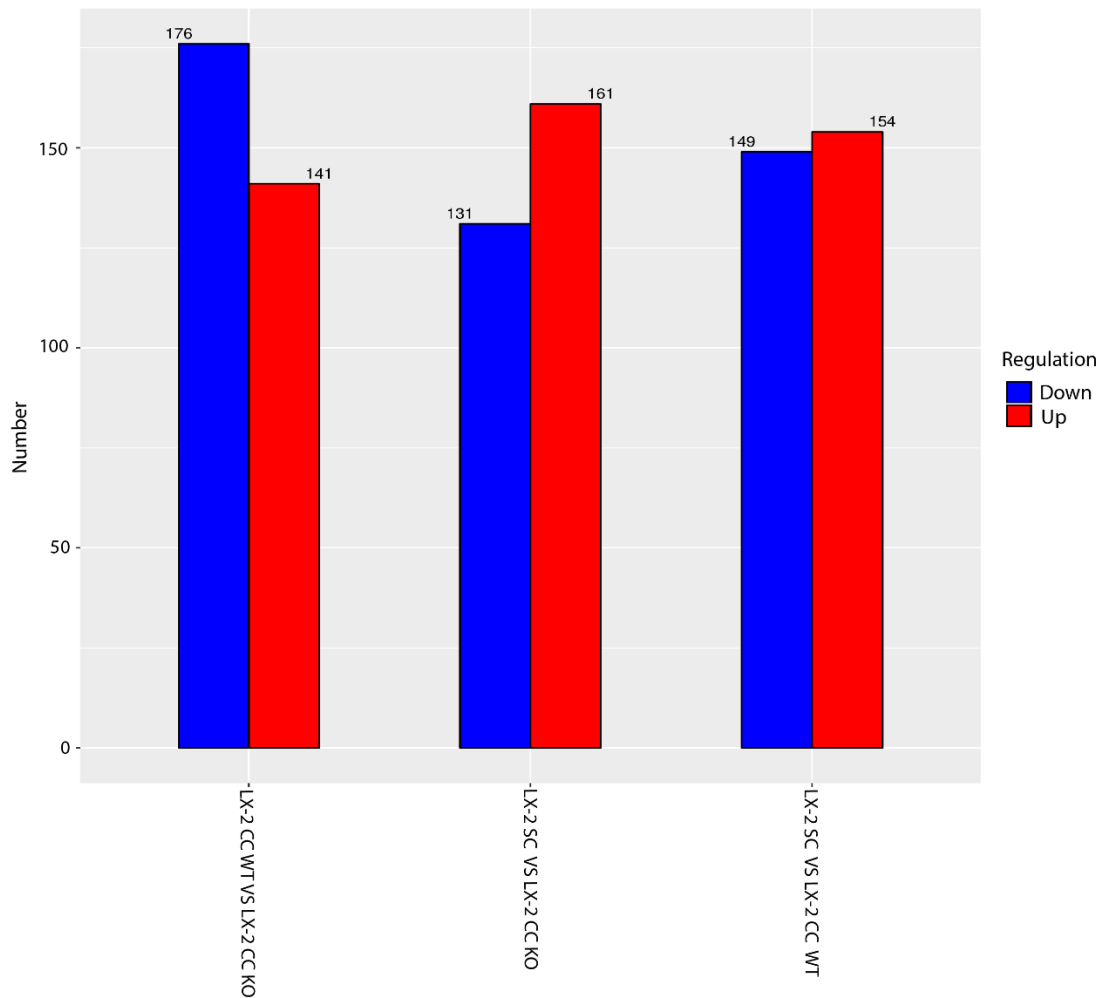
(A) A Boxplot graph illustrating the log<sub>10</sub> (FPKM) gene expression of each biological sample analysed. The mean of each sample displayed to be ~ 0. (B) The Pearson correlation coefficient demonstrating the degree of linear relationship between samples is  $\geq 0.98$ . (C) A PCA plot determining relationships of samples based on sample-to-sample distance. Clusters LX-2 SC, LX-2 CC WT and LX-2 CC KO circled blue, green and red, respectively.

#### **6.4.1.2 Differential gene expression analysis - LX-2 SC versus LX-2 CC WT versus LX-2 CC KO experimental groups**

Differential expression analysis was performed to compare the differentially expressed gene (DEG) profiles of LX-2 SC, LX-2 CC WT and LX-2 CC KO experimental groups. Figure 6.2A represents a heat map with DEGs of each population. The expression profiles of LX-2 SC, LX-2 CC WT and LX-2 CC KO comparison groups show similar numbers of DEGs (Figure 6.2B) (fold change (FC)  $>2$  or  $<-2$ , false discovery rate (FDR)  $<0.05$ ).

(A)



**(B)**

**Figure 6.2: Differential expression analysis of LX-2 SC, LX-2 CC WT and LX-2 CC KO experimental groups.**

(A) A heatmap illustrating the DEGs of biological replicates of groups LX-2 SC, LX-2 CC WT and LX-2 CC KO. (B) A bar graph demonstrating the numbers of DEGs between analysis groups LX-2 SC versus LX-2 CC WT, LX-2 SC versus LX-2 CC KO and LX-2 CC WT versus LX-2 CC KO.

### 6.4.1.3 Differential gene expression analysis - LX-2 SC versus LX-2 CC WT experimental groups

In total, 303 DEGs were identified in the LX-2 SC versus LX-2 CC WT comparison group with FC >2 or <-2 and FDR<0.05 (Figure 6.3). Table 6.2 highlights specific up- and downregulated genes between the LX-2 SC versus LX-2 CC WT comparison group involved in liver disease, with several genes associated with EMT, shown bolded.

The results identify that LX-2 cells, which have been co-cultured with BMOL-TAT<sup>c-MET</sup> WT cells, upregulate epithelial genes (*Krt5*, *Pxdnl* and *Lcn2*) while downregulating EMT-associated genes (*Matn1* and *Zeb2-as1*).

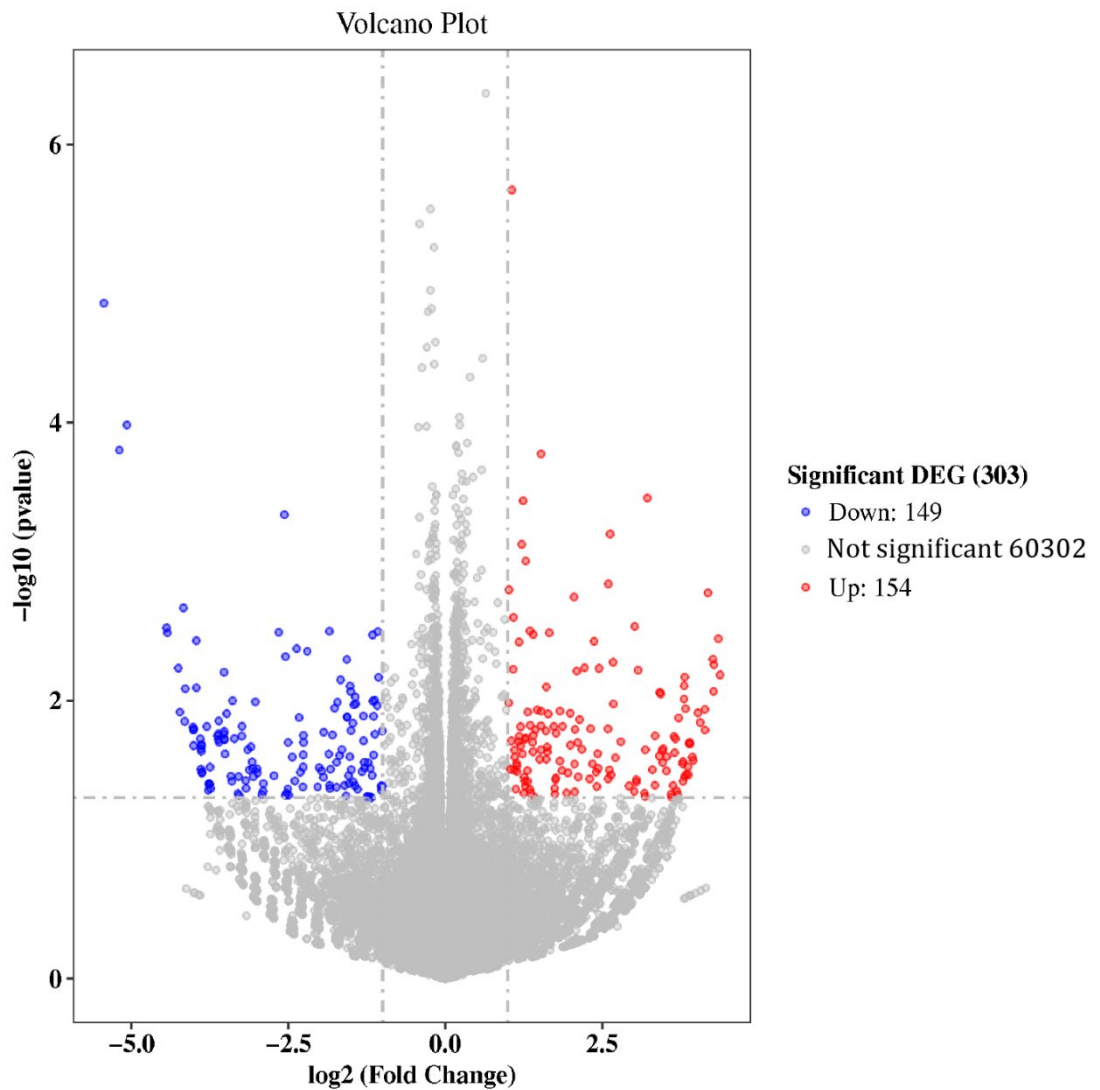


**Figure 6.3: Volcano plot of DEGs between LX-2 SC versus LX-2 CC WT experimental groups.**

The LX-2 SC versus LX-2 CC WT comparison group identified 303 DEGs. Red dots denoting upregulated genes and blue dots denoting downregulated genes.

All DEGs FC >2 or <-2 and FDR<0.05.



Gene	Log2 fold change	P-value	Literature
<b><i>Krt5</i></b>	<b>4.275731014</b>	<b>0.008570117</b>	<b>Involved in epithelial cell proliferation (Alam, Sehgal, Kundu, Dalal, &amp; Vaidya, 2011)</b>
<b><i>Pxdn1</i></b>	<b>3.811135775</b>	<b>0.035189357</b>	<b>Involved in epithelial cell differentiation (Sigurdardottir et al., 2021)</b>
<b><i>Sox5</i></b>	<b>3.788941549</b>	<b>0.037968384</b>	<b>Linked to fibrosis and EMT (D. Wang, Han, Wang, Peng, &amp; Li, 2015)</b>
<b><i>Lcn2</i></b>	<b>3.218570005</b>	<b>0.000348316</b>	<b>Negative regulator of EMT (Y. P. Wang et al., 2013)</b>
<i>Il2ra</i>	2.426171999	0.024052635	Increased expression with disease severity (Kao et al., 2021)
<i>Pik3c2g</i>	-3.761550047	0.039668431	Regulates HSC activation, proliferation and promotes fibrosis (Son, Hines, Lindquist, Schrum, & Rippe, 2009)
<b><i>Matn1</i></b>	<b>-3.391928201</b>	<b>0.010008924</b>	<b>Expressed by mesenchymal fibroblasts (Pei, Luo, &amp; Chen, 2008)</b>
<b><i>Zeb2-as1</i></b>	<b>-2.992917297</b>	<b>0.033098964</b>	<b>Linked to EMT (Jiang et al., 2020)</b>

**Table 6.2: DEGs between LX-2 SC versus LX-2 CC WT comparison groups involved in liver disease.**

DEGs associated with liver disease regulation, as identified in previous studies. Red colouring denotes upregulation and blue colouring denotes downregulation. Bolded genes are known to be involved in EMT/MET.

All DEGs FC >2 or <-2 and FDR<0.05.

#### 6.4.1.4 Differential gene expression analysis - LX-2 CC WT versus LX-2 CC KO experimental group

Since data obtained from LX-2 cells in single culture cannot be directly analysed in relation to LX-2 co-cultures with BMOL-TAT<sup>c-MET KO</sup> cells (LX-2 CC KO), a comparison with only one variable was performed: LX-2 CC WT versus LX-2 CC KO - where only the status of c-MET signalling activity is different.

In total, 317 DEGs were identified in the LX-2 CC WT versus LX-2 CC KO comparison group (FC >2 or <-2 and FDR<0.05) (Figure 6.4). Of the DEGs, ones relevant to the context of liver disease are displayed in Table 6.3. As previously, several genes associated with EMT are shown bolded.

The results identify that LX-2 cells that are co-cultured with BMOL-TAT<sup>c-MET KO</sup> cells upregulate fibrogenic and mesenchymal genes (*Tnf* and *Matn1*), while downregulating epithelial genes (*Krt5* and *Lcn2*).

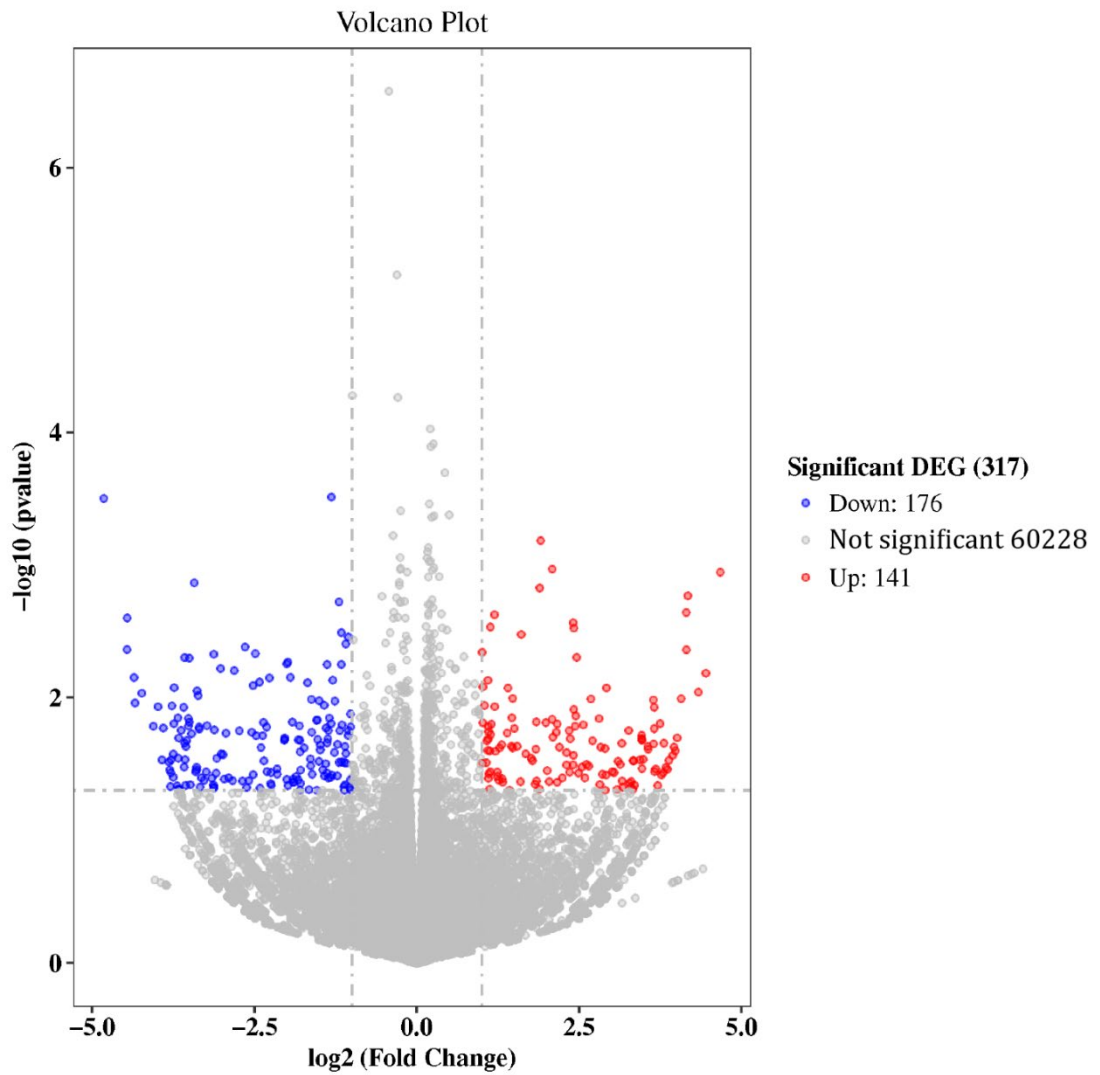


**Figure 6.4: Volcano plot of DEGs between LX-2 CC WT versus LX-2 CC KO experimental groups.**

The volcano plot illustrates 317 DEGs between the LX-2 CC WT versus LX-2 CC KO comparison group. Red dots denoting upregulated genes and blue dots denoting downregulated genes.

All DEGs FC >2 or <-2 and FDR<0.05.

Gene	Log2 fold change	P-value	Literature
<i>Tnf</i>	4.072453052	0.010166953	Promotes inflammation and liver fibrosis (Y. M. Yang & Seki, 2015)
<b><i>Matn1</i></b>	<b>3.010237691</b>	<b>0.036230652</b>	<b>Expressed by mesenchymal fibroblasts (Pei et al., 2008)</b>
<i>Krt5</i>	-4.235125908	0.009260408	Involved with epithelial cell proliferation (Alam et al., 2011)
<b><i>Sox5</i></b>	<b>-3.74840415</b>	<b>0.039769008</b>	<b>Linked to fibrosis and EMT (D. Wang et al., 2015)</b>
<i>Saa1</i>	-3.571938427	0.02194835	Promotes inflammation, proliferation, and cell death in HSCs (Siegmond et al., 2016)
<b><i>Lcn2</i></b>	<b>-2.485696561</b>	<b>0.004650947</b>	<b>Negative regulator of EMT (Y. P. Wang et al., 2013)</b>
<i>Il2ra</i>	-2.398284532	0.023782242	Increased expression with disease severity (Kao et al., 2021)

**Table 6.3: DEGs between LX-2 CC WT versus LX-2 CC KO cells involved in liver disease.**

DEGs associated with liver disease regulation, as identified in previous studies. Red colouring denotes upregulation and blue colouring denotes downregulation. Bolded genes involved in EMT/MET.

All DEGs FC >2 or <-2 and FDR<0.05.

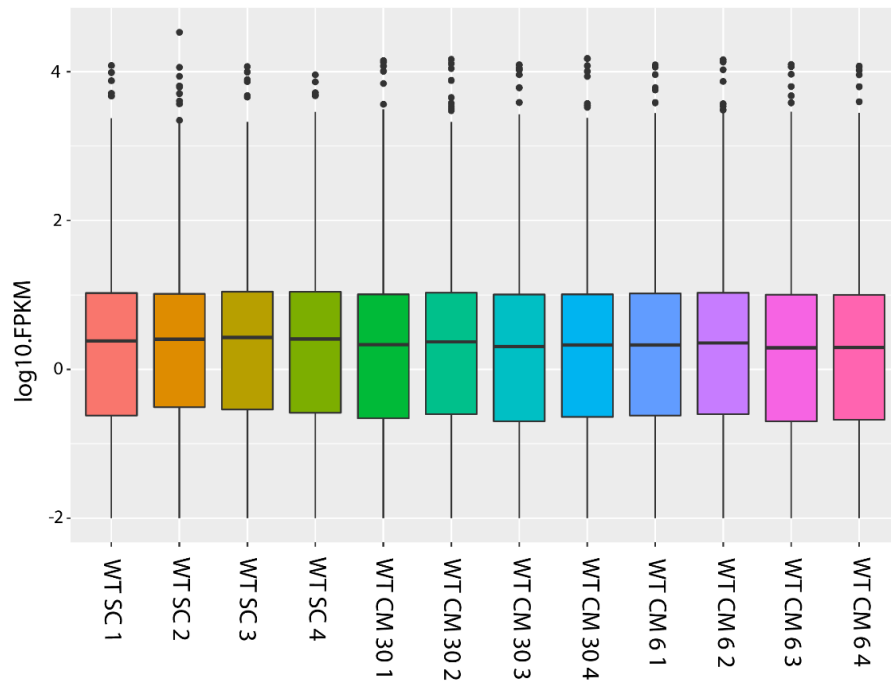
## 6.4.2 Transcriptional profile of BMOL-TAT<sup>c-MET</sup> WT and BMOL-TAT<sup>c-MET</sup> KO cells in single culture and LX-2-conditioned medium

### 6.4.2.1 Quality control analysis

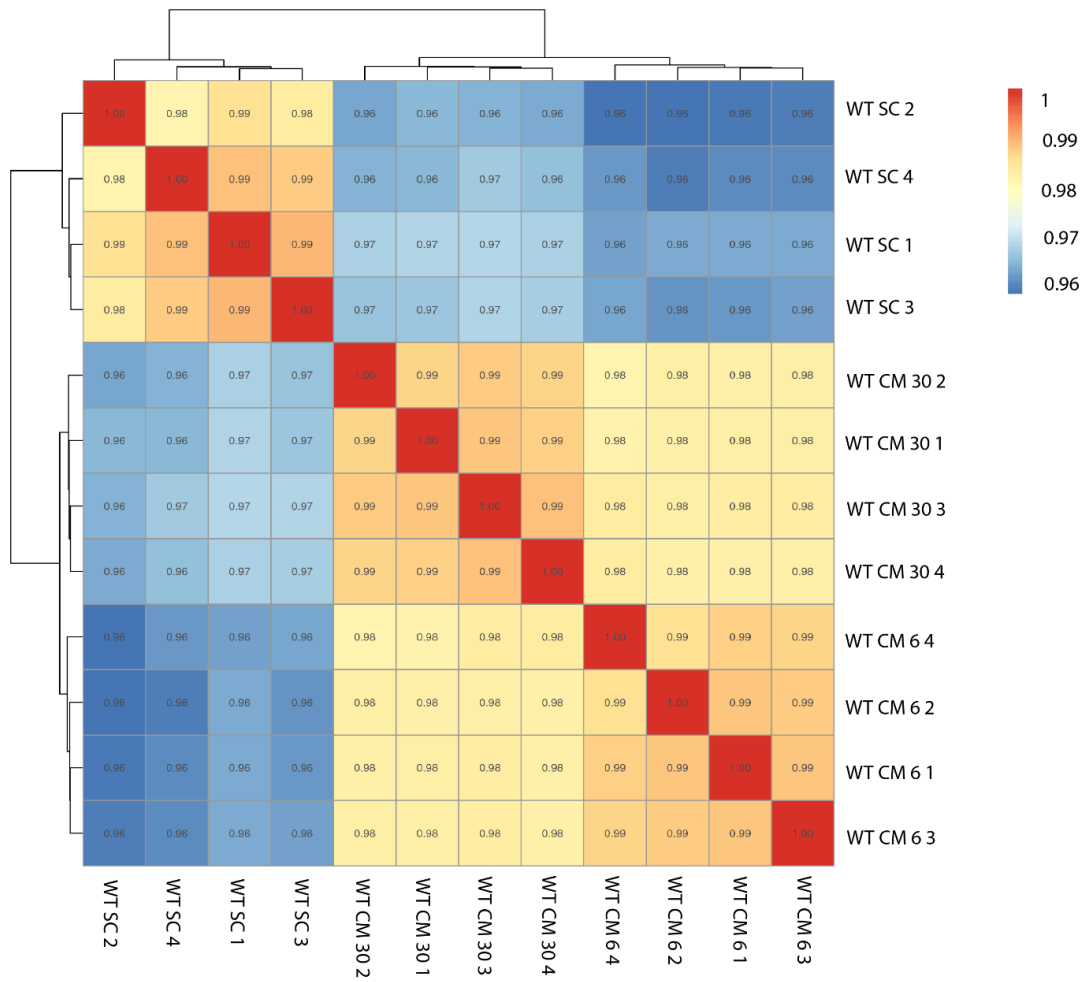
Appropriate quality of the samples WT SC, WT CM 30, WT CM 6, KO CM 30, KO CM 6 was confirmed before further analysis ensued (RIN $\geq$ 7).

Figures 6.5A and 6.6A represent a Boxplot of the log<sub>10</sub> (FPKM) gene expression, demonstrating consistency of samples (mean  $\sim$  0). Sample quality was further validated by the Pearson correlation coefficient with values  $\geq$  0.96, demonstrating a positive linear relationship between samples (Figures 6.5B and 6.6B). A lower sample relationship was observed between single culture and conditioned medium experimental groups, evidenced by values closer to 0.96 (Figure 6.5B). This was also demonstrated when comparing wildtype and c-MET knockout BMOL-TAT experimental groups (Figure 6.6B).

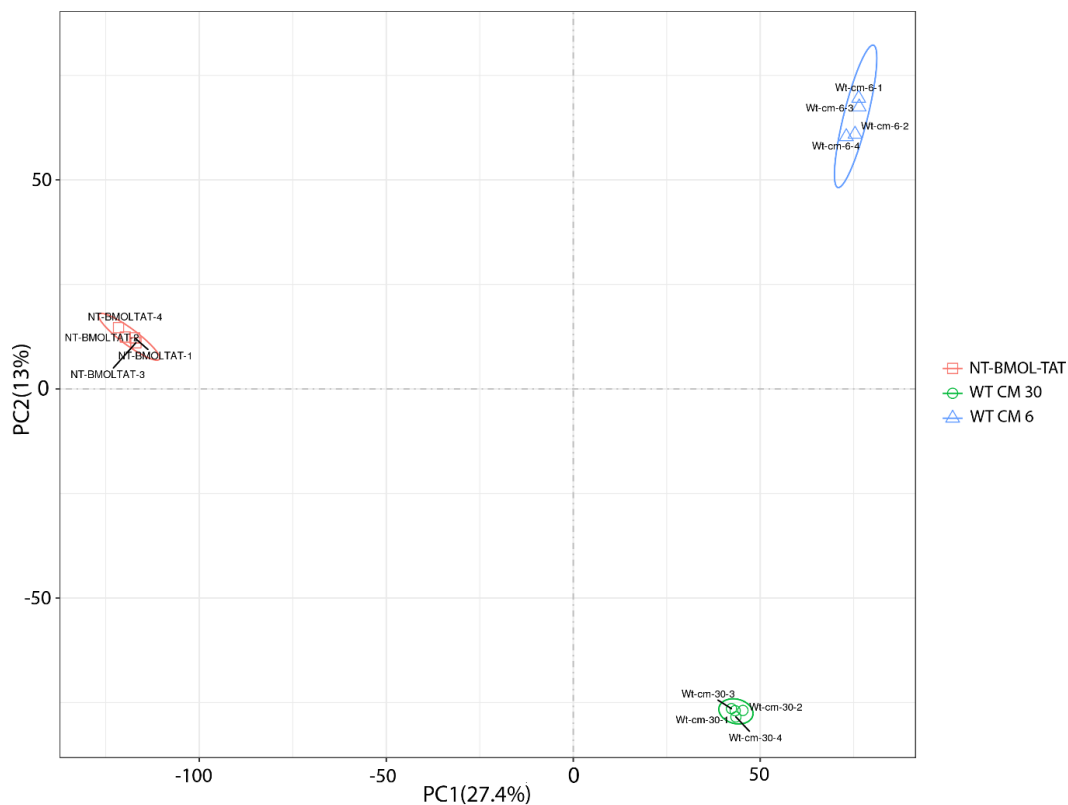
The lower similarity between single culture and conditioned medium groups is further represented in the PCA plot in Figure 6.5C as a greater distance between treatment groups is indicative of distinct transcriptional profiles. Wildtype and c-MET knockout BMOL-TAT cells were also evidenced to display transcriptionally distinct profiles (Figure 6.6C). Still, biological samples of each group tended to cluster together due to their high sample relationship.

**(A)**

(B)



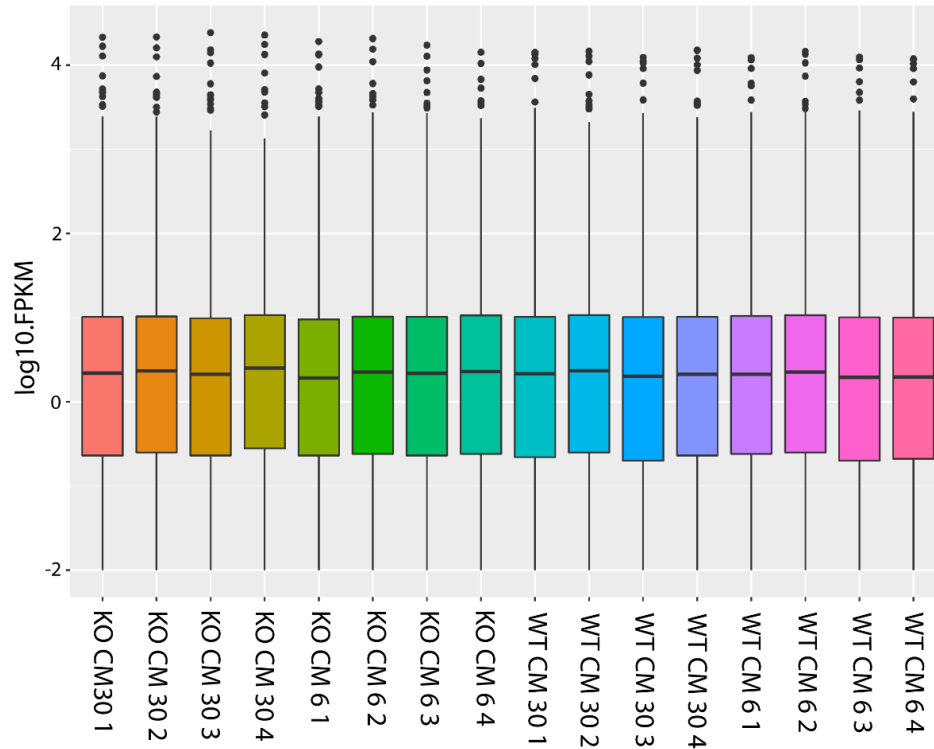
(C)



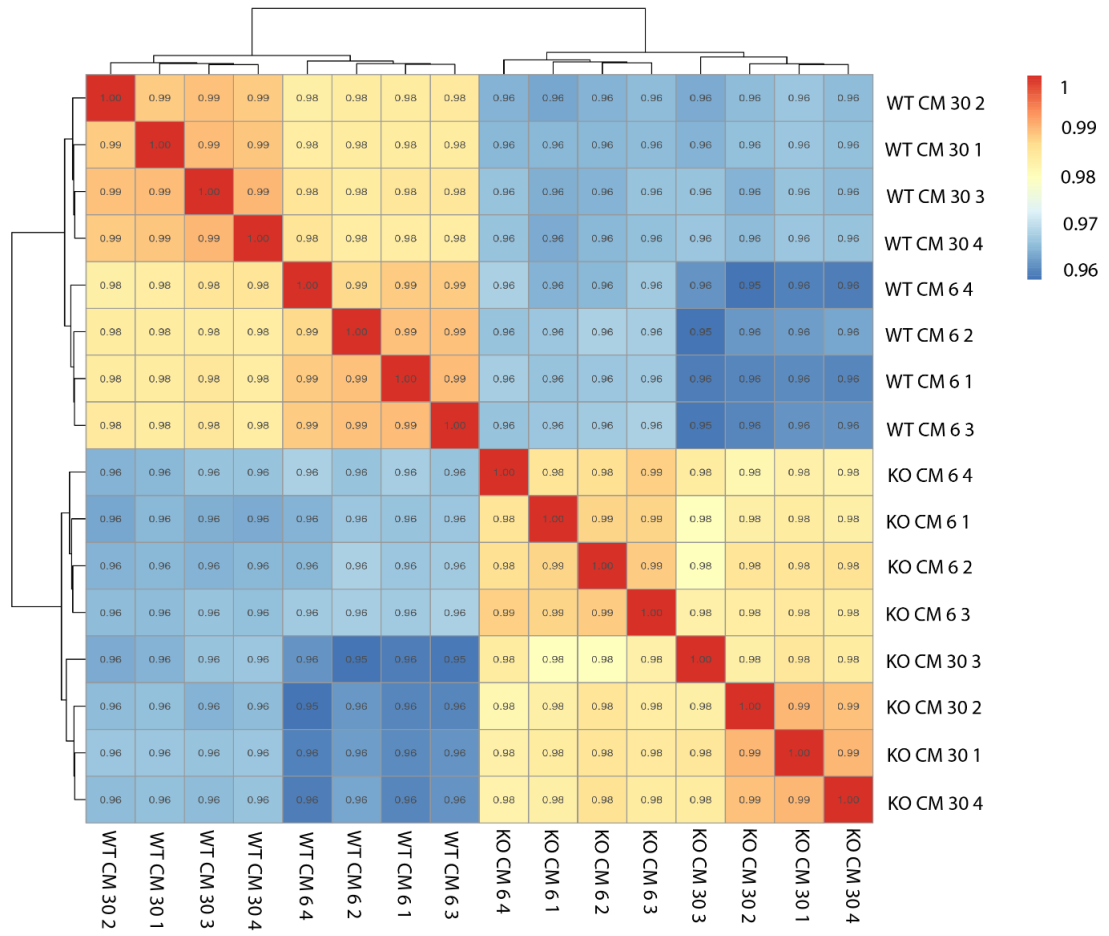
**Figure 6.5: Quality control analysis of BMOL-TAT<sup>c-MET</sup> WT cells.**

(A) A Boxplot illustrating the log<sub>10</sub> (FPKM) gene expression of each biological sample measured, will the means approximately 0. (B) The Pearson correlation coefficient demonstrating the degree of linear relationship between samples is  $\geq 0.96$ . (C) A PCA plot determining relationships of samples based on distance between them. Clusters WT SC, WT CM 30 and WT CM 6 circled red, green and blue, respectively, display transcriptionally distinct profiles. NT-BMOL-TAT denoting WT SC.



**(A)**

(B)



(C)

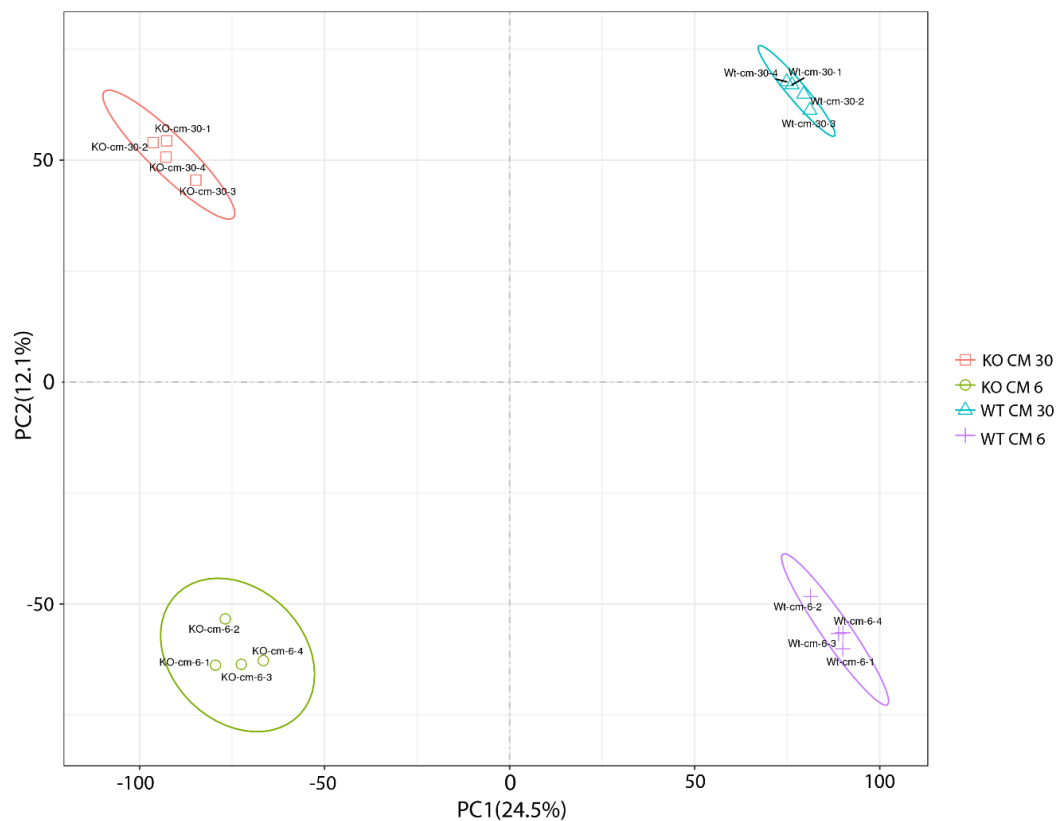


**Figure 6.6: Quality control analysis of BMOL-TAT<sup>c-MET</sup> WT and BMOL-TAT<sup>c-MET</sup> KO cells in conditioned medium experiments.**

(A) A Boxplot illustrating the log<sub>10</sub> (FPKM) gene expression of each biological sample measured, with the mean of each sample  $\sim 0$ . (B) The Pearson correlation coefficient demonstrating the degree of linear relationship between samples is  $\geq 0.96$ . (C) PCA plot determining relationships of samples based on distance between them. Clusters KO CM 30, KO CM 6, WT CM 30, WT CM 6 circled red, green, blue and purple, respectively, display transcriptionally distinct profiles.

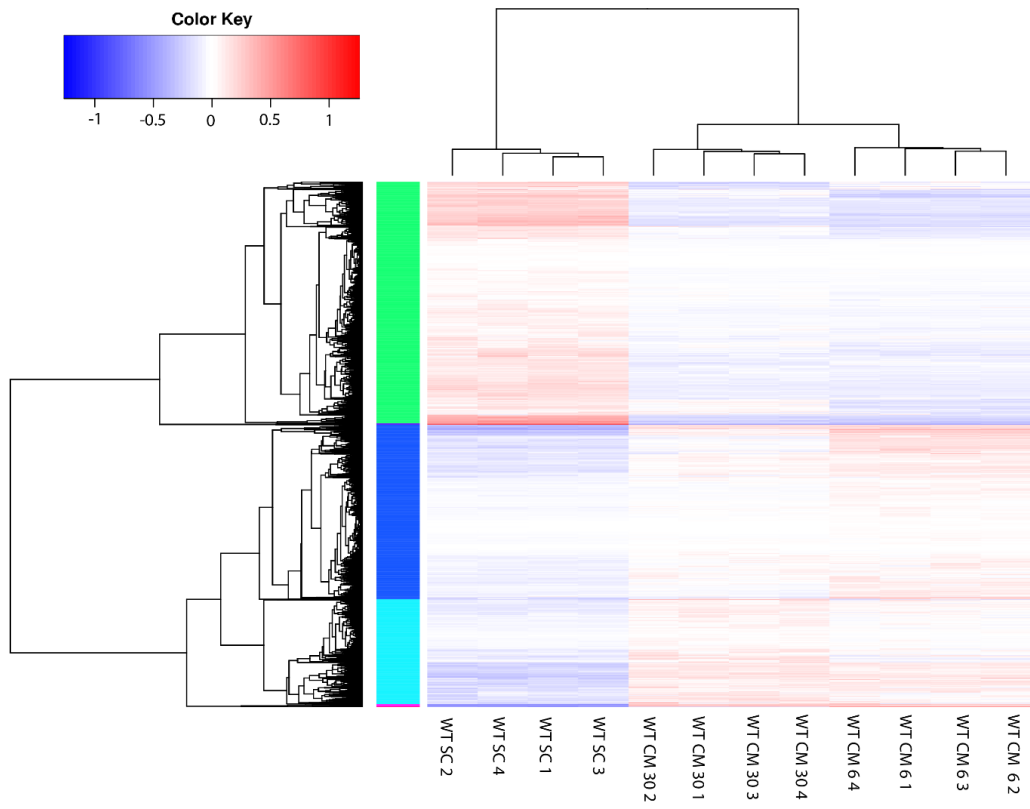
#### **6.4.2.2 Differential gene expression analysis - WT SC versus WT CM 30 versus WT CM 6 experimental groups**

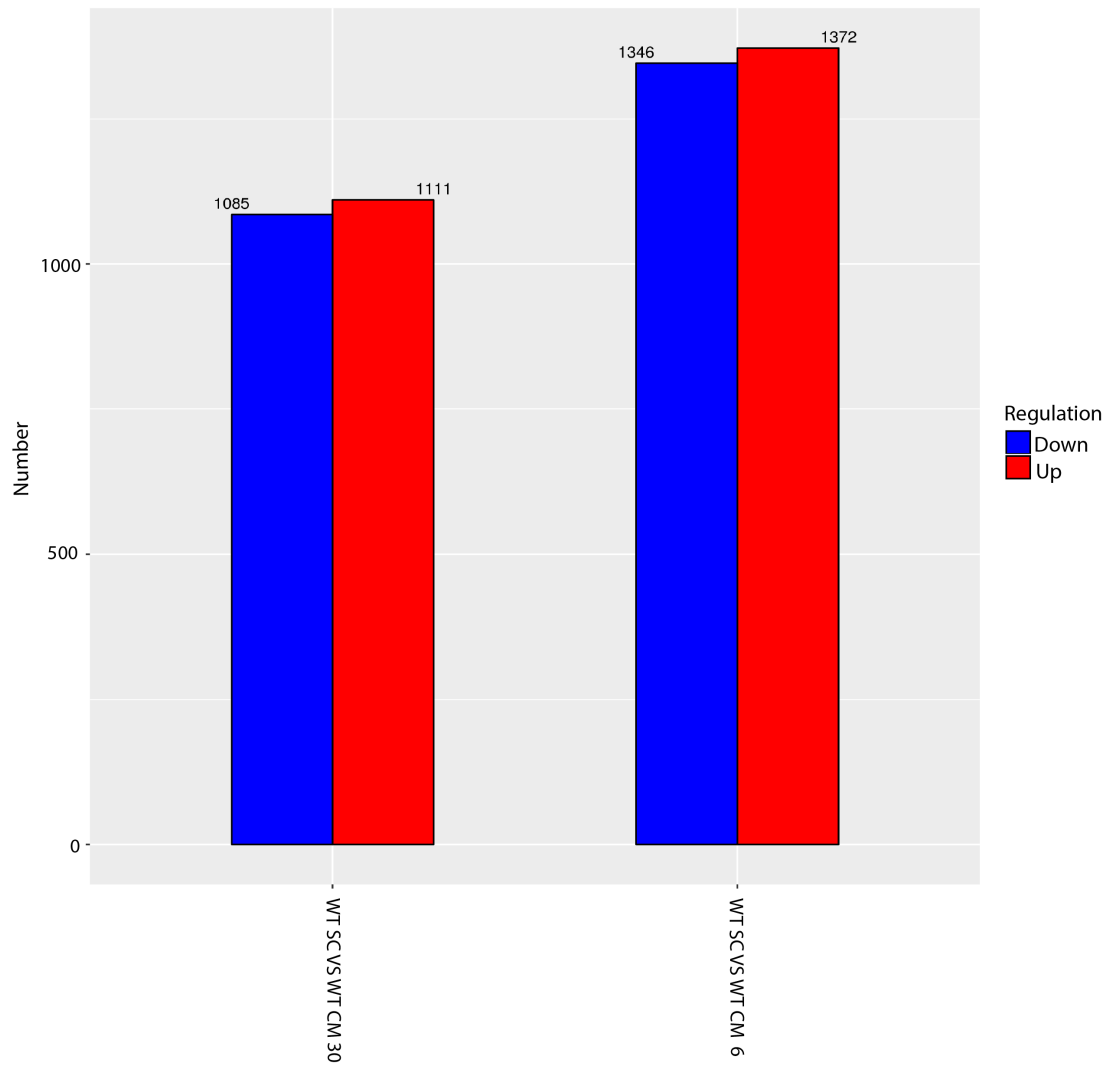
Differential expression analysis was performed to compare wildtype BMOL-TAT cells in single culture and in LX-2-conditioned medium for either 30 minutes or 6 hours (WT SC, WT CM 30 and WT CM 6). Figure 6.7A displays all DEGs between each sample population. The DEG profiles are similar between WT CM 30 and WT CM 6 treatment groups, suggesting that the timeframe of conditioned medium experiments did not impact the overall transcriptional activity greatly. However, between WT SC and WT CM experimental groups, major changes in gene expression were evident (Figure 6.7A).

Although Figure 6.7B identified similar DEG changes between WT CM 30 and WT CM 6 treatment groups, it was also identified that a greater number of up- or downregulated genes were present in the WT SC versus WT CM 6 comparison group, relative to the WT SC versus WT CM 30 comparison group ((FC) >2 or <-2, (FDR) <0.05).

Further, the Venn diagram in Figure 6.7C corroborated this finding, as a greater number of uniquely identified DEGs (1087) were present in the WT SC versus WT CM 6 comparison group. Therefore, further analysis was carried out using the WT SC versus WT CM 6 experimental group.

(A)



**(B)**

(C)

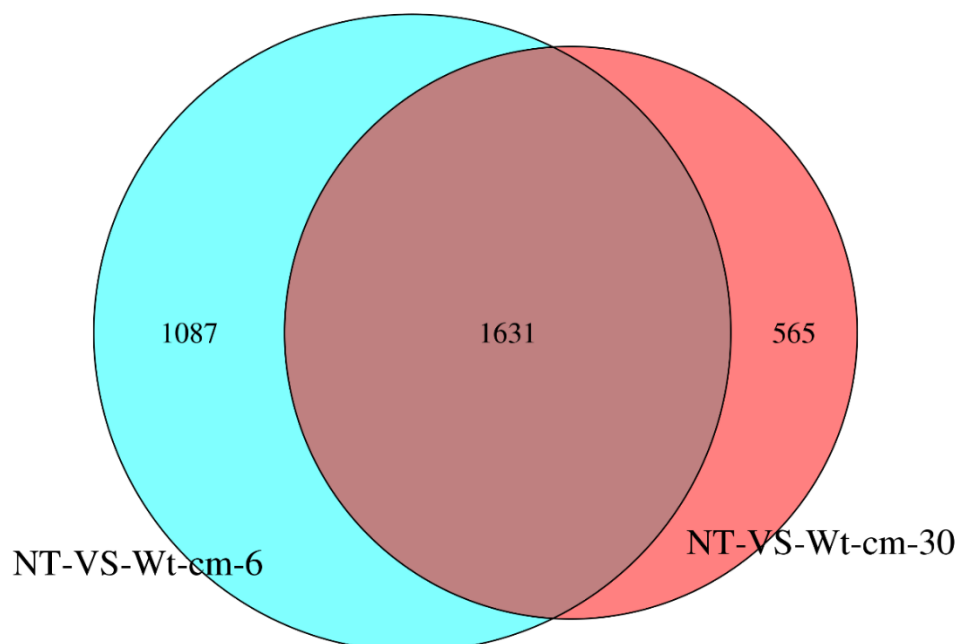


**Figure 6.7: Differential gene expression analysis of WT SC versus WT CM 30 versus WT CM 6 comparison groups.**

(A) A heatmap illustrating the DEGs in biological replicates of experimental groups WT SC, WT CM 30 and WT CM 6. (B) A bar graph demonstrating a greater number of DEGs were present between the WT SC versus WT CM 6 comparison group, as compared to the WT SC versus WT CM 30 experimental group. (C) A Venn diagram displaying a higher number of unique DEGs between the WT SC and WT CM 6 comparison group, as compared to the WT SC versus WT CM 30 experimental group. NT denoting the WT SC experimental group.

All DEGs with FC >2 or <-2 and FDR<0.05.

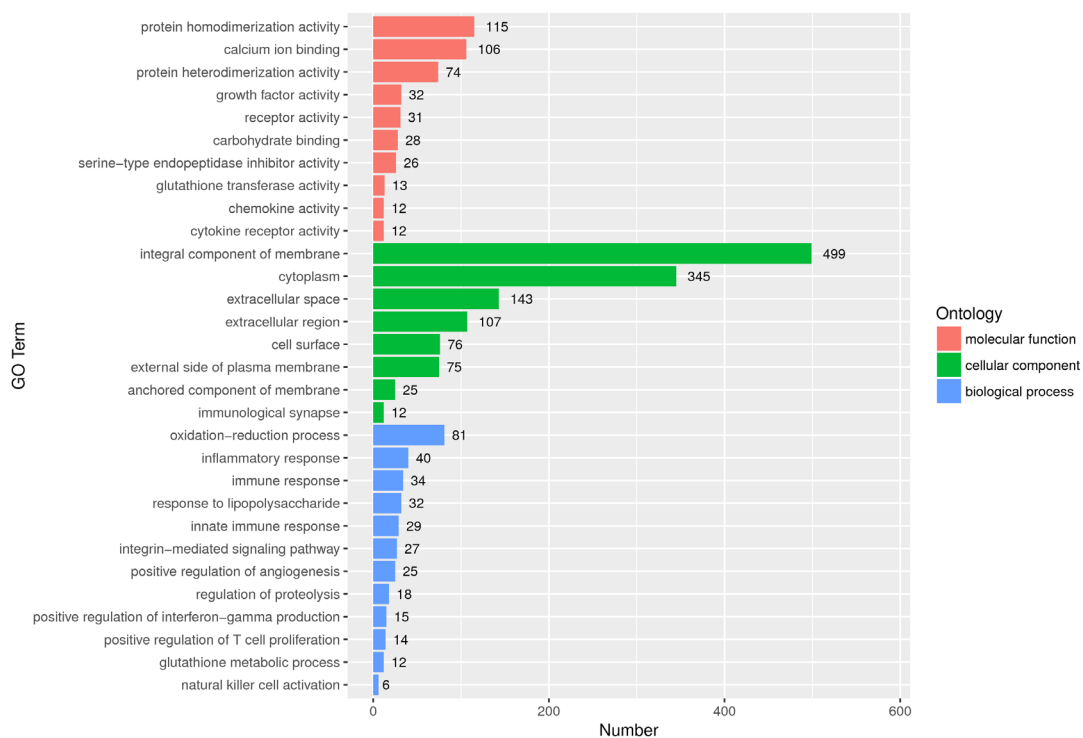
#### **6.4.2.3 Enrichment analysis - WT SC versus WT CM 6 experimental group**

Gene ontology (GO) analysis of upregulated DEGs on the WT SC versus WT CM 6 experimental group was performed, which demonstrated significant enrichment of a range of biological processes, displayed in Figure 6.8A.

Moreover, KEGG pathway analysis revealed that several pathways are enriched, highlighted in Figure 6.8B. Changes were not restricted to LPC biology, although enrichment profiles in cancer and cell adhesion provided insight into LPC function during cellular crosstalk. Therefore, investigating the specific up- and downregulated genes in the WT SC versus WT CM 6 experimental group was of interest to provide a deeper understanding of potential cellular changes upon the addition of LX-2-conditioned medium.



(A)



(B)

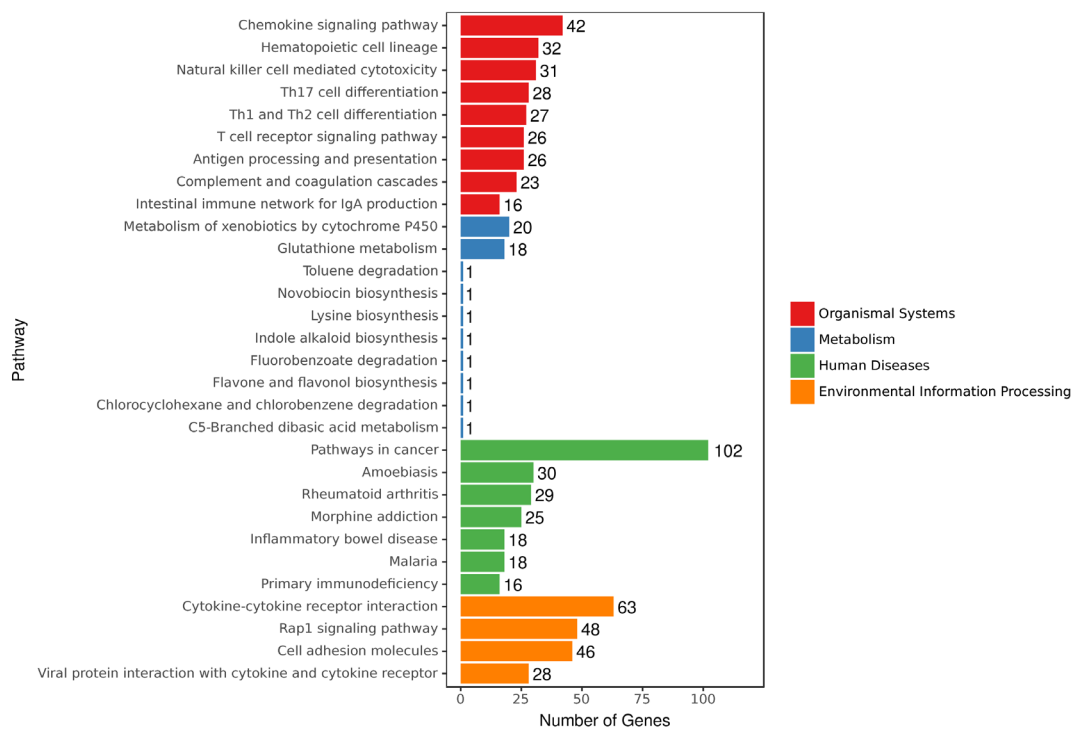


**Figure 6.8: Enrichment analysis of the WT SC versus WT CM 6 experimental group.**

(A) GO analysis and (B) KEGG pathway analysis of upregulated DEGs in WT SC versus WT CM 6 cells, demonstrating an enrichment in several pathways. FDR, <math><0.05</math>,

#### 6.4.2.4 Differential gene expression analysis - WT SC versus WT CM 6 experimental group

In total, 2718 DEGs were identified in the WT SC versus WT CM 6 comparison group (FC >2 or <-2 and FDR<0.05) (Figure 6.9). Table 6.4 illustrates all up- or downregulated genes in the context of liver disease. Of the DEGs, several were involved in ECM remodelling and cell adhesion, shown bolded.

The identified DEGs demonstrate that subjecting the BMOL-TAT<sup>c-MET</sup> WT cells to LX-2-conditioned medium for 6 hours, induced the upregulation of ECM remodelling genes *Mmp3*, *Mmp10*, *Igfa4*, *Mmp2*, *Mmp12* and *Mmp13* and downregulation of ECM deposition genes *Col16a1*, *Lama4*, *Cldn6*, *Timp3*, *Col8a1*, *Col6a2*, *Col28a1*, *Matn1* and *Col4a6*. Additionally, BMOL-TAT<sup>c-MET</sup> WT cells under the same conditions, downregulated cell adhesion genes including *Cdh13*, *Krt20*, *Cdh10*, *Cdhr1*, *Jam3*, *Krt7* and *Bcam* (Table 6.4). This suggests that the BMOL-TAT<sup>c-MET</sup> WT cells are altering their surrounding ECM in response to LX-2-regulated signalling, while downregulating their adhesion to facilitate their migration.

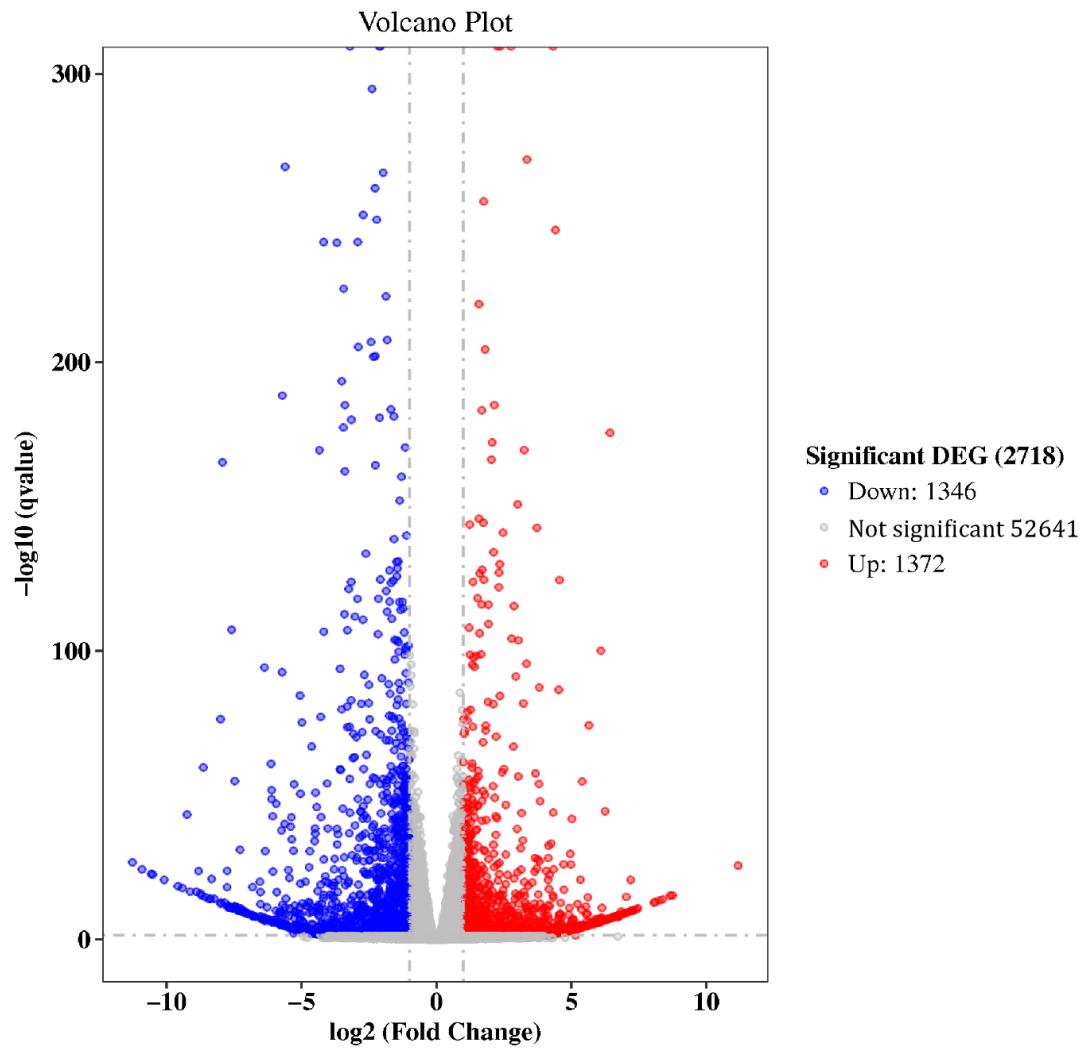


**Figure 6.9: Volcano plot of DEGs between WT SC versus WT CM 6 experimental groups.**

In total, 2718 statistically significant genes were identified between the WT SC versus WT CM 6 comparison group. Red dots denoting upregulated genes and blue dots denoting downregulated genes.

All DEGs FC >2 or <-2 and FDR<0.05.

Gene	Log2 fold change	P-value	Literature
<b>Mmp3</b>	<b>11.1733453</b>	<b>1.09E-27</b>	<b>Increased expression during liver disease progression (Geervliet &amp; Bansal, 2020)</b>
<i>Saa2</i>	6.54618949	3.18E-09	Promotes inflammation, proliferation, and cell death in HSCs (Siegmund et al., 2016)
<b>Mmp10</b>	<b>6.244224134</b>	<b>7.29E-47</b>	<b>Increased expression during liver fibrosis (Geervliet &amp; Bansal, 2020)</b>
<i>Saa1</i>	5.992750937	1.55E-07	Promotes inflammation, proliferation, and cell death in HSCs (Siegmund et al., 2016)
<b>Itga4</b>	<b>5.54349091</b>	<b>2.58E-10</b>	<b>Upregulated in LPCs during regeneration (Peter Siig Vestentoft et al., 2013)</b>
<b>Mmp2</b>	<b>5.41413899</b>	<b>1.78E-06</b>	<b>Increased expression during liver fibrosis (Geervliet &amp; Bansal, 2020)</b>
<i>Ang2</i>	5.33615911	1.76E-05	Increased expression with liver disease severity (Siddiqui, Rawal, Bihari, Arora, & Kaur, 2020)
<i>Fgl2</i>	4.744323198	0.000455981	Promotes tumour progression (B.-Q. Liu, Bao, Zhu, & Liu, 2021)
<b>Col5a3</b>	<b>4.609582725</b>	<b>0.001690933</b>	<b>Increased expression during liver fibrosis (Lai et al., 2011)</b>
<i>Rac2</i>	4.601482338	1.98E-14	Promotes inflammation during liver injury (Zou, Xiong, Ma, Wang, & Qian, 2017)
<b>Mmp12</b>	<b>4.515656401</b>	<b>0.001653143</b>	<b>Increased expression during liver fibrosis (Geervliet &amp; Bansal, 2020)</b>
<i>Saa3</i>	4.409996914	1.10E-249	Promotes inflammation, proliferation, and cell death in HSCs (Siegmund et al., 2016)
<b>Cdh5</b>	<b>4.165474431</b>	<b>2.16E-19</b>	<b>Involved in progenitor cell activation (Anderson et al., 2015)</b>
<i>Ddr2</i>	4.06352566	7.72E-26	Involved in liver fibrosis resolution (Olaso, Arteta, Benedicto, Crende, & Friedman, 2011)
<i>Stat4</i>	3.753441119	0.005573992	Increased expression with liver disease severity (Y. Wang, Qu, & Wang, 2015)

<i>Casp1</i>	3.074712593	0.000196908	Role in inflammation and fibrosis (Dixon, Berk, Thapaliya, Papouchado, & Feldstein, 2012)
<b><i>Mmp13</i></b>	<b>2.762988005</b>	<b>0</b>	<b>Increased expression during liver fibrosis (Geervliet &amp; Bansal, 2020)</b>
<i>Bex2</i>	-8.893841915	1.99E-18	Involved in liver disease progression (Tamai et al., 2020)
<i>Bex1</i>	-7.749154307	7.71E-26	Importance in LPC expansion (Gu et al., 2018)
<i>Pparg</i>	-7.480444769	2.97E-13	Reduces LPC expansion (Gu et al., 2018)
<b><i>Cdh13</i></b>	<b>-7.144014109</b>	<b>4.90E-11</b>	<b>Importance in cell adhesion (Andreeva &amp; Kutuzov, 2010)</b>
<i>Igfbp5</i>	-6.537633022	5.81E-22	Promotes fibrosis (Nguyen, Muhammad, Nietert, & Feghali-Bostwick, 2018)
<i>Hnf1a</i>	-6.064366066	3.96E-45	Increased expression with liver disease severity (Xue Wang et al., 2019)
<b><i>Krt20</i></b>	<b>-5.935049046</b>	<b>1.68E-49</b>	<b>Provides structural integrity for epithelial cells (C. W. Chan et al., 2009)</b>
<i>Pdgfd</i>	-5.806269581	4.73E-11	Increased expression during liver fibrosis (Borkham-Kamphorst et al., 2007)
<b><i>Col16a1</i></b>	<b>-5.713396442</b>	<b>1.62E-95</b>	<b>Increased expression during liver fibrosis (Lai et al., 2011)</b>
<b><i>Lama4</i></b>	<b>-5.066761152</b>	<b>3.67E-08</b>	<b>Increased expression during liver cancer (Zheng et al., 2020)</b>
<b><i>Cdh10</i></b>	<b>-4.962088368</b>	<b>3.02E-14</b>	<b>Importance in cell adhesion (Luo, Lin, Liao, Li, &amp; Qin, 2021)</b>
<i>Sox2</i>	-4.765301183	0.00136351	Importance in tissue regeneration and survival (Arnold et al., 2011)
<i>Lefty1</i>	-4.693849729	2.91E-14	Stemness marker (Kim, Cha, Ahn, Kim, & Park, 2014)
<b><i>Cldn6</i></b>	<b>-4.62142678</b>	<b>1.46E-69</b>	<b>Increased expression in HCC (Lu et al., 2021)</b>
<i>Sox12</i>	-4.235765202	0.001240168	Promotes HCC (W. Huang et al., 2015)
<b><i>Cdhr1</i></b>	<b>-4.224415967</b>	<b>0.00155327</b>	<b>Importance in cell adhesion (Luo et al., 2021)</b>
<b><i>Timp3</i></b>	<b>-4.114022022</b>	<b>5.99E-24</b>	<b>Fibro-protective role in the liver (Casagrande et al., 2017)</b>

<i>Col8a1</i>	<b>-3.968433677</b>	<b>7.27E-05</b>	<b>Increased expression during liver fibrosis (Lai et al., 2011)</b>
<i>Jam3</i>	<b>-3.699964893</b>	<b>2.23E-09</b>	<b>Role in cell adhesion (Hintermann et al., 2018)</b>
<i>Sox5</i>	-3.519531392	0.018126518	Linked to fibrosis and EMT (D. Wang et al., 2015)
<i>Fgf1</i>	-3.446360641	6.82E-181	Fibro-protective role in the liver (Z. Xu et al., 2020)
<i>Col6a2</i>	<b>-3.426074449</b>	<b>3.26E-06</b>	<b>Increased expression during liver fibrosis (Lai et al., 2011)</b>
<i>Krt7</i>	<b>-3.29760534</b>	<b>3.57E-110</b>	<b>Increased expression with liver disease severity (Sancho-Bru et al., 2012)</b>
<i>Tgfb3</i>	-3.221267094	4.63E-09	Potential negative regulator of fibrosis (Chu et al., 2011)
<i>Col28a1</i>	<b>-3.100074683</b>	<b>0.009251527</b>	<b>Increased expression during liver fibrosis (Lai et al., 2011)</b>
<i>Bcam</i>	<b>-2.915170594</b>	<b>1.72E-245</b>	<b>Role in liver regeneration (Miura et al., 2018)</b>
<i>Alb</i>	-2.862688064	1.30E-10	Increased expression with liver disease severity (Fujita et al., 2019)
<i>Matn2</i>	<b>-2.826528454</b>	<b>1.34E-17</b>	<b>Role in tissue remodelling (Szabó et al., 2008)</b>
<i>Ndr2</i>	-2.7562422	2.83E-38	Fibro-protective role (J. Yang et al., 2011)
<i>Prom1</i>	-2.709370392	0.003467182	Stemness marker (F. Liu & Qian, 2021)
<i>Mmp15</i>	<b>-2.671282799</b>	<b>2.88E-12</b>	<b>Increased expression during liver fibrosis (Geervliet &amp; Bansal, 2020)</b>
<i>Mapk15</i>	-2.639406457	8.85E-06	Increased expression with liver disease severity (Westenberger et al., 2021)
<i>Bmp6</i>	-2.600935611	2.49E-05	Fibro-protective role during liver disease (Arndt et al., 2015)
<i>Col4a6</i>	<b>-2.528437593</b>	<b>6.38E-06</b>	<b>Increased expression during liver fibrosis (Lai et al., 2011)</b>

**Table 6.4: DEGs between the WT SC versus WT CM 6 comparison group involved in liver disease.**

A list of DEGs associated with liver disease regulation, as identified in previous studies. Red colouring denotes upregulation and blue colouring denotes downregulation. Bolded genes involved in ECM remodelling and cell adhesion. All DEGs FC >2 or <-2 and FDR<0.05.

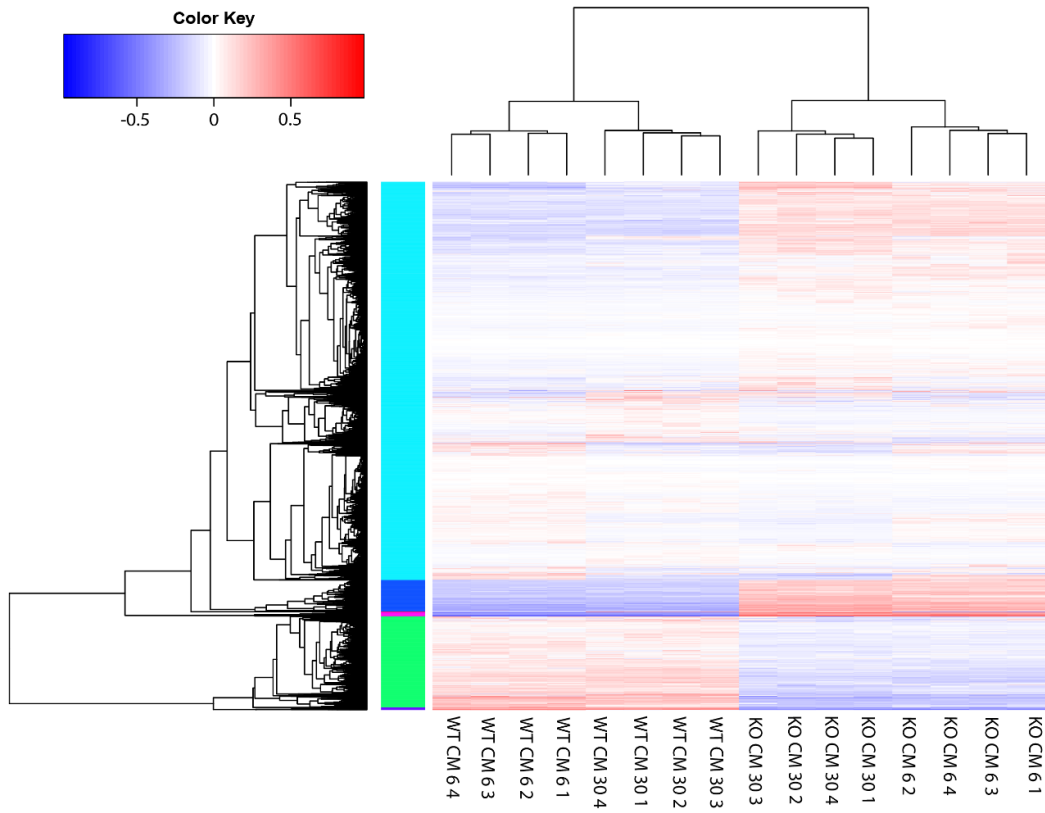
#### **6.4.2.5 Differential gene expression analysis - WT CM 30, WT CM 6, KO CM 30, KO CM 6 experimental groups**

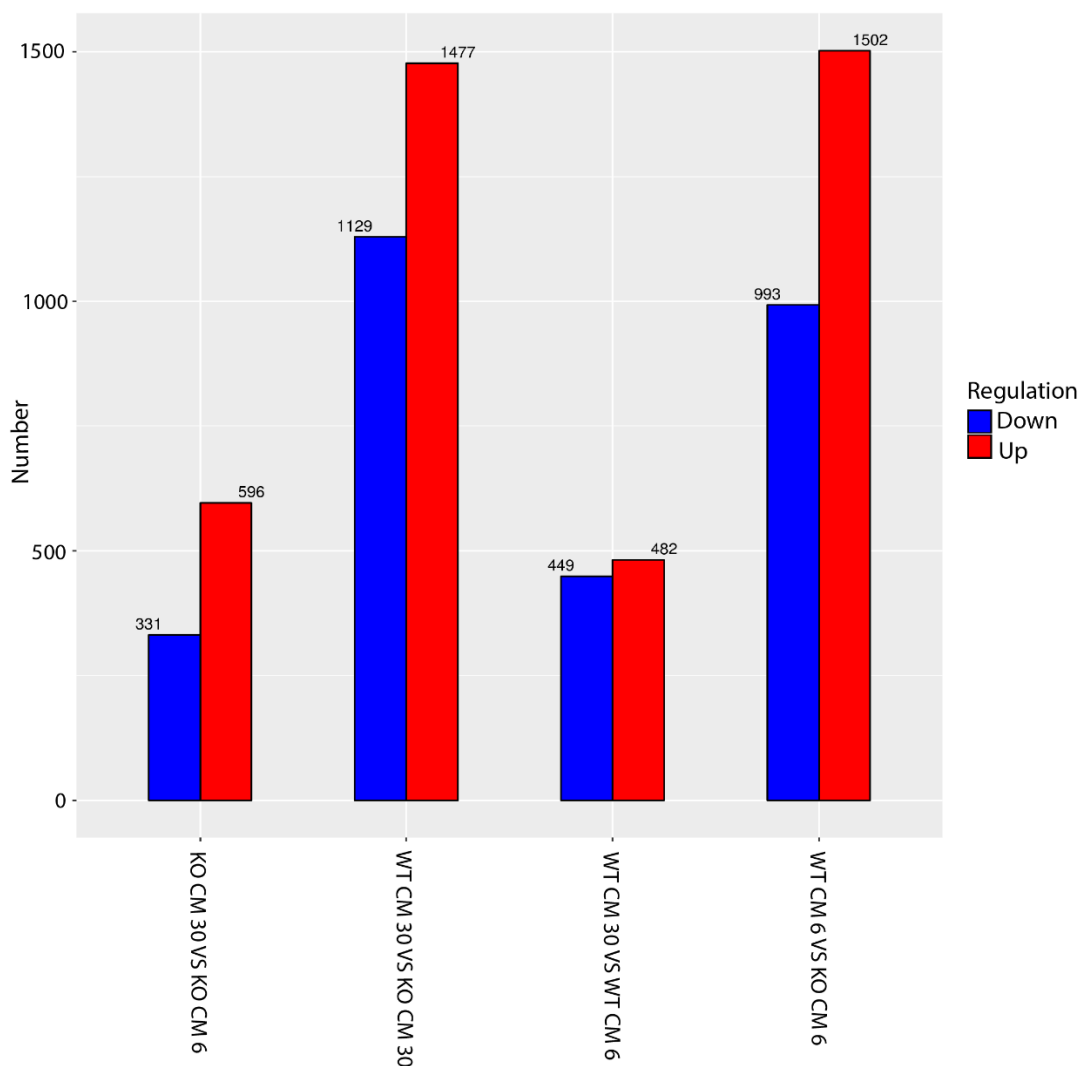
Differentially expressed genes between wildtype and c-MET knockout BMOL-TAT cells in LX-2-conditioned medium for either 30 minutes or 6 hours were assessed (WT CM 30, WT CM 6, KO CM 30, KO CM 6). Figure 6.10A represents all DEGs in each biological sample. It is evident that there are great differences in transcriptional activity between WT and KO cells, displayed by the difference in red/up and blue/downregulation of genes.

Fewer DEGs were evident between comparison groups WT CM 30 versus WT CM 6 (Figure 6.10B), solidifying the choice to proceed with 6-hour conditioned medium experiments in previous parts of this Chapter. Similarly, less significant changes were apparent between KO CM 30 versus KO CM 6 cells, further suggesting that the time frame of conditioned medium experiments does not greatly impact transcriptional activity. Therefore, to maintain consistency, the KO CM 6 group was selected for further investigation. When comparing the WT CM 6 and KO CM 6 experimental groups, many DEGs were demonstrated (Figure 6.10B) ((FC) >2 or <-2, (FDR) <0.05), suggesting that deletion of the c-MET receptor affects the overall transcriptional profile of the cells.



(A)



**(B)**

**Figure 6.10: Differential expression analysis of WT CM 30, WT CM 6, KO CM 30 and KO CM 6 comparison groups.**

(A) A Heatmap illustrating the DEGs in biological samples of WT CM 30, WT CM 6, KO CM 30 and KO CM 6 comparison groups. (B) A bar graph demonstrating a greater number of DEGs are present between groups WT CM 30 versus KO CM 30 and WT CM 6 versus KO CM 6, as compared to groups WT CM 30 versus WT CM 6 and KO CM 30 versus KO CM 6.

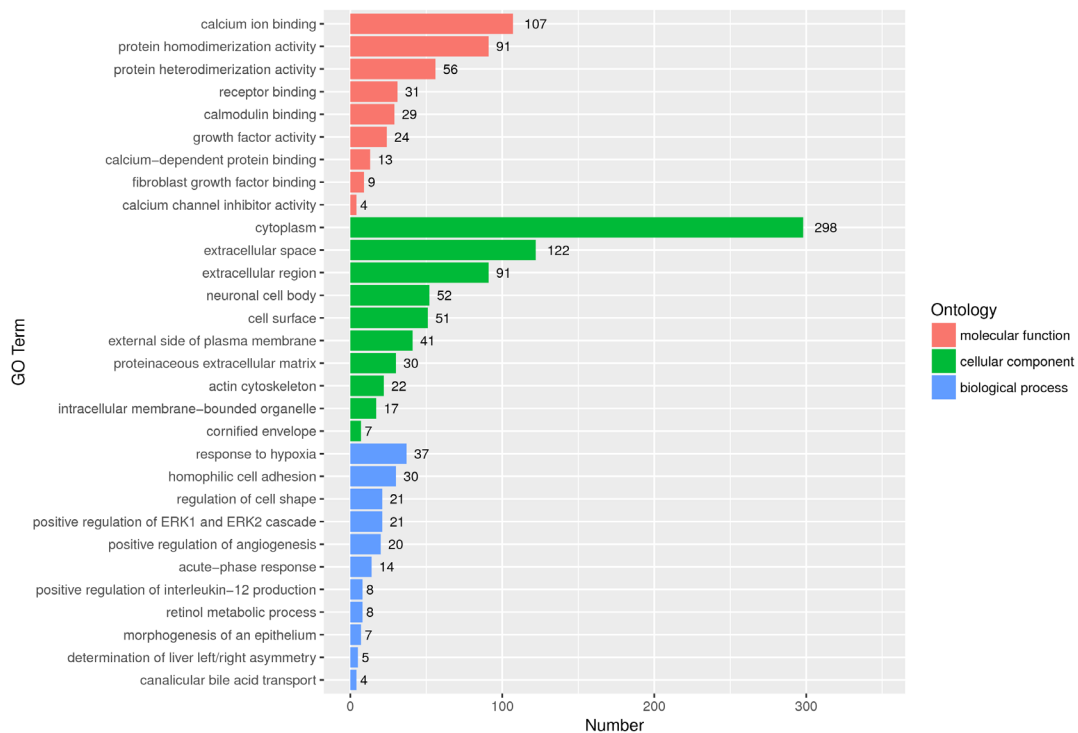
All DEGs with  $FC > 2$  or  $< -2$  and  $FDR < 0.05$ .

#### **6.4.2.6 Enrichment analysis - WT CM 6 versus KO CM 6 comparison groups**

Gene ontology (GO) analysis of upregulated DEGs in the WT CM 6 versus KO CM 6 comparison group demonstrated enrichment of a range of molecular functions, cellular components and biological processes including receptor binding, proteinaceous extracellular matrix, actin cytoskeleton, homophilic cell adhesion and regulation of cell shape (Figure 6.11A).

Moreover, KEGG pathway analysis highlighted that several pathways were highly enriched (Figure 6.11B). Specifically, pathways in cancer, Rap1 signalling, ECM-receptor interaction and focal adhesion are relevant to liver disease.

(A)



(B)

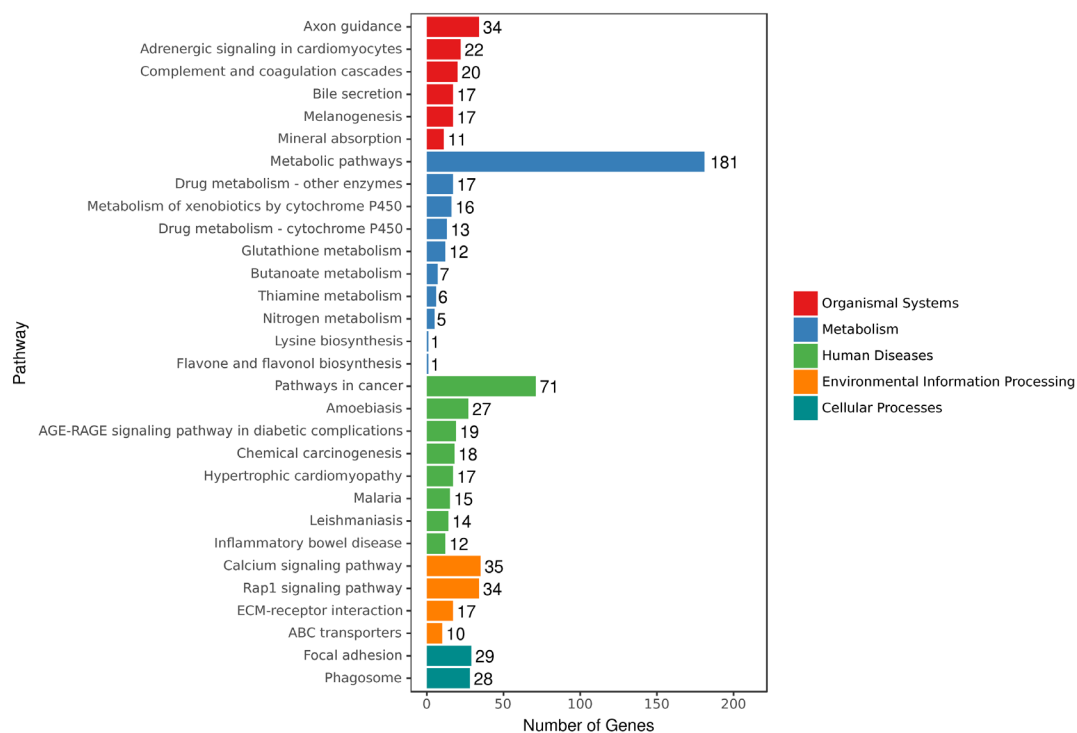


**Figure 6.11: Enrichment analysis of WT CM 6 versus KO CM 6 comparison groups.**

(A) GO analysis and (B) KEGG pathway analysis of upregulated DEGs in the WT CM 6 versus KO CM 6 experimental group demonstrating enrichment of several pathways.

FDR, <0.05,  $p < 0.05$ .

#### 6.4.2.7 Differential gene expression analysis - WT CM 6 versus KO CM 6 experimental group

In total, 2495 DEGs were identified in the WT CM 6 versus KO CM 6 comparison group (FC >2 or <-2 and FDR<0.05) (Figure 6.12).

In Table 6.5, all up- or downregulated genes in the context of liver disease are displayed. Of the DEGs present, several were associated with ECM remodelling and cell adhesion, and therefore bolded. Following culture in LX2-conditioned medium for 6 hours, the BMOL-TAT<sup>c-MET KO</sup> cells upregulate the cell adhesion genes *Cdh13*, *Jam3*, *Bcam* and *Cdh10*. In addition, the BMOL-TAT<sup>c-MET KO</sup> line had greater expression of the ECM deposition genes *Col22a1*, *Col4a6*, *Timp3*, *Lama4*, *Col4a4*, *Col26a1*, *Adam12* and *Col4a3* as well as downregulated levels of ECM remodelling genes *Mmp3*, *Mmp10* and *Mmp12*, suggesting that BMOL-TAT<sup>c-MET KO</sup> cells deposit ECM, rather than clearing it and increase their adherence in culture. Further, these DEGs are oppositely regulated in BMOL-TAT BMOL-TAT<sup>c-MET WT</sup> cells when cultured in LX-2 conditioned medium for 6 hours (Figure 6.13), suggesting that the regulation of genes involved in cell adhesion, ECM deposition and ECM remodelling may be c-MET dependent.

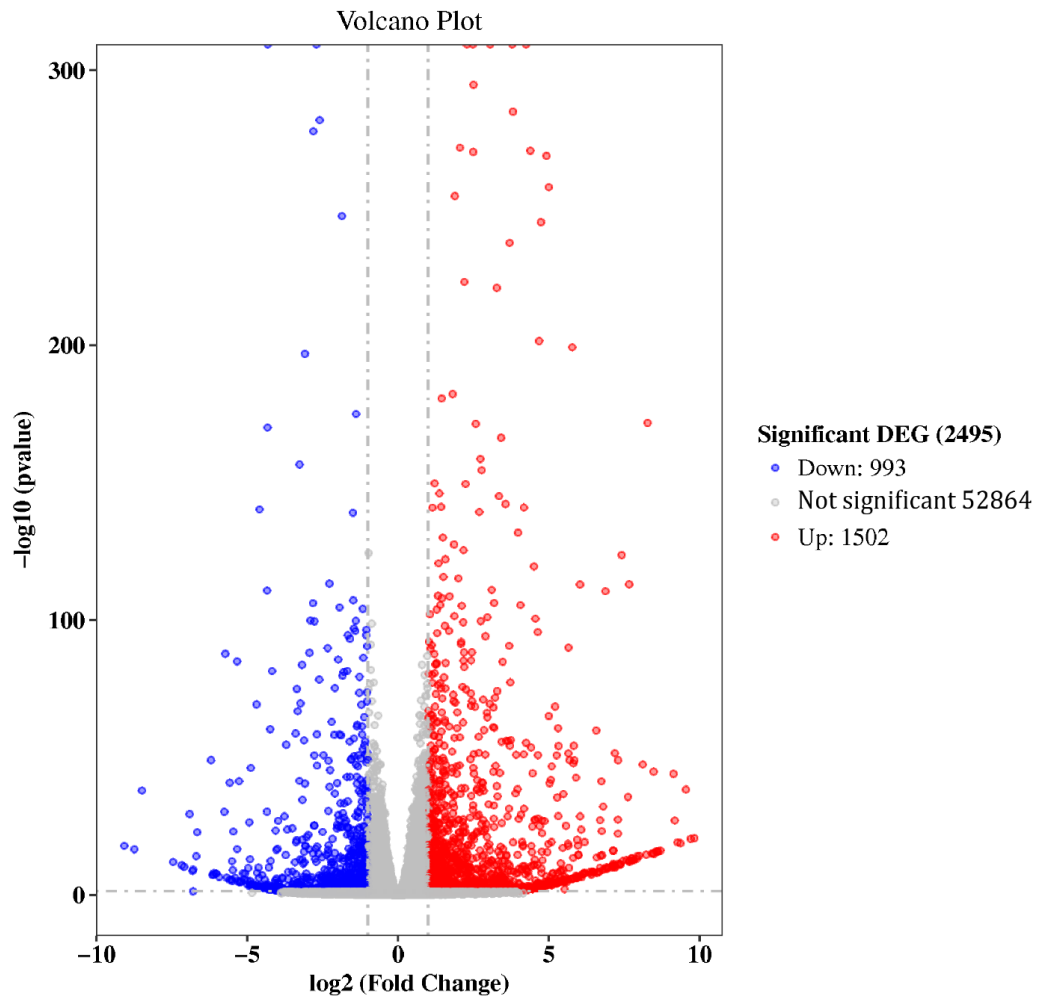


**Figure 6.12: Volcano plot of DEGs between WT CM 6 versus KO CM 6 experimental groups.**

In total, 2495 significant DEGs were identified between the WT CM 6 versus KO CM 6 comparison group. Red dots denoting upregulated genes and blue dots denoting downregulated genes.

All DEGs FC >2 or <-2 and FDR<0.05.

Gene	Log2 fold change	P-value	Literature
<i>Bex1</i>	9.538249272	4.10E-39	Importance in LPC expansion (Gu et al., 2018)
<i>Bex2</i>	9.260712116	7.09E-20	Involved in liver disease progression (Tamai et al., 2020)
<i>Pparg</i>	7.91614077	8.85E-15	Reduces LPC expansion (Gu et al., 2018)
<b><i>Cdh13</i></b>	<b>7.813449425</b>	<b>2.43E-13</b>	<b>Importance in cell adhesion (Andreeva &amp; Kutuzov, 2010)</b>
<b><i>Tnc</i></b>	<b>7.406604156</b>	<b>2.10E-124</b>	<b>Promotes liver fibrosis (El-Karef et al., 2007)</b>
<b><i>Col22a1</i></b>	<b>7.176960349</b>	<b>5.19E-11</b>	<b>Increased expression during liver fibrosis (Lai et al., 2011)</b>
<i>Tlr5</i>	6.791942133	6.07E-10	Anti-fibrotic (Zhou et al., 2020)
<b><i>Col16a1</i></b>	<b>6.027830635</b>	<b>1.07E-113</b>	<b>Increased expression during liver fibrosis (Lai et al., 2011)</b>
<i>Hnfa1</i>	5.897178908	1.93E-43	Increased expression with liver disease severity (Xue Wang et al., 2019)
<i>Hoxb7</i>	5.822280369	5.06E-55	Promotes HCC (W. M. Wang et al., 2017)
<b><i>Col4a6</i></b>	<b>5.809057788</b>	<b>1.17E-48</b>	<b>Increased expression during liver fibrosis (Lai et al., 2011)</b>
<i>Pdgfra</i>	5.478354234	1.78E-05	Increased expression with increased disease severity (Lim et al., 2018)
<i>Megf6</i>	5.203764927	2.78E-69	Promotes EMT (H. Hu et al., 2018)
<b><i>Timp3</i></b>	<b>5.021978176</b>	<b>2.33E-41</b>	<b>Fibro-protective role in the liver (Casagrande et al., 2017)</b>
<b><i>Jam3</i></b>	<b>4.97738944</b>	<b>2.62E-19</b>	<b>Role in cell adhesion (Hintermann et al., 2018)</b>
<b><i>Lama4</i></b>	<b>4.91060307</b>	<b>1.53E-07</b>	<b>Increased expression during liver cancer (Zheng et al., 2020)</b>
<i>Sox12</i>	4.538985545	0.000255736	Promotes HCC (W. Huang et al., 2015)
<b><i>Bcam</i></b>	<b>4.243095444</b>	<b>0</b>	<b>Role in liver regeneration (Miura et al., 2018)</b>
<b><i>Cdh10</i></b>	<b>3.970338926</b>	<b>8.13E-09</b>	<b>Importance in cell adhesion (Andreeva &amp; Kutuzov, 2010)</b>
<b><i>Col4a4</i></b>	<b>3.957026596</b>	<b>2.91E-39</b>	<b>Increased expression during liver fibrosis (Lai et al., 2011)</b>
<b><i>Col26a1</i></b>	<b>3.622732929</b>	<b>0.030221977</b>	<b>Increased expression during liver fibrosis (Lai et al., 2011)</b>



<b>Adam12</b>	<b>3.546191159</b>	<b>0.013641099</b>	<b>Increased expression with increased disease severity (Du et al., 2022)</b>
<i>Lefty1</i>	3.319551468	1.13E-06	Stemness marker (Kim et al., 2014)
<i>Tgfbr3</i>	3.313677364	1.33E-09	Potential negative regulator of fibrosis (Chu et al., 2011)
<i>Mapk15</i>	2.817953539	2.96E-06	Increased expression with liver disease severity (Westenberger et al., 2021)
<b>Col4a3</b>	<b>2.501978907</b>	<b>1.54E-22</b>	<b>Increased expression during liver fibrosis (Lai et al., 2011)</b>
<i>Gas6</i>	2.479812763	0	Increased expression during liver fibrosis (Bárcena et al., 2015)
<b>Mmp15</b>	<b>2.272369973</b>	<b>1.43E-07</b>	<b>Increased expression during liver fibrosis (Geervliet &amp; Bansal, 2020)</b>
<b>Mmp3</b>	<b>-8.48779476</b>	<b>9.15E-39</b>	<b>Increased expression during liver fibrosis (Geervliet &amp; Bansal, 2020)</b>
<b>Mmp10</b>	<b>-6.200498042</b>	<b>8.36E-50</b>	<b>Increased expression during liver fibrosis (Geervliet &amp; Bansal, 2020)</b>
<i>Alb</i>	-5.519149805	2.07E-06	Increased expression with liver disease severity (Fujita et al., 2019)
<i>Ndgr2</i>	-4.504904858	5.51E-08	Anti-fibrotic (J. Yang et al., 2011)
<i>Saa3</i>	-3.327889685	1.28E-67	Promotes inflammation, proliferation, and cell death in HSCs (Siegmund et al., 2016)
<b>Mmp12</b>	<b>-3.151988406</b>	<b>0.019041344</b>	<b>Increased expression during liver fibrosis (Geervliet &amp; Bansal, 2020)</b>
<i>Saa2</i>	-3.014247506	9.64E-07	Promotes inflammation, proliferation, and cell death in HSCs (Siegmund et al., 2016)
<i>Sod3</i>	-2.937191574	7.34E-89	Anti-fibrotic (Sun et al., 2021)
<b>Cdh5</b>	<b>-2.725992535</b>	<b>1.53E-17</b>	<b>Involved in progenitor cell activation (Anderson et al., 2015)</b>
<i>Casp1</i>	-2.458257886	0.000367304	Role in inflammation and fibrosis (Dixon et al., 2012)
<i>Saa1</i>	-2.457416142	0.000219263	Promotes inflammation, proliferation, and cell death in HSCs (Siegmund et al., 2016)

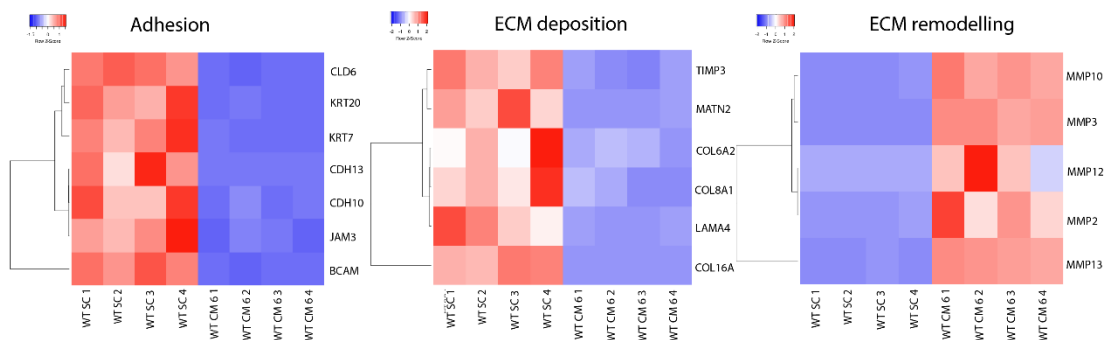
**Table 6.5: DEGs between the WT CM 6 versus KO CM 6 comparison group involved in liver disease.**

A list of DEGs associated with liver disease regulation, as identified in previous studies. Red colouring denotes upregulation and blue colouring denotes downregulation. Bolded genes are involved in ECM remodelling and cell adhesion.

All DEGs FC >2 or <-2 and FDR<0.05.

(A)

WT SC VS WT CM 6



(B)

WT CM 6 VS KO CM 6

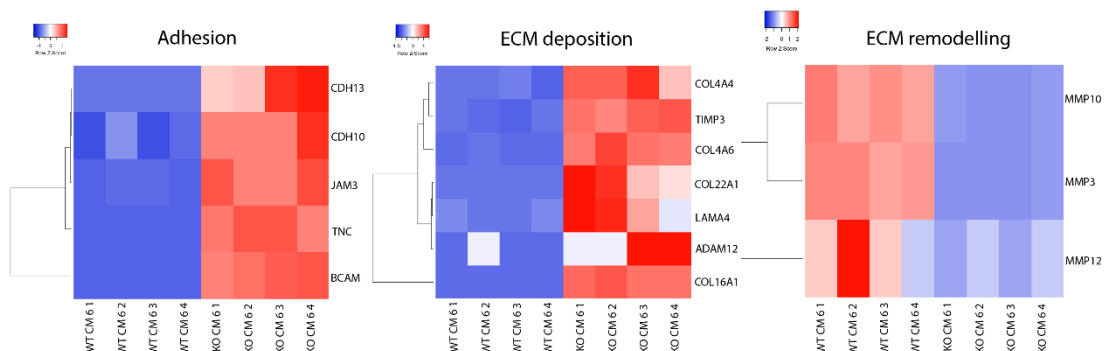


Figure 6.13 Heatmaps graphically representing the top DEGs between WT SC versus WT CM 6 and WT CM 6 versus KO CM 6 experimental groups. Heatmaps illustrating the top differentially expressed genes between (A) WT SC versus WT CM 6 and (B) WT CM 6 versus KO CM 6 experimental groups for cell adhesion, ECM deposition and ECM remodelling. All DEGs  $FC > 2$  or  $< -2$  and  $FDR < 0.05$ .

## 6.5 Discussion

It was established in Chapter 5 that the BMOL-TAT<sup>c-MET<sup>WT</sup></sup> and BMOL-TAT<sup>c-MET<sup>KO</sup></sup> cells are highly communicative with LX-2 cells. To gain a deeper understanding of the signalling networks used during their crosstalk, bulk RNA-sequencing was employed.

In Chapter 5, a 48-hour co-culture was suitable to display changes in protein expression in LX-2 cells following their co-culture with either BMOL-TAT<sup>c-MET<sup>WT</sup></sup> or BMOL-TAT<sup>c-MET<sup>KO</sup></sup> cells. Other studies also suggest 48 hours as a suitable timepoint for mRNA analysis (Bota-Rabassedas et al., 2021) (Bilandzic et al., 2019) (Gratte et al., 2021). Using this timepoint for RNA-sequencing, the LX-2 cells demonstrated limited numbers of DEGs specific to liver disease, following their co-culture with BMOL-TAT<sup>c-MET<sup>WT</sup></sup> or BMOL-TAT<sup>c-MET<sup>KO</sup></sup> cells, suggesting that either the timeframe of co-culture had been suboptimal to detect differences or that LX-2 cells are not greatly impacted at the transcriptional level by BMOL-TAT<sup>c-MET<sup>WT</sup></sup> and BMOL-TAT<sup>c-MET<sup>KO</sup></sup> cells. Nonetheless, following LX-2 co-culture with BMOL-TAT<sup>c-MET<sup>WT</sup></sup> cells, an upregulation of epithelial genes *Krt5*, *Pxdn1* and *Lcn2* and a downregulation of EMT-associated genes *Matn1* and *Zeb2-as1* was revealed. This suggests that LX-2 cells may present a more epithelial cell phenotype when communicating with BMOL-TAT<sup>c-MET<sup>WT</sup></sup> cells.

Next, RNA-sequencing analysis was performed on LX-2 CC WT versus LX-2 CC KO experimental groups, with the absence of the c-MET receptor in the LPC line BMOL-TAT as the only outstanding variable between groups. Evaluation of DEGs revealed an upregulation of fibrosis-driving and EMT-associated genes *Tnf* and *Matn1*, while downregulation of epithelial-like genes *Krt5* and *Lcn2* in LX-2 cells, following their co-culture with BMOL-TAT<sup>c-MET<sup>KO</sup></sup> cells. With inverse expression of the epithelial genes *Krt5* and *Lcn2* in LX-2 cells, depending on their co-culture status, this suggested that the deletion of c-MET in BMOL-TAT cells, impacts the transcriptional activity of LX-2 cells.

It was not possible to achieve cell harvests of optimal RNA quality and quantity from BMOL-TAT cells located in Boyden chamber inserts during co-culture

with LX2 cells, therefore an alternative approach involved exposure of traditionally cultured BMOL-TAT cells to LX-2-conditioned medium. Since marginally more DEGs were present in the 6-hour compared to the 30-minute incubation period, the longer timepoint was chosen for all further analyses.

Analysis of the WT SC versus WT CM 6 comparison group identified ECM and cell adhesion gene changes when the BMOL-TAT<sup>c-MET<sup>WT</sup></sup> cells were in conditioned medium for 6 hours. An upregulation of ECM remodelling genes *Mmp3*, *Mmp10*, *Igfa4*, *Mmp2*, *Mmp12* and *Mmp13* and downregulation of ECM deposition genes *Col16a1*, *Lama4*, *Cldn6*, *Timp3*, *Col8a1*, *Col6a2*, *Col28a1*, *Matn1* and *Col4a6* was revealed. Further, BMOL-TAT<sup>c-MET<sup>WT</sup></sup> cells in LX-2-conditioned medium were evidenced to downregulate cell adhesion genes *Cdh13*, *Krt20*, *Cdh10*, *Cdhr1*, *Jam3*, *Krt7* and *Bcam*. This suggests that BMOL-TAT<sup>c-MET<sup>WT</sup></sup> cells, upon contact with LX-2 secretions, remodel their surrounding ECM and downregulate their adhesion to facilitate their migration to sites of injury. Suarez-Causado and colleagues identified that active HGF/c-MET signalling increases LPC migration through deposited extracellular matrix, evidenced by the expression of metalloproteinases (Suárez-Causado et al., 2015). Therefore, establishment and remodelling of the ECM is important for LPC activation and migration to sites of injury and ultimately, liver regeneration.

Analysis of the WT CM 6 and KO CM 6 experimental group demonstrated inverse gene expression of ECM remodelling, ECM deposition and cell adhesion genes, as compared to WT SC versus WT CM 6 experimental group. Active HGF/c-MET signalling is vital for LPC migration (Suárez-Causado et al., 2015) (Ishikawa et al., 2012). Therefore, with the absence of the c-MET receptor, the BMOL-TAT cells upregulated cell adhesion genes *Cdh13*, *Jam3*, *Bcam* and *Cdh10*, when in LX-2-conditioned medium. These data validate the finding in Chapter 4, where BMOL-TAT<sup>c-MET<sup>KO</sup></sup> cells displayed a decrease in migration when subjected to a wound healing assay. The upregulation of ECM deposition genes *Col22a1*, *Col4a6*, *Timp3*, *Lama4*, *Col4a4*, *Col26a1*, *Adam12* and *Col4a3* and downregulation of ECM remodelling genes *Mmp3*, *Mmp10* and *Mmp12* was observed in BMOL-TAT<sup>c-MET<sup>KO</sup></sup> cells following culture in LX-

2-conditioned medium, suggesting that the cells deposit ECM, rather than clearing it, and demonstrate pro-fibrotic potential. Considering that the regulation of these genes varies depending on the presence or absence of the c-MET receptor, demonstrates that the observed cellular responses in LPCs are HGF/c-MET-dependent and regulated via HSCs.

Further, *Mmp* expression changes were pronounced between WT SC versus WT CM 6 and WT CM 6 versus KO CM 6 comparison groups. Active HGF/c-MET signalling has previously been noted to increase *Mmp2* expression in human chondrosarcoma cells (Tsou et al., 2013). Similarly, *Mmp2* upregulation was evident in BMOL-TAT<sup>c-MET WT</sup> cells, following 6-hour incubation in LX-2-conditioned medium. Additionally, *Mmp13* was also upregulated under the same conditions, with this gene reported to be activated by HGF and described to accelerate recovery from experimental liver fibrosis (Endo et al., 2011). Further, the expression of HGF-induced *Mmp3* has been noted to increase the invasion of HCC cells (Monvoisin et al., 2002). Here, placing BMOL-TAT<sup>c-MET WT</sup> cells in LX-2-conditioned medium led to a significant upregulation of *Mmp3*, suggesting similar regulatory mechanisms in LPCs. *Mmp3* was greatly downregulated in BMOL-TAT<sup>c-MET KO</sup> cells in LX-2-conditioned medium, corroborating previous studies that demonstrated *Mmp3* regulation through HGF/c-MET signalling. This further suggests the ECM-degrading and invasive role of actively HGF/c-MET-signalling LPCs during liver fibrosis, to migrate to sites of injury and potentially regenerate the injured parenchyma.

In conclusion, the results presented in this chapter have identified that BMOL-TAT<sup>c-MET WT</sup> and BMOL-TAT<sup>c-MET KO</sup> cells are greatly affected at the transcriptomic level by signalling molecules present in LX-2-conditioned medium. This further reinforces the communicative relationship of LPCs and HSCs in diseased liver states. Additionally, upon co-culture of BMOL-TAT<sup>c-MET KO</sup> cells with LX-2 cells, deletion of the c-MET receptor in BMOL-TAT cells had a profound effect on the expression of adhesion genes, along with ECM remodelling and deposition genes, which were contrary to BMOL-TAT<sup>c-MET WT</sup> expression of the same genes under the same conditions, suggesting an

importance of this pathway for LPC behaviour following HSC crosstalk. Finally, the RNA-sequencing data provided a detailed picture of other potential candidates for future study into molecular pathways involved in LPC-HSC signalling crosstalk.

## **General Discussion**



In 2020, it was estimated that liver cancer was the third leading cause of cancer-related death worldwide (Ferlay et al., 2015). With a strong upward trend of obesity, alcohol consumption, hepatitis and metabolic syndrome observed in recent years, mortality rates are expected to rise (Cheemerla & Balakrishnan, 2021). Reversal of end-stage CLD is challenging, as tyrosine kinase inhibitors (TKIs) in combination with immunotherapies, demonstrate poor treatment success due to drug resistance by suppression of immune system regulators (Marcellin & Kutala, 2018) (Onuma et al., 2020). Therefore, there is a clear need for intervention at earlier stages before the disease becomes irreversible or very difficult to treat.

Upon chemical, viral or carcinogenic insult, fibrosis is the body's natural wound healing response (T. A. Wynn, 2008). Dysregulated fibrosis results in excessive scarring due to the imbalance between tissue inhibitor of metalloproteinases (TIMPs), which favour matrix deposition, and matrix metalloproteinases (MMPs), which degrade ECM. Further, there is excessive accumulation of (ECM) components, particularly collagen, by the main fibrosis-driving cells, the HSCs. This leads to distortion of regular tissue architecture (T. A. Wynn, 2008) (Bataller & Brenner, 2005). Once activated, myofibroblastic HSCs have a pro-fibrotic effect on hepatocytes and inflammatory cells through the upregulation of TGF $\beta$ 1, a key pro-fibrotic signalling pathway (Mikula, Proell, Fischer, & Mikulits, 2006) (Yin, Evason, Asahina, & Stainier, 2013) (Q. Yang, Yan, & Gong, 2018). However, limited studies are available on the disease-associated interactions between other cell types of the liver, including the liver progenitor cells.

The role of liver progenitor cells in chronic liver disease has been controversially discussed over time. In the early days of LPC research, it became clear that the cells are strongly associated with the progression of CLD, since LPC numbers directly and positively correlate to the stage of underlying chronic liver disease (Lowe et al., 1999). However, LPCs are now generally thought to have pro-regenerative roles in the early stages of chronic liver injury, where they are capable of replacing lost parenchymal tissue by differentiation into biliary epithelial cells or hepatocytes (Kohn-Gaone et al.,

2016) (Raven et al., 2017). Later, when LPCs are chronically activated to a proliferative phenotype, they may become targets of transformation and assume a cancer-stem cell-like phenotype (Kohn-Gaone et al., 2016). The pro- and/or anti-regenerative role that LPCs perform may therefore be dependent on the injury stimulus, context, and interaction with other cells within the microenvironment.

The previously described injury and regeneration niche exemplifies the space in which the LPCs, HSCs and inflammatory cell populations travel to and reside upon injury (Kohn-Gaone et al., 2016). As these cell types are spatially proximal there, this proposes cellular crosstalk as a key theme for either resolution or progression of disease, with this communicative relationship being largely unexplored. (Kohn-Gaone et al., 2016).

It has only been recently proposed that LPCs may have regulatory potential over HSCs and aid in liver regeneration (Gratte et al., 2021). Interestingly, the HGF/c-MET signalling pathway has been noted to promote regeneration during chronic liver injury (Petrini, 2015) (Huh et al., 2004). HGF is localised on HSCs, whereas the receptor, c-MET is expressed by the LPCs, suggesting an intimate relationship between cell types during wound healing (Z. Hu et al., 1993). Activation of the pathway induces a variety of cellular responses, including epithelial cell proliferation, differentiation, survival, motility and overall liver regeneration (Suárez-Causado et al., 2015). However, all investigations on the pro-regenerative role of HGF/c-MET have assessed LPCs and HSCs in isolation. Considering that LPCs and HSCs are known to proliferate and then migrate together to sites of injury, my project focused on the crosstalk between both cell types and hypothesised the potential regulatory role of LPCs on HSC behaviour during chronic liver disease.

The HGF/c-MET signalling pathway has been previously studied in the DDC animal model of disease (Ishikawa et al., 2012). However, no reports on the relationship of the signalling pathway and the CDE model have been established. Investigation into this dietary model revealed a decrease in HGF/c-MET signalling with increasing stages of disease, suggesting the anti-

fibrotic role of the pathway is inhibited. This provided a novel proof-of-principle model as a basis for further experiments.

Liver progenitor cells have been previously reported to be essential for liver regeneration (del Castillo et al., 2008) (Gratte et al., 2021), with few studies attributing the cells regenerative capacity to the HGF/c-MET pathway (Suárez-Causado et al., 2015) (Ishikawa et al., 2012). Investigating LPC biology *in vitro* following deletion of the c-MET receptor using CRISPR/Cas9 technology, provided a controlled setting without having to account for the complex microenvironment that an *in vivo* study delivers. The findings presented in Chapter 4 demonstrated that following deletion of c-MET, the LPC phenotype was significantly altered, displaying an overall rounder appearance in combination with increased adherence and clump-like growth. Cell scattering has been previously reported to be regulated by active HGF/c-MET signalling (G. K. Y. Chan et al., 2008), suggesting that maintenance of the LPC phenotype is largely HGF/c-MET signalling-dependent. Additionally, BMOL-TAT<sup>c-MET KO</sup> displayed a significant decrease in viability and proliferative and migratory capacities, solidifying findings from previous reports that note apoptosis and growth arrest following deletion of c-MET in LPCs (Suárez-Causado et al., 2015) (Ishikawa et al., 2012) and proposing that the cells cannot migrate to sites of injury, to aid in the wound healing process. Further, BMOL-TAT<sup>c-MET KO</sup> cells revealed an increased expression of TGF $\beta$  signalling components compared to wildtype BMOL-TAT cells, suggesting that without c-MET regulation, LPCs exhibit a pro-fibrotic nature. Here, establishment of a novel LPC-specific c-MET knockout cell culture model provides an important contribution to our understanding of the vital role of the HGF/c-MET pathway in terms of LPC biology *in vitro*.

Since LPCs and fibrosis-driving HSCs are generally spatially proximal during liver injury (Kohn-Gaone et al., 2016), there is the significant potential for cellular crosstalk to drive liver regeneration or encourage disease progression. Following chronic injury, the hepatic microenvironment is complex, making LPC-HSC crosstalk difficult to study when using an *in vivo* model. Currently, there are few *in vitro* LPC-HSC co-culture reports (Gratte et al., 2021)

(Xuanyan Cai et al., 2020), suggesting a gap in knowledge of the communicative relationship between cell types. Through a controlled *in vitro* model of crosstalk, this thesis reported that LPCs and HSCs are highly chemoattracted, as evidenced by a Boyden Chamber migration assay. Further, wildtype BMOL-TAT cells in LX-2-conditioned medium for 6 hours, displayed an increase in *Mmp3* expression. A previous report demonstrated this result in hepatocytes, which revealed that dose-dependent administration of HGF induced their expression of pro-MMP3, followed by the cells' increased invasion. This suggests that the expression of *Mmp3* in LPCs may aid in their migration and invasion to sites of injury, not previously described (Monvoisin et al., 2002). This bulk RNA-seq dataset of LPCs in LX-2-conditioned medium was accompanied by a significant increase in other ECM remodelling genes including *Mmp10*, *Igfa4*, *Mmp2*, *Mmp12* and *Mmp13* and a downregulation of ECM deposition genes *Col16a1*, *Lama4*, *Cldn6*, *Timp3*, *Col8a1*, *Col6a2*, *Col28a1*, *Matn1* and *Col4a6* and cell adhesion genes *Cdh13*, *Krt20*, *Cdh10*, *Cdhr1*, *Jam3*, *Krt7* and *Bcam*. Suarez-Cuasado and colleagues reported no loss of expression of cell-cell adhesion proteins upon HGF administration to LPCs (Suárez-Causado et al., 2015). This suggests that LPC interaction with HSCs alters their adhesive properties, previously not reported. Moreover, RNA-seq data propose that LPCs, once interacting with HSCs, clear ECM rather than depositing it, to migrate to sites of injury and aid in wound healing, with this co-migratory relationship of LPCs and HSCs previously reported in mice (Van Hul et al., 2009) (Ruddell et al., 2009).

Recently published data, also presented in this thesis, suggest that LPCs are involved in the regulation of HSCs and, therefore, indirectly fibrogenesis (Gratte et al., 2021). HSCs co-cultured with LPCs in a Boyden Chamber for 48 hours, displayed a decrease in collagen secretion compared to single culture. This corroborates previous findings on the regulatory and pro-regenerative role of LPCs during chronic liver injury (del Castillo et al., 2008) (Gratte et al., 2021) (Ishikawa et al., 2012) (Dai et al., 2020). Though potentially regenerative, LPCs have also demonstrated to increase pro-fibrotic protein expression of HSCs (Knight et al., 2008) (Kaur, Siddiqui, & Bhat, 2015). Interestingly, in Chapter 5, this was shown to be LPC-specific, as HSC co-

culture with the HCC line SNU-449 evidenced no alterations in fibrogenic marker expression. Taken together, establishment of an *in vitro* co-culture model demonstrated that LPCs and HSCs do indeed have a highly communicative and mutually regulatory relationship. Significant chemoattraction was exemplified between cell types, along with the modulation of LPC behaviour at a transcriptional level to expand their invasive potential. Further, expression of fibrosis-associated markers in HSCs was presented to be strongly impacted by LPCs. These data provide a novel contribution to the field, with LPC-HSC behaviour not previously investigated in a controlled, isolated setting.

It was established in Chapter 4 that deletion of the c-MET receptor in LPCs altered their biology. The importance of active HGF/c-MET signalling has been reported in previous studies, (Ishikawa et al., 2012) (Almalé et al., 2019) (del Castillo et al., 2008), however ablation of active signalling, in the context of LPC-HSC crosstalk has yet to be reported. Suarez-Causado and colleagues described that HGF induces c-MET-dependent LPC migration (Suárez-Causado et al., 2015). Evidence presented in Chapter 5 solidifies this finding, as ablation of the c-MET receptor in BMOL-TAT cells significantly decreased their chemoattraction to the HSC line LX-2, suggesting that HSC and LPC co-migration to sites of injury *in vivo* is HGF/c-MET signalling-dependent. Additionally, in bulk-RNA-seq data obtained from BMOL-TAT<sup>c-MET KO</sup> cells in LX-2-conditioned medium for 6 hours, an increase in expression of cell adhesion genes *Cdh13*, *Jam3*, *Bcam* and *Cdh10* was identified. Considering that the expression of cell adhesion genes decreased upon co-culture of wildtype BMOL-TAT cells with LX-2 cells, this highlights that the HGF/c-MET signalling pathway may be an important regulator of cell adhesion in single and co-culture *in vitro* systems.

In Chapter 5, it was presented that HSCs co-cultured with LPCs decreased their secretion of collagen. This result was mirrored following HSC co-culture with c-MET-deleted LPCs, suggesting that HGF/c-MET may not be a regulator of collagen production in HSCs. Although Ishikawa *et al.* reported that LPC-specific, conditional c-MET knockout mice demonstrated increased collagen

expression in liver injury areas (Ishikawa et al., 2012), it is challenging to compare controlled *in vitro* LPC-HSC crosstalk with a whole organ system, where the complexity of the microenvironment differs greatly. Suarez-Causado *et al.* previously reported that HGF stimulation of LPCs increased invasion through ECM by their release of MMPs (Suárez-Causado et al., 2015). Bulk RNA-seq data from BMOL-TAT<sup>c-MET</sup> KO cells in LX-2-conditioned medium for 6 hours demonstrated an increase in cell deposition genes *Col22a1*, *Col4a6*, *Timp3*, *Lama4*, *Col4a4*, *Col26a1*, *Adam12* and *Col4a3* and a decrease in MMP genes *Mmp3*, *Mmp10* and *Mmp12*. The resulting data imply that without active HGF/c-MET signalling, LPCs are depositing ECM, rather than clearing it, ultimately inhibiting their regenerative ability. These findings provide novel insights into the essential role of HGF/c-MET signalling during LPC-HSC crosstalk.

Although cell-cell interaction studies are valuable for determining cell-specific responses, few studies have investigated LPC-HSC interactions *in vitro* (Gratte et al., 2021). Accurate recapitulation of the complex *in vivo* liver microenvironment is difficult to achieve, presenting a limitation of *in vitro* experimentation. Due to COVID-related laboratory shutdowns, the maintenance of mice for primary HSC isolations was unfeasible, terminating further experimentation using primary-isolated HSCs. Further, previous to the COVID outbreak, primary-isolated HSCs from normal chow-fed control autoactivated on tissue culture plastic, demonstrating a limitation to the establishment of differing HSC phenotypes (Appendix Figure A1, A2, A3, A4). Culturing primary HSCs with an optimised growth medium containing epidermal growth factor (EGF) and fibroblast growth factor 2 (FGF2) may eliminate this issue, as it retains cells in an undifferentiated state (El Taghdouini et al., 2015). Therefore, the work presented in this thesis primarily focused on clonal cell lines, allowing ease of their continuous culture.

In Chapter 4, it was revealed that deletion of the c-MET receptor in LPCs altered their phenotype to create a rounder cell, increased their adherence and decreased their proliferative and migratory potential. Further, in Chapters 5, the potential regulatory role of LPCs on HSC behaviour was investigated. It

was revealed that wildtype LPCs are greatly chemoattracted to HSCs, and that their co-culture decreases HSC collagen secretion significantly, while increasing the expression of TGF $\beta$  signalling components. Conversely, c-MET knockout LPCs, when co-cultured with HSCs, demonstrated a repulsive effect, however, did not alter the expression of TGF $\beta$  signalling components. As deletion of the c-MET receptor altered the LPC phenotype and ultimately had an effect on LPC-HSC chemoattraction, it can be deduced that the HGF/c-MET signalling pathway is important for the maintenance of LPC biology and LPC-HSC crosstalk *in vitro*. However, due to the use of clonal cell lines, this result may be context-specific, hence it cannot be confirmed that HGF/c-MET signalling is vital for the regulatory role of LPCs in an *in vivo* system, due to the lack of respective animal model investigations.

In the future, investigating LPC-HSC crosstalk using primary LPCs and HSCs will be of interest, to establish a model that more closely mimics the liver microenvironment. Irrespective of the injury stimulus, LPCs are spatially proximal to activated HSCs as well as immune cells (X. Cai et al., 2020). Therefore, examining the communicative relationship between the cell types in the injury and regeneration niche will provide insight into their unexplored crosstalk. Further, creating a conditional c-MET KO mouse would provide a more complex *in vivo* model to characterise disease development and cell-cell interactions. In Chapter 6, bulk RNA-sequencing data demonstrated that LPCs, upon stimulation with LX-2-conditioned medium, upregulated the expression of ECM remodelling genes while downregulating the expression of ECM deposition and cell adhesion genes. This suggests that the LPCs, once stimulated by HSCs, clear ECM, to aid in their migration to sites of injury and ultimately regenerate the liver. Therefore, substantial increases in up-/down-regulated genes upon LPC exposure to HSCs uncovers avenues for additional signalling pathways to be investigated in relation to LPC-HSC crosstalk.

The ever-increasing prevalence of liver cancer and lack of widespread effective treatment options highlights the need for early intervention. LPCs present as a key regulatory cell type, that are activated upon chronic liver injury and crosstalk with fibrosis-driving HSCs, portraying them as attractive

therapeutic target cells. Additionally, the HGF/c-MET signalling pathway is known for its anti-fibrotic effects in the liver, with LPCs presenting the c-MET receptor on their surface and the HSCs secreting the ligand, HGF. The regulatory potential of LPCs on activated HSCs in relation to the HGF/c-MET pathway had previously not been reported.

The work presented in this thesis has (a) characterised fibrosis-related models in relation to the HGF/c-MET signalling pathway and (b) demonstrated that deletion of c-MET in LPCs alters the cells' biology. Further, (c) co-culture of wildtype LPCs with HSCs demonstrated their strong communicative relationship, which was impacted upon co-culture of HSCs with c-MET knockout LPCs. Lastly, (d) transcriptional analysis of LPCs and HSCs in co-culture or following administration of conditioned medium, highlighted the cells' communicative relationship further, providing a platform for further crosstalk research to be built upon.



## **References**

Every reasonable effort has been made to acknowledge the owners of copyright material. I would be pleased to hear from any copyright owner who has been omitted or incorrectly acknowledged.

- Abdel-Misih, S. R., & Bloomston, M. (2010). Liver anatomy. *Surgical Clinics of North America*, 90(4), 643-653. doi:10.1016/j.suc.2010.04.017
- Afdhal, N. H., & Nunes, D. (2004). Evaluation of liver fibrosis: a concise review. *American Journal of Gastroenterology*, 99(6), 1160-1174. doi:10.1111/j.1572-0241.2004.30110.x
- Akhurst, R. J., & Hata, A. (2012). Targeting the TGF $\beta$  signalling pathway in disease. *Nature Reviews Drug Discovery*, 11(10), 790-811. doi:10.1038/nrd3810
- Alam, H., Sehgal, L., Kundu, S. T., Dalal, S. N., & Vaidya, M. M. (2011). Novel function of keratins 5 and 14 in proliferation and differentiation of stratified epithelial cells. *Molecular Biology of the Cell*, 22(21), 4068-4078. doi:10.1091/mbc.e10-08-0703
- Almalé, L., García-Álvaro, M., Martínez-Palacián, A., García-Bravo, M., Lazcanoiturburu, N., Addante, A., . . . Sánchez, A. (2019). c-Met Signaling Is Essential for Mouse Adult Liver Progenitor Cells Expansion After Transforming Growth Factor- $\beta$ -Induced Epithelial–Mesenchymal Transition and Regulates Cell Phenotypic Switch. *Stem Cells*, 37(8), 1108-1118. doi:10.1002/stem.3038
- Anderson, H., Patch, T. C., Reddy, P. N., Hagedorn, E. J., Kim, P. G., Soltis, K. A., . . . Shah, D. I. (2015). Hematopoietic stem cells develop in the absence of endothelial cadherin 5 expression. *Blood*, 126(26), 2811-2820. doi:10.1182/blood-2015-07-659276
- Andreeva, A. V., & Kutuzov, M. A. (2010). Cadherin 13 in cancer. *Genes Chromosomes Cancer*, 49(9), 775-790. doi:10.1002/gcc.20787

- Arndt, S., Wacker, E., Dorn, C., Koch, A., Saugspier, M., Thasler, W. E., . . . Hellerbrand, C. (2015). Enhanced expression of BMP6 inhibits hepatic fibrosis in non-alcoholic fatty liver disease. *Gut*, *64*(6), 973-981. doi:10.1136/gutjnl-2014-306968
- Arnold, K., Sarkar, A., Yram, M. A., Polo, J. M., Bronson, R., Sengupta, S., . . . Hochedlinger, K. (2011). Sox2(+) adult stem and progenitor cells are important for tissue regeneration and survival of mice. *Cell Stem Cell*, *9*(4), 317-329. doi:10.1016/j.stem.2011.09.001
- Asrani, S. K., Devarbhavi, H., Eaton, J., & Kamath, P. S. (2019). Burden of liver diseases in the world. *Journal of Hepatology*, *70*(1), 151-171. doi:10.1016/j.jhep.2018.09.014
- Aydin, A. F., Küskü-Kiraz, Z., Doğru-Abbasoğlu, S., Güllüoğlu, M., Uysal, M., & Koçak-Toker, N. (2010). Effect of carnosine against thioacetamide-induced liver cirrhosis in rat. *Peptides*, *31*(1), 67-71. doi:10.1016/j.peptides.2009.11.028
- Bao, Y.-l., Wang, L., Pan, H.-t., Zhang, T.-r., Chen, Y.-h., Xu, S.-j., . . . Li, S.-w. (2021). Animal and Organoid Models of Liver Fibrosis. *Frontiers in Physiology*, *12*(763). doi:10.3389/fphys.2021.666138
- Bárcena, C., Stefanovic, M., Tutusaus, A., Joannas, L., Menéndez, A., García-Ruiz, C., . . . Morales, A. (2015). Gas6/Axl pathway is activated in chronic liver disease and its targeting reduces fibrosis via hepatic stellate cell inactivation. *Journal of Hepatology*, *63*(3), 670-678. doi:10.1016/j.jhep.2015.04.013
- Bataller, R., & Brenner, D. A. (2005). Liver fibrosis. *The Journal of clinical investigation*, *115*(2), 209-218. doi:10.1172/JCI24282

- Best, J., Manka, P., Syn, W.-K., Dollé, L., van Grunsven, L. A., & Canbay, A. (2015). Role of liver progenitors in liver regeneration. *Hepatobiliary Surgery and Nutrition*, 4(1), 48-58. doi:10.3978/j.issn.2304-3881.2015.01.16
- Bi, Y., Mukhopadhyay, D., Drinane, M., Ji, B., Li, X., Cao, S., & Shah, V. H. (2014). Endocytosis of collagen by hepatic stellate cells regulates extracellular matrix dynamics. *American Journal of Physiology-Cell Physiology*, 307(7), C622-C633. doi:10.1152/ajpcell.00086.2014
- Bilandzic, M., Rainczuk, A., Green, E., Fairweather, N., Jobling, T. W., Plebanski, M., & Stephens, A. N. (2019). Keratin-14 (KRT14) Positive Leader Cells Mediate Mesothelial Clearance and Invasion by Ovarian Cancer Cells. *Cancers*, 11(9). doi:10.3390/cancers11091228
- Birchmeier, C., Birchmeier, W., Gherardi, E., & Vande Woude, G. F. (2003). Met, metastasis, motility and more. *Nature Reviews Molecular Cell Biology*, 4(12), 915-925. doi:10.1038/nrm1261
- Bladt, F., Riethmacher, D., Isenmann, S., Aguzzi, A., & Birchmeier, C. (1995). Essential role for the c-met receptor in the migration of myogenic precursor cells into the limb bud. *Nature*, 376(6543), 768-771. doi:10.1038/376768a0
- Bolotin, A., Quinquis, B., Sorokin, A., & Ehrlich, S. D. (2005). Clustered regularly interspaced short palindrome repeats (CRISPRs) have spacers of extrachromosomal origin. *Microbiology (Reading)*, 151(Pt 8), 2551-2561. doi:10.1099/mic.0.28048-0
- Borkham-Kamphorst, E., van Roeyen, C. R., Ostendorf, T., Floege, J., Gressner, A. M., & Weiskirchen, R. (2007). Pro-fibrogenic potential of PDGF-D in liver fibrosis. *Journal of Hepatology*, 46(6), 1064-1074. doi:10.1016/j.jhep.2007.01.029

- Borowiak, M., Garratt, A. N., Wüstefeld, T., Strehle, M., Trautwein, C., & Birchmeier, C. (2004). Met provides essential signals for liver regeneration. *Proceedings of the National Academy of Sciences of the United States of America*, *101*(29), 10608. doi:10.1073/pnas.0403412101
- Bota-Rabassedas, N., Banerjee, P., Niu, Y., Cao, W., Luo, J., Xi, Y., . . . Kurie, J. M. (2021). Contextual cues from cancer cells govern cancer-associated fibroblast heterogeneity. *Cell Reports*, *35*(3), 109009. doi: 10.1016/j.celrep.2021.109009
- Bria, A., Marda, J., Zhou, J., Sun, X., Cao, Q., Petersen, B. E., & Pi, L. (2017). Hepatic progenitor cell activation in liver repair. *Liver Research*, *1*(2), 81-87. doi:10.1016/j.livres.2017.08.002
- Brown, Z. J., Heinrich, B., & Greten, T. F. (2018). Mouse models of hepatocellular carcinoma: an overview and highlights for immunotherapy research. *Nature Reviews Gastroenterology Hepatology*, *15*(9), 536-554. doi:10.1038/s41575-018-0033-6
- Cai, X., Wang, J., Wang, J., Zhou, Q., Yang, B., He, Q., & Weng, Q. (2020). Intercellular crosstalk of hepatic stellate cells in liver fibrosis: New insights into therapy. *Pharmacological Research*, *155*, 104720. doi:10.1016/j.phrs.2020.104720
- Carlessi, R., Denisenko, E., Boslem, E., Koehn-Gaone, J., Main, N., Abu Bakar, N. D. B., . . . Tirnitz-Parker, J. E. E. (2022). Single Nucleus RNA Sequencing of Pre-Malignant Liver Reveals Disease-Associated Hepatocyte State with HCC Prognostic Potential. *Cell Genomics*, *3*(1), 2666-2979. doi: 10.1016/j.xgen.2023.100301

- Casagrande, V., Mauriello, A., Bischetti, S., Mavilio, M., Federici, M., & Menghini, R. (2017). Hepatocyte specific TIMP3 expression prevents diet dependent fatty liver disease and hepatocellular carcinoma. *Scientific Reports*, 7(1), 6747. doi:10.1038/s41598-017-06439-x
- Chan, C. W., Wong, N. A., Liu, Y., Bicknell, D., Turley, H., Hollins, L., . . . Bodmer, W. F. (2009). Gastrointestinal differentiation marker Cytokeratin 20 is regulated by homeobox gene CDX1. *Proceedings of the National Academy of Sciences of the United States of America*, 106(6), 1936-1941. doi:10.1073/pnas.0812904106
- Chan, G. K. Y., Lutterbach, B. A., Pan, B.-S., Kariv, I., & Szewczak, A. A. (2008). High-Throughput Analysis of HGF-Stimulated Cell Scattering. *Journal of Biomolecular Screening*, 13(9), 847-854. doi:10.1177/1087057108324497
- Cheemerla, S., & Balakrishnan, M. (2021). Global Epidemiology of Chronic Liver Disease. *Clinical Liver Disease*, 17(5), 365-370. doi:10.1002/cld.1061
- Cheng, J. Y.-K., & Wong, G. L.-H. (2017). Advances in the diagnosis and treatment of liver fibrosis. *Hepatoma Research*, 3, 156-169. doi:10.20517/2394-5079.2017.27
- Chu, W., Li, X., Li, C., Wan, L., Shi, H., Song, X., . . . Yang, B. (2011). TGFBR3, a potential negative regulator of TGF- $\beta$  signaling, protects cardiac fibroblasts from hypoxia-induced apoptosis. *Journal of Cellular Physiology*, 226(10), 2586-2594. doi:10.1002/jcp.22604
- Chung, S. I., Moon, H., Kim, D. Y., Cho, K. J., Ju, H. L., Kim, D. Y., . . . Ro, S. W. (2016). Development of a transgenic mouse model of hepatocellular carcinoma with a liver fibrosis background. *BMC Gastroenterology*, 16, 13. doi:10.1186/s12876-016-0423-6

- Cunningham, R. P., & Porat-Shliom, N. (2021). Liver Zonation – Revisiting Old Questions With New Technologies. *Frontiers in Physiology*, 12. doi:10.3389/fphys.2021.732929
- Dai, Z., Song, G., Balakrishnan, A., Yang, T., Yuan, Q., Möbus, S., . . . Sharma, A. D. (2020). Growth differentiation factor 11 attenuates liver fibrosis via expansion of liver progenitor cells. *Gut*, 69(6), 1104-1115. doi:10.1136/gutjnl-2019-318812
- del Castillo, G., Factor, V. M., Fernández, M., Alvarez-Barrientos, A., Fabregat, I., Thorgeirsson, S. S., & Sánchez, A. (2008). Deletion of the Met tyrosine kinase in liver progenitor oval cells increases sensitivity to apoptosis in vitro. *The American Journal of Pathology*, 172(5), 1238-1247. doi:10.2353/ajpath.2008.070793
- DeLeve, L. D., & Maretta-Mira, A. C. (2017). Liver Sinusoidal Endothelial Cell: An Update. *Seminars in Liver Disease*, 37(4), 377-387. doi:10.1055/s-0037-1617455
- Dixon, L. J., Barnes, M., Tang, H., Pritchard, M. T., & Nagy, L. E. (2013). Kupffer cells in the liver. *Comprehensive Physiology*, 3(2), 785-797. doi:10.1002/cphy.c120026
- Dixon, L. J., Berk, M., Thapaliya, S., Papouchado, B. G., & Feldstein, A. E. (2012). Caspase-1-mediated regulation of fibrogenesis in diet-induced steatohepatitis. *Laboratory Investigation*, 92(5), 713-723. doi:10.1038/labinvest.2012.45
- Dollé, L., Best, J., Mei, J., Al Battah, F., Reynaert, H., van Grunsven, L. A., & Geerts, A. (2010). The quest for liver progenitor cells: A practical point of view. *Journal of Hepatology*, 52(1), 117-129. doi:10.1016/j.jhep.2009.10.009

- Domenicali, M., Caraceni, P., Giannone, F., Baldassarre, M., Lucchetti, G., Quarta, C., . . . Bernardi, M. (2009). A novel model of CCl<sub>4</sub>-induced cirrhosis with ascites in the mouse. *Journal of Hepatology*, *51*(6), 991-999. doi:10.1016/j.jhep.2009.09.008
- Dooley, S., & Dijke, P. (2012). TGF-beta in progression of liver disease. *Cell Tissue Research*, *347*. doi:10.1007/s00441-011-1246-y
- Du, S., Sun, L., Wang, Y., Zhu, W., Gao, J., Pei, W., & Zhang, Y. (2022). ADAM12 is an independent predictor of poor prognosis in liver cancer. *Scientific Reports*, *12*(1), 6634. doi:10.1038/s41598-022-10608-y
- Dwyer, B., Olynyk, J., Ramm, G., & Tirnitz-Parker, J. (2014). TWEAK and LTβ Signaling during Chronic Liver Disease. *Frontiers in Immunology*, *5*(39). doi:10.3389/fimmu.2014.00039
- El-Karef, A., Yoshida, T., Gabazza, E. C., Nishioka, T., Inada, H., Sakakura, T., & Imanaka-Yoshida, K. (2007). Deficiency of tenascin-C attenuates liver fibrosis in immune-mediated chronic hepatitis in mice. *Journal of Pathology*, *211*(1), 86-94. doi:10.1002/path.2099
- El Taghdouini, A., Najimi, M., Sancho-Bru, P., Sokal, E., & van Grunsven, L. A. (2015). In vitro reversion of activated primary human hepatic stellate cells. *Fibrogenesis Tissue Repair*, *8*, 14. doi:10.1186/s13069-015-0031-z
- Endo, H., Niioka, M., Sugioka, Y., Itoh, J., Kameyama, K., Okazaki, I., . . . Watanabe, T. (2011). Matrix Metalloproteinase-13 Promotes Recovery from Experimental Liver Cirrhosis in Rats. *Pathobiology*, *78*(5), 239-252. doi:10.1159/000328841



- Fabregat, I., Moreno-Càceres, J., Sánchez, A., Dooley, S., Dewidar, B., Giannelli, G., & Ten Dijke, P. (2016). TGF- $\beta$  signalling and liver disease. *Febs journal*, 283(12), 2219-2232. doi:10.1111/febs.13665
- Ferlay, J., Soerjomataram, I., Dikshit, R., Eser, S., Mathers, C., Rebelo, M., . . . Bray, F. (2015). Cancer incidence and mortality worldwide: sources, methods and major patterns in GLOBOCAN 2012. *International Journal of Cancer*, 136(5), E359-386. doi:10.1002/ijc.29210
- Fontana, R. J., & Lok, A. S. (2002). Noninvasive monitoring of patients with chronic hepatitis C. *Hepatology*, 36(5 Suppl 1), S57-64. doi:10.1053/jhep.2002.36800
- Friedman, S. L. (2008). Hepatic stellate cells: protean, multifunctional, and enigmatic cells of the liver. *Physiological Reviews*, 88(1), 125-172. doi:10.1152/physrev.00013.2007
- Fujita, K., Oura, K., Yoneyama, H., Shi, T., Takuma, K., Nakahara, M., . . . Masaki, T. (2019). Albumin-bilirubin score indicates liver fibrosis staging and prognosis in patients with chronic hepatitis C. *Hepatology Research*, 49(7), 731-742. doi:10.1111/hepr.13333
- Gajalakshmi, P., Majumder, S., Viebahn, C. S., Swaminathan, A., Yeoh, G. C., & Chatterjee, S. (2016). Interleukin-6 secreted by bipotential murine oval liver stem cells induces apoptosis of activated hepatic stellate cells by activating NF- $\kappa$ B-inducible nitric oxide synthase signaling. *Biochemistry and Cell Biology*, 95(2), 263-272. doi:10.1139/bcb-2016-0011
- Gandillet, A., Alexandre, E., Holl, V., Royer, C., Bischoff, P., Cinqualbre, J., . . . Richert, L. (2003). Hepatocyte ploidy in normal young rat. *Comparative biochemistry and physiology*, 134(3), 665-673. doi:10.1016/s1095-6433(02)00374-4

- Ge, JY., Zheng, YW., Tsuchida, T. (2020) Hepatic stellate cells contribute to liver regeneration through galectins in hepatic stem cell niche. *Stem Cell Research and Therapy* 11, 425. doi:10.1186/s13287-020-01942-x
- Geerts, A. (2001). History, heterogeneity, developmental biology, and functions of quiescent hepatic stellate cells. *Seminars in Liver Disease*, 21(3), 311-335. doi:10.1055/s-2001-17550
- Geervliet, E., & Bansal, R. (2020). Matrix Metalloproteinases as Potential Biomarkers and Therapeutic Targets in Liver Diseases. *Cells*, 9(5). doi:10.3390/cells9051212
- Giuliano, C. J., Lin, A., Girish, V., & Sheltzer, J. M. (2019). Generating Single Cell-Derived Knockout Clones in Mammalian Cells with CRISPR/Cas9. *Current Protocols in Molecular Biology*, 128(1), e100. doi: 10.1002/cpmb.100
- Gogoi-Tiwari, J., Köhn-Gaone, J., Giles, C., Schmidt-Arras, D., Gratte, F. D., Elsegood, C. L., . . . Tirnitz-Parker, J. E. E. (2017). The Murine Choline-Deficient, Ethionine-Supplemented (CDE) Diet Model of Chronic Liver Injury. *Journal of visualized experiments*, (128), 56138. doi:10.3791/56138
- Goyal, L., Muzumdar, M. D., & Zhu, A. X. (2013). Targeting the HGF/c-MET pathway in hepatocellular carcinoma. *Clinical cancer research : an official journal of the American Association for Cancer Research*, 19(9), 2310-2318. doi:10.1158/1078-0432.CCR-12-2791
- Gratte, F. D., Pasic, S., Abu Bakar, N. D. B., Gogoi-Tiwari, J., Liu, X., Carlessi, R., . . . Tirnitz-Parker, J. E. E. (2021). Previous liver regeneration induces fibro-protective mechanisms during thioacetamide-induced chronic liver injury. *The International Journal of Biochemistry & Cell Biology*, 134, 105933. doi: 10.1016/j.biocel.2021.105933

- Greenbaum, L. E., & Wells, R. G. (2011). The role of stem cells in liver repair and fibrosis. *International Journal of Biochemistry and Cell Biology*, 43(2), 222-229. doi:10.1016/j.biocel.2009.11.006
- Greenfield, E. A. (2019). Single-Cell Cloning of Hybridoma Cells by Limiting Dilution. *Cold Spring Harbor Protocols*, 2019(11). doi:10.1101/pdb.prot103192
- Gu, Y., Wei, W., Cheng, Y., Wan, B., Ding, X., Wang, H., . . . Jin, M. (2018). A pivotal role of BEX1 in liver progenitor cell expansion in mice. *Stem Cell Research & Therapy*, 9(1), 164. doi:10.1186/s13287-018-0905-2
- Hintermann, E., Bayer, M., Conti, C. B., Fuchs, S., Fausther, M., Leung, P. S., . . . Christen, U. (2018). Junctional adhesion molecules JAM-B and JAM-C promote autoimmune-mediated liver fibrosis in mice. *Journal of Autoimmunity*, 91, 83-96. doi:10.1016/j.jaut.2018.05.001
- Hu, C.-T., Wu, J.-R., Cheng, C.-C., & Wu, W.-S. (2017). The Therapeutic Targeting of HGF/c-Met Signaling in Hepatocellular Carcinoma: Alternative Approaches. *Cancers*, 9(6), 58. doi:10.3390/cancers9060058
- Hu, H., Wang, M., Wang, H., Liu, Z., Guan, X., Yang, R., . . . Wang, X. (2018). MEGF6 Promotes the Epithelial-to-Mesenchymal Transition via the TGF $\beta$ /SMAD Signaling Pathway in Colorectal Cancer Metastasis. *Cellular Physiology and Biochemistry*, 46(5), 1895-1906. doi:10.1159/000489374
- Hu, Z., Evarts, R. P., Fujio, K., Marsden, E. R., & Thorgeirsson, S. S. (1993). Expression of hepatocyte growth factor and c-met genes during hepatic differentiation and liver development in the rat. *American Journal of Pathology*, 142(6), 1823-1830.

- Huang, A., Yang, X.-R., Chung, W.-Y., Dennison, A. R., & Zhou, J. (2020). Targeted therapy for hepatocellular carcinoma. *Signal Transduction and Targeted Therapy*, 5(1), 146. doi:10.1038/s41392-020-00264-x
- Huang, W., Chen, Z., Shang, X., Tian, D., Wang, D., Wu, K., . . . Xia, L. (2015). Sox12, a direct target of FoxQ1, promotes hepatocellular carcinoma metastasis through up-regulating Twist1 and FGFBP1. *Hepatology*, 61(6), 1920-1933. doi:10.1002/hep.27756
- Huh, C.-G., Factor, V. M., Sánchez, A., Uchida, K., Conner, E. A., & Thorgeirsson, S. S. (2004). Hepatocyte growth factor/c-met signaling pathway is required for efficient liver regeneration and repair. *Proceedings of the National Academy of Sciences of the United States of America*, 101(13), 4477. doi:10.1073/pnas.0306068101
- Inagaki, Y., Higashi, K., Kushida, M., Hong, Y. Y., Nakao, S., Higashiyama, R., . . . Okazaki, I. (2008). Hepatocyte Growth Factor Suppresses Profibrogenic Signal Transduction via Nuclear Export of Smad3 With Galectin-7. *Gastroenterology*, 134(4), 1180-1190. doi:10.1053/j.gastro.2008.01.014
- Ishikawa, T., Factor, V. M., Marquardt, J. U., Raggi, C., Seo, D., Kitade, M., & Conner, E. A. (2012). Hepatocyte growth factor/c-met signaling is required for stem-cell-mediated liver regeneration in mice. *Hepatology*, 55. doi:10.1002/hep.24796
- Jakubowski, A., Ambrose, C., Parr, M., Lincecum, J. M., Wang, M. Z., Zheng, T. S., & Browning, B. (2005). TWEAK induces liver progenitor cell proliferation. *Journal of Clinical Investigation*, 115. doi:10.1172/jci23486
- Jiang, Y., Liu, G., Ye, W., Xie, J., Shao, C., Wang, X., & Li, X. (2020). ZEB2-AS1 Accelerates Epithelial/Mesenchymal Transition Through miR-

1205/CRKL Pathway in Colorectal Cancer. *Cancer Biotherapy and Radiopharmaceuticals*, 35(2), 153-162. doi:10.1089/cbr.2019.3000

Jungermann, K., & Katz, N. (1989). Functional specialization of different hepatocyte populations. *Physiological Reviews*, 69(3), 708-764. doi:10.1152/physrev.1989.69.3.708

Kao, W. Y., Lin, Y. F., Chang, I. W., Chen, C. L., Tang, J. H., Chang, C. C., . . . Wang, W. (2021). Interleukin-2 receptor alpha as a biomarker for nonalcoholic fatty liver disease diagnosis. *Journal of the Chinese Medical Association*, 84(3), 261-266. doi:10.1097/jcma.0000000000000469

Karsdal, M. A., Daniels, S. J., Holm Nielsen, S., Bager, C., Rasmussen, D. G. K., Loomba, R., . . . Schuppan, D. (2020). Collagen biology and non-invasive biomarkers of liver fibrosis. *Liver International*, 40(4), 736-750. doi:10.1111/liv.14390

Kato, T. (2017). Biological roles of hepatocyte growth factor-Met signaling from genetically modified animals. *Biomedical Reports*, 7(6), 495-503. doi:10.3892/br.2017.1001

Kaur, S., Siddiqui, H., & Bhat, M. H. (2015). Hepatic Progenitor Cells in Action: Liver Regeneration or Fibrosis? *The American Journal of Pathology*, 185(9), 2342-2350. doi:10.1016/j.ajpath.2015.06.004

Kawai, T., Yasuchika, K., Ishii, T., Katayama, H., Yoshitoshi, E. Y., Ogiso, S., . . . Uemoto, S. (2015). Keratin 19, a Cancer Stem Cell Marker in Human Hepatocellular Carcinoma. *Clinical Cancer Research*, 21(13), 3081-3091. doi:10.1158/1078-0432.CCR-14-1936

Kholodenko, I. V., & Yarygin, K. N. (2017). Cellular Mechanisms of Liver Regeneration and Cell-Based Therapies of Liver Diseases. *Biomedical Research International*, 8910821. doi:10.1155/2017/8910821

- Kietzmann, T. (2017). Metabolic zonation of the liver: The oxygen gradient revisited. *Redox Biology*, 11, 622-630. doi:10.1016/j.redox.2017.01.012
- Kiss, A., Wang, N. J., Xie, J. P., & Thorgeirsson, S. S. (1997). Analysis of transforming growth factor (TGF)-alpha/epidermal growth factor receptor, hepatocyte growth Factor/c-met, TGF-beta receptor type II, and p53 expression in human hepatocellular carcinomas. *Clinical cancer research : an official journal of the American Association for Cancer Research*, 3(7), 1059-1066.
- Knight, B., Tirnitz-Parker, J. E., & Olynyk, J. K. (2008). C-kit inhibition by imatinib mesylate attenuates progenitor cell expansion and inhibits liver tumor formation in mice. *Gastroenterology*, 135(3), 969-979, 979.e961. doi:10.1053/j.gastro.2008.05.077
- Köhn-Gaone, J., Dwyer, B. J., Grzelak, C. A., Miller, G., Shackel, N. A., Ramm, G. A., . . . Tirnitz-Parker, J. E. E. (2016). Divergent Inflammatory, Fibrogenic, and Liver Progenitor Cell Dynamics in Two Common Mouse Models of Chronic Liver Injury. *American Journal of Pathology*, 186(7), 1762-1774. doi:10.1016/j.ajpath.2016.03.005
- Kohn-Gaone, J., Gogoi-Tiwari, J., Ramm, G. A., Olynyk, J. K., & Tirnitz-Parker, J. E. (2016). The role of liver progenitor cells during liver regeneration, fibrogenesis, and carcinogenesis. *American Journal of Physiology-Gastrointestinal and Liver Physiology*, 310(3), G143-154. doi:10.1152/ajpgi.00215.2015
- Kruepunga, N., Hakvoort, T. B. M., Hikspoors, J., Köhler, S. E., & Lamers, W. H. (2019). Anatomy of rodent and human livers: What are the differences? *BBA Molecular Basis of Disease*, 1865(5), 869-878. doi:10.1016/j.bbadis.2018.05.019
- Kuramitsu, K., Sverdlov, D. Y., Liu, S. B., Csizmadia, E., Burkly, L., Schuppan, D., . . . Popov, Y. (2013). Failure of Fibrotic Liver Regeneration in Mice

Is Linked to a Severe Fibrogenic Response Driven by Hepatic Progenitor Cell Activation. *The American Journal of Pathology*, 183(1), 182-194. doi:10.1016/j.ajpath.2013.03.018

Kwiecinski, M., Noetel, A., Elfimova, N., Trebicka, J., Schievenbusch, S., Strack, I., . . . Odenthal, M. (2011). Hepatocyte growth factor (HGF) inhibits collagen I and IV synthesis in hepatic stellate cells by miRNA-29 induction. *PLoS One*, 6(9), e24568. doi:10.1371/journal.pone.0024568

Lai, K. K., Shang, S., Lohia, N., Booth, G. C., Masse, D. J., Fausto, N., . . . Beretta, L. (2011). Extracellular matrix dynamics in hepatocarcinogenesis: a comparative proteomics study of PDGFC transgenic and Pten null mouse models. *PLoS Genetics*, 7(6), e1002147. doi:10.1371/journal.pgen.1002147

Lee, H. S., Choi, J., Son, T., Lee, E. J., Kim, J. G., Ryu, S. H., . . . Kim, K. W. (2018). A-kinase anchoring protein 12 is downregulated in human hepatocellular carcinoma and its deficiency in mice aggravates thioacetamide-induced liver injury. *Oncology Letters*, 16(5), 5907-5915. doi:10.3892/ol.2018.9396

Li, N., Dou, Z., Liu, J., Chai, B., Li, Y., An, X., . . . Zhang, X. (2018). Therapeutic Effect of HGF on NASH Mice Through HGF/c-Met and JAK2-STAT3 Signalling Pathway. *Annals of Hepatology*, 17(3), 501-510. doi:10.5604/01.3001.0011.7395

Liedtke, C., Luedde, T., Sauerbruch, T., Scholten, D., Streetz, K., Tacke, F., . . . Weiskirchen, R. (2013). Experimental liver fibrosis research: update on animal models, legal issues and translational aspects. *Fibrogenesis & Tissue Repair*, 6(1), 19. doi:10.1186/1755-1536-6-19

Lim, B. J., Lee, W.-K., Lee, H. W., Lee, K. S., Kim, J. K., Chang, H. Y., & Lee, J. I. (2018). Selective deletion of hepatocyte platelet-derived growth factor receptor  $\alpha$  and development of liver fibrosis in mice. *Cell*

*Communication and Signaling*, 16(1), 93. doi:10.1186/s12964-018-0306-2

Liu, B.-Q., Bao, Z.-Y., Zhu, J.-Y., & Liu, H. (2021). Fibrinogen-like protein 2 promotes the accumulation of myeloid-derived suppressor cells in the hepatocellular carcinoma tumor microenvironment. *Oncology Letters*, 21(1), 47. doi:10.3892/ol.2020.12308

Liu, F., & Qian, Y. (2021). The role of CD133 in hepatocellular carcinoma. *Cancer Biology and Therapy*, 22(4), 291-300. doi:10.1080/15384047.2021.1916381

Liu, Y., Meyer, C., Xu, C., Weng, H., Hellerbrand, C., ten Dijke, P., & Dooley, S. (2012). Animal models of chronic liver diseases. *American Journal of Physiology-Gastrointestinal and Liver Physiology*, 304(5), G449-G468. doi:10.1152/ajpgi.00199.2012

Liu, Z., Mo, H., Liu, R., Niu, Y., Chen, T., Xu, Q., . . . Yang, N. (2021). Matrix stiffness modulates hepatic stellate cell activation into tumor-promoting myofibroblasts via E2F3-dependent signaling and regulates malignant progression. *Cell Death & Disease*, 12(12), 1134. doi:10.1038/s41419-021-04418-9

Lowes, K. N., Brennan, B. A., Yeoh, G. C., & Olynyk, J. K. (1999). Oval Cell Numbers in Human Chronic Liver Diseases Are Directly Related to Disease Severity. *American Journal of Pathology*, 154(2), 537-541. doi:10.1016/S0002-9440(10)65299-6

Lu, Y., Dang, Q., Bo, Y., Su, X., Wang, L., Sun, J., . . . Li, Y. (2021). The Expression of CLDN6 in Hepatocellular Carcinoma Tissue and the Effects of CLDN6 on Biological Phenotypes of Hepatocellular Carcinoma Cells. *Journal of Cancer*, 12(18), 5454-5463. doi:10.7150/jca.55727



- Luo, S., Lin, R., Liao, X., Li, D., & Qin, Y. (2021). Identification and verification of the molecular mechanisms and prognostic values of the cadherin gene family in gastric cancer. *Scientific Reports*, 11(1), 23674. doi:10.1038/s41598-021-03086-1
- Marcellin, P., & Kutala, B. K. (2018). Liver diseases: A major, neglected global public health problem requiring urgent actions and large-scale screening. *Liver International*, 38(S1), 2-6. doi:10.1111/liv.13682
- Maroni, L., Haibo, B., Ray, D., Zhou, T., Wan, Y., Meng, F., . . . Alpini, G. (2015). Functional and structural features of cholangiocytes in health and disease. *Cellular and Molecular Gastroenterology and Hepatology*, 1(4), 368-380. doi:10.1016/j.jcmgh.2015.05.005
- Marquardt, J. U., Seo, D., Gómez-Quiroz, L. E., Uchida, K., Gillen, M. C., Kitade, M., . . . Thorgeirsson, S. S. (2012). Loss of c-Met accelerates development of liver fibrosis in response to CCl<sub>4</sub> exposure through deregulation of multiple molecular pathways. *Biochimica et Biophysica Acta (BBA) - Molecular Basis of Disease*, 1822(6), 942-951. doi:10.1016/j.bbadis.2012.02.012
- Marrone, G., Shah, V. H., & Gracia-Sancho, J. (2016). Sinusoidal communication in liver fibrosis and regeneration. *Journal of Hepatology*, 65(3), 608-617. doi:10.1016/j.jhep.2016.04.018
- Maulik, G., Shrikhande, A., Kijima, T., Ma, P. C., Morrison, P. T., & Salgia, R. (2002). Role of the hepatocyte growth factor receptor, c-Met, in oncogenesis and potential for therapeutic inhibition. *Cytokine & Growth Factor Reviews*, 13(1), 41-59. doi:10.1016/S1359-6101(01)00029-6
- Mederacke, I., Dapito, D. H., Affò, S., Uchinami, H., & Schwabe, R. F. (2015). High-yield and high-purity isolation of hepatic stellate cells from normal

- and fibrotic mouse livers. *Nature Protocols*, 10(2), 305-315. doi:10.1038/nprot.2015.017
- Michalopoulos, G. K. (2010). Liver regeneration after partial hepatectomy: critical analysis of mechanistic dilemmas. *American Journal of Pathology*, 176(1), 2-13. doi:10.2353/ajpath.2010.090675
- Michelotti, G. A., Xie, G., Swiderska, M., Choi, S. S., Karaca, G., Krüger, L., . . . Diehl, A. M. (2013). Smoothed is a master regulator of adult liver repair. *Journal of Clinical Investigations*, 123(6), 2380-2394. doi:10.1172/jci66904
- Mikula, M., Proell, V., Fischer, A. N. M., & Mikulits, W. (2006). Activated hepatic stellate cells induce tumor progression of neoplastic hepatocytes in a TGF- $\beta$  dependent fashion. *Journal of Cellular Physiology*, 209(2), 560-567. doi:10.1002/jcp.20772
- Miura, Y., Matsui, S., Miyata, N., Harada, K., Kikkawa, Y., Ohmuraya, M., . . . Tanaka, M. (2018). Differential expression of Lutheran/BCAM regulates biliary tissue remodeling in ductular reaction during liver regeneration. *Elife*, 7. doi:10.7554/eLife.36572
- Monvoisin, A., Bisson, C., Si-Tayeb, K., Balabaud, C., Desmoulière, A., & Rosenbaum, J. (2002). Involvement of matrix metalloproteinase type-3 in hepatocyte growth factor-induced invasion of human hepatocellular carcinoma cells. *International Journal of Cancer*, 97(2), 157-162. doi:10.1002/ijc.1595
- Mungunsukh, O., McCart, E. A., & Day, R. M. (2014). Hepatocyte Growth Factor Isoforms in Tissue Repair, Cancer, and Fibrotic Remodeling. *Biomedicines*, 2(4), 301-326. doi:10.3390/biomedicines2040301
- Naito, M., Hasegawa, G., & Takahashi, K. (1997). Development, differentiation, and maturation of Kupffer cells. *Microscopy Research*

*and Technique*, 39(4), 350-364. doi:10.1002/(sici)1097-0029(19971115)39:4<350::Aid-jemt5>3.0.Co;2-l

Narmada, B. C., Kang, Y., Venkatraman, L., Peng, Q., Sakban, R. B., Nugraha, B., . . . Yu, H. (2013). Hepatic Stellate Cell–Targeted Delivery of Hepatocyte Growth Factor Transgene via Bile Duct Infusion Enhances Its Expression at Fibrotic Foci to Regress Dimethylnitrosamine-Induced Liver Fibrosis. *Human Gene Therapy*, 24(5), 508-519. doi:10.1089/hum.2012.158

Nguyen-Lefebvre, A. T., & Horuzsko, A. (2015). Kupffer Cell Metabolism and Function. *Journal of Enzymology and Metabolism*, 1(1).

Nguyen, X.-X., Muhammad, L., Nietert, P. J., & Feghali-Bostwick, C. (2018). IGFBP-5 Promotes Fibrosis via Increasing Its Own Expression and That of Other Pro-fibrotic Mediators. *Frontiers in Endocrinology*, 9. doi:10.3389/fendo.2018.00601

Ogawa, H., Kaji, K., Nishimura, N., Takagi, H., Ishida, K., Takaya, H., . . . Yoshiji, H. (2021). Lenvatinib prevents liver fibrosis by inhibiting hepatic stellate cell activation and sinusoidal capillarization in experimental liver fibrosis. *Journal of Cellular and Molecular Medicine*, 25(8), 4001-4013. doi:10.1111/jcmm.16363

Olaso, E., Arteta, B., Benedicto, A., Crende, O., & Friedman, S. L. (2011). Loss of discoidin domain receptor 2 promotes hepatic fibrosis after chronic carbon tetrachloride through altered paracrine interactions between hepatic stellate cells and liver-associated macrophages. *American Journal of Pathology*, 179(6), 2894-2904. doi:10.1016/j.ajpath.2011.09.002

Onuma, A. E., Zhang, H., Huang, H., Williams, T. M., Noonan, A., & Tsung, A. (2020). Immune Checkpoint Inhibitors in Hepatocellular Cancer: Current Understanding on Mechanisms of Resistance and Biomarkers

of Response to Treatment. *Gene Expression*, 20(1), 53-65.  
doi:10.3727/105221620x15880179864121

Organ, S. L., & Tsao, M.-S. (2011). An overview of the c-MET signaling pathway. *Therapeutic advances in medical oncology*, 3(1 Suppl), S7-S19. doi:10.1177/1758834011422556

Papa, E., Weller, M., Weiss, T., Ventura, E., Burghardt, I., & Szabó, E. (2017). Negative control of the HGF/c-MET pathway by TGF- $\beta$ : a new look at the regulation of stemness in glioblastoma. *Cell Death Diseases*, 8(12), 3210. doi:10.1038/s41419-017-0051-2

Pei, M., Luo, J., & Chen, Q. (2008). Enhancing and maintaining chondrogenesis of synovial fibroblasts by cartilage extracellular matrix protein matrilins. *Osteoarthritis Cartilage*, 16(9), 1110-1117. doi:10.1016/j.joca.2007.12.011

Petrini, I. (2015). Biology of MET: a double life between normal tissue repair and tumor progression. *Annals of Translational Medicine*, 3(6), 82. doi:10.3978/j.issn.2305-5839.2015.03.58

Raven, A., Lu, W. Y., Man, T. Y., Ferreira-Gonzalez, S., O'Duibhir, E., Dwyer, B. J., . . . Forbes, S. J. (2017). Cholangiocytes act as facultative liver stem cells during impaired hepatocyte regeneration. *Nature*, 547(7663), 350-354. doi:10.1038/nature23015

Rodríguez-Rodríguez, D. R., Ramírez-Solís, R., Garza-Elizondo, M. A., Garza-Rodríguez, M. L., & Barrera-Saldaña, H. A. (2019). Genome editing: A perspective on the application of CRISPR/Cas9 to study human diseases (Review). *International Journal of Molecular Medicine*, 43(4), 1559-1574. doi:10.3892/ijmm.2019.4112

Roskams, T. (2006). Liver stem cells and their implication in hepatocellular and cholangiocarcinoma. *Oncogene*, 25(27), 3818-3822. doi:10.1038/sj.onc.1209558

- Ruddell, R. G., Knight, B., Tirnitz-Parker, J. E. E., Akhurst, B., Summerville, L., Subramaniam, V. N., . . . Ramm, G. A. (2009). Lymphotoxin- $\beta$  receptor signaling regulates hepatic stellate cell function and wound healing in a murine model of chronic liver injury. *Hepatology*, *49*(1), 227-239. doi:10.1002/hep.22597
- Sancho-Bru, P., Altamirano, J., Rodrigo-Torres, D., Coll, M., Millán, C., José Lozano, J., . . . Bataller, R. (2012). Liver progenitor cell markers correlate with liver damage and predict short-term mortality in patients with alcoholic hepatitis. *Hepatology*, *55*(6), 1931-1941. doi:10.1002/hep.25614
- Schmidt, C., Bladt, F., Goedecke, S., Brinkmann, V., Zschiesche, W., Sharpe, M., . . . Birchmeier, C. (1995). Scatter factor/hepatocyte growth factor is essential for liver development. *Nature*, *373*(6516), 699-702. doi:10.1038/373699a0
- Schulze, R. J., Schott, M. B., Casey, C. A., Tuma, P. L., & McNiven, M. A. (2019). The cell biology of the hepatocyte: A membrane trafficking machine. *Journal of Cell Biology*, *218*(7), 2096-2112. doi:10.1083/jcb.201903090
- Sear, J. (1992). Anatomy and physiology of the liver. *Baillière's Clinical Anaesthesiology*, *6*(4), 697-727. doi:10.1016/S0950-3501(05)80304-6
- Seif, F., Khoshmirsafa, M., Aazami, H., Mohsenzadegan, M., Sedighi, G., & Bahar, M. (2017). The role of JAK-STAT signaling pathway and its regulators in the fate of T helper cells. *Cell Communication and Signaling*, *15*(1), 23. doi:10.1186/s12964-017-0177-y

- Shang, L., Hosseini, M., Liu, X., Kisseleva, T., & Brenner, D. A. (2018). Human hepatic stellate cell isolation and characterization. *Journal of Gastroenterology*, *53*(1), 6-17. doi:10.1007/s00535-017-1404-4
- Shetty, S., Lalor, P. F., & Adams, D. H. (2018). Liver sinusoidal endothelial cells - gatekeepers of hepatic immunity. *Nature Reviews Gastroenterology and Hepatology*, *15*(9), 555-567. doi:10.1038/s41575-018-0020-y
- Shukla, M. N., Rose, J. L., Ray, R., Lathrop, K. L., Ray, A., & Ray, P. (2009). Hepatocyte growth factor inhibits epithelial to myofibroblast transition in lung cells via Smad7. *American journal of respiratory cell and molecular biology*, *40*(6), 643-653. doi:10.1165/rcmb.2008-0217OC
- Siddiqui, H., Rawal, P., Bihari, C., Arora, N., & Kaur, S. (2020). Vascular Endothelial Growth Factor Promotes Proliferation of Epithelial Cell Adhesion Molecule-Positive Cells in Nonalcoholic Steatohepatitis. *J Clinical and Experimental Hepatology*, *10*(4), 275-283. doi:10.1016/j.jceh.2019.11.011
- Siegmund, S. V., Schlosser, M., Schildberg, F. A., Seki, E., De Minicis, S., Uchinami, H., . . . Schwabe, R. F. (2016). Serum Amyloid A Induces Inflammation, Proliferation and Cell Death in Activated Hepatic Stellate Cells. *PLoS One*, *11*(3), e0150893. doi:10.1371/journal.pone.0150893
- Sigurdardottir, A. K., Jonasdottir, A. S., Asbjarnarson, A., Helgudottir, H. R., Gudjonsson, T., & Traustadottir, G. A. (2021). Peroxidasin Enhances Basal Phenotype and Inhibits Branching Morphogenesis in Breast Epithelial Progenitor Cell Line D492. *Journal of Mammary Gland Biology and Neoplasia*, *26*(4), 321-338. doi:10.1007/s10911-021-09507-1
- Son, G., Hines, I. N., Lindquist, J., Schrum, L. W., & Rippe, R. A. (2009). Inhibition of phosphatidylinositol 3-kinase signaling in hepatic stellate

cells blocks the progression of hepatic fibrosis. *Hepatology*, 50(5), 1512-1523. doi:10.1002/hep.23186

Spee, B., Carpino, G., Schotanus, B. A., Katoonizadeh, A., Vander Borght, S., Gaudio, E., & Roskams, T. (2010). Characterisation of the liver progenitor cell niche in liver diseases: potential involvement of Wnt and Notch signalling. *Gut*, 59. doi:10.1136/gut.2009.188367

Stravitz, R. T., & Lee, W. M. (2019). Acute liver failure. *Lancet*, 394(10201), 869-881. doi:10.1016/s0140-6736(19)31894-x

Suárez-Causado, A., Caballero-Díaz, D., Bertrán, E., Roncero, C., Addante, A., García-Álvaro, M., . . . Sánchez, A. (2015). HGF/c-Met signaling promotes liver progenitor cell migration and invasion by an epithelial–mesenchymal transition-independent, phosphatidyl inositol-3 kinase-dependent pathway in an in vitro model. *BBA Molecular Cell Research*, 1853(10, Part A), 2453-2463. doi:10.1016/j.bbamcr.2015.05.017

Sun, Y.-L., Bai, T., Zhou, L., Zhu, R.-T., Wang, W.-J., Liang, R.-P., . . . Gou, J.-J. (2021). SOD3 deficiency induces liver fibrosis by promoting hepatic stellate cell activation and epithelial–mesenchymal transition. *Journal of Cellular Physiology*, 236(6), 4313-4329. doi:10.1002/jcp.30174

Suzuki, K., Hayashi, N., Yamada, Y., Yoshihara, H., Miyamoto, Y., Ito, Y., . . . et al. (1994). Expression of the c-met protooncogene in human hepatocellular carcinoma. *Hepatology*, 20(5), 1231-1236.

Szabó, E., Korpos, E., Batmunkh, E., Lotz, G., Holczbauer, A., Kovalszky, I., . . . Kiss, A. (2008). Expression of matrilin-2 in liver cirrhosis and hepatocellular carcinoma. *Pathology and Oncology Research*, 14(1), 15-22. doi:10.1007/s12253-008-9005-4

- Tabibian, J. H., Masyuk, A. I., Masyuk, T. V., O'Hara, S. P., & LaRusso, N. F. (2013). Physiology of cholangiocytes. *Comprehensive Physiology*, 3(1), 541-565. doi:10.1002/cphy.c120019
- Tamai, K., Nakamura-Shima, M., Shibuya-Takahashi, R., Kanno, S.-I., Yasui, A., Mochizuki, M., . . . Satoh, K. (2020). BEX2 suppresses mitochondrial activity and is required for dormant cancer stem cell maintenance in intrahepatic cholangiocarcinoma. *Scientific Reports*, 10(1), 21592. doi:10.1038/s41598-020-78539-0
- Tarlow, B. D., Pelz, C., Naugler, W. E., Wakefield, L., Wilson, E. M., Finegold, M. J., & Grompe, M. (2014). Bipotential adult liver progenitors are derived from chronically injured mature hepatocytes. *Cell Stem Cell*, 15(5), 605-618. doi:10.1016/j.stem.2014.09.008
- Theise, N. D., Saxena, R., Portmann, B. C., Thung, S. N., Yee, H., Chiriboga, L., . . . Crawford, J. M. (1999). The canals of Hering and hepatic stem cells in humans. *Hepatology*, 30(6), 1425-1433. doi:10.1002/hep.510300614
- Tirnitz-Parker, J. E., Viebahn, C. S., Jakubowski, A., Klopčič, B. R., Olynyk, J. K., Yeoh, G. C., & Knight, B. (2010). Tumor necrosis factor-like weak inducer of apoptosis is a mitogen for liver progenitor cells. *Journal of Hepatology*, 52(1), 291-302. doi:10.1002/hep.23663
- Tirnitz-Parker, J. E. E., Tonkin, J. N., Knight, B., Olynyk, J. K., & Yeoh, G. C. T. (2007). Isolation, culture and immortalisation of hepatic oval cells from adult mice fed a choline-deficient, ethionine-supplemented diet. *International Journal of Biochemistry and Cell Biology*, 39(12), 2226-2239. doi:10.1016/j.biocel.2007.06.008
- Trefts, E., Gannon, M., & Wasserman, D. H. (2017). The liver. *Current Biology*, 27(21), R1147-r1151. doi:10.1016/j.cub.2017.09.019



- Troeger, J. S., Mederacke, I., Gwak, G. Y., Dapito, D. H., Mu, X., Hsu, C. C., . . . Schwabe, R. F. (2012). Deactivation of hepatic stellate cells during liver fibrosis resolution in mice. *Gastroenterology*, *143*(4), 1073-1083.e1022. doi:10.1053/j.gastro.2012.06.036
- Tsou, H.-K., Chen, H.-T., Hung, Y.-H., Chang, C.-H., Li, T.-M., Fong, Y.-C., & Tang, C.-H. (2013). HGF and c-Met Interaction Promotes Migration in Human Chondrosarcoma Cells. *PLoS One*, *8*(1), e53974. doi:10.1371/journal.pone.0053974
- Tsuchida, T., & Friedman, S. L. (2017). Mechanisms of hepatic stellate cell activation. *Nature Reviews Gastroenterology and Hepatology*, *14*(7), 397-411. doi:10.1038/nrgastro.2017.38
- Uchikawa, E., Chen, Z., Xiao, G.-Y., Zhang, X., & Bai, X.-c. (2021). Structural basis of the activation of c-MET receptor. *Nature Communications*, *12*(1), 4074. doi:10.1038/s41467-021-24367-3
- Uddin, F., Rudin, C. M., & Sen, T. (2020). CRISPR Gene Therapy: Applications, Limitations, and Implications for the Future. *Frontiers in Oncology*, *10*, 1387. doi:10.3389/fonc.2020.01387
- Uehara, T., Pogribny, I. P., & Rusyn, I. (2014). The DEN and CCl<sub>4</sub> -Induced Mouse Model of Fibrosis and Inflammation-Associated Hepatocellular Carcinoma. *Current Protocols in Pharmacology*, *66*, 14.30.11-14.30.10. doi:10.1002/0471141755.ph1430s66
- Uehara, Y., Minowa, O., Mori, C., Shiota, K., Kuno, J., Noda, T., & Kitamura, N. (1995). Placental defect and embryonic lethality in mice lacking hepatocyte growth factor/scatter factor. *Nature*, *373*(6516), 702-705. doi:10.1038/373702a0
- Van Hul, N. K. M., Abarca-Quinones, J., Sempoux, C., Horsmans, Y., & Leclercq, I. A. (2009). Relation between liver progenitor cell expansion and extracellular matrix deposition in a CDE-induced murine model of

chronic liver injury. *Hepatology*, 49(5), 1625-1635.  
doi:10.1002/hep.22820

Venepalli, N. K., & Goff, L. (2013). Targeting the HGF-cMET Axis in Hepatocellular Carcinoma. *International Journal of Hepatology*, 2013, 341636. doi:10.1155/2013/341636

Vestentoft, P. S., Jelnes, P., Andersen, J. B., Tran, T. A. T., Jørgensen, T., Rasmussen, M., . . . Bisgaard, H. C. (2013). Molecular constituents of the extracellular matrix in rat liver mounting a hepatic progenitor cell response for tissue repair. *Fibrogenesis & Tissue Repair*, 6(1), 21. doi:10.1186/1755-1536-6-21

Vestentoft, P. S., Jelnes, P., Hopkinson, B. M., Vainer, B., Møllgård, K., Quistorff, B., & Bisgaard, H. C. (2011). Three-dimensional reconstructions of intrahepatic bile duct tubulogenesis in human liver. *BMC Developmental Biology*, 11, 56. doi:10.1186/1471-213x-11-56

Wallace, M. C., Hamesch, K., Lunova, M., Kim, Y., Weiskirchen, R., Strnad, P., & Friedman, S. L. (2015). Standard operating procedures in experimental liver research: thioacetamide model in mice and rats. *Laboratory Animals*, 49(1 Suppl), 21-29. doi:10.1177/0023677215573040

Wang, D., Han, S., Wang, X., Peng, R., & Li, X. (2015). SOX5 promotes epithelial-mesenchymal transition and cell invasion via regulation of Twist1 in hepatocellular carcinoma. *Medical Oncology*, 32(2), 461. doi:10.1007/s12032-014-0461-2

Wang, H., Rao, B., Lou, J., Li, J., Liu, Z., Li, A., . . . Yu, Z. (2020). The Function of the HGF/c-Met Axis in Hepatocellular Carcinoma. *Frontiers in Cell and Developmental Biology*, 8(55). doi:10.3389/fcell.2020.00055

- Wang, W. M., Xu, Y., Wang, Y. H., Sun, H. X., Sun, Y. F., He, Y. F., . . . Fan, J. (2017). HOXB7 promotes tumor progression via bFGF-induced activation of MAPK/ERK pathway and indicated poor prognosis in hepatocellular carcinoma. *Oncotarget*, 8(29), 47121-47135. doi:10.18632/oncotarget.17004
- Wang, X., Foster, M., Al-Dhalimy, M., Lagasse, E., Finegold, M., & Grompe, M. (2003). The Origin and Liver Repopulating Capacity of Murine Oval Cells. *Proceedings of the National Academy of Sciences of the United States of America*, 100, 11881-11888. doi:10.1073/pnas.1734199100
- Wang, X., Hassan, W., Zhao, J., Bakht, S., Nie, Y., Wang, Y., . . . Huang, Z. (2019). The impact of hepatocyte nuclear factor-1 $\alpha$  on liver malignancies and cell stemness with metabolic consequences. *Stem Cell Research & Therapy*, 10(1), 315. doi:10.1186/s13287-019-1438-z
- Wang, Y., Qu, A., & Wang, H. (2015). Signal Transducer and Activator of Transcription 4 in Liver Diseases. *International Journal of Biological Sciences*, 11(4), 448-455. doi:10.7150/ijbs.11164
- Wang, Y. P., Yu, G. R., Lee, M. J., Lee, S. Y., Chu, I. S., Leem, S. H., & Kim, D. G. (2013). Lipocalin-2 negatively modulates the epithelial-to-mesenchymal transition in hepatocellular carcinoma through the epidermal growth factor (TGF-beta1)/Lcn2/Twist1 pathway. *Hepatology*, 58(4), 1349-1361. doi:10.1002/hep.26467
- Weidner, K. M., Arakaki, N., Hartmann, G., Vandekerckhove, J., Weingart, S., Rieder, H., . . . et al. (1991). Evidence for the identity of human scatter factor and human hepatocyte growth factor. *Proceedings of the National Academy of Sciences of the United States of America*, 88(16), 7001-7005. doi:10.1073/pnas.88.16.7001

- Westenberger, G., Sellers, J., Fernando, S., Junkins, S., Han, S. M., Min, K., & Lawan, A. (2021). Function of Mitogen-Activated Protein Kinases in Hepatic Inflammation. *Journal of Cellular Signaling*, 2(3), 172-180.
- Wu, Y., Cheng, M., Shi, Z., Feng, Z., & Guan, X. (2014). Dynamic expression and localization of c-MET isoforms in the developing rat pancreas. *International journal of clinical and experimental pathology*, 7(12), 8563-8572. Retrieved from <https://pubmed.ncbi.nlm.nih.gov/25674220>
- Wynn, T. A. (2008). Cellular and molecular mechanisms of fibrosis. *The Journal of pathology*, 214(2), 199-210. doi:10.1002/path.2277
- Wynn, T. A., & Ramalingam, T. R. (2012). Mechanisms of fibrosis: therapeutic translation for fibrotic disease. *Nature medicine*, 18(7), 1028-1040. doi:10.1038/nm.2807
- Xie, B., Xing, R., Chen, P., Gou, Y., Li, S., Xiao, J., & Dong, J. (2010). Down-regulation of c-Met expression inhibits human HCC cells growth and invasion by RNA interference. *Journal of Surgical Research*, 162(2), 231-238. doi:10.1016/j.jss.2009.04.030
- Xu, L., Hui, A. Y., Albanis, E., Arthur, M. J., O'Byrne, S. M., Blaner, W. S., . . . Eng, F. J. (2005). Human hepatic stellate cell lines, LX-1 and LX-2: new tools for analysis of hepatic fibrosis. *Gut*, 54(1), 142-151. doi:10.1136/gut.2004.042127
- Xu, Z., Wu, Y., Wang, F., Li, X., Wang, P., Li, Y., . . . Liu, Y. (2020). Fibroblast Growth Factor 1 Ameliorates Diabetes-Induced Liver Injury by Reducing Cellular Stress and Restoring Autophagy. *Frontiers in Pharmacology*, 11. doi:10.3389/fphar.2020.00052
- Yamada, K. M., & Sixt, M. (2019). Mechanisms of 3D cell migration. *Nature Reviews Molecular Cell Biology*, 20(12), 738-752. doi:10.1038/s41580-019-0172-9

- Yan, Y., Zeng, J., Xing, L., & Li, C. (2021). Extra- and Intra-Cellular Mechanisms of Hepatic Stellate Cell Activation. *Biomedicines*, 9(8). doi:10.3390/biomedicines9081014
- Yang, J., Zheng, J., Wu, L., Shi, M., Zhang, H., Wang, X., . . . Dou, K. (2011). NDRG2 ameliorates hepatic fibrosis by inhibiting the TGF- $\beta$ 1/Smad pathway and altering the MMP2/TIMP2 ratio in rats. *PLoS One*, 6(11), e27710. doi:10.1371/journal.pone.0027710
- Yang, Q., Yan, C., & Gong, Z. (2018). Interaction of hepatic stellate cells with neutrophils and macrophages in the liver following oncogenic kras activation in transgenic zebrafish. *Scientific Reports*, 8(1), 8495. doi:10.1038/s41598-018-26612-0
- Yang, Y. M., & Seki, E. (2015). TNF $\alpha$  in liver fibrosis. *Current Pathobiological Reports*, 3(4), 253-261. doi:10.1007/s40139-015-0093-z
- Yanguas, S. C., Cogliati, B., Willebrords, J., Maes, M., Colle, I., van den Bossche, B., . . . Vinken, M. (2016). Experimental models of liver fibrosis. *Archives of toxicology*, 90(5), 1025-1048. doi:10.1007/s00204-015-1543-4
- Ye, M., Wilhelm, M., Gentschev, I., & Szalay, A. (2021). A Modified Limiting Dilution Method for Monoclonal Stable Cell Line Selection Using a Real-Time Fluorescence Imaging System: A Practical Workflow and Advanced Applications. *Methods Protocols*, 4(1). doi:10.3390/mps4010016
- Yin, C., Evason, K. J., Asahina, K., & Stainier, D. Y. R. (2013). Hepatic stellate cells in liver development, regeneration, and cancer. *The Journal of clinical investigation*, 123(5), 1902-1910. doi:10.1172/JCI66369
- Yuan-yuan, M., Mu-qing, Y., Zhi-gang, H., Qing, W., & Ji-yu, L. (2017). The Biological Function of Kupffer Cells in Liver Disease. In G. Anirban (Ed.), *Biology of Myelomonocytic Cells* (pp. Ch. 3). Rijeka: IntechOpen.

- Zhang, Y., Xia, M., Jin, K., Wang, S., Wei, H., Fan, C., . . . Xiong, W. (2018). Function of the c-Met receptor tyrosine kinase in carcinogenesis and associated therapeutic opportunities. *Molecular Cancer*, *17*(1), 45. doi:10.1186/s12943-018-0796-y
- Zheng, B., Qu, J., Ohuchida, K., Feng, H., Chong, S. J. F., Yan, Z., . . . Nakamura, M. (2020). LAMA4 upregulation is associated with high liver metastasis potential and poor survival outcome of Pancreatic Cancer. *Theranostics*, *10*(22), 10274-10289. doi:10.7150/thno.47001
- Zhou, Z., Kim, J. W., Qi, J., Eo, S. K., Lim, C. W., & Kim, B. (2020). Toll-Like Receptor 5 Signaling Ameliorates Liver Fibrosis by Inducing Interferon  $\beta$ -Modulated IL-1 Receptor Antagonist in Mice. *American Journal of Pathology*, *190*(3), 614-629. doi:10.1016/j.ajpath.2019.11.012
- Zou, Y., Xiong, J. B., Ma, K., Wang, A. Z., & Qian, K. J. (2017). Rac2 deficiency attenuates CCl(4)-induced liver injury through suppressing inflammation and oxidative stress. *Biomedical Pharmacotherapy*, *94*, 140-149. doi:10.1016/j.biopha.2017.07.074

## Appendix

**UCSC browser for single nucleus RNA-sequencing data**

<http://prealignantliver.s3-website-ap-southeast-2.amazonaws.com/>



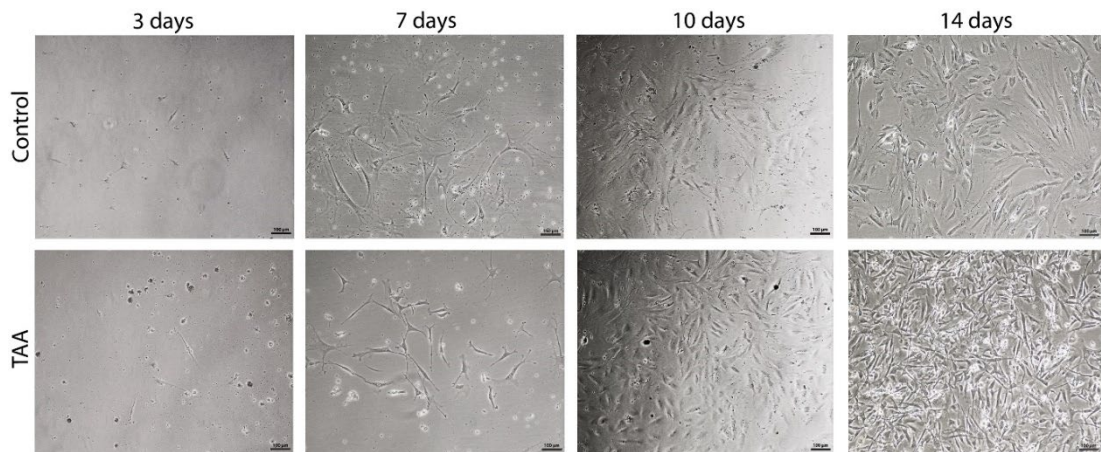


**Figure A.1: *In vitro* growth of primary control and TAA-treated HSCs in 2D culture.**

Brightfield microscopy images revealed that TAA-treated isolated primary HSCs display a mesenchymal shape, suggesting activation. Control isolated primary HSCs also display a mesenchymal morphology, suggesting autoactivation in culture, from their quiescent phenotype.

Scale bar depicting 100 μm.

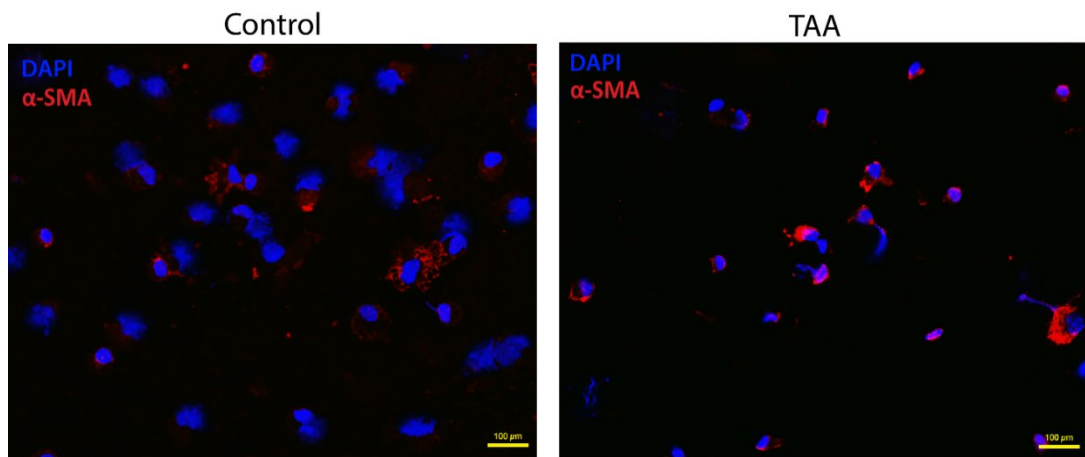


**Figure A.2: Fluorescent detection of  $\alpha$ SMA expression in primary HSCs of control and TAA-treated mice.**

Immunofluorescent staining confirming primary HSCs isolated from control and TAA-treated mice both express  $\alpha$ SMA. This suggests that TAA-treated HSCs are activated, and control isolated HSCs have autoactivated in culture. Scale bar depicting 100  $\mu$ m.

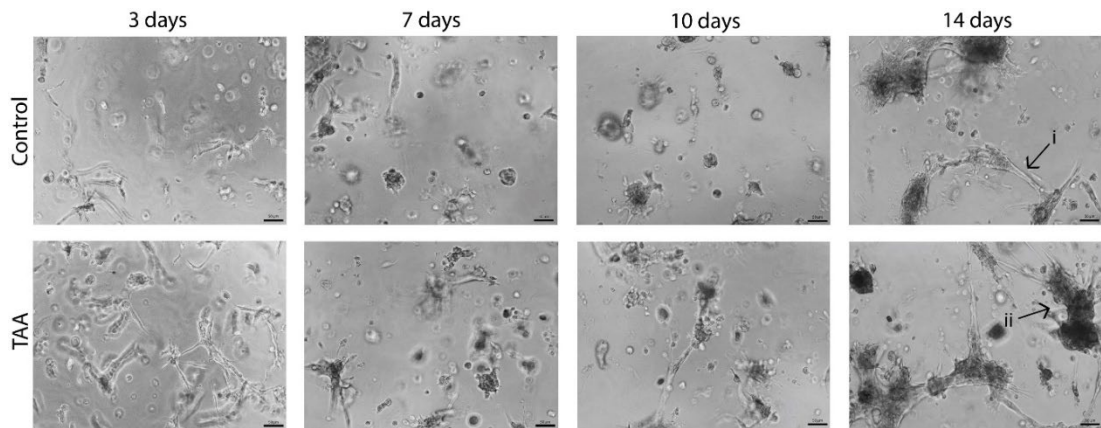


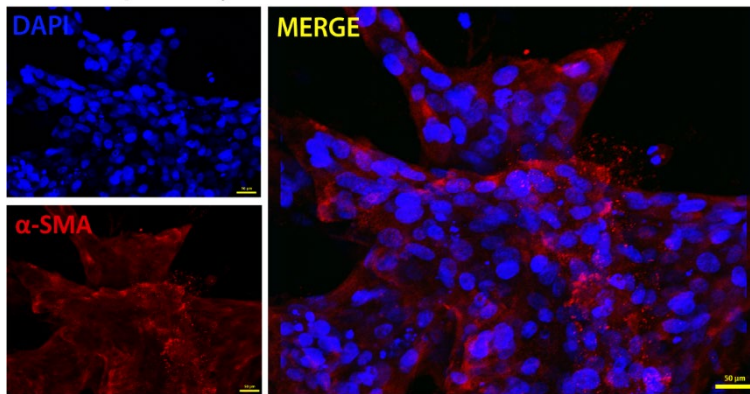
**Figure A.3: Brightfield microscopy of primary HSCs from control and TAA-treated mice in 3D culture.**

Three-dimensional bioprinted primary HSCs from control and TAA-treated mice form cell networks (i) and cell spheroids (ii) over 14 days in culture.

Scale bar depicting 100 μm.

**(A)**

Control primary HSCs



**(B)**

TAA primary HSCs

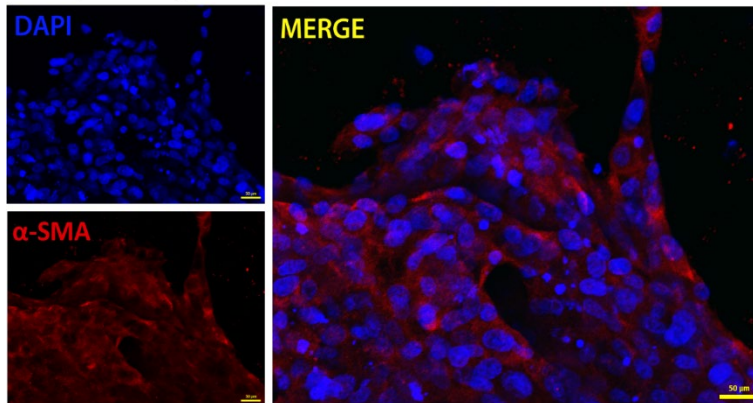


**Figure A.4: Immunofluorescent detection of  $\alpha$ SMA expression in 3D cultured primary HSCs isolated from control and TAA-treated mice.**

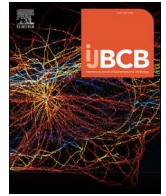
Primary HSCs from control and TAA-treated mice both express  $\alpha$ SMA in culture, following 3D bioprinting.

Scale bar depicting 100  $\mu$ m.

## **Bulk RNA-sequencing data**

<https://data.mendeley.com/datasets/cdj36h5nfj/1>

Pasic, Sara (2023), "Transcriptional profile of LPCs and HSCs following co-culture or conditioned-medium experiments", Mendeley Data, V1, doi: 10.17632/cdj36h5nfj.1



## Previous liver regeneration induces fibro-protective mechanisms during thioacetamide-induced chronic liver injury

Francis D. Gratte<sup>a,b</sup>, Sara Pasic<sup>b</sup>, N. Dianah B. Abu Bakar<sup>b</sup>, Jully Gogoi-Tiwari<sup>a,b</sup>, Xiao Liu<sup>c</sup>, Rodrigo Carlessi<sup>b</sup>, Tatiana Kisseleva<sup>c</sup>, David A. Brenner<sup>d</sup>, Grant A. Ramm<sup>e,f</sup>, John K. Olynyk<sup>g,h</sup>, Janina E.E. Tirnitz-Parker<sup>b,\*</sup>

<sup>a</sup> School of Veterinary and Life Sciences, Murdoch University, Perth, WA, Australia

<sup>b</sup> Curtin Medical School, Curtin Health Innovation Research Institute, Curtin University, Perth, Australia

<sup>c</sup> Department of Surgery, University of California, San Diego, La Jolla, CA, USA

<sup>d</sup> School of Medicine, University of California, San Diego, La Jolla, CA, USA

<sup>e</sup> QIMR Berghofer Medical Research Institute, Brisbane, QLD, Australia

<sup>f</sup> The University of Queensland, Brisbane, QLD, Australia

<sup>g</sup> Fiona Stanley and Fremantle Hospital Group, Perth, WA, Australia

<sup>h</sup> School of Medical and Health Sciences, Edith Cowan University, Perth, WA, Australia

### ARTICLE INFO

#### Keywords:

Chronic liver disease  
Liver progenitor cells  
Hepatic stellate cells  
Fibrosis  
Thioacetamide

### ABSTRACT

Chronic liver injury is characterised by continuous or repeated epithelial cell loss and inflammation. Hepatic wound healing involves matrix deposition through activated hepatic stellate cells (HSCs) and the expansion of closely associated Ductular Reactions and liver progenitor cells (LPCs), which are thought to give rise to new epithelial cells. In this study, we used the murine thioacetamide (TAA) model to reliably mimic these injury and regeneration dynamics and assess the impact of a recovery phase on subsequent liver injury and fibrosis. Age-matched naïve or 6-week TAA-treated/4-week recovered mice (C57BL/6 J, n = 5–9) were administered TAA for six weeks (C57BL/6 J, n = 5–9). Sera and liver tissues were harvested at key time points to assess liver injury biochemically, by real-time PCR for fibrotic mediators, Sirius Red staining and hydroxyproline assessment for collagen deposition as well as immunofluorescence for inflammatory, HSC and LPC markers. In addition, primary HSCs and the HSC cell line LX-2 were co-cultured with the well-characterised LPC line BMOL and analysed for potential changes in expression of fibrogenic mediators. Our data demonstrate that recovery from a previous TAA insult, with LPCs still present on day 0 of the second treatment, led to a reduced TAA-induced disease progression with less severe fibrosis than in naïve TAA-treated animals. Importantly, primary activated HSCs significantly reduced pro-fibrogenic gene expression when co-cultured with LPCs. Taken together, previous TAA injury established a fibro-protective molecular and cellular microenvironment. Our proof-of principle HSC/LPC co-culture data demonstrate that LPCs communicate with HSCs to regulate fibrogenesis, highlighting a key role for LPCs as regulatory cells during chronic liver disease.

### 1. Background

Liver fibrosis is a component of wound healing in response to hepatic insults during chronic liver diseases, including viral hepatitis, alcoholic liver disease and non-alcoholic fatty liver disease or steatohepatitis. Key fibrogenic drivers in this process are activated hepatic stellate cells

(HSCs), which transdifferentiate into myofibroblasts and initiate accumulation of extracellular matrix (ECM) components to provide structural support when the liver architecture becomes compromised (Tsuchida and Friedman, 2017). A consistent and unresolved injury stimulus may promote fibrosis progression to cirrhosis, which can become irreversible in severe cases (Lee et al., 2015; Trautwein et al.,

\* Corresponding author.

E-mail addresses: [32707216@student.murdoch.edu.au](mailto:32707216@student.murdoch.edu.au) (F.D. Gratte), [sara.pasic@postgrad.curtin.edu.au](mailto:sara.pasic@postgrad.curtin.edu.au) (S. Pasic), [nurdianah.abubakar@postgrad.curtin.edu.au](mailto:nurdianah.abubakar@postgrad.curtin.edu.au) (N.D.B. Abu Bakar), [jully.gogoi@murdoch.edu.au](mailto:jully.gogoi@murdoch.edu.au) (J. Gogoi-Tiwari), [xil094@ucsd.edu](mailto:xil094@ucsd.edu) (X. Liu), [Rodrigo.Carlessi@curtin.edu.au](mailto:Rodrigo.Carlessi@curtin.edu.au) (R. Carlessi), [tkisseleva@health.ucsd.edu](mailto:tkisseleva@health.ucsd.edu) (T. Kisseleva), [dbrenner@health.ucsd.edu](mailto:dbrenner@health.ucsd.edu) (D.A. Brenner), [Grant.Ramm@qimrberghofer.edu.au](mailto:Grant.Ramm@qimrberghofer.edu.au) (G.A. Ramm), [John.Olynyk@health.wa.gov.au](mailto:John.Olynyk@health.wa.gov.au) (J.K. Olynyk), [n.tirnitz-parker@curtin.edu.au](mailto:n.tirnitz-parker@curtin.edu.au) (J.E.E. Tirnitz-Parker).

<https://doi.org/10.1016/j.biociel.2021.105933>

Received 18 August 2020; Received in revised form 20 January 2021; Accepted 20 January 2021

Available online 1 February 2021

1357-2725/© 2021 Elsevier Ltd. All rights reserved.



2015). Underlying macro- and micro-morphological changes, including the development of fibrotic septa in the parenchyma, forming 'regenerative nodules', may lead to reduced liver functionality, portal hypertension and are a significant risk factor for the development of hepatocellular carcinoma (HCC) (Schuppan and Afdhal, 2008). It is therefore not surprising that a lot of research has focussed on the development of anti-fibrotic therapies in order to inhibit disease progression and carcinogenesis (Chen et al., 2019; Hicks et al., 2017; Lemoine and Friedman, 2019; Zhou et al., 2020).

Knowledge of the remarkably dynamic nature of the liver during disease and regeneration (Tirnitz-Parker et al., 2019) has prompted investigations into the plasticity of native hepatic cells relevant to the production of liver fibrosis, particularly HSCs. The mechanism of HSC activation from a resident quiescent cell to a collagen-producing myofibroblastic phenotype is well-studied and the clearance of activated HSCs at the cessation of fibrosis has typically been attributed to a combination of HSC senescence and apoptosis (Koyama et al., 2016; Schnabl et al., 2003). Inducible genetic labelling of activated HSCs in mice withdrawn from alcohol- or carbon tetrachloride (CCl<sub>4</sub>)-induced fibrosis revealed that 40-50% of these cells escaped apoptosis and 'inactivated' to a phenotype determined to be similar to quiescent HSCs but distinct in terms of quicker myofibroblast reactivation during adoptive transfer and cell culture activation (Kisseleva et al., 2012; Troeger et al., 2012). While the role of HSCs during fibrogenesis and fibrosis reversal cannot be understated, it is clear that these cells do not work in isolation. Other key cell populations in the CLD injury and regeneration niche are represented by inflammatory cells, mainly macrophages (Kisseleva and Brenner, 2020), and reactive biliary or liver progenitor cells (LPCs). LPCs are always seen in a very close temporal and spatial relationship to HSCs (Köhn-Gaone et al., 2016a; b; Ruddell et al., 2009; Tirnitz-Parker et al., 2014), however are much less studied in the context of fibrotic regression. Recent reports have reinforced the significance of a cellular and matrix-based microenvironment or 'niche' in which LPCs, HSCs and inflammatory cells interact with each other and the surrounding matrix to regulate wound healing during regenerative phases and fibrosis progression (Dwyer et al., 2014; Grzelak et al., 2014; Van Hul et al., 2009; Wood et al., 2014). Importantly, the number of proliferating LPCs is generally directly proportional to the underlying disease severity (Loves et al., 1999; Prakoso et al., 2014) and their main role has been thought to lie in the regeneration of lost liver mass through differentiation into biliary epithelial cells and hepatocytes (Raven et al., 2017). However, the LPC pool consists of a very heterogeneous population of cells with greatly varying, often context-specific marker expression profiles, which may reflect distinct cellular functions that are yet to be identified (Köhn-Gaone et al., 2016b). The current study used thioacetamide (TAA) supplementation and withdrawal to induce LPC-mediated regeneration (Köhn-Gaone et al., 2016a) prior to a second round of TAA treatment to examine disease progression in a cohort of TAA-pre-treated compared to TAA-naïve mice. Our data demonstrate differential fibrogenic dynamics in both experimental groups and reveal a novel HSC-regulatory role for LPCs during chronic liver disease, potentially mediated via LPC-HSC cross-talk.

## 2. Methods

### 2.1. Animal experimentation

Five-week-old male C57BL/6J mice were acquired from the Animal Resources Centre (Murdoch, Australia) and housed under PC2 animal facility guidelines, in temperature-controlled individually ventilated cages, exposed to a 12h day-to-night cycle. Up to six mice were housed together in one cage, on wheaten chaff bedding with *ad libitum* access to food and water and acclimatised for one week before commencing any experimental treatment. The mice were then randomised into two groups: (1) The 'pre-treatment' group was administered TAA in the drinking water (300 mg/L, Sigma-Aldrich, Castle Hill, Australia) for six

weeks, followed by a recovery period on normal chow and water for four weeks and a second round of TAA treatment for six weeks, (2) the 'naïve' group was fed normal laboratory chow and water for 10 weeks, followed by one round of TAA treatment for six weeks (Supplementary Fig. 1). Tissue and sera were taken and snap-frozen at 0, 1, 2, 3 days, 1 week and 6 weeks in the second round of TAA treatment for pre-treated mice, and following the first exposure to TAA for naïve animals, respectively. For co-culture experiments, HSCs were isolated from mice in groups of five: (i) healthy (quiescent HSCs), (ii) 6-week TAA-treated (activated HSCs) and (iii) 6-week TAA-treated and 4-weeks normal diet recovery ('inactivated' HSCs). All animal experiments were performed in accordance with the Australian code for the care and use of animals for scientific purposes at Curtin University, Perth, Australia with local Animal Ethics Committee approval.

### 2.2. Hepatic stellate cell isolation

Primary HSCs were isolated at high-yield and high-purity from livers of three groups of mice: healthy, fibrotic and recovering (outlined above), using retrograde pronase, collagenase and DNase I (all obtained from Sigma-Aldrich) perfusion, followed by density-gradient centrifugation, adapted from a previously published protocol (Mederacke et al., 2015). Isolated cells were adhered overnight in HSC growth medium: DMEM (Thermo Fisher, Waltham, MA, USA) supplemented with 10% fetal bovine serum (FBS), 4.5 g D-Glucose, 2 mM L-glutamine and antibiotics. Adhered cells were routinely assessed for purity by harnessing the HSC-endogenous fluorescence of vitamin A retinoid droplets in response to UV light exposure.

### 2.3. Co-culture assay

Primary HSCs or the HSC line LX-2 (Merck KGaA, Darmstadt, Germany) were seeded in replicate wells of 24-well (for RNA extraction) or 12-well plates (for protein extraction) at densities of 100,000 or 50,000 cells/cm<sup>2</sup>, respectively. Immortalised bipotential murine oval liver (BMOL) and BMOL-TAT progenitor cells (Tirnitz-Parker et al., 2007) were routinely cultured in Williams' E medium (Thermo Fisher), supplemented with 5 µg/mL insulin (Eli Lilly, IN, USA), 2 mM L-glutamine, 5% FBS, 10 ng/mL epidermal growth factor (EGF, BD Biosciences, Sydney, Australia), and 15 ng/mL insulin-like growth factor (IGF-II, Gropep, Adelaide, Australia). Prior to experimentation, BMOL, BMOL-TAT cells and the hepatocellular carcinoma cell line SNU-449 (ATCC, Manassas, VA, USA) were cultured in HSC growth medium. Cells were seeded and adhered to the porous polycarbonate membrane surface of trans-well inserts (0.4 µm pores, Sigma-Aldrich) at a density of 100,000 cells/cm<sup>2</sup>. Inserts containing BMOL, BMOL-TAT or SNU-446 cells were incubated overnight to adapt to their new conditions before being placed in 24- or 12-well plates containing HSCs, producing modified Boyden chambers. The co-culture system was incubated for 24 h (RNA extraction) or 48 h (protein extraction) in fresh HSC growth medium under normal cell culture conditions (37 °C in 5% CO<sub>2</sub>). Trans-well inserts were then carefully removed and plates containing HSCs were immediately homogenised for RNA or protein isolations.

### 2.4. Hydroxyproline assay

Using approximately 130 mg of snap-frozen liver tissue for each mouse, hydroxyproline quantitation of collagen content in whole liver was determined as previously described (Köhn-Gaone et al., 2016a).

### 2.5. Serum alanine aminotransferase assessment

Liver injury was assessed by measuring levels of serum alanine aminotransferase (ALT), according to the manufacturer's instructions (Sigma-Aldrich).

## 2.6. Transcriptional analysis

Total RNA was extracted from whole liver, cell lines and primary cells using Isolate II RNA Mini Kit (Bioline, London, UK), according to the manufacturer's instructions. Following quantitation using a Nano-Drop 1000 spectrophotometer, experiment-dependent concentrations of RNA were reverse-transcribed using High-Capacity cDNA Reverse Transcription Kit (Thermo Fisher). Real-time expression analysis of the resultant cDNA was performed with SYBR Green-based GoTaq qPCR Master Mix (Promega, Alexandria, NSW, Australia) on the ViiA 7 Real-Time PCR System (Life Technologies, Scoresby, VIC, Australia) or with SensiFAST SYBR® No-ROX Kit (Bioline) on the CFX Connect Real-Time PCR Detection System (Bio-Rad, Hercules, CA, USA). Data were normalised to the 18S RNA subunit (18S rRNA) and expressed relative to assay-dependent controls. In addition, RT<sup>2</sup> Profiler™ PCR Array Mouse Fibrosis analysis was performed on activated HSCs co-cultured with the BMOL LPC line (Tirnitz-Parker et al., 2007), according to the manufacturer's instructions (Qiagen).

## 2.7. Primers

Primers used for qPCR were: 18 s rRNA – forward 5'- CGGCTACCA-CATCCAAGGAA -3' and reverse 5'- GCTGGAATTACCGCGGCT -3', alpha-smooth muscle actin (αSMA) – forward 5'- CTGACAGAGCCACACTGAA -3' and reverse 5'- CATCTCCAGAGTCCAGCACA -3', collagen 1 alpha subunit 1 (Col1a1) – forward 5'- CAAGGTCTTCTGGATCAAGTG -3' and reverse 5'- CCTTTATGCCTCTGTCACCTTG -3', desmin – forward 5'- GAGAAACCAGCCCCGAGCAAAG -3' and reverse 5'- AGCCTCGCTGACAACTCTCCA -3', matrix metalloproteinase 2 (MMP2) – forward 5'- GTCGCCCTAAACAGACAA -3' and reverse 5'- GGTCTCGATGGTGTTCTGGT -3', tissue inhibitor of matrix metalloproteinases 1 (TIMP1) – forward 5'- ATTC AAGCTGTGGGAAATG -3', transforming growth factor-beta 1 (TGF-β1) – forward 5'- GCGGACTACTATGCTAAAGAGG -3', and reverse 5'- GTAGAGTTCACATGTTGCTCC -3' all obtained from Sigma Aldrich.

## 2.8. Protein extraction

BMOL-TAT, LX-2 and SNU-449 cells were cultured in modified Boyden chamber co-culture plates for 48 h, as described previously. LX-2 cells were detached using Accutase (Sigma-Aldrich), centrifuged at 500 × g for 5 min and pellets were resuspended in 1x RIPA buffer (Sigma-Aldrich) supplemented with 1x protease/phosphatase inhibitor cocktail (Cell Signaling Technologies). The lysates were then sonicated, centrifuged for 10 min at 14,000 × g and supernatants were collected. Protein concentration was determined using a bicinchoninic acid (BCA) protein assay kit (Pierce), following the manufacturer's instructions.

## 2.9. Western Blot protein analysis

A 1:10 ratio of 10x Reducing Agent (Thermo Fisher) in 1x NuPAGE LDS sample buffer (Thermo Fisher) and water was added to LX-2 cell lysates to achieve a final total protein concentration of 1 µg/µL. Then, samples were denatured for 5 min at 95 °C for all samples, except samples being run for Collagen 1 detection. Precision Plus Protein Standards (Bio-Rad) was used as a ladder. Samples (20 µg per lane) were loaded and separated in Bolt™ 4–12% Bis-Tris Plus SDS-PAGE gels (Thermo Fisher) at 200 V for 30 min. Gels were transferred onto nitrocellulose membranes (Bio-Rad) for 1 h at 100 V. Revert Total Protein Stain (Li-Cor) was added to membranes for 5 min in the dark at RT prior to washing with Revert Wash Solution (Li-Cor) and imaging on the ChemiDoc™ Xrt System (Bio-Rad). Membranes were blocked with 5% skim milk powder in 1X Tris-buffered saline with 0.1% Tween-20 (TBST) for 1 h and then washed three times with 1× TBST. They were then incubated with primary antibodies TGF-β1 (Abcam, ab92486, 1:1,000), αSMA (Abcam, ab32575, 1:10,000) and Collagen 1 (Abcam, ab34710,

1:1,000) overnight at 4 °C, with 3% BSA in TBST. Anti-rabbit IgG-HRP (1:2,000) secondary antibody (Cell Signalling, 7074S) was diluted in 5% skim milk powder in TBST and then added for 1 h at RT. Three final TBST washes were performed before enhanced chemiluminescent (ECL) detection (Biorad) was completed and proteins were detected on the ChemiDoc™ Xrt System (Bio-Rad). Western blot semi-quantification was completed using the Bio-Rad ImageLab software.

## 2.10. Immunohistochemistry and immunofluorescence

Tissue for histological processing was formalin-fixed and embedded in paraffin for storage, prior to cutting into 4 µm thin sections, dewaxing, and rehydration as per standard protocols and mounting with a gelatin-based aqueous mounting medium. Immunofluorescent staining was performed on snap-frozen liver tissue cut to 7 µm sections. Depending on the antibody, frozen sections were fixed with either 1:1 (v/v) methanol: acetone solution for 5 min, then air-dried and rehydrated in PBS, or fixed in 4% paraformaldehyde (PFA) and rinsed thoroughly in PBS, before and between antibody incubation steps. Immunofluorescent stains were mounted with ProLong Gold Antifade Reagent containing DAPI nuclear counter-stain (Invitrogen, Melbourne, Australia). Positively stained cells were either manually counted or sections were scanned with a Zeiss Axio Scan.Z1 Digital Slide Scanner for quantitation using positive pixel count analysis.

## 2.11. Antibodies

The following antibodies used for immunofluorescent stains were diluted in Dako REAL, Ready-to-use diluent (Dako, North Sydney, NSW, Australia): mouse anti-alpha smooth muscle actin (αSMA, 1:2000, Sigma-Aldrich), rat anti-CD45 (1:200, BD Biosciences), rabbit anti-desmin (1:200, Abcam, VIC, Australia), rat anti-glial fibrillary acidic protein (GFAP, 1:500, Thermo Fisher) rabbit anti-pan cytokeratin (PanCK, 1:300, Dako), rat anti-F4/80 (1:150, eBioscience), rat anti-Ly6G (1:50, BD Pharmingen), and rat anti-CD11b (1:400 eBioscience). All secondary antibodies used for fluorescent labelling were Alexa Fluor dyes (1:400, Life Technologies).

## 2.12. Picro-Sirius Red staining

Collagen staining of liver sections was performed by Picro-Sirius Red staining (PSR - Polysciences Inc., Warrington, PA), according to the manufacturer's instructions. Visualisation was performed with bright-field light microscopy, and fibrosis staging was undertaken by an independent clinical gastrointestinal pathologist in an unbiased and blinded manner. Tissue collagen deposition was quantitated by imaging PSR-stained sections through polarised light and quantification of the resulting birefringence. Hue histograms of the 256 colours present in RGB images were generated using ImageJ software (NIH), in the following classifications: (a) thinner fibres, green (52–128) and yellow (39–51), (b) thicker fibres, orange (10–38) and red (2–9, 230–256), and the interstitial space (129–229). Pixels positive for collagen birefringence (all birefringence hues) were presented as a percentage of total area (including interstitial space).

## 2.13. Statistical analysis

Data obtained from qPCR analyses and cell counts are presented as means ± standard error of the mean (SEM). Statistical significance was assessed by parametric one-way analysis of variance (ANOVA) of log-transformed data (co-culture data) or two-way ANOVA (all other data) with multiple comparisons using Graphpad Prism 7 for Windows (Graphpad Software, Inc., San Diego, CA, USA).



### 3. Results

#### 3.1. TAA pre-treatment provides protection against effects of subsequent TAA toxicity

To compare the effects of TAA treatment on the liver biology of naïve and pre-injured/recovered mice, ‘pre-treated’ (six weeks TAA/four

weeks recovery) mice and a ‘naïve’ (10 weeks normal chow) age-matched group were subjected to a 6-week course of TAA to assess the respective injury responses.

The first round of TAA treatment in the ‘pre-treated’ experimental group resulted in reduced weight gain compared to control chow-fed mice, as described previously (Köhn-Gaone et al., 2016a). However, mice subjected to the second round of TAA treatment following a 4-week

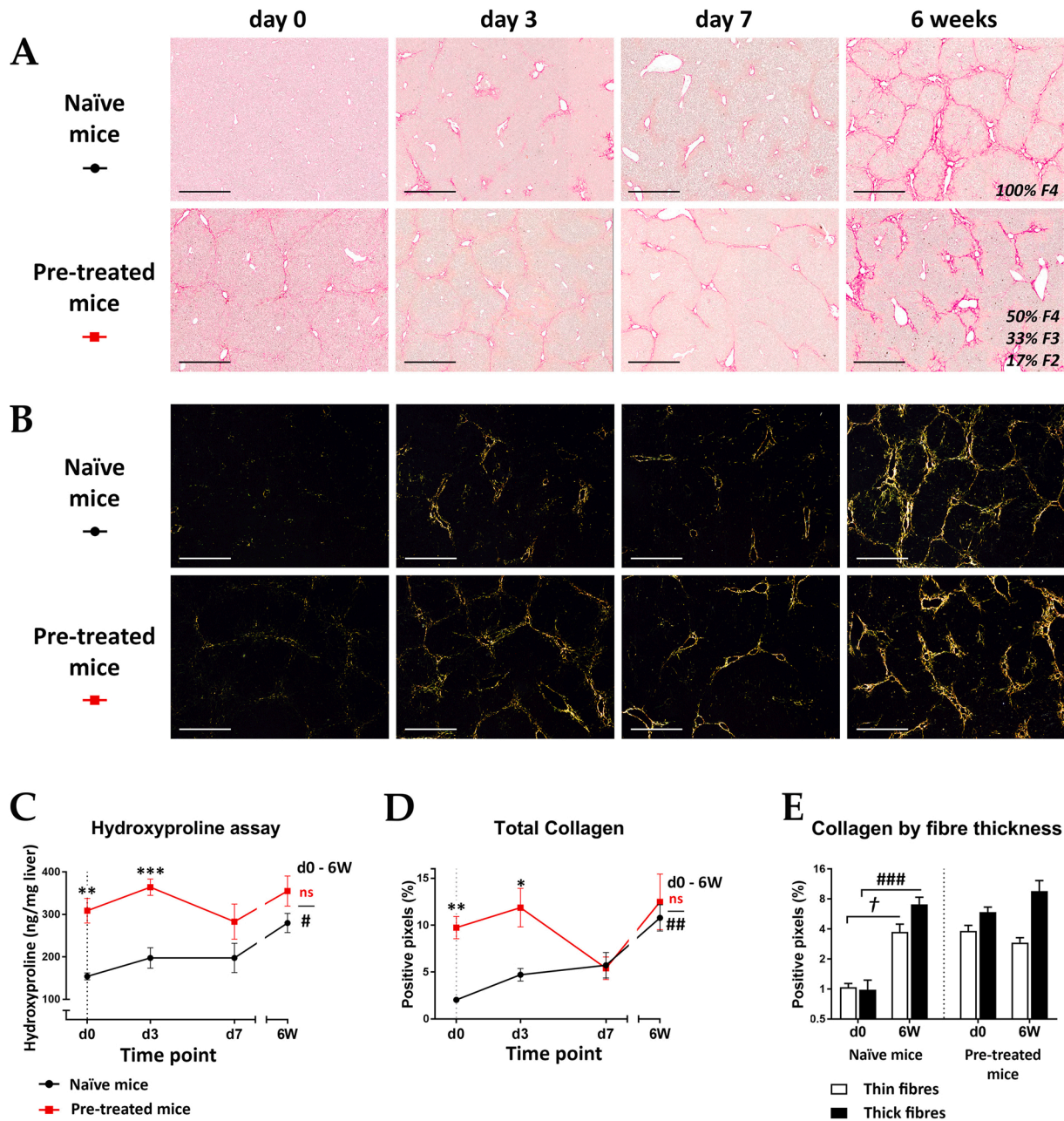


**Fig. 1.** Pre-treatment with TAA reduced fibrogenic effects of TAA toxicity. Liver sections taken at day 0, 1, 2, 3, 7 and 6 weeks into TAA treatment of naïve and TAA-pre-treated mice were stained for collagen deposition using PicroSirius Red and viewed using (A) brightfield and (B) polarised light microscopy. Collagen staining (red) observed under brightfield light showed that fibrosis in TAA-pre-treated mice presented earlier (day 0, d0) but was comparatively severe and advanced in naïve mice by late stage treatment (six weeks, 6 W). Polarised light revealed different collagen distribution patterns developing during TAA treatment of pre-treated mice. (C) Hydroxyproline levels (biochemical collagen assay) were significantly higher in whole liver of pre-treated mice at day 0 (d0,  $**P < 0.01$ ) and day 3 (d3,  $***P < 0.001$ ), compared to naïve mice, an effect which was reflected in (D) image analysis software-based quantitation of collagen birefringence generated with polarised light (day 0;  $**P < 0.01$ , day 3;  $*P < 0.05$ ). Hydroxyproline and collagen quantitation both demonstrated convergent progression of total collagen between the experimental groups by day 7 (d7). However significant increases in collagen from day 0 to the end of TAA treatment (six weeks) were only seen in naïve mice (hydroxyproline;  $\#P < 0.05$ , quantitation;  $\#\#P < 0.05$ ). (E) Analysis of thin (yellow and green birefringence) and thick (orange and red birefringence) collagen fibrils under polarised light illustrated that naïve mice had near significant ( $\dagger P = 0.0554$ ) and significant ( $\#\#\#P < 0.001$ ) increases of thin and thick fibrils, respectively.  $n = 4-9$  mice per group. Data expressed as mean  $\pm$  SEM. Statistical significance is given relative to the complementary experimental group at the same time point, unless indicated. Scale bar = 500  $\mu$ m. ns, not significant.

recovery period continued to gain weight over time, while the weight of naïve TAA-treated mice stagnated (Supplementary Fig. 1). This growth inhibition in the naïve group was consistent with the development of major tissue damage, manifesting in eosinophilic bands of hepatocytes as early as day 1, persisting throughout the six weeks of treatment (Supplementary Fig. 2A). Pre-treated mice appeared unaffected by perivenular necrosis typical of acute TAA injury, whereas more than one third of naïve mice experienced zonal, pericentral liver necrosis at days 3 and 7 and 6 weeks (Supplementary Fig. 3). Despite histological similarity to naïve mouse livers, pre-treated mice had notably reduced contrast between basophilic and eosinophilic staining from day 0 up to 6 weeks, indicating a lower degree of tissue damage. Taken in context with low and relatively stable serum ALT levels (Supplementary Fig. 2B) over the same period - only expressing a total mean range of 12.4–33.5 - pre-treated mice appeared to exhibit lower levels of structural and biochemical evidence for hepatic injury. In significant contrast, ALT levels of naïve mice rose from day 0 levels of  $13.8 \pm 1.6$  U/L to  $77.7 \pm 6.7$  by day 3 and remained significantly elevated ( $42.8 \pm 8.1$ ) relative to day 0 by the end of six weeks, indicating more liver injury and reduced liver function as compared to animals with previous TAA exposure.

### 3.2. Inhibition of TAA-induced fibrogenesis and cirrhosis in response to TAA pre-treatment

Visualisation of collagen depositions by PSR staining and brightfield light microscopy as well as polarised light for the study of collagen birefringence revealed that TAA toxicity in the pre-treatment group led to reduced fibrosis progression compared to TAA-treated naïve mice (Fig. 1A, B). While livers of naïve mice had completely healthy liver histology on day 0 with collagen levels of  $154.2 \pm 8.3$  ng/mg liver, TAA-pre-treated mice still presented with remnants of collagen bands after the 4-week recovery period, measuring  $308.8 \pm 29.0$  ng/mg liver, and presumed to be the result of incomplete fibrosis resolution (Fig. 1A, B). Despite the clear pre-existing collagen deposition, TAA-pre-treated mice did not progress to cirrhosis from TAA reintroduction to the 6-week

endpoint, whereas naïve mice showed gradual development of bridging fibrosis and the formation of nodules by week 6, consistent with cirrhosis. Interestingly, an early spike in quantified collagen around day 3 was observed in pre-treated mice, followed by a reduction to stabilised levels at later time points (Fig. 1C, D). Naïve mice experienced overall accumulation of both thick and thin collagen fibrils, while unresolved day 0 collagen levels in pre-treated mice remained stable but underwent structural conversion from thin to thick fibrils (Fig. 1E). In agreement with these results, qPCR analysis revealed higher day 0 transcription of the general HSC marker desmin ( $P < 0.05$ ) and a trend towards increased expression of the collagen degradation enzyme matrix metalloproteinase (MMP) 2 (ns) in pre-treated mice, followed by a reduction during TAA administration (day 3; Fig. 2). Naïve mice exhibited significant upregulation of profibrogenic transcription from day 0 to the end of TAA treatment (transforming growth factor beta, TGF- $\beta$ 1,  $###P < 0.001$ ; MMP2,  $####P < 0.0001$ ), compared with slightly lower levels in pre-treated mice (TGF- $\beta$ 1,  $##P < 0.01$ ; MMP2,  $##P < 0.01$ ). Transcriptomic analyses of fibrosis readouts confirmed the reduced fibrogenic effect of TAA treatment in pre-treated compared to naïve mice, as judged by day 3 mRNA regulation patterns of collagen, desmin (general HSC marker) and  $\alpha$ SMA, (activated HSCs) as well as the fibrogenic mediators TGF- $\beta$ 1, MMP2 and tissue inhibitor of matrix metalloproteinases (TIMP) 1 (Fig. 2).

### 3.3. A unique cellular profile is generated in the liver during recovery from TAA pre-treatment

Mice not previously exposed to TAA administration presented with the expected proliferation of inflammatory cells, HSCs and LPCs upon TAA exposure (Köhn-Gaone et al., 2016a). Representative images show that the number of cells positive for the leukocyte common antigen marker CD45 increased over the course of the 6-week TAA administration in naïve mouse liver (Fig. 3A). In contrast, TAA pre-treatment reduced the early (day 3) wave of CD45<sup>+</sup> inflammatory cells to only  $35 \pm 2.7$  cells per field of view (FOV), significantly lower ( $**P < 0.01$ )

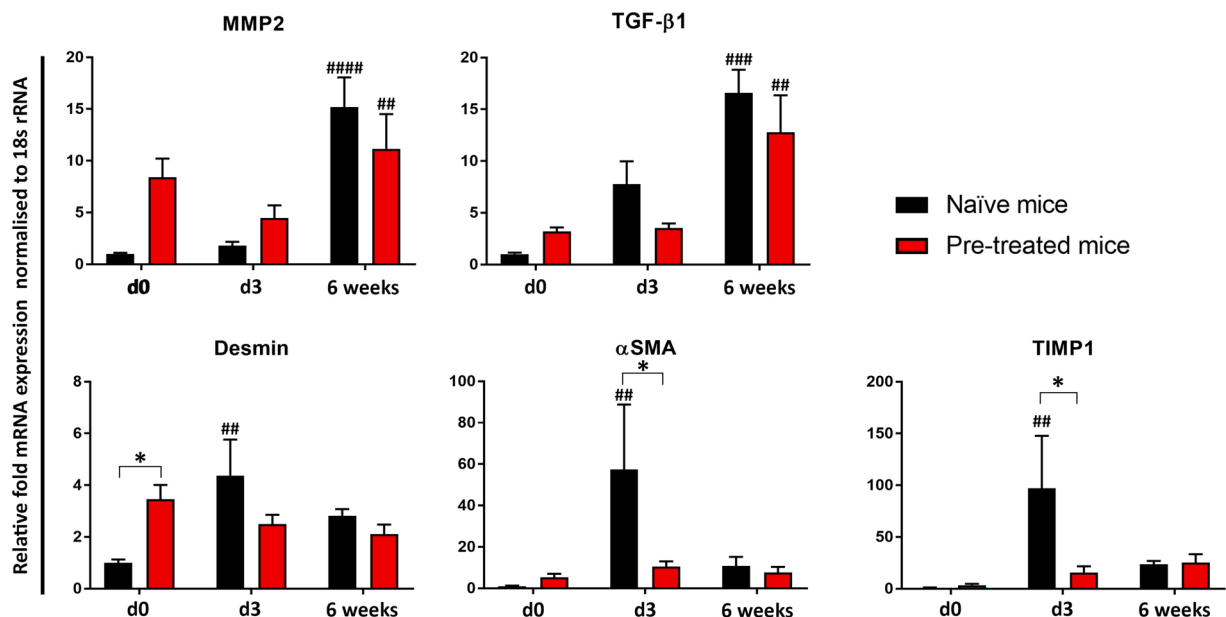


**Fig. 2.** TAA pre-treatment modulates profibrogenic gene transcription during subsequent TAA-induced fibrosis. In comparison to naïve mice, pre-treated mice had significantly reduced transcript levels of  $\alpha$ SMA and TIMP1 at day 3 (d3), and higher desmin expression at day 0 (d0,  $*P < 0.05$ ). When comparing other time points to healthy uninjured mice, prior to TAA treatment, naïve mice have greater upregulation of  $\alpha$ SMA (d3,  $###P < 0.01$ ), TGF- $\beta$ 1 (6 weeks, 6W,  $###P < 0.001$ ), desmin (d3,  $###P < 0.01$ ), MMP2 (6 weeks,  $####P < 0.001$ ) and TIMP1 (d3,  $##P < 0.01$ ) than exhibited by mice pre-treated with TAA.  $n = 5-8$  mice per group. Data are normalised to the 18S RNA subunit (18S rRNA) and expressed as mean  $\pm$  SEM and are relative to healthy mice with no history of liver injury.  $\alpha$ SMA, alpha-smooth muscle actin; HSC, hepatic stellate cell; MMP2, matrix metalloproteinase 2; TAA, thioacetamide; TIMP1, tissue inhibitor of matrix metalloproteinases 1; TGF- $\beta$ 1, transforming growth factor beta 1.

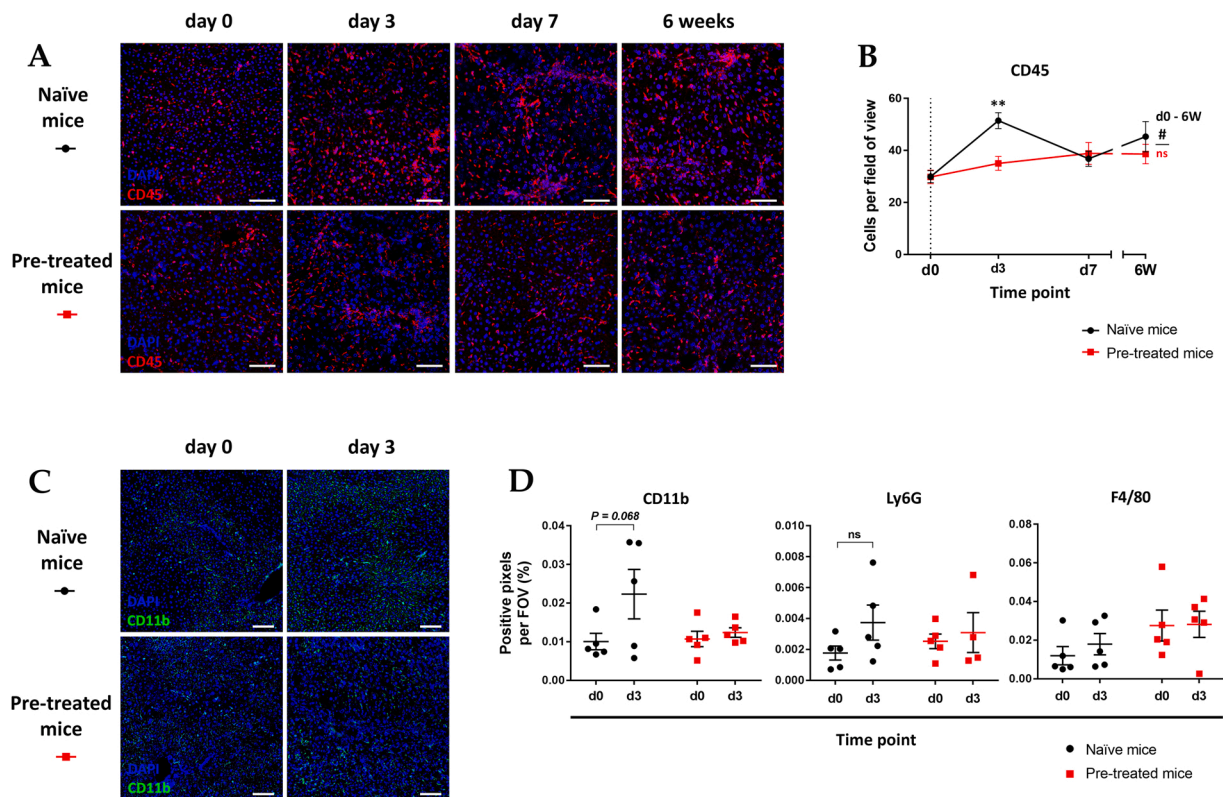


**Fig. 3.** Mice pre-treated with TAA lacked CD45<sup>+</sup> inflammatory cell expansion during subsequent TAA administration. (A) Immunofluorescent staining for the leukocyte common antigen marker CD45 and (B) quantitation by manual cell count at day 0, 3, 7 and 6 weeks of TAA treatment showed a significantly higher ( $**P < 0.01$ ) number of CD45<sup>+</sup> cells present in naïve mice at day 3 (d3). Naïve mice also experienced a significant increase in CD45<sup>+</sup> cells ( $\#P < 0.05$ ), which was not reflected in livers from pre-treated mice.  $n = 5-7$  mice per group. Data expressed as mean  $\pm$  SEM. Statistical significance presented relative to the complementary experimental group at the same time point. Scale bar = 100  $\mu$ m. (C) Immunofluorescent detection of CD11b in naïve and pre-treated mice at day 0 and day 3 suggests increased cell numbers at day 3 in mice that had not previously been exposed to TAA. (D) Quantitation of positively stained cells reveals no changes in F4/80<sup>+</sup> macrophages or LY6G<sup>+</sup> neutrophils across all groups and slightly but insignificantly increased CD11b<sup>+</sup> monocyte-derived macrophage cell numbers with three days of TAA re-exposure in naïve mice. CD45, cluster of differentiation 45; CD11b, cluster of differentiation 11b; CLD, chronic liver disease; F4/80, protein corresponding to the gene encoding EGF module-containing mucin-like receptor; Ly6G, lymphocyte antigen 6 complex locus G; ns, no significance; TAA, thioacetamide.

than observed in naïve mice ( $51.5 \pm 3.1$ ) during exposure to TAA (Fig. 3B). This trend of reduced inflammation following re-treatment with TAA remained consistent, as there was no significant increase in CD45<sup>+</sup> expression by week 6, contrasting with significant increases in the naïve mice compared over the time-course ( $\#P < 0.05$ ). To analyse the inflammatory component in the injury and regeneration niche further, we performed immunofluorescent cell quantitations for the pan-macrophage marker F4/80, the neutrophil marker Ly6G and the monocyte-derived macrophage marker CD11b at days 0 and 3. While inflammatory cell numbers were similar in all investigated groups for F4/80 and Ly6G, there was a statistically insignificant trend towards increased infiltrating CD11b<sup>+</sup> macrophages in the naïve compared to the pre-treated mice at day 3 (Fig. 3D).

Triple staining for GFAP,  $\alpha$ SMA and desmin revealed that pre-treated mice exhibited higher levels of overall desmin (total HSC) expression at day 0 of TAA treatment but reached similar levels to those of naïve mice at later time points (Fig. 4A). HSC populations were categorised as follows: quiescent (qHSC, Des<sup>+</sup>/ $\alpha$ SMA<sup>-</sup>/GFAP<sup>+</sup>), activated (aHSC, Des<sup>+</sup>/ $\alpha$ SMA<sup>+</sup>/GFAP<sup>+</sup>) and inactivated (iHSC, Des<sup>+</sup>/ $\alpha$ SMA<sup>-</sup>/GFAP<sup>-</sup>). Quantitation of cell numbers illustrated similar trends in both experimental groups over time for quiescent and activated HSCs, however inactivated HSCs were only detected at days 0–3 in the group of mice that had gone through an earlier time course of TAA treatment, followed by a 4-week recovery period (Fig. 4B–D).

Livers were also stained for the LPC and biliary marker PanCK, which is routinely used for detection of the total pool of LPCs (Müller et al., 2016; Tirmitz-Parker et al., 2010). On day 0, only a relatively low

number of cells stained positively with PanCK ( $10.9 \pm 2.7$  per FOV) in portal areas of naïve mice, representing biliary cells, and numbers of PanCK<sup>+</sup> biliary cells and LPCs increased slowly over time. In contrast, mice that had undergone a previous round of 6-week TAA treatment displayed a significantly higher number of PanCK<sup>+</sup> cells ( $28.4 \pm 3.6$  cells per FOV) in portal, central and parenchymal areas, indicating the continued presence and activity of LPCs even after four weeks of recovery from TAA. A steady-state presence of PanCK<sup>+</sup> biliary cells and LPCs was observed over time in the pre-treatment group (Fig. 5A, B).

#### 3.4. Liver progenitor cells regulate the fibrogenic potential of primary hepatic stellate cells

To investigate the significance of LPC presence prior to TAA treatment and their potential role in modulating HSC-mediated fibrogenesis directly, we performed primary cell isolations of HSCs in different activation states and co-cultured them with the well-characterised BMOL LPC line (Tirmitz-Parker et al., 2007). For generation of the HSC populations representing different activation states, quiescent HSCs were isolated from healthy mice, activated HSCs from 6-week TAA-treated mice and inactivated HSCs from mice that had undergone six weeks of TAA treatment and had been allowed to recover for four weeks (Fig. 6A). The HSC activation status was confirmed using representative cell aliquots immediately after isolation by exposure to UV light (Fig. 6A, shown for activated HSCs) and by transcriptomic analyses of  $\alpha$ SMA and Col1a1 expression, corroborating the expected low expression of both genes in quiescent and inactivated cells but high





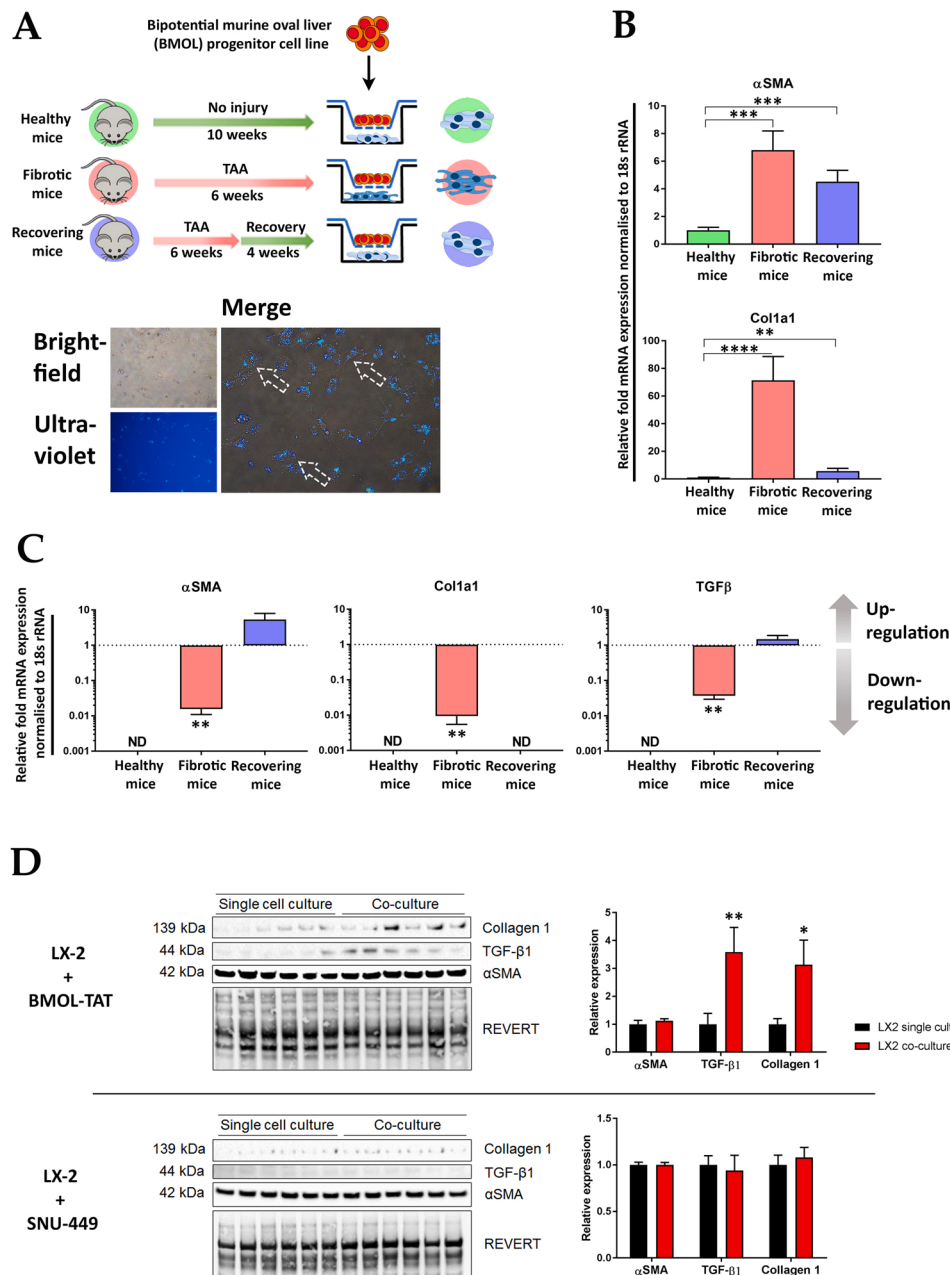


**Fig. 6.** Co-culture with LPCs modulates the expression of HSC fibrogenic markers in primary HSCs isolated from fibrotic TAA-treated mice and in the human HSC line LX-2. (A) HSCs isolated from healthy, fibrotic or recovering mice and assessed for purity by morphological analysis and detection of retinoid autofluorescence under UV light (arrows, vitamin A<sup>+</sup> HSCs). (B) Transcriptomic analyses of  $\alpha$ SMA and Col1a1 expression reflected levels expected of quiescent HSCs in healthy, activated HSCs in fibrotic and inactivated HSCs in recovering mice. (C) Upon co-culture with the LPC line BMOL, HSCs from fibrotic mice significantly downregulated expression of profibrogenic markers  $\alpha$ SMA and Col1a1, and TGF- $\beta$ 1.  $**P < 0.01$ ,  $***P < 0.001$ ,  $****P < 0.0001$ .  $n = 3-5$  replicates per group. Data were normalised to the 18S RNA subunit (18S rRNA) and expressed as mean  $\pm$  SEM. (D) Co-culture of LX-2 cells with SNU-449 HCC cells did not induce any changes, while LX-2 exposure to the LPC line BMOL-TAT significantly increased the protein expression of TGF- $\beta$ 1 and collagen 1.  $*P < 0.05$ ,  $**P < 0.01$ .  $n = 6$  replicates per group.  $\alpha$ SMA, alpha-smooth muscle actin; Col1a1, collagen 1 alpha subunit 1; HSC, hepatic stellate cell; ND, not detected; REVERT, total protein stain; TGF- $\beta$ 1, transforming growth factor-beta 1.

fibrogenic potential, activated primary HSCs significantly downregulated  $\alpha$ SMA, Col1a1 and TGF- $\beta$ 1 after they had been co-cultured with LPCs (Fig. 6C). To assess the potential for fibrogenesis-regulating cross-talk between HSCs and LPCs at the protein level, we performed co-culture experiments using the well-established human HSC line LX-2 and either the LPC line BMOL-TAT or the non-LPC cell line SNU-449, derived from a human hepatocellular carcinoma. While the LX-2 expression of  $\alpha$ SMA, TGF- $\beta$ 1 and collagen 1 remained unchanged after the 48h co-culture exposure to SNU-449 HCC cells, the presence of BMOL-TAT cells in the Boyden chambers significantly increased the expression of TGF- $\beta$ 1 and collagen 1 in the HSC line, importantly, reflecting context-specific modulation of the HSC fibrogenic potential in response to LPC-derived signals.

#### 4. Discussion

Recent investigations into unique cellular dynamics that occur during recovery from CCL<sub>4</sub>-induced hepatic fibrosis and lead to the

generation of an inactivated HSC phenotype (Kisseleva et al., 2012; Troeger et al., 2012) prompted us to establish a similar model of recurrent injury after a recovery period using TAA. While CCL<sub>4</sub> is a rapid, effective and convenient model of hepatic fibrosis and cirrhosis, it is known to induce discrepant pathology compared with human CLD and lower numbers of reactive biliary cells and LPCs than observed in other models such as CDE or TAA (Köhn-Gaone et al., 2016a; Liedtke et al., 2013). To overcome these limitations, investigators often use CCL<sub>4</sub> at incrementally higher concentrations (Español-Suñer et al., 2012), or combined with other compounds (such as 2-acetylaminofluorene; 2-AAF) (Chen et al., 2015; Kallis et al., 2011) in order to increase induction of inflammation and more severe chronic fibrosis to prompt LPC expansion. A study by Kisseleva et al. revealed that recurrent CCL<sub>4</sub>-induced injury, separated by a 6-month recovery period, resulted in increased fibrosis compared to mice that were naive to CCL<sub>4</sub>. The inactivated HSCs, which had developed from activated HSCs during the recovery phase, demonstrated a greater propensity to activate in culture and contributed more to the myofibroblast pool during adoptive transfer

to CCl<sub>4</sub>-treated mice than quiescent HSCs. Therefore, we initially expected similar results in our model of TAA reintroduction after a recovery phase. However, in contrast to increased fibrosis progression in CCl<sub>4</sub>-pre-treated as compared to CCl<sub>4</sub>-naïve mice, we observed the opposite using TAA supplementation to the drinking water. Pre-treated mice still gained weight upon TAA reintroduction and demonstrated less morphological aberrations and hepatotoxic biochemistry at the end-point (6 weeks) of TAA treatment than naïve mice, indicating that pre-treatment resulted in protection from the effects of TAA toxicity. Despite pre-existing collagen deposition at day 0 of the second TAA treatment, the mice in the pre-treatment group did not show significantly increased collagen accumulation as seen in the TAA-naïve mice. At the last time point, the fibrotic bands appeared thickened in some areas, however importantly, they did not bridge and crosslink to cirrhotic levels in mice that had been pre-exposed to TAA. Thus, pre-treatment with TAA conferred some level of protection from further fibrosis in subsequent TAA-induced injury. A significant number of cells with a Des<sup>+</sup>/αSMA<sup>-</sup>/GFAP<sup>-</sup> phenotype reflective of inactivated HSCs were identified in pre-treated and recovered mice, but this population declined rapidly from day 0 to day 3. The fate of this iHSC population is unclear, and additional investigations are required to assess the possibility that they reactivate upon re-injury, as has been seen in other murine models of fibrosis (Kisseleva et al., 2012; Troeger et al., 2012). While both groups displayed similar numbers of activated HSCs during TAA-induced injury, progression of fibrosis was significantly reduced in pre-treated mice, for which an alternative compensatory mechanism, such as anti-fibrotic cellular cross-talk, may be responsible. Proliferation of several resident and transient cell types in the liver during TAA-induced injury have been previously extensively characterised (Köhn-Gaone et al., 2016a). The spike in the presence of CD45-positive inflammatory cells on day 3 was observed in naïve mice but not evident in TAA pre-treated mice. Given that we identified a trend of monocyte-derived CD11b<sup>+</sup> macrophages entering naïve livers around day 3 of TAA exposure and inflammatory cells have the potential to activate HSCs into myofibroblasts (Kisseleva and Brenner, 2020; Koyama et al., 2016), a reduction in their numbers is likely one of the factors that contributed to a less fibrotic microenvironment in mice with previous TAA exposure. A noteworthy difference between the studies using CCl<sub>4</sub> (Kisseleva et al., 2012) and TAA reintroduction after a recovery phase is the presence of a significant number of LPCs in our TAA model. Historically, LPCs have been thought to simply replace lost tissue during chronic injury when hepatocytes undergo replicative arrest and are inhibited to proliferate (Köhn-Gaone et al., 2016b). However, a potential regulatory role for LPCs has recently been emerging. Our group previously reported the cellular cross-talk between LPCs and HSCs, facilitating co-migration through the parenchyma to sites of injury (Dwyer et al., 2014; Ruddell et al., 2009; Tirmitz-Parker et al., 2014). A recent study reported that growth differentiation factor 11 attenuates fibrosis through expansion of Lgr5-expressing LPCs, suggesting a potential anti-fibrotic role for LPCs. Using two mouse models of fibrotic liver disease (CCl<sub>4</sub> administration and the 3,5-diethoxycarbonyl-1,4-dihydrocollidine diet), the authors demonstrated reduced liver fibrosis when Lgr5<sup>+</sup> progenitor cells were transplanted (Dai et al., 2020). Our own novel data now confirm this new, regulatory aspect of LPC biology during chronic liver disease and demonstrate through proof-of-principle experiments that LPCs can directly modulate the fibrogenic potential of HSCs in co-culture. Primary HSCs, which were isolated from a highly fibrotic niche, downregulated fibrosis-associated genes. When we performed additional experiments with the gold standard HSC cell line LX-2, co-culture with non-LPC HCC cells SNU-449 had no effect. However, when the LX-2 cells were exposed to signals derived from the LPC line BMOL-TAT, they significantly upregulated expression of the central fibrosis regulator TGF-β1 as well as collagen 1. While the primary HSC data suggest an anti- and the cell line results a pro-fibrotic HSC effect, mediated by LPCs, the data are not surprising. In contrast, they suggest (a) different effects of LPCs on HSCs derived from a

complex fibrotic *in vivo* niche compared to cell culture-adapted cell lines, and (b) may also reflect a highly adaptable nature of LPCs, which are present within ductular reactions during all stages of human chronic liver disease (Dwyer et al., 2020; Grzelak et al., 2017; Lowes et al., 1999; Prakoso et al., 2014). LPCs may have very context-specific regulatory roles to modulate the biology of surrounding cells. The specific paracrine pathways that regulate HSC-LPC cross-talk, resulting in modulation of fibrogenesis and potentially other HSC functions, remain to be determined (Cai et al., 2020). Nonetheless, a picture of LPCs as regulatory or ‘dimmer switch’ cells during chronic liver injury and regeneration is definitely emerging and highlights the potential for their therapeutic targeting (Breitkopf-Heinlein and Syn, 2020)

## 5. Conclusion

In conclusion, the process of liver injury and recovery observed in the TAA model stimulates compensatory mechanisms that limit hepatotoxicity, inflammation and fibrosis during subsequent hepatic insults. One key component of the altered cellular niche in pre-treated livers is the presence of a persistent population of parenchymal LPCs that closely associate inflammatory cells and fibrosis-driving HSCs upon re-exposure to the hepatotoxin. We now demonstrate that LPCs are capable of direct modulation of the HSC fibrogenic potential through intercellular communication. The LPC-derived fibrosis modulators are currently unknown, and further studies are required to identify the underlying cross-talk mechanisms, which may also include cellular communication to key inflammatory cells in the injury niche.

## Ethical approval and consent to participate

All animal experiments were performed in accordance with the Australian code for the care and use of animals for scientific purposes at Curtin University, Perth, Australia with local Animal Ethics Committee approval.

## Funding

This research was supported by the National Health and Medical Research Council provided Project Grant funding (APP1087125 and APP1160323). The Spinnaker-Health Research Foundation and Murdoch University co-funded a Belberry Medical Research PhD scholarship, while Curtin University provided Australian Government-funded Research Training Program PhD scholarships.

## CRediT authorship contribution statement

**Francis D. Gratte:** Conceptualization, Methodology, Validation, Formal analysis, Investigation, Writing - original draft, Writing - review & editing, Project administration, Funding acquisition. **Sara Pasic:** Methodology, Formal analysis, Investigation. **N. Dianah B. Abu Bakar:** Methodology, Formal analysis, Investigation. **Jully Gogoi-Tiwari:** Investigation. **Xiao Liu:** Methodology. **Rodrigo Carlessi:** Formal analysis, Investigation. **Tatiana Kisseleva:** Resources, Writing - review & editing, Supervision. **David A. Brenner:** Resources, Writing - review & editing, Supervision. **Grant A. Ramm:** Conceptualization, Writing - review & editing, Supervision, Funding acquisition. **John K. Olynyk:** Conceptualization, Writing - review & editing, Supervision, Funding acquisition. **Janina E.E. Tirmitz-Parker:** Conceptualization, Methodology, Resources, Writing - original draft, Writing - review & editing, Supervision, Project administration, Funding acquisition.

## Acknowledgements

The National Health and Medical Research Council provided Project Grant funding (APP1087125 and APP1160323). The Spinnaker-Health Research Foundation and Murdoch University co-funded a Belberry



Medical Research PhD scholarship, while Curtin University provided Australian Government-funded Research Training Program PhD scholarships.

## Appendix A. Supplementary data

Supplementary material related to this article can be found, in the online version, at doi:<https://doi.org/10.1016/j.biocel.2021.105933>.

## References

- Breitkopf-Heinlein, K., Syn, W.K., 2020. Harnessing liver progenitors in the treatment of liver fibrosis: a step in the right direction? *Gut* 69 (6), 975–976.
- Cai, X., Wang, J., Wang, J., Zhou, Q., Yang, B., He, Q., Weng, Q., 2020. Inter-cellular crosstalk of hepatic stellate cells in liver fibrosis: new insights into therapy. *Pharmacol. Res.* 155, 104720.
- Chen, J., Zhang, X., Xu, Y., Li, X., Ren, S., Zhou, Y., Duan, Y., Zern, M., Zhang, H., Chen, G., Liu, C., Mu, Y., Liu, P., 2015. Hepatic progenitor cells contribute to the progression of 2-acetylaminofluorene/carbon tetrachloride-induced cirrhosis via the non-canonical Wnt pathway. *PLoS One* 10 (6), e0130310.
- Chen, L., Brenner, D.A., Kisseleva, T., 2019. Combatting fibrosis: exosome-based therapies in the regression of liver fibrosis. *Hepatology* 69 (2), 180–192.
- Dai, Z., Song, G., Balakrishnan, A., Yang, T., Yuan, Q., Möbus, S., Weiss, A.C., Bentler, M., Zhu, J., Jiang, X., Shen, X., Bantel, H., Jaeckel, E., Kispert, A., Vogel, A., Saborowski, A., Büning, H., Manns, M., Cantz, T., Ott, M., Sharma, A.D., 2020. Growth differentiation factor 11 attenuates liver fibrosis via expansion of liver progenitor cells. *Gut* 69 (6), 1104–1115.
- Dwyer, B.J., Olynyk, J.K., Ramm, G.A., Tirmitz-Parker, J.E., 2014. TWEAK and LTP signaling during chronic liver disease. *Front. Immunol.* 5, 39.
- Dwyer, B.J., Jarman, E.J., Gogoi-Tiwari, J., Ferreira-Gonzalez, S., Boulter, L., Guest, R.V., Kendall, T.J., Kurian, D., Kilpatrick, A.M., Robson, A.J., O'Duibhir, E., Man, T.Y., Campana, L., Starkey Lewis, P.J., Wigmore, S.J., Olynyk, J.K., Ramm, G.A., Tirmitz-Parker, J.E.E., Forbes, S.J., 2020. TWEAK/Fn14 signalling promotes cholangiocarcinoma niche formation and progression. *J. Hepatol.* <https://doi.org/10.1016/j.jhep.2020.11.018>.
- Español-Suñer, R., Carpentier, R., Van Hul, N., Legry, V., Achouri, Y., Cordi, S., Jacquemin, P., Lemaigre, F., Leclercq, I.A., 2012. Liver progenitor cells yield functional hepatocytes in response to chronic liver injury in mice. *Gastroenterology* 143 (6), 1564–1575 e1567.
- Grzelak, C.A., Martelotto, L.G., Sigglekow, N.D., Patkunanathan, B., Ajami, K., Calabro, S.R., Dwyer, B.J., Tirmitz-Parker, J.E., Watkins, D.N., Warner, F.J., Shackel, N.A., McCaughan, G.W., 2014. The intrahepatic signalling niche of hedgehog is defined by primary cilia positive cells during chronic liver injury. *J. Hepatol.* 60 (1), 143–151.
- Grzelak, C.A., Sigglekow, N.D., Tirmitz-Parker, J.E., Hamson, E.J., Warren, A., Maneck, B., Chen, J., Patkunanathan, B., Boland, J., Cheng, R., Shackel, N.A., Seth, D., Bowen, D.G., Martelotto, L.G., Watkins, D.N., McCaughan, G.W., 2017. Widespread GLI expression but limited canonical hedgehog signaling restricted to the ductular reaction in human chronic liver disease. *PLoS One* 12 (2), e0171480.
- Hicks, D.F., Goossens, N., Blas-Garcia, A., Tsuchida, T., Wooden, B., Wallace, M.C., Nieto, N., Lade, A., Redhead, B., Cederbaum, A.I., Dudley, J.T., Fuchs, B.C., Lee, Y.A., Hoshida, Y., Friedman, S.L., 2017. Transcriptome-based repurposing of apigenin as a potential anti-fibrotic agent targeting hepatic stellate cells. *Sci. Rep.* 7, 42563.
- Kallis, Y.N., Robson, A.J., Fallowfield, J.A., Thomas, H.C., Alison, M.R., Wright, N.A., Goldin, R.D., Iredale, J.P., Forbes, S.J., 2011. Remodelling of extracellular matrix is a requirement for the hepatic progenitor cell response. *Gut* 60 (4), 525–533.
- Kisseleva, T., Brenner, D., 2020. Molecular and cellular mechanisms of liver fibrosis and its regression. *Nat. Rev. Gastroenterol. Hepatol.* <https://doi.org/10.1038/s41575-020-00372-7>.
- Kisseleva, T., Cong, M., Paik, Y., Scholten, D., Jiang, C., Benner, C., Iwaisako, K., Moore-Morris, T., Scott, B., Tsukamoto, H., Evans, S.M., Dillmann, W., Glass, C.K., Brenner, D.A., 2012. Myofibroblasts revert to an inactive phenotype during regression of liver fibrosis. *Proc. Natl. Acad. Sci. U.S.A.* 109 (24), 9448–9453.
- Köhn-Gaone, J., Dwyer, B.J., Grzelak, C.A., Miller, G., Shackel, N.A., Ramm, G.A., McCaughan, G.W., Elsegood, C.L., Olynyk, J.K., Tirmitz-Parker, J.E.E., 2016a. Divergent inflammatory, fibrogenic, and liver progenitor cell dynamics in two common mouse models of chronic liver injury. *Am. J. Pathol.* 186 (7), 1762–1774.
- Köhn-Gaone, J., Gogoi-Tiwari, J., Ramm, G.A., Olynyk, J.K., Tirmitz-Parker, J.E., 2016b. The role of liver progenitor cells during liver regeneration, fibrogenesis, and carcinogenesis. *Am. J. Physiol. Gastrointest. Liver Physiol.* 310 (3), G143–154.
- Koyama, Y., Xu, J., Liu, X., Brenner, D.A., 2016. New developments on the treatment of liver fibrosis. *Dig. Dis.* 34 (5), 589–596.
- Lee, Y.A., Wallace, M.C., Friedman, S.L., 2015. Pathobiology of liver fibrosis: a translational success story. *Gut* 64 (5), 830–841.
- Lemoine, S., Friedman, S.L., 2019. New and emerging anti-fibrotic therapeutics entering or already in clinical trials in chronic liver diseases. *Curr. Opin. Pharmacol.* 49, 60–70.
- Liedtke, C., Luedde, T., Sauerbruch, T., Scholten, D., Streetz, K., Tacke, F., Tolba, R., Trautwein, C., Trebicka, J., Weiskirchen, R., 2013. Experimental liver fibrosis research: update on animal models, legal issues and translational aspects. *Fibrogenesis Tissue Repair* 6 (1), 19.
- Lowes, K.N., Brennan, B.A., Yeoh, G.C., Olynyk, J.K., 1999. Oval cell numbers in human chronic liver diseases are directly related to disease severity. *Am. J. Pathol.* 154 (2), 537–541.
- Mederacke, I., Dapito, D.H., Affò, S., Uchinami, H., Schwabe, R.F., 2015. High-yield and high-purity isolation of hepatic stellate cells from normal and fibrotic mouse livers. *Nat. Protoc.* 10 (2), 305–315.
- Müller, M., Wetzel, S., Köhn-Gaone, J., Chalupsky, K., Lüllmann-Rauch, R., Barikbin, R., Bergmann, J., Wöhner, B., Zbodakova, O., Leuschner, I., Martin, G., Tiegs, G., Rose-John, S., Sedlacek, R., Tirmitz-Parker, J.E., Saftig, P., Schmidt-Arras, D., 2016. A disintegrin and metalloprotease 10 (ADAM10) is a central regulator of murine liver tissue homeostasis. *Oncotarget* 7 (14), 17431–17441.
- Prakoso, E., Tirmitz-Parker, J.E., Clouston, A.D., Kayali, Z., Lee, A., Gan, E.K., Ramm, G.A., Kench, J.G., Bowen, D.G., Olynyk, J.K., McCaughan, G.W., Shackel, N.A., 2014. Analysis of the intrahepatic ductular reaction and progenitor cell responses in hepatitis C virus recurrence after liver transplantation. *Liver Transplant.* 20 (12), 1508–1519.
- Raven, A., Lu, W.Y., Man, T.Y., Ferreira-Gonzalez, S., O'Duibhir, E., Dwyer, B.J., Thomson, J.P., Meehan, R.R., Bogorad, R., Koteliensky, V., Kotelevtsev, Y., Ffrench-Constant, C., Boulter, L., Forbes, S.J., 2017. Cholangiocytes act as facultative liver stem cells during impaired hepatocyte regeneration. *Nature* 547 (7663), 350–354.
- Ruddell, R.G., Knight, B., Tirmitz-Parker, J.E., Akhurst, B., Summerville, L., Subramanian, V.N., Olynyk, J.K., Ramm, G.A., 2009. Lymphotoxin-beta receptor signaling regulates hepatic stellate cell function and wound healing in a murine model of chronic liver injury. *Hepatology* 49 (1), 227–239.
- Schnabl, B., Purbeck, C.A., Choi, Y.H., Hagedorn, C.H., Brenner, D., 2003. Replicative senescence of activated human hepatic stellate cells is accompanied by a pronounced inflammatory but less fibrogenic phenotype. *Hepatology* 37 (3), 653–664.
- Schuppan, D., Afdhal, N.H., 2008. Liver cirrhosis. *Lancet* 371 (9615), 838–851.
- Tirmitz-Parker, J.E., Tonkin, J.N., Knight, B., Olynyk, J.K., Yeoh, G.C., 2007. Isolation, culture and immortalisation of hepatic oval cells from adult mice fed a choline-deficient, ethionine-supplemented diet. *Int. J. Biochem. Cell Biol.* 39 (12), 2226–2239.
- Tirmitz-Parker, J.E., Viebahn, C.S., Jakubowski, A., Klopčič, B.R., Olynyk, J.K., Yeoh, G.C., Knight, B., 2010. Tumor necrosis factor-like weak inducer of apoptosis is a mitogen for liver progenitor cells. *Hepatology* 52 (1), 291–302.
- Tirmitz-Parker, J.E., Olynyk, J.K., Ramm, G.A., 2014. Role of TWEAK in coregulating liver progenitor cell and fibrogenic responses. *Hepatology* 59 (3), 1198–1201.
- Tirmitz-Parker, J.E.E., Forbes, S.J., Olynyk, J.K., Ramm, G.A., 2019. Cellular plasticity in liver regeneration: spotlight on cholangiocytes. *Hepatology* 69 (5), 2286–2289.
- Trautwein, C., Friedman, S.L., Schuppan, D., Pinzani, M., 2015. Hepatic fibrosis: concept to treatment. *J. Hepatol.* 62 (1 Suppl), S15–24.
- Troeger, J.S., Mederacke, I., Gwak, G.Y., Dapito, D.H., Mu, X., Hsu, C.C., Pradere, J.P., Friedman, R.A., Schwabe, R.F., 2012. Deactivation of hepatic stellate cells during liver fibrosis resolution in mice. *Gastroenterology* 143 (4), 1073–1083 e1022.
- Tsuchida, T., Friedman, S.L., 2017. Mechanisms of hepatic stellate cell activation. *Nat. Rev. Gastroenterol. Hepatol.* 14 (7), 397–411.
- Van Hul, N.K., Abarca-Quinones, J., Sempoux, C., Horsmans, Y., Leclercq, I.A., 2009. Relation between liver progenitor cell expansion and extracellular matrix deposition in a CDE-induced murine model of chronic liver injury. *Hepatology* 49 (5), 1625–1635.
- Wood, M.J., Gadd, V.L., Powell, L.W., Ramm, G.A., Clouston, A.D., 2014. Ductular reaction in hereditary hemochromatosis: the link between hepatocyte senescence and fibrosis progression. *Hepatology* 59 (3), 848–857.
- Zhou, J., Cui, S., He, Q., Guo, Y., Pan, X., Zhang, P., Huang, N., Ge, C., Wang, G., Gonzalez, F.J., Wang, H., Hao, H., 2020. SUMOylation inhibitors synergize with FXR agonists in combating liver fibrosis. *Nat. Commun.* 11 (1), 240.